LUTETIUM ISOTOPES

A STUDY OF LUTETIUM ISOTOPES USING SINGLE PARTICLE TRANSFER REACTIONS

by

ROBERT ARTHUR O'NEIL, B.Sc.

A Thesis

Submitted to the School of Graduate Studies

in Partial Fulfilment of the Requirements

for the Degree of

Doctor of Philosophy

McMaster University

August, 1972

DOCTOR OF PHILOSOPHY (1972)
(Physics)

McMASTER UNIVERSITY
Hamilton, Ontario

TITLE: A Study of Lutetium Isotopes Using Single Particle Transfer Reactions

AUTHOR: Robert Arthur O'Neil, B. Sc. (University of Calgary)

SUPERVISOR: Dr. D. G. Burke

NUMBER OF PAGES: xi, 231

SCOPE AND CONTENTS:

The nuclear energy level structure of the three odd-Z nuclei ^{173}Lu, ^{175}Lu and ^{177}Lu have been investigated using the (^{3}He,d) and (α,t) reactions. The resulting spectra have been interpreted using the Nilsson model with corrections for Coriolis coupling and pairing effects. The present work confirms the earlier assignments of the $7/2^{+}[404]$ and $5/2^{+}[402]$ proton orbitals in all three nuclei. New assignments are made for the $9/2^{-}[514]$ orbital in ^{173}Lu and the $1/2^{-}[541]$ orbital in ^{177}Lu. The assignment of these states is confirmed in the remaining nuclei in each case. The assignment of the $1/2^{+}[411]$ orbital is confirmed in ^{173}Lu and ^{177}Lu but the state has not been assigned in ^{175}Lu. In addition, assignments are proposed for the $1/2^{-}[530]$ and $3/2^{-}[532]$ proton orbitals above 1 MeV excitation in all three nuclei.

The structure of the odd-odd nucleus ^{174}Lu has also been studied using the (^{3}He,d), (α,t), (^{3}He,α) and (d,t) reactions. The proton transfer data have enabled the assignment

of the $1/2^-[541]$, $5/2^+[402]$, $9/2^-[514]$ and the $1/2^-[530]$ proton orbitals coupled to the $5/2^-[512]$ neutron in both spin triplet and singlet configurations. Strong Coriolis coupling has been observed in bands formed by the transfer of the $1/2^-[541]$ and the $1/2^-[530]$ protons. The neutron transfer data have been used to confirm previous assignments of the $5/2^-[512]$, $1/2^-[521]$ and $3/2^-[521]$ neutron orbitals coupled to the $7/2^+[404]$ proton. The observation of levels populated by high-ℓ transfers in the $(^3He,\alpha)$ reaction has led to a revised assignment of the $K^\pi = 7^+$, $\{7/2^+[633]_n + 7/2^+[404]_p\}$ rotational band. Similarly the spin triplet $K^\pi = 0^+$ configuration of these two orbitals has also been identified.

ACKNOWLEDGEMENTS

I would like to thank Dr. Dennis Burke, my research supervisor, for his friendship throughout my stay at McMaster. The initial patient explanations and subsequent discussions were much appreciated. In particular the help given in the writing of the papers which form the body of the discussion part of this thesis was very instructive.

I am very grateful to have been able to collaborate with Professor W. P. Alford of the University of Rochester Nuclear Structure Research Laboratory where a considerable fraction of the experiments was performed. His interest in all the aspects of my work has been most encouraging.

Appreciation is also expressed to Dr. W. V. Prestwich and Dr. K. Fritze, who were members of my supervisory committee.

I would also like to thank Dr. R. Bloch, who before going on to bigger and better things, gave me an appreciation for the power of physical insight when applied to other fields. Discussions with Dr. J. C. Waddington have always been fruitful, particularly in the earlier stages of this work.

It has been very interesting and enjoyable to be a member of the same research group as J. C. Tippett and D. E. Nelson. I am pleased to acknowledge their efforts which contributed to the success of our group.

In addition I would like to thank:

Geoff Frank whose careful examination of GREAT revealed several errors;

Aadu Pilt for many enlightening discussions in nuclear theory;
Judith Balogh for preparing most of the drawings;
The counting girls and in particular Mrs. Jacque Prestwich who scanned many meters of plates as the first step in the data reduction process;
The operations groups of the McMaster FN tandem accelerator and the Rochester MP tandem accelerator, in particular, Phil Ashbaugh, John McKay and Arnold Peterson, bigwigs;
And the girls of the Physics Office for the skill and patience required to type a manuscript written by the worst writer in the department.

Financial support was provided by the National Research Council of Canada in the form of a bursary and scholarships to the author, and an operating grant to his supervisor, Dr. D. G. Burke.

Ex ungue leonem.

TABLE OF CONTENTS

LIST OF FIGURES

LIST OF TABLES

CHAPTER 1

INTRODUCTION

The study of nuclear physics is concerned with attempting to probe the internal structure of the nucleus. In nuclear physics, as in all physics, there are two goals: one is the actual measurement of gross nuclear parameters as well as the details of individual nuclear states, and the second is the explanation of these results in addition to the prediction of hitherto unobserved effects. In the course of the explanation, models or theories of the nucleus are formed which in turn suggest further measurements. These subsequent measurements frequently strengthen the basic ideas embedded in the models and just as often suggest refinements which should be considered in later theories.

One of the best known characteristics of heavier rare earth nuclei is the fact that they are deformed. Except possibly in the region of transition from a spherical to a deformed shape, the nuclear deformation is prolate (implying a football shaped object). Because the nucleus is not spherical, nuclear states which are manifestations of the nucleus rotating about its center of mass may be observed. These rotational states are grouped to form "bands" which are among the most prominent features of the

low energy spectrum. Using the predictions of the Nilsson model, in which a single particle moves in the deformed potential well of the nuclear core, it is possible to learn something of the structure of these nuclei. In the last ten years these models have been very successfully applied to the interpretation of nuclei with an unpaired neutron outside a rotating deformed core.

When this investigation was initiated the existing experimental data on the structure of odd-proton nuclei was mainly derived from β-decay studies and from (n,γ) reaction work. Assignments of the intrinsic nuclear structure were made of the lowest energy states from measurements of energy level spacings within rotational bands as well as γ-ray transition probabilities. It was typical of these early investigations that many ambiguities remained even after the measurement of some of the spins and parities of the low lying levels. In the case of odd-odd deformed nuclei, where the nucleus has both an unpaired proton and an unpaired neutron, the situation was similar in that only the lowest configurations had been observed and assigned.

It was decided to study a series of odd mass nuclei using single particle transfer reactions, a technique which had only rarely been applied to deformed odd-proton nuclei. It had been shown, using the transfer of a single neutron, that these reactions could be used to measure the magnitude

of the Nilsson wavefunction components in the final deformed nucleus. The results were in impressive agreement with the predictions of the Nilsson model. These components were extracted using the characteristic relative intensity pattern of the rotational band built on a specific intrinsic configuration. This "fingerprint" of the rotational band has been used extensively in the present work to establish the origin of the observed bands. Such unambiguous determinations of the intrinsic states are often quite difficult using γ-ray techniques, though ideally all experimental methods available should be brought to bear on the nucleus being studied.

It is characteristic of single particle transfer reactions such as the (^{3}He,d) and (α,t) reaction that there is only one transition (peak) per level in the final nucleus. Thus, the energy spectrum obtained is much less complicated than the spectrum from an experiment involving the measurement of γ-ray transitions or internal conversion electrons where several transitions are observed per energy level. The energy resolution obtained in single particle transfer reactions is much poorer than that which may be obtained using modern Ge(Li) detectors to study γ-rays; so the simple spectrum of the transfer reactions is a significant advantage in regions where the level density is high. It is worth noting too, that the energy of the peaks observed in single particle transfer reactions is directly related to the excitation energy of the state in the final nucleus. This again is an advantage

in nuclei with complicated level schemes.

Single proton transfer reactions were not done until fairly recently on deformed rare earth targets because of the low cross sections with which these reactions sometimes take place. Of particular significance to the technique, was the development of accelerators with very intense (several μA) beams of ^{3}He and α-particles at energies greater than the Coulomb barrier of the deformed target (≈ 22 MeV). To complement these accelerators high resolution magnetic spectrographs with large solid angles of acceptance have become available.

In the present work the structures of ^{173}Lu, ^{175}Lu and ^{177}Lu has been studied. The results of these experiments have been interpreted as proton orbitals in the Nilsson model description of the nucleus. Several of the rotational bands identified are strongly coupled by the Coriolis interaction and calculations have been done to show the observed effects are consistent with this interpretation. In addition to the study of the odd mass isotopes, the odd-odd nucleus ^{174}Lu has been investigated. In this case the interpretation of the levels was made using rotational bands built on excitation of only the proton or only the neutron from the ground state configuration. Here again, calculations have shown the energies and cross sections of some of the rotational bands to be strongly perturbed by the Coriolis interaction.

CHAPTER 2

EXPERIMENTAL DETAILS

The present work reports the results of the experiments listed in Table 2.0.1 to study the single particle level structure of the three odd-mass nuclei ^{173}Lu, ^{175}Lu and ^{177}Lu and the two quasi-particle levels in the odd-odd nucleus ^{174}Lu.

As may be seen, most of the experiments were performed at the University of Rochester Nuclear Structure Research Laboratory. There were several reasons for this, the first being that the (^{3}He,d) exposures on the even mass targets were by-products of (^{3}He,α) experiments into the odd-mass ytterbium isotopes (Burke et al. 1971) performed at Rochester because the McMaster accelerator had not been completed. The second reason was the Rochester MP Tandem Van de Graaff accelerator was capable of higher beam energies and intensities especially of ^{3}He ions and α-particles than was available at the time from the McMaster FN Tandem Van de Graaff accelerator. The latter reason is especially important in the (α,t) reactions on rare earth targets where large negative Q-values and high Coulomb barriers cause low cross sections. Subsequent experiments with lower beam energies on even mass targets were performed at McMaster.

Table 2.0.1

Experiments Performed

Reaction	E_{in} (MeV)	θ_{out} (degrees)	Laboratory
$^{172}Yb(^{3}He,d)^{173}Lu$	28	10,20,25,30,40, 50,60	Rochester
	24[a]	≈0, 10,15	McMaster
$^{172}Yb(\alpha,t)^{173}Lu$	30	45,60	Rochester
$^{174}Yb(^{3}He,d)^{175}Lu$	28	10,20,25,30,40,50 70,80	Rochester
	25[a]	≈0 ,6 ,10 ,15	McMaster
$^{174}Yb(\alpha,t)^{175}Lu$	30	45,60	Rochester
$^{176}Yb(^{3}He,d)^{177}Lu$	28	15,20,25,40	Rochester
	24[a]	≈0, 15	McMaster
$^{176}Yb(\alpha,t)^{177}Lu$	30	45	Rochester
	25[a]	90, 130	McMaster
	24[a]	90	McMaster
$^{173}Yb(^{3}He,d)^{174}Lu$	24	30,38,50	McMaster
$^{173}Yb(\alpha,t)^{174}Lu$	28.5	20,60,75	Rochester
	26[a]	90	McMaster
	25[a]	60,120	McMaster
$^{175}Lu(^{3}He,\alpha)^{174}Lu$	24	25,35,45	McMaster
$^{175}Lu(d,t)^{174}Lu$	12	40,60,120	McMaster
	16[a]	6,15,20,30,60,120	McMaster
	18[a]	6	McMaster

a) not reported in the present work

However, they were not a significant improvement over the Rochester data. In the case of the ^{173}Yb target the experiments were initially attempted at McMaster with the lower beam energies. The (α,t) exposures, though useable, exhibited extremely small cross sections, particularly above 500 keV. The cross section was expected to be much improved at the higher beam energies available using an MP tandem accelerator. Thus, the experiments were repeated at the University of Rochester using 28.5 MeV α-particles. The present discussion considers only the 28.5 MeV data.

2.1 Construction of targets

The ytterbium targets were made from isotopically enriched Yb_2O_3 purchased from the Stable Isotopes Division of the Oak Ridge National Laboratory. The isotopic compositions of these oxides, as stated by the supplier, appear in Table 2.1.1. The manufacture of these targets followed essentially the same method given by Westgaard and Bjørnholm (1966). In this case a mixture of fresh lanthanum filings and Yb_2O_3 powder were placed in a tantalum crucible. The amount of lanthanum was approximately 1.5 times the amount indicated by the stoichiometric ratio for the reduction reaction. The crucible was then heated in a vacuum using electron bombardment which resulted in the following reaction:

$$Yb_2O_3 + 2La \rightarrow La_2O_3 + 2Yb\uparrow \ .$$

Table 2.1.1

Isotopic composition of the targets

Target	Abundance of isotope in target								
	^{168}Yb	^{170}Yb	^{171}Yb	^{172}Yb	^{173}Yb	^{174}Yb	^{176}Yb	^{175}Lu	^{176}Lu
^{172}Yb	<0.01%	0.05%	0.75%	97.15%	1.01%	0.87%	0.19%		
^{173}Yb	<0.02%	0.05%	0.3 %	1.41%	95%	2.89%	0.34%		
^{174}Yb	<0.01%	0.05%	0.41%	0.99%	2.2 %	95.8%	0.57%		
^{176}Yb	<0.01%	0.05%	0.32%	0.52%	0.56%	2.12%	96.43%		
^{175}Lu [a]								99.94%	0.06%

a) The total Yb content in the ^{175}Lu was stated to be 0.02% by the supplier

In this manner the oxide was reduced and the ytterbium metal simultaneously evaporated. The metal was condensed onto 50 μgm/cm^2 carbon foils on glass microscope slides. For some of the even mass targets a mask was placed in between the crucible and the carbon foils to allow ytterbium to be deposited in a 1/2 mm wide line. The carbon foils were then floated off the glass slides and onto aluminum target frames suitable for mounting in the target chamber. The thickness of metal deposited was estimated initially using the α scattering apparatus of Burke and Tippett (1968) and later, a more accurate measurement was obtained during the actual exposures. For the even mass targets, the thicknesses of metal were found to be between 50 μgm/cm^2 to 150 μgm/cm^2. In the case of ^{173}Yb targets of thicknesses between 40 and 70 μgm/cm^2 were used in an attempt to enhance the resolution.

The ^{175}Lu targets for the neutron transfer work were made from enriched $^{175}Lu_2O_3$ from the same supplier as the ytterbium isotopes. In order to prevent the powdered oxide from becoming charged and flying out of the crucible under electron bombardment, the powder was compressed into a small thin pellet. This pellet was heated to its melting point and the resulting $^{175}Lu_2O_3$ vapours were condensed onto 50 μgm/cm^2 carbon foils in the same manner as for ytterbium. For the (d,t) exposures targets of between 20 and 30 μgm/cm^2 were used; whereas, the (^{3}He,α) exposures employed targets of up to 125 μgm/cm^2 thickness because the cross section for the reaction was very small and the peak widths are quite large for reasons to be

discussed in section 2.2.

2.2 The Enge magnetic spectrograph

Single particle transfer reactions into deformed rare earth nuclei populate large numbers of states with fairly small cross sections. The design of a spectrograph for such experiments must take these two important facts into consideration. The Enge split pole magnetic spectrographs (Spencer and Enge 1967) such as installed at the University of Rochester and McMaster accelerator laboratories have large solid angles of acceptance and high resolving powers.

Fig. 2.2.1 shows a schematic diagram of the median plane of the spectrograph. The two pole pieces are encircled by a common field coil. The purpose of the split in the pole piece and the non-normal angles of entry and exit of the trajectories into the magnetic fields is to provide enough design parameters that second order aberrations are eliminated at the same time as the desired dispersion and magnifications are maintained.

For an Enge spectrograph of the type installed at McMaster and Rochester with a maximum radius of curvature ρ_{max} = 91 cm the energy dispersion is approximately 1 keV/mm per MeV of particle energy. For example, in an experiment where 9 MeV particles are detected there would be about 1 mm between peaks separated by 9 keV. Including the fact that the particles strike the focal plane at approximately 45°

Figure 2.2.1

Schematic diagram of an Enge split pole magnetic spectrograph. Several trajectories through the magnetic field are shown for particle groups on the focal plane.

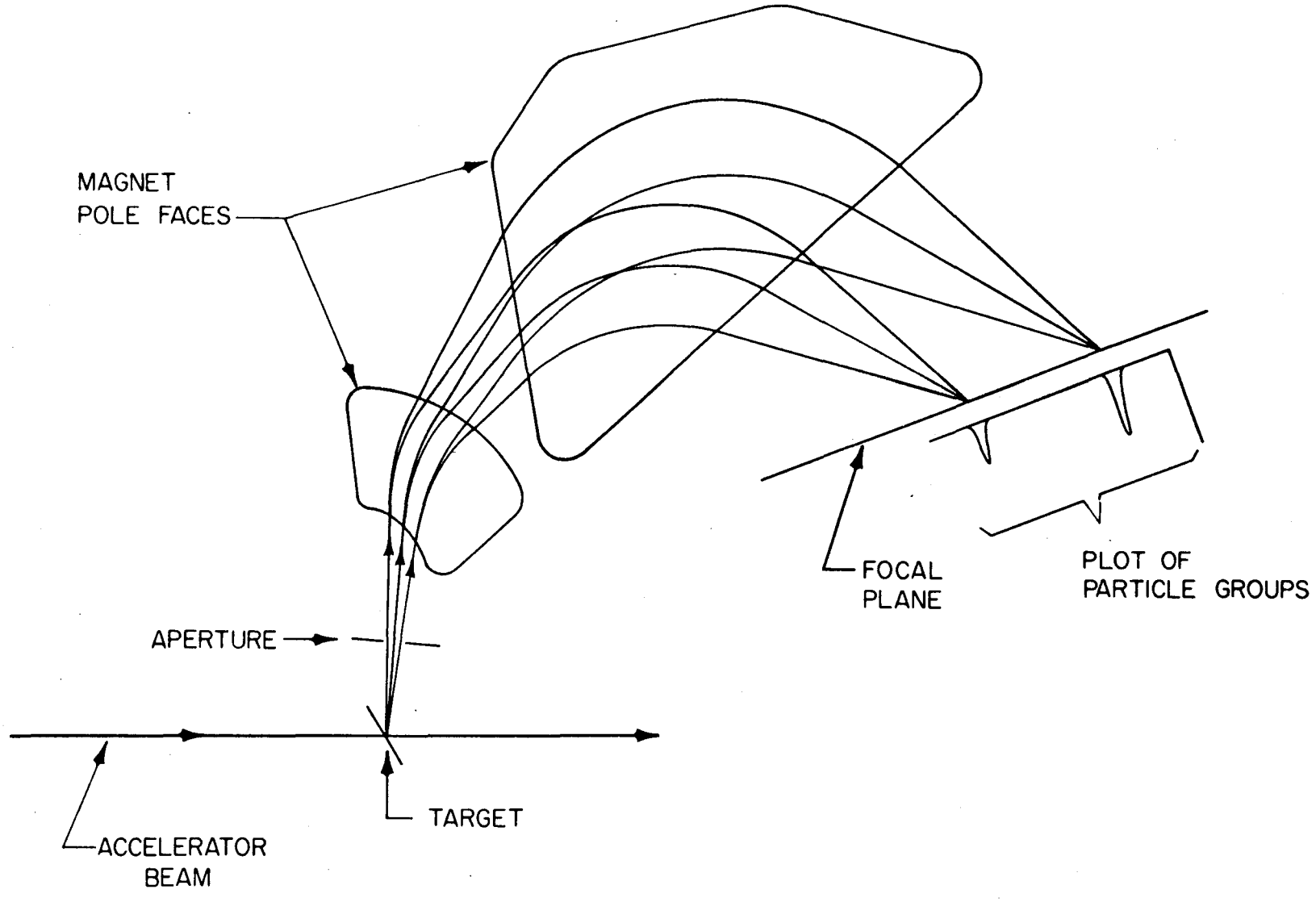
MAGNET
POLE FACES
APERTURE
FOCAL
PLANE
PLOT OF
PARTICLE GROUPS
TARGET
ACCELERATOR
BEAM

in the median plane, the horizontal width of the image formed by the spectrograph on the emulsions is about half as wide as the beam spot in the target chamber. Vertical (out of the median plane) focussing also exists in these spectrographs in order to obtain large solid angles. In the vertical direction the particles are spread over about one centimeter in the focal plane, making tracks easier to count on nuclear emulsions.

The energy of a particle leaving a nuclear reaction varies with the outgoing angle as a result of the recoil of the residual nucleus. When a large solid angle spectrograph is used the energy of a particle entering one side of the aperture is different than the energy of a particle entering on the opposite side. This effect is the so-called kinematic broadening of the peaks. The Enge spectrograph is able to compensate for this broadening for a specific reaction by shifting of the focal plane along the particle trajectories. The shift is calculated using the known kinematics for each reaction and the procedure described by Spencer and Enge (1967).

The McMaster spectrograph is located, relative to the analyzing magnet and switching magnet, such that the focal plane of the spectrograph is dispersion compensated. This is to say that the ion optics of the system are such that small fluctuations in the beam energy, which cause the beam spot to move from left to right on the target will not result in broadened peaks on the focal plane of the spectrograph. If

the experiment is performed with the spectrograph looking at the outcoming particles being transmitted by the target, (the most common mode of operation because it includes the angles forward of $\theta = 60°$) the beam optics are set so that the beam passes through one more focus than it has when the outcoming particles are "reflected" from the target. Though it is not so easy to focus the beam onto the target when doing an experiment in the reflection geometry, the reduction in the peak width obtained by removing the one focus is significant.

The particles were detected on the focal plane with nuclear emulsions. For the (^{3}He,d), (α,t) and (d,t) reactions Kodak type NTB emulsions 50 μm thick were used. In the case of the (^{3}He,α) exposures, 50 μm thick Ilford K minus 1 emulsions were more desirable because they were quite insensitive to the deuterons of the same magnetic rigidity as the α-particles of interest, and which would otherwise cause a large background.

The nuclear emulsions were covered with aluminum absorbers to discriminate against unwanted particles arising from reactions in the target. It is rather interesting that carbon ions may be knocked out of the target backing and appear at the same radius of curvature as the tritons of interest in the (α,t) reactions. The absorber thicknesses in the four reactions were: in the (α,t) reaction between 0.05 mm and 0.1 mm of Al; in the (d,t) reaction 0.1 mm Al; in the (^{3}He,d) reaction, 0.7 mm Al; and in the (^{3}He,α) reaction a graded Al absorber

was used which varied in thickness from 0.3 mm near the ground state to 0.25 mm at 3 MeV excitation.

The typical solid angles used at Rochester were 3.29 msr in the even mass target experiments and 2.32 msr for the $^{173}Yb(\alpha,t)^{174}Lu$ exposures. At McMaster the aperture was varied in order to strike a compromise between a small solid angle which tended to make the observed peaks more symmetric and the length of time available for the exposure. The value chosen was usually about 1 msr and never more than 2.6 msr.

The reactions of the beam on light materials in the target, for example the carbon backing and silicon from the pump oil, cause very broad high intensity plateaus which can obscure large parts of the spectrum of interest. The large widths of these peaks is caused by the large kinematic broadening of peaks from light nuclei. For the rare earth nuclei the kinematic shift is rather small compared to that which is needed for the light impurities so the latter are not well focussed in the reactions on lutetium and ytterbium targets. Moderately heavy impurities ($A<150$) in the target can also be detected because the energies of their peaks appear to move to higher excitation energies as the reaction angle is increased. This again is due to kinematic effects. The easiest way of detecting isotopic impurities is with a knowledge of the relative Q-values of the various contaminants and the spectrum of each. In general, the angles chosen for these experiments were such that the very broad carbon peaks from the target backing fell

outside the first two MeV of excitation of the nucleus of interest.

There are several important factors affecting the resolution obtained in these experiments. The first is the energy stability of the beam and the centering of the beam on the target. At McMaster early attempts were made to minimize these contributions using 1/2 mm slits just before the target. Recently, due to improvements in the terminal voltage stabilizers (Cairns, 1972) it has been possible to use 1 mm slits with almost as good results and have much higher beam currents on the target. The dispersion compensation of the McMaster spectrograph undoubtedly helps reduce the peak width when using the wider slits. The approach tried at Rochester was to use targets on which the material had been deposited in only a 0.5 mm wide vertical line so there was no reaction of interest if the beam was not correctly centered. It is worth pointing out, that no better resolution has been obtained in any of the present experiments using line targets. In both locations the beam spot was approximately 1/2 mm wide and 2 mm high. The horizontal magnification, being $\tilde{\sim}$ 0.5, would yield an intrinsic peak width on the focal plane of about 0.25 mm. The second major contribution to the resolution is the target thickness. According to the Bohr theory of straggling (Bohr 1948 or Enge 1966) the energy of the incident beam is reduced by electronic scattering and the energy distribution of the beam after passage through a target is approximately gaussian.

The width of the gaussian, and hence the contribution to the resolution, varies in the following manner:

$$\Delta E \gtrsim 18\ Z\sqrt{t}.$$

Where: ΔE is the energy spread after the passage through the material (keV)

Z is the atomic number of the charged particle

t is the target thickness (mg/cm^2).

The energy spread in this theory is independent of the incident energy. It may be seen that a very large reduction in the target thickness is needed for even modest gains in the peak width (energy spread). This expression also leads one to expect twice the peak width in reactions with ^3He and α-particles because these particles are doubly charged. The straggling is a major contribution to the poorer energy resolution in the $(^3He,\alpha)$ reaction.

Table 2.2.1 lists the resolutions obtained in the experiments into the lutetium isotopes. In the $(^3He,\alpha)$ reaction where the reaction Q-value is large and positive the peak width is more than 0.75 mm which corresponds to approximately 30 keV. The peak width in the (α,t) reactions is similar but this corresponds to about 12 keV because the triton energy is so low. The best resolution was attained in the (d,t) exposures when small entrance apertures and thin targets were used. The actual peak width in the (d,t) reaction is about 0.6 mm.

Table 2.2.1

Resolution obtained

Reaction	Beam Energy (MeV)	Target Thickness [a] ($\mu gm/cm^2$)	Observed Resolution (keV)
Yb(^{3}He,d)Lu	28	50-150	18-21
	24	70-100	16-20
Yb(α,t)Lu	30	50-150	14-17
	28.5	70-100	12
^{175}Lu(d,t)^{174}Lu	12	30-50	7-12
^{175}Lu(^{3}He,α)^{174}Lu	24	70-100	$\approx$30

a) does not include the 50 $\mu gm/cm^2$ carbon backings.

2.3 Normalization of the cross sections

In order to make assignments of certain peaks in the spectrum, it is necessary to have some measure of the absolute cross section for the state's formation in the reaction. Accurate measurements of the absolute cross sections are very difficult. In the odd mass lutetium isotopes angular distributions were attempted in order to extract the orbital angular momentum, ℓ, of the transition forming the peak. In such cases it is necessary to be able to measure at least relative cross sections from angle to angle.

The reaction cross sections were normalized using the known elastic scattering cross section for the incident beam on the target. At the same time as the spectrum was being taken, a small counter placed in the target chamber was used to observe the elastically scattered events. At the University of Rochester, the detector was a small NaI crystal with a photomultiplier. This particular system had a resolution of several hundreds of keV. At McMaster, small Si(Li) detectors were used. These initially had a resolution of about 50 keV which soon started to deteriorate due to neutron damage and the temperature of the target chamber while the beam was on. The spectrum was recorded in a multichannel analyzer and also a gate was set around the elastic peak of interest so the experiment's progress could be monitored on a scaler. In addition the beam current which passed through the target and was collected

in the Faraday cup was integrated, giving the total charge through the target during the experiment.

It is necessary to separate the events resulting from elastic scattering of the beam from the target material from those events arising from the carbon, silicon or oxygen. Having ascertained the number of elastic events in the course of the experiment the cross section for a peak on the plates is given by:

$$\left(\frac{d\sigma}{d\Omega}\right)_R = \frac{\left(\frac{d\sigma}{d\Omega}\right)_e \Omega_e}{N_e \Omega_R} N_R \cdot A \qquad (2.3.1)$$

where: $\left(\frac{d\sigma}{d\Omega}\right)_R$ is the center of mass cross section of the peak on the plate

$\left(\frac{d\sigma}{d\Omega}\right)_e$ is the elastic scattering cross section for the incident particles in the lab frame

Ω_e is the monitor solid angle

Ω_R is the spectrograph solid angle

N_R is the number of counts appearing in the peak on the plate

A is the factor which converts the reaction cross section from the lab to the center of mass frame. For rare earth nuclei it is essentially unity.

This arises simply because the spectrograph and the monitor detector are looking at the same target for the duration of the experiment.

Of the quantities in the above expression only the elastic cross section for the incident particle is difficult to calculate. In general the monitor was set at a lab angle

$\theta = 30°$ though in some instances it was at $\theta = 45°$. At these angles for 28.5 and 30 MeV α-particles and 28 MeV ^{3}He particles the elastic cross section is significantly less than Rutherford. The elastic cross section of a 28 MeV ^{3}He beam on ^{174}Yb was measured as a function of angle before these experiments were begun. The cross sections observed were in excellent agreement with the values predicted using the optical model parameters discussed in sect. 3.4. At $\theta=30°$ the elastic cross section for the $^{174}Yb(^{3}He,^{3}He)^{174}Yb$ reaction is 76% of the Rutherford cross section at an incident energy of 28 MeV. The elastic cross sections used in the normalization of the spectra using equation 2.3.1 were taken subsequently from the optical model calculations.

The normalization obtained in this manner was checked several times by measuring the elastic cross section by making a short exposure before and after the long experiments. Also the ratio of elastic events to the charge through the target was used to check for consistency, though this latter method assumed the beam strikes the same part of the target for all exposures and that the target angle has not been adjusted. In general these three methods gave results which were within 20% of each other; and hence, this is the estimate of the error placed on the absolute cross sections. In addition to this error, there are the statistical errors in the cross sections from the stripping and integration of the peaks. The statistical errors, which gave an estimate of the relative errors in the cross sections of

the peaks in a given exposure, are the only errors quoted in Chapters 4 and 5.

2.4 Calculation of the experimental energies and cross sections

The energy of the peak and the cross section for the transition to the level is found by measuring the peak position on the plate and the number of tracks appearing in the group. In the case of a well isolated peak, the procedure for finding the centroids and integrating the peak is straightforward. However, this is not as easily accomplished for peaks which are only partially resolved; for example, which appear as a shoulder on the side of another.

In the deformed rare earth nuclei, the level density is such that many spectra exhibit unresolved multiplets. As an aid to locating centroids and stripping areas the computer program SPECTR (O'Neil, 1972) was used. This program attempts to fit all the peaks in the spectrum to a standard shape, namely a gaussian with an exponential tail on the high excitation energy side. The four parameters which describe the peak shape are found by fitting a sample region in the spectrum which ideally contains only well resolved singlet peaks. The shape parameters are then fixed and applied to all the peaks in the spectrum. Only the position and height of the peaks are varied in a non-linear least-squares technique to find the best fit. In some cases the program "resolved" states which were separated by less than half of the full width half maximum (FWHM). Some consideration was given

to these peaks if this effect appeared consistently with different peak shape parameters and in several different spectra. Knowing the shape parameters and the height the program is able to integrate the number of counts in each peak. Using eq. 2.3.1 it is then possible to convert this number into a cross section.

From the plate position it is possible to find the radius of curvature of the trajectories in the magnetic field. The calibration (polynomial) curve, relating the radius of curvature and the plate position, was determined empirically using α-particles of known magnetic rigidity emitted from a radioactive source placed at the target position.

Having the radius of curvature of the detected particle in the spectrograph it is a straightforward calculation to obtain the excitation energy of the level corresponding to the observed group (Marion and Young 1968 or Enge 1966). The masses used in this calculation were from Liran and Zeldes (1969) and the mass of ^{174}Lu was taken from the (d,t) Q-value measurement by Jones and Sheline (1969). The absolute Q-values were not measured at the Univeristy of Rochester because an emulsion was not put on the focal plane to measure the position of the elastically scattered particles. Attempts to measure the Q-values in these reactions at McMaster were hampered because of difficulties with the system for placing index marks on the plates. The Q-values

obtained from these masses were consistent with the observed location of the ground state peaks on the emulsion so there was no problem in measuring the excitation energies relative to the ground state group.

The most recent calibration of the Rochester spectrograph is significantly different from the curve used in the calculation of the published energies of the odd mass lutetium isotopes (O'Neil et al. 1971). It is now believed that the later calibration generates the correct calibration curve. The energies in Chapter 4 were calculated using the most recent calibration curve. The new calibration makes about 10 keV/MeV difference in the (^{3}He,d) energies at 28 MeV bombarding energy, and brings some of the energies observed in the particle transfer work into better agreement with the reported β-decay and γ-decay studies.

The experimental spectra and tabulations of energies and cross sections may be found in Chapter 4 for the odd mass lutetium isotopes and in Chapter 5 in the case of ^{174}Lu.

CHAPTER 3

CALCULATIONS

In order to compare the experimental energies and cross sections to the theoretical predictions of the Nilsson model a number of calculations must be performed. In general the theoretical justification of many of these steps may be found in the literature. In particular, Elbek and Tjøm (1969) have published an excellent review article which includes an outline of the techniques used to compare the results of single particle transfer reactions and the Nilsson model in the deformed rare earth region.

In the present work levels in four lutetium nuclei have been interpreted in terms of the Nilsson model where the main assumption is that a single particle moves in a deformed potential well created by the core nucleons. In the rare earth nuclei the well has a prolate spheroidal shape. The various angular momentum vectors and their projections useful for such a description of the nucleus are shown in fig. 3.0.1. Because the nucleus is assumed to be symmetrical about its body fixed axis, there can be no observable component of the rotational angular momentum along the body axis. Hence the rotational angular momentum vector, $\vec{R}$, is perpendicular to the body axis. This then implies that K, the projection of the total angular

Figure 3.0.1

The angular momentum vectors, their coupling sums and projections for a deformed odd-odd nucleus. Because the nucleus has an axis of symmetry, $\vec{R}$ must be perpendicular to the body fixed axis. For an odd proton nucleus considered in the present work, the scheme is the same except there is no contribution from the angular momentum of the neutron. The term "body fixed axis" is used synonymously with the term "nuclear symmetry axis".

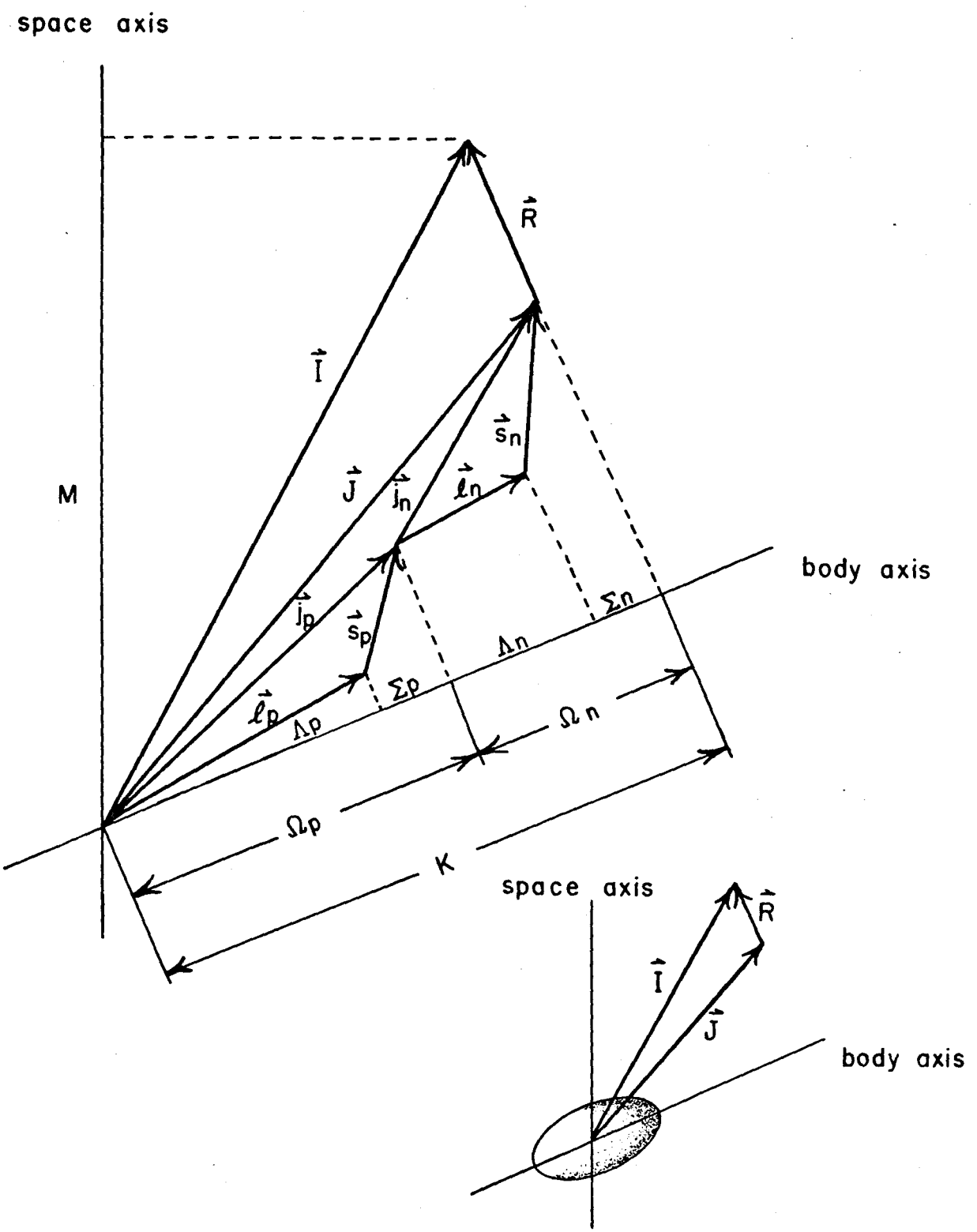
space axis
M
$\vec{R}$
$\vec{I}$
$\vec{J}$
$\vec{j}_n$
$\vec{\ell}_n$
$\vec{s}_n$
$\vec{j}_p$
$\vec{s}_p$
$\vec{\ell}_p$
body axis
Σn
Λn
Σp
Λp
Ωn
Ωp
K
space axis
$\vec{R}$
$\vec{I}$
$\vec{J}$
body axis

momentum on the body axis is the same as Ω, the projection of the intrinsic angular momentum on the body axis. Fig. 3.0.1 is drawn for the case of an odd-odd nucleus, for an odd proton nucleus the vectors labelled with a subscript n are simply zero because all the neutrons are paired up and give no contribution to the intrinsic nuclear angular momentum. The Nilsson model itself predicts only the wave functions of the odd particle outside the deformed core.

In order to predict the excitation energies and cross sections of the levels in the nucleus the Nilsson model states must be corrected for the effect of the pairing of the nucleons. These states form the band heads for a series of rotational states which often lead to the very characteristic energy spacings of groups of levels.

$$E_I = E_o + \frac{\hbar^2}{2\mathcal{J}} (I(I+1)) \qquad (3.0.1)$$

where: E_I is the excitation energy of the state with angular momentum I

E_o is related to the intrinsic energy of the configuration

I is the total nuclear spin of the state

$\mathcal{J}$ is the nuclear moment of inertia

$\hbar$ is Planck's constant $/2\pi$.

The factor $\frac{\hbar^2}{2\mathcal{J}}$ is referred to as the rotational parameter.

Rotational bands built on different intrinsic configurations may be mixed by the Coriolis interaction which can strongly perturb the rotational spacings and the cross

sections of the transitions to the various band members. The effects of the Coriolis coupling are particularly striking in the odd-odd nucleus ^{174}Lu.

All the experimental results in this work were obtained using single particle transfer reactions. The effects of the reaction mechanism on the cross sections were found using a Distorted Wave Born Approximation (DWBA) calculation with the optical model. These results, combined with the nuclear structure calculations referred to above, enable comparison of the experimental data with the theoretical predictions. In the case of the odd-odd nucleus ^{174}Lu, the comparisons with experiment appear more clearly if the calculation is carried through to the point of the prediction of the actual cross section. In the odd-A nuclei the contribution of the particular reaction to the experimental cross section was removed for the states assigned to the Nilsson model configurations so that the nuclear structure factors obtained from the different reactions into the various nuclei could be compared to the structure factor predicted by the model.

The nuclear Hamiltonian, H, has been assumed to be composed of a sum of five terms:

$$H = H_n + H_p + H_{rot} + H_{rpc} + H_{int} . \qquad (3.0.2)$$

H_n and H_p are due to the single particle motion of the odd nucleon or nucleons. These terms are calculated using the Nilsson model. The third term originates from the rotation of the

core and the unpaired particles. To this point the assumption has been that the rotational energy is very small in comparison to the single particle energies so these three terms are independent: the so-called "adiabatic approximation". H_{rpc} includes the non-adiabatic coupling of the rotations to the single particle states. In the present work only the Coriolis coupling term has been included in H_{rpc}. H_{int} is the interaction between the odd proton and the odd neutron in the odd-odd nucleus. Each of these terms will be discussed in this chapter.

It should be noted that the Hamiltonian (eq. (3.0.2)) could also contain terms referring to the vibrational states of the nucleus and their coupling to the particle states and the rotations. However, most of the states of interest lie below the energy of the first vibrational levels in the neighbouring even-even nuclei so interactions with the vibrational states have been ignored. The nucleus was also assumed to be in its vibrational ground state.

3.1 The Nilsson model

The intrinsic motion of a particle coupled to a deformed core was considered by Nilsson (1955). The potential chosen was essentially a cylindrical harmonic oscillator with spin orbit coupling. The Nilsson Hamiltonion H_N is:

$$\frac{H_N}{\hbar\omega_o} = \frac{1}{2}(-\nabla^2 + \rho^2) + \frac{4}{3}\sqrt{\frac{\pi}{5}}\,\delta\rho^2 Y_2^o$$

$$-2\kappa\vec{\ell}\cdot\vec{s} - \mu\kappa\vec{\ell}\cdot\vec{\ell} \qquad (3.1.1)$$

where: δ is the deformation, $\delta > 0$ implies a prolate shape

μ and κ are the well parameters

$$\nabla^2 \equiv \frac{\hbar}{m\omega_o(\delta)} \sum_{i=1}^{3} \frac{\partial^2}{\partial x_i^2}$$

$$\rho^2 \equiv \frac{m\omega_o(\delta) r^2}{\hbar}$$

r is the radius vector, the angular parts are contained in the Legendre polynomial

m is the reduced mass of the orbiting particle

A is the mass number of the deformed core

$$\omega_o(\delta) = 41A^{-1/3} \left(1 - \frac{4}{3}\delta^2 - \frac{16}{27}\delta^3\right)^{-1/6} \quad . \quad (3.1.2)$$

The term $(-\nabla^2+\rho^2)$ in the Hamiltonian is the usual simple harmonic oscillator potential characterized by the quantum number N. Though states of the same N and ℓ quantum numbers are not degenerate, the term in $\vec{\ell}\cdot\vec{\ell}$ controls the magnitude of the splitting of states of different orbital angular momentum in each oscillator shell; and the term in $\vec{\ell}\cdot\vec{s}$ enables the energy of the state with $j = \ell+\frac{1}{2}$ to be lowered relative to the state with $j = \ell-\frac{1}{2}$. These three terms are essentially a simple shell model for a single particle in a spherical nucleus. The purpose of the remaining term in the Hamiltonian, the one with the spherical harmonic, Y_2^o , is to introduce a deformation into the potential.

The parameters μ and κ are adjusted to give the best fit to the observed level spacings and sequences at deformation

$\delta = 0$. The values chosen were those recommended by Lamm (1969). For rare earth nuclei they are as follows:

$$\mu_{proton} = 0.600 \ , \ \mu_{neutron} = 0.420$$
$$\kappa_{proton} = 0.0637, \ \kappa_{neutron} = 0.0637 \qquad (3..1.3)$$

The factor of 41 in the expression for $\omega_o(\delta)$ was also arrived at by fitting observed energies in spherical states.

The most convenient basis to choose for single particle transfer reactions is the following coupled representation:

$$\tfrac{1}{2}(-\nabla^2+\rho^2)\,|N\ell j\,\Omega\rangle = (N+\tfrac{3}{2})\,|N\ell j\,\Omega\rangle, \ N = 0,1...$$
$$\ell^2|N\ell j\Omega\rangle = \ell(\ell+1)\,|N\ell j\Omega\rangle \quad , \ \ell = N, N-2...\text{to 1 or 0}$$
$$j^2|N\ell j\Omega\rangle = j(j+1)\,|N\ell j\Omega\rangle \quad , \ j = \ell \pm \tfrac{1}{2}$$
$$j_z|N\ell j\Omega\rangle = \Omega|N\ell j\Omega\rangle \quad , \ \Omega = -j, -j+1..., \ j \ . \qquad (3.1.4)$$

Because $\vec{j} = \vec{\ell}+\vec{s} = \vec{\ell}\pm\frac{1}{2}$ the operator s^2 is also a conserved quantity in this basis. With the exception of the term containing the spherical harmonic, the Hamiltonian matrixis diagonal in this representation. The necessary matrix elements for the deformation term in the potential may be found in Nilsson (1955) and by the application of the Wigner-Eckart theorem in this coupled representation. This deformation term mixes all the quantum numbers except Ω. The basis wave functions $|N\ell j\Omega\rangle$ represent simple single particle shell model states which have $(2j+1)$-fold degeneracy. The deformation lifts the $(2j+1)$-fold degeneracy leaving a state with $+\Omega$ degenerate

with the $-\Omega$ state (or more correctly, the state and its time reverse are degenerate). Thus the Nilsson model has only one good quantum number: Ω.

The eigenfunction resulting from this diagonalization yields for Nilsson wave function:

$$|\nu\Omega> = \sum_{j=\Omega}^{N'} C^{\nu}_{j\Omega} \; |N\ell j\,\Omega>. \qquad (3.1.5)$$

The $C^{\nu}_{j\Omega}$ is the Nilsson expansion coefficient. The sum extends over all j-values from Ω to $N' = (2N_{max}+1)/2$ which represents maximum allowable Ω from the largest oscillator shell included in the calculation. The parity of the basis wavefunctions, and hence, the Nilsson orbitals is $(-1)^N$. This then implies that for each j there is a corresponding ℓ. For positive parity states only even ℓ-values are possible and for negative parity states only odd ℓ-values are allowed.

In the present work the calculations were performed using a program due originally to Chi (1967). In this case the Hamiltonian matrix was diagonalized using all the states of a particular oscillator shell N with a given Ω. The coupling of states differing by two units in N was not included. Fig. 3.1.1 shows the results of a Nilsson calculation for neutron states. The energy of the state is plotted as a function of the deformation. Similarly fig. 3.1.2 shows the results of a calculation for proton states. In the limit of large deformations ℓ_z, N_z and s_z become constants of the motion,

Figure 3.1.1

Nilsson calculations for single neutron states in the rare earth region. The energy of the state is plotted as a function of the deformation. Each Nilsson state can contain two neutrons, one with $+\Omega$ and the other with $-\Omega$. Notice the $2j+1$ fold degeneracy of the shell model states which is lifted by deformation. (From Lederer *et al.* 1968).

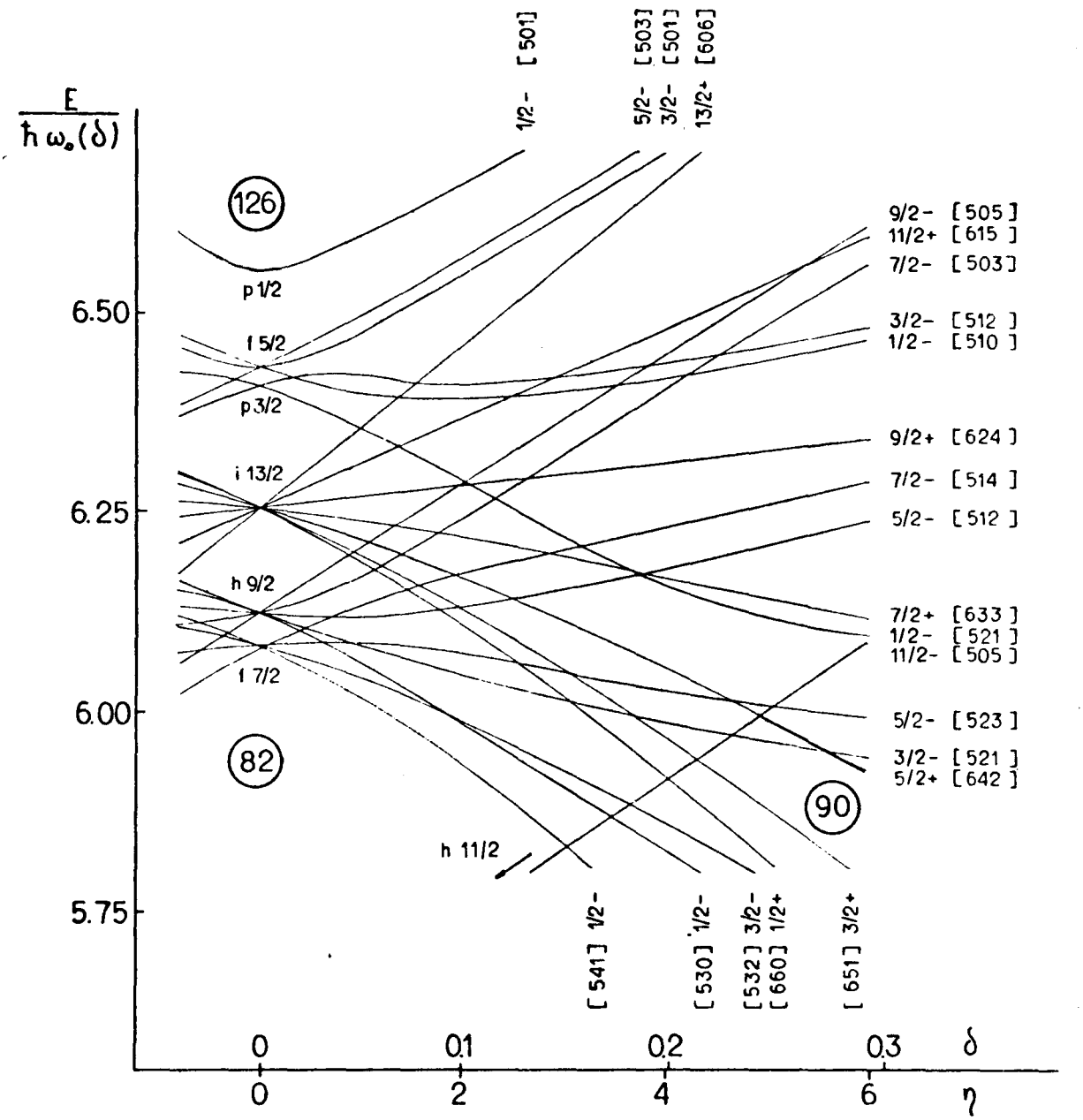
E / ħω₀(δ)
6.50
6.25
6.00
5.75
126
82
90
p 1/2
f 5/2
p 3/2
i 13/2
h 9/2
f 7/2
h 11/2
1/2- [501]
5/2- [503]
3/2- [501]
13/2+ [606]
9/2- [505]
11/2+ [615]
7/2- [503]
3/2- [512]
1/2- [510]
9/2+ [624]
7/2- [514]
5/2- [512]
7/2+ [633]
1/2- [521]
11/2- [505]
5/2- [523]
3/2- [521]
5/2+ [642]
[541] 1/2-
[530] 1/2-
[532] 3/2-
[660] 1/2+
[651] 3/2+
0
0.1
0.2
0.3
δ
0
2
4
6
η

Figure 3.1.2

Nilsson calculation for single proton states in the rare earth region (Adapted from Lederer *et al.* 1968)

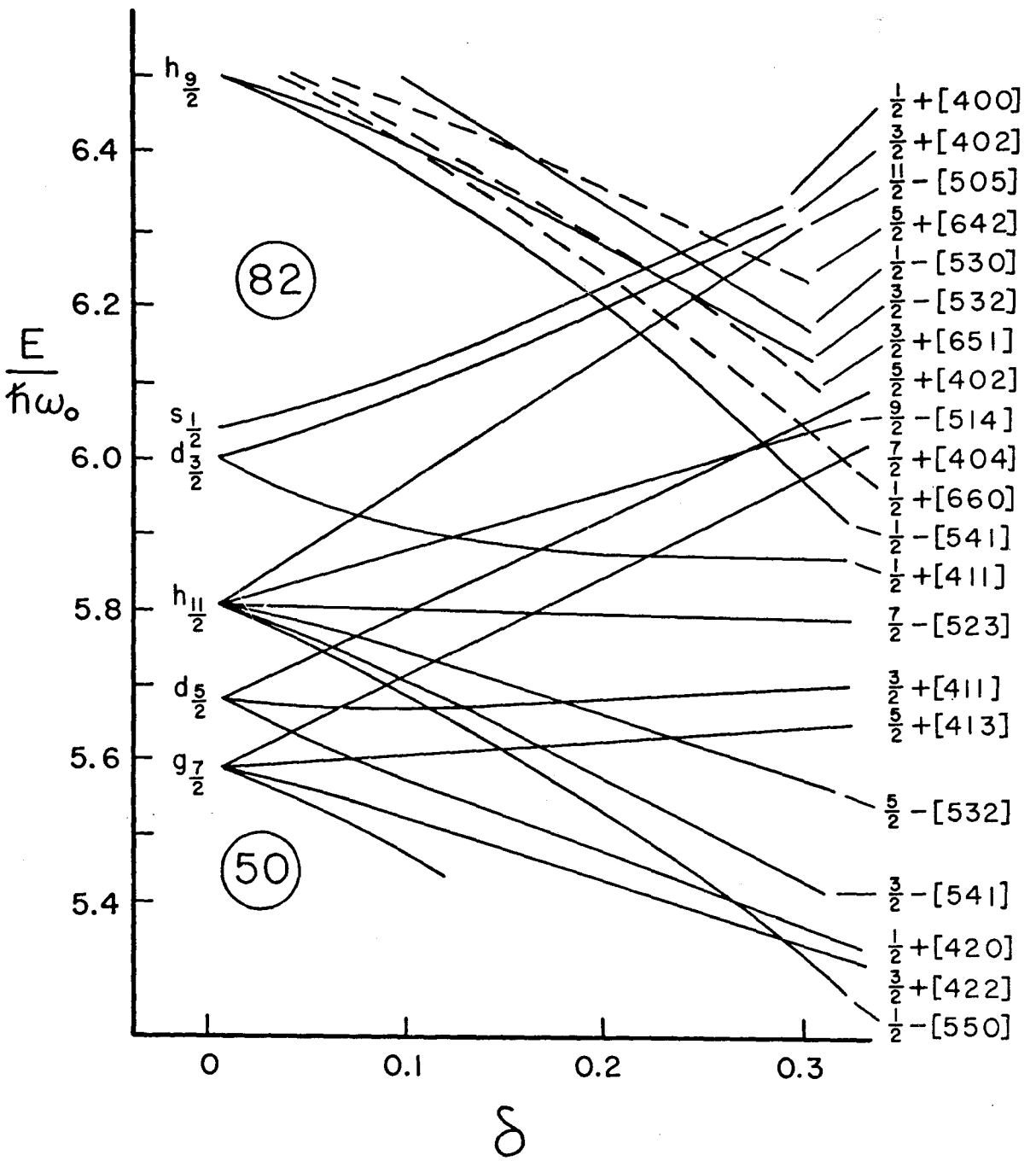
E/ħω₀
6.4
6.2
6.0
5.8
5.6
5.4
0
0.1
0.2
0.3
δ
82
50
h 9/2
s 1/2
d 3/2
h 11/2
d 5/2
g 7/2
1/2 +[400]
3/2 +[402]
11/2 −[505]
5/2 +[642]
1/2 −[530]
3/2 −[532]
3/2 +[651]
5/2 +[402]
9/2 −[514]
7/2 +[404]
1/2 +[660]
1/2 −[541]
1/2 +[411]
7/2 −[523]
3/2 +[411]
5/2 +[413]
5/2 −[532]
3/2 −[541]
1/2 +[420]
3/2 +[422]
1/2 −[550]

where the z subscript refers to the body axis in fig. 3.0.1. The corresponding quantum numbers are Λ, n_z, Σ; here n_z is the number of oscillator quanta along the body axis. The Nilsson orbitals are labelled by the asymptotic quantum numbers in the following form:

$$\Omega^{\pi}[Nn_z\Lambda] \ .$$

The letter $\pi = (-1)^N$ stands for the parity of the state. At a positive deformation for a given Ω and N the lowest energy state has $n_z = N$, the next most energetic has $n_z = N-1$ and so on. Λ is determined such that $\Lambda = \Omega \pm \frac{1}{2}$ and the sum $N + n_z + \Lambda$ is even.

Each Nilsson orbital may accommodate two particles, one in the state $|\nu\Omega\rangle$ and the other in its time reversed state $|\nu\tilde{\Omega}\rangle$. It is important in the mixing calculation that the difference in these two wave functions be noted. The present work uses the following relations when dealing with the time reversed state $|\nu\tilde{\Omega}\rangle$.

$$|\nu\tilde{\Omega}\rangle = (-1)^{\Omega-\frac{1}{2}}\,\pi|\nu-\Omega\rangle$$

$$|\nu-\Omega\rangle = \sum_{j=\Omega}^{N'} C_{j-\Omega}|N\ell j-\Omega\rangle$$

and

$$C^{\nu}_{j-\Omega} = (-1)^{j-\frac{1}{2}}\,\pi C^{\nu}_{j\Omega} \qquad (3.1.6)$$

$\pi = (-1)^N$, the parity of the state.

The actual calculation of the Nilsson wave function was performed with the parameters recommended by Lamm (1969) and with a deformation $\delta = 0.27$ as a part of the Coriolis coupling calculations (sect. 3.3). The Nilsson expansion

coefficients $C_{j\Omega}$ are very similar to those published by Chi (1967) at deformation $\delta = 0.3$. For the particular neutron and proton states of interest the more elaborate calculations of Rost (1967), (or see Jones 1969) using a Woods-Saxon potential show only small differences for the $C_{j\Omega}$ coefficients for $j \leq (2N+1)/2$. The same is true of the recent calculation by Nilsson et al. (1969) with a hexadecapole deformation. For $j > (2N+1)/2$ these coefficients are very small. In the calculation used for the present analysis the latter coefficients were zero. The more complex calculations referred to above may predict Nilsson energies which are in better agreement with the observed spectra especially when the states from different oscillator shells are being compared.

3.2 The effect of pairing

Nathan and Nilsson (1965) give a brief introduction to the concepts and results of pairing theory. The probability of any orbital being occupied by a pair is predicted to vary smoothly from unity (completely filled) to zero (completely unoccupied) as higher and higher energy orbitals are examined. This is in analogy to a Fermi gas at non-zero temperature. Two parameters characterize this nuclear Fermi surface. The first is the energy gap parameter, Δ, which is essentially a measure of the diffuseness of the occupation probability curve. The second is the Fermi energy, λ, at which the occupation probability is a half.

The first result of pairing theory to be considered is important in the calculation of direct reaction cross sections (sec. 3.5). The probability, V^2, that a particular single particle orbital with energy ε_ν is occupied by a pair is:

$$V^2 = \frac{1}{2}\left(1 - \frac{\varepsilon_\nu - \lambda}{\sqrt{(\varepsilon_\nu - \lambda)^2 + \Delta^2}}\right) \qquad (3.2.1)$$

This factor modifies the pick-up reaction cross section. In making predictions of the cross sections of stripping reactions one must take into account the emptiness U^2 of the orbital into which the particle is transferred where:

$$U^2 = 1 - V^2 \ . \qquad (3.2.2)$$

The second important result is the compression of the single particle energies in an odd mass nucleus by the pairing force. The energy of the resulting single quasi-particle state is given by

$$E_\nu = \sqrt{(\varepsilon_\nu - \lambda)^2 + \Delta^2} \ . \qquad (3.2.3)$$

Thus the excitation of any state $|\nu'>$ relative to the ground state $|\nu>$ is simply the difference in the quasi-particle energies

$$\begin{aligned} E_o = E_{\nu'} - E_\nu &= \sqrt{(\varepsilon_{\nu'} - \lambda^2) + \Delta^2} - \sqrt{(\varepsilon_\nu - \lambda) + \Delta^2} \\ &\approx \sqrt{(\varepsilon_{\nu'} - \lambda)^2 + \Delta^2} - \Delta \ . \end{aligned} \qquad (3.2.4)$$

The wavefunction of the single quasi-particle is identical to the single particle wave functions calculated from the Nilsson

model for the calculations necessary in the present work. Only the energy has been changed in the quasi-particle formulation.

In both equations (3.2.1) and (3.2.4) the single particle energies referred to are the intrinsic Nilsson energies.

The factor, Δ, for the proton states of an even-even nucleus (Z,N) may be calculated from the proton separation energy $S_p(Z,N)$ in the neighbouring nuclei in the following manner:

$$\Delta_p(Z,N) \approx \frac{1}{4}[2S_p(Z,N)-S_p(Z+1,N)-S_p(Z-1,N)] \quad . \qquad (3.2.5)$$

Similarly the neutron gap parameter, Δ_n, may be evaluated from neutron binding energies. Δ, then represents approximately half the energy required to break a nucleon pair. Neergård and Vogel (1970) show a plot of the neutron and proton pairing gap parameters evaluated from formula (3.2.5) for rare earth nuclei. In the region of the lutetium isotopes of interest the following average values were estimated:

$$\begin{aligned} \Delta_p &= 0.85 \text{ MeV}, \\ \Delta_n &= 0.70 \text{ MeV}. \end{aligned} \qquad (3.26)$$

These are the values chosen for the subsequent cross section calculations.

The Fermi energy, λ, represents the point of inflection of the occupation probability for the ground state of the even-

even core of the nucleus. The optimum value of λ for the proton states was found by the simultaneous adjustment of λ and the deformation δ so that the predicted band heads of the $5/2^+[402]$ and $1/2^+[411]$ states appeared close to the observed energy relative to the $7/2^+[404]$ ground state orbital. This method is not particularly good if the energies ε_ν from the Nilsson model are not reliable. It appeared for the proton states that λ was about 300 keV below the energy of the $7/2^+[404]$ ground state orbital. For the neutron states, it appears from Burke et al. (1966) that the Fermi surface is very close to the ground state of the odd-N nuclei studied (in particular ^{173}Yb). For the neutron transfer experiments into ^{174}Lu the energy of the Fermi surface was considered to be approximately coincident with, or slightly below, that of the $5/2^-[512]$ neutron orbital.

The observed cross sections in the odd-odd nucleus ^{174}Lu as well as those in the odd mass lutetium and ytterbium isotopes are consistent with the values of the gap parameter, Δ_p and Δ_n, and the Fermi energy, λ, chosen. It should be noticed that it is possible to calculate U^2 and V^2 using the predicted intrinsic energy of the state relative to the ground state. It is also not unreasonable, knowing the experimental energy and Δ, to estimate V^2 if the quasi-particle is known to have mostly the character of a hole or a particle.

It will be mentioned in Appendix A that the occupation probabilities also make a small correction to the Coriolis matrix element.

3.3 Nuclear rotations

The discussion in this section may also be found in more detail in Jones' thesis (1969). The expression for the rotational wavefunction may be also found in Davidson (1968) and the details of the rotational Hamiltonian are very similar to the treatment in the standard texts (for example: Preston (1962) and the Elliott (1958) notes).

The total rotational Hamiltonian is simply:

$$T_{rot} = \frac{\hbar^2}{2\mathcal{J}} \vec{R}^2 \ . \qquad (3.3.1)$$

The nucleus is assumed to be axially symmetric so there can be no projection of the rotational angular momentum on the nuclear symmetry axis, therefore $R_z = 0$. The subscripts x, y and z will be used to refer to the body fixed frame, the p and n subscripts refer to the odd proton and the odd neutron respectively in the odd-odd nucleus. In that $\vec{R} = \vec{I}-\vec{J}$ and that $\vec{J} = \vec{j}_p + \vec{j}_n$ as may be seen in fig. 3.0.1 it is possible to expand equation (3.3.1).

$$T_{rot} = H_{rot} + H_{prot} + H_{nrot} + H_{rpc} + H_{pp} \qquad (3.3.2)$$

where:
$$H_{rot} = \frac{\hbar^2}{2\mathcal{J}} (I^2 - I_z^2 - j_{pz}^2 - j_{nz}^2) \qquad (3.3.3)$$

$$H_{prot} = \frac{\hbar^2}{2\mathcal{J}} (\vec{j}_p^{\,2}) \qquad (3.3.4)$$

$$H_{nrot} = \frac{\hbar^2}{2\mathcal{J}} (\vec{j}_n^{\,2}) \qquad (3.3.5)$$

$$H_{pp} = \frac{\hbar^2}{2\mathcal{J}} (j_{p+}j_{n-} + j_{p-}j_{n+}) \qquad (3.3.6)$$

$$H_{rpc} = -\frac{\hbar^2}{2\mathcal{J}} (I_+J_- + I_-J_+). \qquad (3.3.7)$$

Here the following angular momentum raising and lowering operators are defined:

$$\begin{aligned} I_\pm &= I_x \pm iI_y \\ j_{p\pm} &= j_{px} \pm ij_{py} \\ j_{n\pm} &= j_{nx} \pm ij_{ny} \\ J_+ &= j_{p+} + j_{n+} \\ J_- &= j_{p-} + j_{n-} \quad . \end{aligned} \qquad (3.3.8)$$

For an odd-Z nucleus the terms H_{nrot} and H_{pp} of the total rotational Hamiltonian T_{rot}, of course, vanish. The raising and lowering operators are then simplified.

The rotational wavefunction of an odd-odd nucleus is assumed to have the form

$$|IMK\Omega_p\Omega_n\rangle = \sqrt{\frac{2I+1}{8\pi^2}}\, D^I_{MK}\, |\Omega_p\rangle|\Omega_n\rangle \; . \qquad (3.3.9)$$

D^I_{MK} is the properly normalized D-function as defined by Edmonds (1957). The D-function is the eigenfunction for the rotational motion. The $|\Omega_p\rangle$ is an abbreviation for the Nilsson wave function of the odd proton as defined in eq. 3.1.5. In order to make the notation more compact the following defi-

nition is made:

$$|\Omega_p> = \sum_{j_p} C_{j_p\Omega_p} |j_p\Omega_p> \ . \qquad (3.1.5)$$

The neutron single particle wave function is defined in a completely analogous manner. This form of the odd-odd wave function assumes the proton and the neutron each move independently, and their motion is uncorrelated to that of the core. The wavefunction though must be properly antisymmetrized using the time reversal operator giving the following:

$$|IMK\Omega_p\Omega_n> = \sqrt{\frac{2I+1}{16\pi^2}} \sum_{j_p} \sum_{j_n} C_{j_p\Omega_p} C_{j_n\Omega_n}$$

$$[D^I_{MK}|j_n\Omega_n>|j_p\Omega_p>$$

$$+(-1)^{I-j_p-j_n} D^I_{M,-K}|j_n-\Omega_n>|j_p-\Omega_p>]. \qquad (3.3.10)$$

Eliminating the reference to the neutron wavefunction and recalling that because of axial symmetry $K = \Omega$, the wavefunction to be used for an odd-Z nucleus becomes:

$$|IMK> = \sqrt{\frac{2I+1}{16\pi^2}} \sum_j C_{jK} [D^I_{MK}|jK>+(-1)^{I-j} D^I_{M-K}|j-K>]. \qquad (3.3.11)$$

Again using the assumption of axial nuclear symmetry, the projection of $\vec{I}$ onto the symmetry axis must be $K = |\Omega_p+\Omega_n|$. This gives two values of K, as each Ω may be positive or negative:

$$K = |\Omega_p| + |\Omega_n|$$

or (3.3.12)

$$K = \left| |\Omega_p| - |\Omega_n| \right| .$$

For this study K has been defined to be positive. Either Ω_p or Ω_n is chosen to have the negative sign such that

$$K = \Omega_p + \Omega_n \geq 0$$

for the smaller K-value. The state of larger K is formed by coupling the neutron and proton with both Ω_p and Ω_n positive.

It is important in the wavefunction (eq. 3.3.10) of the odd-odd nucleus that these signs of Ω are carefully manipulated. The correct phase relationship for the $C_{j\Omega}$'s must be included in the wavefunction, and hence in the derived matrix elements. This phase relationship is:

$$C_{j-\Omega} = (-1)^{j-\frac{1}{2}} \pi C_{j\Omega} \, . \qquad (3.1.6)$$

The parity of the coupled configuration, $\pi_{odd-odd}$, is the product of the parity of the orbital occupied by the neutron and the parity of the orbital occupied by the proton:

$$\pi_{odd-odd} = \pi_n \pi_p \, .$$

The matrix elements of the rotational Hamiltonian may be found in Appendix A.

A program was written which considered all the terms in the rotational Hamiltonian with the exception of H_{prot} and H_{nrot}. The program GREAT (O'Neil 1972) will perform the entire calculation for an odd mass nucleus in which up to 10 rotational bands may be coupled simultaneously. The program GREATER (O'Neil 1972) does a similar calculation considering the coupling of up to 10 proton orbitals to the orbital of the odd target neutron. Thus,

in the odd-odd nucleus up to 20 configurations may be considered simultaneously. These programs carry out the diagonalization to calculate the perturbed energies and mixing amplitudes. The mixed wavefunction, $|\psi>$, may be expressed in the form:

$$|\psi> = \sum_i a_i \, |IMK\Omega_n\Omega_p>_i \, . \qquad (3.3.13)$$

The square of the mixing amplitude, a_i, gives the fraction of the i^{th} configuration in the final mixed wavefunction. These mixing amplitudes, and the properties of the various admixed states may be used to calculate the cross sections for single particle reactions as will be discussed in section 3.5.

The philosophy used in this calculation was to generate a typical prediction showing the observed results were consistent with the Nilsson model with Coriolis coupling and pairing effects included.

In the odd mass lutetium nuclei, the Coriolis coupling and cross section calculations were not very sensitive to the exact energy of the band heads so long as the states were separated by approximately the correct energy and the ordering of the band heads was correct. Though the excitation energies change in the three odd-A nuclei studied, the spectroscopic factors are very similar for the corresponding bands. For this reason the actual band head energy and the energies of the band members were not fitted. In the odd-A nuclei, a rotational parameter $\frac{\hbar^2}{2\mathcal{I}}$ of 13 keV was used and with this it was not found necessary to attenuate the Coriolis matrix elements. The Nilsson calculation

used in the present work was not able to reproduce the band head energies within one hundred keV, especially when states from different oscillator shells were being compared.

For the odd-odd nucleus, ^{174}Lu, where the interpretation is more difficult, a more careful attempt was made to fit the observed energies. Initially only the band head energies were varied. For the proton transfer reaction, adequate fits were obtained using a rotational parameter $(\frac{\hbar^2}{2\mathcal{J}})$ = 11.1 keV which is the observed value for the ground state band. It was not necessary to attenuate the Coriolis matrix element in the proton transfer case whereas in the neutron transfer case better agreement with the experiments was obtained if the Coriolis matrix element was reduced by a factor of 0.75. This reduction of the Coriolis matrix element for neutron states has been observed in the odd-A gadolinium isotopes (Løvhøiden et al.1970). The rotational parameter used for the states in ^{174}Lu populated by neutron transfer reactions was $(\frac{\hbar^2}{2\mathcal{J}})$ = 12.1 keV. It would have been more pleasing had it been possible to obtain as good agreement in both the proton and neutron transfer analyses using the same rotational parameter and the same attenuation factor in the Coriolis matrix element.

It is more convenient to discuss the actual details of the coupling calculations in the sections dealing with the interpretation of the experimental results.

3.4 Effects of the Residual Interaction

The odd proton may couple to the odd neutron in an odd-odd nucleus such as ^{174}Lu in two ways:

$$K = |\Omega_n| + |\Omega_p|$$

or

$$K = \left| |\Omega_n| - |\Omega_p| \right| . \qquad (3.3.12)$$

The energies of these two configurations are not degenerate. The lowest state, according to the Gallagher-Moszkowski rule (Gallagher and Moszkowski 1958) is the state in which the intrinsic proton and neutron spins are aligned parallel, the so-called triplet state. The triplet state in the rare earth region usually lies 100 to 200 keV below the spin singlet state in which the spins are aligned antiparallel. The Gallagher-Moszkowski rule for ascertaining the K of the lowest state may be stated as follows:

$$K_{low} = |\Omega_p| + |\Omega_n| \text{ if } \Omega_p = \Lambda_p \pm \tfrac{1}{2} \text{ and } \Omega_n = \Lambda_n \pm \tfrac{1}{2}$$

$$K_{low} = \left| |\Omega_p| - |\Omega_n| \right| \text{ if } \Omega_p = \Lambda_p \pm \tfrac{1}{2} \text{ and } \Omega_n = \Lambda_n \mp \tfrac{1}{2} . \qquad (3.4.1)$$

The quantities Ω and Λ may be found from the labels of the Nilsson orbitals in question. This rule is never violated in the assigned states in ^{174}Lu. Coriolis mixing of the levels and uncertainties in the rotational parameters of the two bands may give rise to apparent contradictions in other nuclei though no such examples are known to the author.

The second effect of the residual interaction in the odd-odd nuclei is the odd-even shift in K=0 bands. The residual interaction causes the odd-spin members to be displaced from their normal I(I+1) energy spacing by a constant amount throughout the entire band. The magnitude of the shift is typically between 30 and 60 keV.

The contribution of the residual interaction to the total diagonal energy of an odd-odd nucleus (eq. A.14) may be parameterized (Newby 1962)

$$E_{int} = A + (-1)^{I}\delta_{KO}B \ . \qquad (3.4.2)$$

All the dependence on the total spin I is written explicitly. The parameters A and B depend on the K of the final configuration as well as on the properties of the individual orbitals coupling to form the configuration. The first term, A, merely displaces the band head energy of the triplet configuration relative to the singlet state. The second term (containing B) may be seen to shift the odd spin members of the band from the even spin members by an amount 2B.

Expressions for quantities related to A and B are given by Pyatov (1963) using a zero range spin dependent force:

$$H_{int} = V(\vec{r}_p-\vec{r}_n)[1-\alpha+\alpha\vec{\sigma}_p\cdot\vec{\sigma}_n] \ ,$$

where: (3.4.3)

$$V(\vec{r}_p-\vec{r}_n) = 4\pi g\delta(\vec{r}_p-\vec{r}_n) \ .$$

The factor α is the magnitude of the exchange admixture and

g is the strength parameter of the force. Jones et al. (1971) have performed calculations with this force, with a finite range force, and with a tensor force. The calculations were compared with all the available data on the spin singlet-triplet splitting energies and odd-even shifts in the rare earths. Calculations show that the type of force proposed by Pyatov (1963) is able to predict the singlet-triplet splitting energies fairly well. A more crucial test of the exchange mixtures comes with the simultaneous fitting of the odd-even shifts and the spin singlet-triplet splitting energies. The odd-even shift in spin triplet K = 0 bands is especially sensitive to the type of residual interaction chosen. Jones et al. (1971) found the best fits including the odd-even shift were obtained using a tensor force, as had been predicted by Newby (1962).

Calculations of the effects of the residual interactions are not presented in this thesis. It is hoped though that the additional data from ^{174}Lu will be included in a future survey of the residual interaction. The singlet-triplet splitting energies of pure two quasiparticle states in even-even nuclei are an additional source of data on the residual interaction which could be included in such a survey. In using results from deformed nuclei to determine the exchange mixtures and the nature of the n-p, p-p or n-n force, the effects of Coriolis coupling, vibrations and rotations must be carefully separated from those effects to be attributed to the residual interaction. Such a separation is difficult and it may not be possible to be sure it is unique.

3.5 Calculation of cross sections

To actually compare the predictions of the Nilsson model and its refinements to reality, it is necessary to calculate the properties which should be displayed by such states in an experiment. It has been shown in previous works (Elbek and Tjøm 1969) that the single particle transfer reactions are a very fruitful method of exploring the structure of deformed rare earth nuclei.

The direct single particle transfer reactions which have been used to study the states in lutetium isotopes are very selective in the states they populate. It is assumed, and also appears to be true experimentally, that these reactions with sufficient bombarding energies do not rearrange the nucleons in the target. One nucleon is simply added to or removed from the target. This transferred particle can be deposited into various orbitals with specific angular momentum. Further angular momentum can be absorbed by the nucleus during these reactions in the form of vibrational or rotational excitations. These collective excitations are then coupled to configurations formed by the target plus the transferred nucleon in a specific orbital. This seems quite reasonable in the case of an even-even target. In an odd-odd nucleus such as ^{174}Lu (or an even-even nucleus), it is possible with different targets to populate states by transferring a neutron or a proton. It is expected then that two completely separate sets of states should be formed: a neutron

transfer set formed by coupling a neutron to the odd target proton, and a proton transfer set formed by coupling a proton to the odd target neutron. In an even-even final nucleus, of course, the transferred proton couples to a target proton to form one set of states and another set is formed in an analogous manner by the neutron transfer reaction. The only states these two sets should have in common are the ground state band and the opposite spin coupling of the same configuration. (It may be possible also to see some components of vibrational states.) If some form of mixing exists between these two sets it is likely the mixed levels will be seen in both types of reactions at the same excitation energy. For example a state which is mainly formed from the neutron set would have large peaks in the neutron transfer spectra and rather smaller ones in the proton transfer. No states of this type have been identified in ^{174}Lu; however, a similar effect has been recently reported (Khoo et al. 1972) in ^{176}Hf. It is to be remembered that there are many other configurations in deformed rare earth nuclei which are not populated by single particle transfer reactions.

These reactions populate different members of rotational bands with different intensities. This relative intensity pattern forms a characteristic fingerprint for the configuration on which the rotational band is built. The present section deals with the calculation of the expected cross sections for the various Nilsson configurations in the nucleus and hence the fingerprints of these rotational bands.

Four reactions are considered in the present work: the (^{3}He,d), the (α,t) the (^{3}He,α) and the (d,t). The (^{3}He,d)

and (α,t) reactions are stripping reactions in which the transferred proton is deposited in an orbital in the target. The largest cross sections are expected to be seen from states which are unoccupied in the target nucleus. It is, then, intuitively appealing to have the cross section for a stripping reaction depending on the emptiness U^2 of the particular orbital in the target. The converse is true in the (d,t) and (^{3}He,α) reactions where a neutron is removed from an occupied target orbital. The largest cross sections should arise from states lying below the Fermi surface. The cross sections vary as the fullness V^2 of the orbital in the target nucleus.

The theory of stripping and pickup reactions is essentially the same except for the differences in the occupation probability factors. The discussion which follows is similar to that given by Elbek and Tjøm (1969) with some of the final expressions being taken from Jones (1969).

The usual treatment of direct single particle reactions is to divide the reaction into three separate parts. The first part has the projectile moving in the average field of the target. The target potential, which is usually described by the optical model, distorts the incoming plane waves in the Distorted Wave Born Approximation (DWBA). This field is the same as is used to describe the elastic scattering of the incident particle from the target. In the second step a particle is transferred to a single particle orbital in the target; the rest of the target

is assumed to be unaffected by this interaction. Finally, the scattered particle moves away from the residual nucleus.

If the A(a,b)B reaction in which a proton p is transferred (a = b+proton), the total Hamiltonian for the initial system is:

$$\begin{aligned} H &= H_a + H_A + T_a + V_a^{opt} + V_{aA} \\ &\approx H_a + H_A + T_a + V_a^{opt} \\ &= H_i^o \ . \end{aligned} \qquad (3.5.1)$$

H_a and H_A are the Hamiltonians of the internal motion of the incident particle and target respectively. T_a is the kinetic energy of the projectile. V_a^{opt} is the optical potential in which the incident particle moves. The last term V_{aA} is the interaction between the projectile and the target which leads to the stripping reaction. It is assumed though that this may be absorbed into V_a^{opt}.

Similarly the total Hamiltonian for the final system is:

$$\begin{aligned} H &= H_b + H_B + T_b + V_b^{opt} + V_{bB} \\ &\approx H_b + H_B + T_b + V_b^{opt} + V_{pb} \\ &= H_f^o + V_{pb} \ . \end{aligned} \qquad (3.5.2)$$

Again H_B describes the internal structure of the residual nucleus; T_b and V_b^{opt} refer to the motion of the scattered particle leaving the nucleus. The scattered particle has its internal Hamiltonian represented by H_b. The assumption is made that the interaction

between the nucleus and the outgoing particle is contained in V_b^{opt} and only the interaction of the scattered particle and the transferred proton V_{pb} is important.

The wavefunction in the incoming channel, $\phi_i(\vec{k}_i)$ is taken to be a product wavefunction of the internal motion of the incident particle, χ_a; the internal motion of the target χ_A; and the motion of the incident particle in the optical potential $\psi_i(\vec{k}_i)$. The linear momentum in the incident channel is designated as $\vec{k}_i$.

$$\phi_i = \chi_a \chi_A \psi_i(\vec{k}_i),$$

thus;

$$H_i^o \phi_i = E\phi_i . \qquad (3.5.3)$$

The wavefunction $\phi_f(\vec{k}_f)$ of the final channel, in analogy to (3.5.3), has the following form:

$$\phi_f = \chi_b \chi_B \psi_f(\vec{k}_f),$$

$$H_f^o \phi_f = E\phi_f . \qquad (3.5.4)$$

The transition amplitude between the initial and final states may be calculated from scattering theory. The transition amplitude from the initial state to the final state is;

$$S_{fi} = \langle\phi_f|V_{pb}|\phi_i\rangle. \qquad (3.5.5)$$

The interaction V_{pb} is being treated as the operator which causes the transition. In Appendix B the steps used in the calculation of S_{fi} are outlined.

$$S_{fi} = \sum_{j_p} \langle I_i, j_p, m_i, m_f - m_i | I_f m_f \rangle \beta_{jp}$$

$$\int \psi_f^* F_{j_p, m_f - m_i} \psi_i d\tau_i d\tau_f \qquad \text{(B.15)}$$

where:

$$\beta_{j_p} = g \sqrt{\frac{2I_i+1}{2I_f+1}} \langle \phi_f | \phi_i \rangle U C_{j_p \Omega_p}$$

$$[\langle I_i j_p K_i \Omega_p | I_f K_f \rangle$$

$$+ (-1)^{I_i - \frac{1}{2}} \pi_n \langle I_i, j_p, K_i, -\Omega_p | I_f - K_f \rangle] \qquad \text{(B.9)}$$

for an odd-odd final nucleus. The factor $g = \sqrt{2}$ if either I_i or $I_f = 0$ and is formed by having nucleons paired to spin zero. Otherwise g is set to unity. The factor $g = \sqrt{2}$ only if the target is an even-even nucleus in its ground state (or possibly in a β-vibrational state) or if the transition is to the ground state or to a completely paired off $K^\pi = 0^+$ state in an even-even nucleus. In the case of an even-even target nucleus:

$$\beta_{j_p} = \sqrt{2} \sqrt{\frac{2I_i+1}{2I_f+1}} U \langle \phi_f | \phi_i \rangle C_{j_p \Omega_p} \delta_{\Omega_p K_p} \delta_{j_p I_f} \qquad \text{(B.11)}$$

The factor $F_{j_p, m_f - m_i}$ is the form factor for the transfer of a proton of angular momentum j_p and projection onto the nuclear symmetry axis $m_f - m_i$.

The cross section is given by Satchler (1964) with the appropriate density of states factors and assuming no spin orbit interactions in the incoming and outgoing waves:

$$\frac{d\sigma}{d\Omega} = \frac{\mu_i \mu_f}{(2\pi\hbar^2)^2} \left(\frac{k_f}{k_i}\right) \Sigma |S_{fi}|^2 \ . \qquad (3.5.6)$$

The reduced masses in the incoming and outgoing channels are represented by μ_i and μ_f respectively. The corresponding linear momenta are k_i and k_f. Because the beam and target are unpolarized, the sum implies an average over the initial substates, of which there are $2I_i+1$, and a sum over the $2I_f+1$ final magnetic substates. The average over the incident channel is because the target has an equal probability to be in any substate. The reaction can proceed to any substate in the final nucleus thus the contributions from the various exit channels are assumed to be equal and hence the sum over m_f yields a factor of $2I_f+1$. It is in summing over the initial and final substates that the interference terms between the different j-values vanish. This allows the contributions to the cross section of the different j-values to be added incoherently (Glendenning 1963).

Equation (3.5.6) may be factored and written:

$$\frac{d\sigma}{d\Omega} = \frac{2I_f+1}{2I_i+1} \sum_{j_p} \beta^2_{j_p}(\ell_p) \ \sigma_{j_p}(\ell_p) \ . \qquad (3.5.7)$$

All the factors pertaining to the integration over the incoming, outgoing and bound particles have been absorbed into $\sigma_{j_p}(\ell_p)$. The dependence of the cross section on the orbital angular momentum, ℓ_p, transferred is implied as it must be specified in order to get the correct parity for the proton transferred of total angular momentum j_p. This fact is discussed in section

3.6. Here it is only necessary to say this represents the intrinsic single particle cross section for the specific reaction under consideration. It includes the Q-value, angular and beam energy dependence of the reaction cross section for the transfer of a proton into a particular shell model state.

For an even-even target expression (3.5.7) reduces to:

$$\frac{d\sigma}{d\Omega} = 2C^2_{j_p\Omega_p} \quad U^2 \quad \sigma_{j_p(\ell_p)}. \qquad (3.5.8)$$

In the present work the nuclear structure factor is defined as:

$$\text{Structure factor} \equiv U^2C^2_{j\Omega} = \frac{d\sigma}{d\Omega}/2\sigma_{j_p(\ell_p)}. \qquad (3.5.9)$$

This is not the usual definition of the spectroscopic factor of Macfarlane and French (1960) and so it has been seen fit to give it a different name. The advantage of the structure factor is that it contains all the nuclear structure information for the state and is independent of the reaction mechanism. Because the single particle cross section does not divide out easily in the transitions to an even-A nucleus, a similar quantity has not been defined for reactions on an odd-A target. In the case of the odd-odd nucleus ^{174}Lu the predicted cross sections were compared directly to the observed cross sections throughout the analysis.

Equation (3.5.7) may be used to predict the relative cross sections of the various spin, I, members in a rotational

band. Using the expression in Appendix A, the relative energy of these states may be calculated. Thus the intensity of the state plotted as a function of the energy of the state forms a characteristic pattern. This fingerprint is exactly what one expects to see in the observed particle spectra when it is plotted on a similar energy scale. The technique of matching fingerprints was one of the methods used to interpret the spectra of all the lutetium isotopes. Numerous fingerprints are shown for the analysis of ^{174}Lu in Chapter 5.

In the case of mixed configurations, such as arise when Coriolis coupling has been considered, the cross section (eq. 3.5.24) becomes

$$\frac{d\sigma}{d\Omega} = \frac{2I_f+1}{2I_i+1} \sum_j \left[\sum_i a_i \beta_{j_p}^{(i)}\right]^2 \sigma_{j_p}(\ell_p) \quad . \qquad (3.5.10)$$

The quantity a_i is the mixing amplitude of the i^{th} configuration into the state of interest. The definition of a_i is implied in eq. (3.3.13).

It should be clear that the formulae developed in this section are equally applicable to pickup reactions, if the occupation probability V^2 is used in place of the emptiness factor U^2 in the expression of the partial widths. Also there is no difference if a neutron is transferred rather than a proton, other than the terms which have been absorbed into the single particle cross section $\sigma_{j(\ell)}$.

The calculation of the Nilsson wavefunction, pairing

corrections, Coriolis coupling and the resulting cross sections is performed by the program GREAT (O'Neil 1972) for the even-even targets and by GREATER (O'Neil 1972) for the odd mass targets. These programs obtained the dependence of the single particle cross sections $\sigma_{j(\ell)}$ on the angle θ, the reaction Q-value and the angular momentum transfer j, from a prior calculation by the program DWUCK (Kunz 1969). This latter calculation is described briefly in the following section.

3.6 The intrinsic single particle cross sections

Detailed discussion of the calculation of the intrinsic single particle cross sections using the Distorted Wave Born Approximation (DWBA) may be found in Satchler (1958 and 1964) and in Bassel et al. (1962).

The intrinsic single particle cross section $\sigma_{j_p(\ell_p)}$ in equation (3.5.7) may be seen to have the form:

$$\sigma_{j_p} = \frac{\mu_i \mu_f}{(2\pi\hbar^2)^2} \frac{k_f}{k_i} N \sum_m \left| \int \psi_f^* F_{j_p,m} \psi_i d\tau_a d\tau_b \right|^2 . \quad (3.6.1)$$

The incident and outgoing channels are labeled by i and f respectively. The factors μ and k are the reduced masses and the linear momenta respectively in the particular channels.

The factor N is a normalizing factor which is a result of choosing a particular internal wavefunction for the incident particle and a particular interaction in the calculation of the form factor (eq. (B-13)). The most common (easiest) interaction

to use is the zero range approximation (eq. (B-14)) and Hulthén wavefunctions.

The integration in equation (3.6.1) extends over the center of mass coordinates of the incoming and exit channels. Lu and Alford (1971) found that better agreement with experimental angular distributions was found if the starting point ("lower cut-off") of the radial integration was increased to about 9 fm. This increases the cross section more at back angles than at forward angles. Some justification for this may be made by saying the reaction takes place only near the nuclear surface. The lower cut-off was zero for the neutron transfer reactions.

The incoming and outgoing wavefunctions, ψ_i and ψ_f, are expanded in terms of partial waves. The incoming and outgoing waves are distorted by the Coulomb potential of the nucleus, as well as the optical potential. The Coulomb potential is screened inside the nucleus but has the usual form outside the nuclear charge radius.

$$V_c = \frac{Ze^2}{2r_{oc}A^{1/3}}\left[3 - \left(\frac{r}{r_{oc}A^{1/3}}\right)^2\right]; \quad r \leq r_{oc}A^{1/3}$$

$$V_c = \frac{Ze^2}{r} \qquad ; \quad r > r_{oc}A^{1/3} \qquad (3.6.2)$$

The symbols Z and A refer to the nuclear charge and mass numbers respectively; the electronic charge is represented by e. The optical potential used in this work is:

$$V_{opt}=V_o\, f(r,r_o,a)+i[W_o f(r,r_o',a') + 4W_D \frac{d}{dr} f(r,r_o',a')]. \qquad (3.6.3)$$

The factor $f(r,r_o,a)$ is a Woods-Saxon well shape:

$$f(r,r_o,a) = [1 + \exp(\frac{r-r_o A^{1/3}}{a})]^{-1} . \qquad (3.6.4)$$

The form factor $F_{j_p,m}$ reduces to the wavefunction of the bound proton angular momentum j_p and projection m when the "zero range" approximation is used. The sum over m in equation (3.6.1) extends over all possible magnetic substates of the transferred proton. It is, of course, the bound proton which was transferred in the reaction. The wavefunction of the bound particle is made to have the correct number of nodes, and the orbital angular momentum ℓ and spin s appropriate to the particle being transferred. The well in which the bound particle resides is of the same form as the optical potential of the entrance channel, however the potential for the bound particle has been modified by the addition of a spin orbit force.

$$V_{bound} = V_{opt} + V_{so}$$

$$V_{so} = -V_o \frac{\lambda}{45.2} \frac{d}{rdr} f(r,r_o,a) \vec{\ell}\cdot\vec{s} . \qquad (3.6.5)$$

The effect of this is to increase the cross section for the states with $j = \ell + \frac{1}{2}$ over those with $j = \ell - \frac{1}{2}$. This change in cross section was calculated for a single ℓ value and the remainder were approximated:

$$\frac{d\sigma}{d\Omega}(\ell + \tfrac{1}{2}) / \frac{d\sigma}{d\Omega}(\ell - \tfrac{1}{2}) \propto 2\ell + 1. \qquad (3.6.6)$$

In some of the calculations the wavefunctions were

modified by a non-local correction term in an attempt to increase the total cross sections. The wavefunction of each particle was modified by the following factor (Kunz 1969)

$$W(r) = \frac{1}{\sqrt{1 + \frac{\beta}{4}\frac{2m}{\hbar^2} V(r)}} . \qquad (3.6.7)$$

V(r) is the optical potential for the distorted waves in the potential well of the bound particle; β is the non local parameter tabulated by Kunz (1969) and m is the mass of the particle.

The calculation of σ_{j_p} was carried out using the program DWUCK (Kunz, 1969). The optical model parameters used for the four reactions are shown in Table 3.6.1. Table 3.6.2 gives the normalization factors used and compares them to the accepted values. The latter table also indicates whether the non-local parameter was used and the value of the lower cut-off in the radial integration for the different calculations.

In the (d,t) reaction, the optical model parameters chosen for the deuterons were from the elastic scattering work of Christensen et al. (1969). The triton parameters were obtained from the study of ^{160}Gd(d,t)^{159}Gd by Jaskola et al. (1967). The (^{3}He,α) parameters were taken from Burke et al. (1971). These originated from the (^{3}He,d) work of Wildenthal et al. (1967) and a (t,α) study by Blair and Armstrong (1966). The (^{3}He,d) and (α,t) potentials were those used by Lu and Alford (1971) at beam energies close to those of the present experiments. The

Table 3.6.1

Optical model parameters used in DWBA Calculation

	V_o(MeV)	r_o(fm)	a(fm)	W_o(MeV)	$4W_D$(MeV)	r_o' (fm)	a'(fm)	V_{so}	r_{oc}(fm)	Non local parameter β
					$^{175}Lu(d,t)^{174}Lu$					
d	-89	1.15	0.909	0.	79.92	1.267	0.78	0.	1.25	0.54
t	-154.	1.1	0.75	0.	48.	1.4	0.65	0.	1.25	0.25
bound neutron	a)	1.25	0.65					λ=8	1.25	0.85
					$^{175}Lu(^3He,\alpha)^{174}Lu$					
^{3}He	-175.	1.14	0.723	-17.5	0.	1.6	0.81	0.	1.4	0.25
α	-206.8	1.41	0.519	-28.8	0.	1.41	0.519	0.	1.3	0.2
bound neutron	a)	1.25	0.65					λ=8	1.25	0.85
					$^{173}Yb(^3He,d)^{174}Lu$					
^{3}He	-175.	1.14	0.723	-17.5	0.	1.6	0.81	0.	1.4	0.25
d	-111.	1.05	0.859	0.	70.8	1.24	0.794	0.	1.25	0.54
bound proton	a)	1.25	0.65					λ=8	1.25	0.85

(continued next page)

Table 3.6.1 (continued)

	V_o (MeV)	r_o (fm)	a (fm)	W_o (MeV)	$4W_D$ (MeV)	r_o' (fm)	a' (fm)	V_{so}	r_{oc} (fm)	Non local parameter β
					$^{173}Yb(\alpha,t)^{174}Lu$					
α	-200.	1.4	0.6	-20.	0.	1.4	0.6	0.	1.3	0.2
t	-200.	1.4	0.6	-50.	0.	1.4	0.6	0.	1.3	0.25
bound proton	a)	1.25	0.65					λ=10	1.25	0.85

a) adjusted to reproduce the separation energy

Table 3.6.2

DWBA Calculations performed

Reaction	Incident Energy (MeV)	Accepted Normalization for DWBA	Normalization Used	Lower Cut-off in rad. int. (fm)	Non-Local parameters
$^{even}_{Yb}(^{3}He,d)^{odd}_{Lu}$	28	4.42	3.45	9.6	no
$^{even}_{Yb}(\alpha,t)^{odd}_{Lu}$	30	$\approx$ 46	52	9.6	no
$^{173}_{Yb}(^{3}He,d)^{174}_{Lu}$	24	4.42	4.42	9.0	yes
$^{173}_{Yb}(\alpha,t)^{174}_{Lu}$	28.5	$\approx$ 46	70	9.0	yes
$^{175}_{Lu}(^{3}He,\alpha)^{174}_{Lu}$	24	$\approx$ 23	23	0	yes
$^{175}_{Lu}(d,t)^{174}_{Lu}$	12	3.33	3.33	0	yes

origin of the proton transfer parameters is the $^{208}Pb(^{3}He,d)^{209}Bi$ reaction (Wildenthal et al. 1967) and the corresponding (α,t) reaction (Lilley and Stein 1967).

For the present study it was felt that the DWBA calculations should yield the Q-dependence and ℓ-dependence for the reactions fairly reliably. However, for complex projectiles and reaction products there is often some uncertainty in the normalization factor. This difficulty is expected to be particularly serious for the (α,t) reaction where the normalization has been found to be extremely sensitive to the finite range parameter (Hering et al. (1970). Finite range parameters, which are similar to the non-local correction in that they multiply the wavefunction by a factor depending on the radius, were not used in the present calculation. In the present work the DWBA results have been used only to obtain the Q-dependence and ℓ-dependence of the reactions, thus really only relative cross sections are being predicted although in most cases the agreement is acceptable on an absolute scale. The angular dependence of the cross section has been used in the $(^{3}He,d)$ reaction at 28 MeV to aid in the assignment of the ℓ-values of transitions to certain peaks. It should be noted too that there is some indication in the study of ^{174}Lu with the (α,t) reaction at 28.5 MeV, that DWBA calculations are not able to predict the Q-dependence of the cross section over ranges of an MeV. The error in the predicted cross section, though, is expected to be small over the several hundred keV spanned by by a typical rotational band.

The number of nodes in the bound state wavefunction is given by the quotient $[\frac{N-\ell}{2}]$. Transitions to states arising from a specific major oscillator shell, of quantum number N, may only take place by transferring particles whose ℓ generates the correct parity. In the neutron transfer reactions, the only identified states populated were by the pick-up of N=5 and 6 neutrons from the target. The proton transfer reactions populated states by depositing protons into N=4 and 5 target orbitals.

The calculations were performed for each of the six entries in Table 3.6.2 for all ℓ-values up to ℓ=5 for proton transfer cases and up to ℓ=6 in the neutron transfer reactions. The cross section varies only slightly with the target so the calculations used for the study of the odd-A lutetium isotopes were only done for the case of a ^{172}Yb target. For each reaction, the reaction Q-value was varied, with the appropriate adjustment of the binding energy so that the cross sections up to several MeV excitation could be interpolated in the following manner:

$$\frac{d\sigma}{d\Omega}(Q,\ell,j,\theta) = \exp(A + BQ + CQ^2 + \ldots). \qquad (3.6.8)$$

The coefficients, A, B and C etc., which are calculated for each ℓ, j and θ combination of interest, were obtained by fitting the predicted Q-dependence. There are as many coefficients as Q-values for which the DWBA calculation was performed. The excitation energy E_x is related to the Q-value in the following

manner:

$$Q = Q_{gs} - E_x \ . \qquad (3.6.9)$$

Q_{gs} is the ground state Q-value.

Figures 3.6.1 to 3.6.4 inclusive show typical angular distributions predicted for these reactions. The predicted shape of the (^{3}He,d) angular distributions did not change a great deal when the beam energy was decreased from 28 MeV to 24 MeV. The same was also true in the (α,t) reaction in going from 30 MeV to 28.5 MeV bombarding energy.

On the proton transfer figures one may see the difference in the cross section if the particle transferred has $j = \ell + \frac{1}{2}$ and $j = \ell - \frac{1}{2}$ for the ℓ=5 transitions. This difference was interpolated using expression (3.6.6) to the other ℓ-values when predicting the experimental cross sections. Though it is not shown in the figures, the ℓ=6 angular distributions in the neutron transfer reactions were calculated for both j = 11/2 and j = 13/2 and a similar interpolation to other ℓ-values was made.

The (^{3}He,d) angular distributions in fig.3.6.1 show some fine structure for the low-ℓ transitions. These features are quite characteristic and proved to be a useful aid in determining the ℓ-value of certain well isolated states in the odd-A lutetium isotopes. It is possible to distinguish between ℓ=1 and 2 transfers as well as between the low and the high-ℓ (ℓ=4 and 5) states) Angular distributions were not measured in the study of ^{174}Lu. Fig. 3.6.5 shows the predicted differential cross section for the (^{3}He,d) reaction as a function of beam

Figure 3.6.1

Angular distributions predicted by DWBA calculations for the $^{172}Yb(^{3}He,d)^{173}Lu$ reaction at 28 MeV and Q = 0 MeV. The ground state Q-value is approximately -0.485 MeV. At $E_{^{3}He}$ = 24 MeV the shape of the angular distributions is quite similar. It is sometimes possible to use the angular distributions to determine the ℓ-values of the transitions, particularly in the low-ℓ cases where some diffraction effects exist.

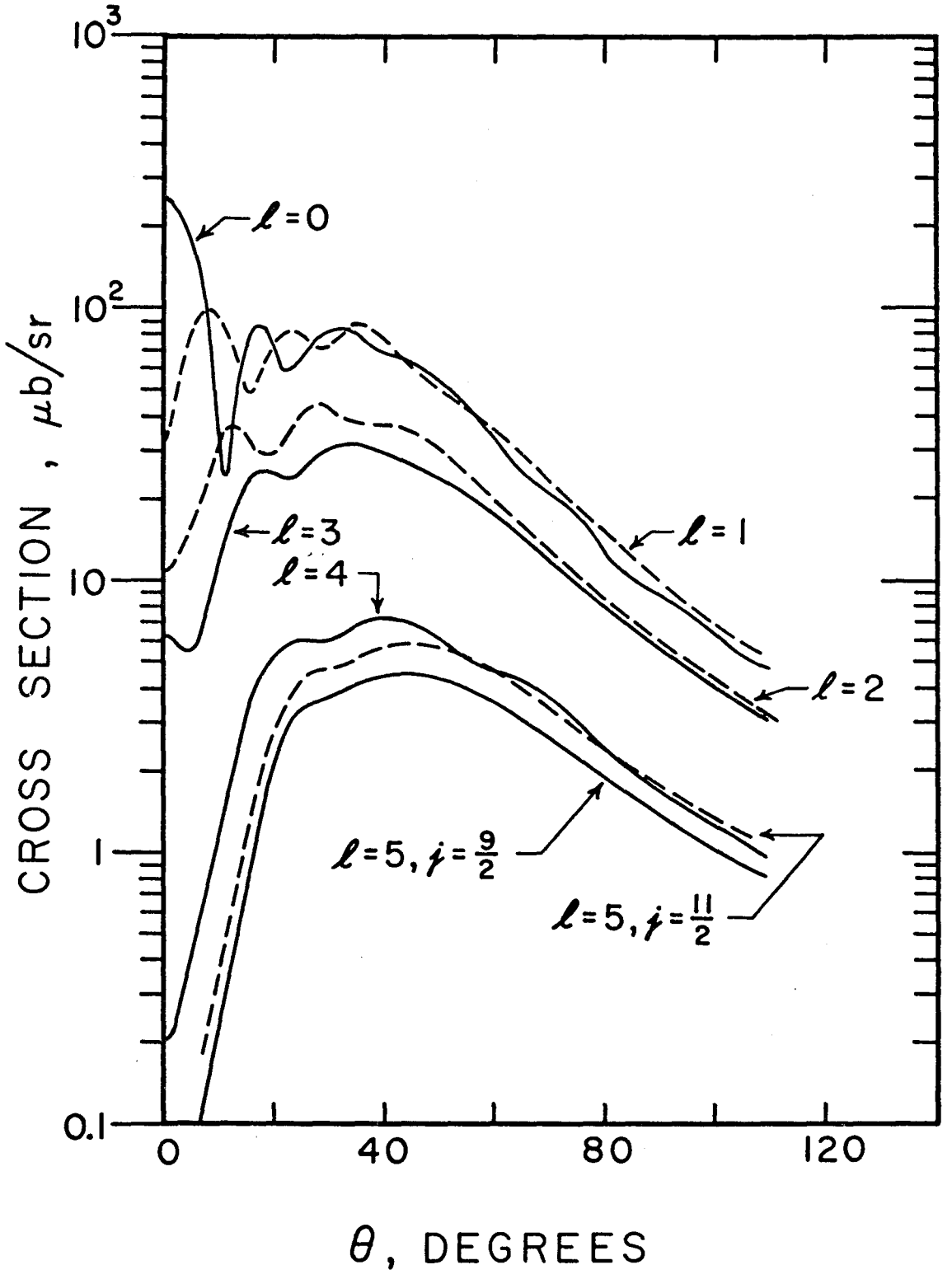
10^3
10^2
10
1
0.1
CROSS SECTION , μb/sr
0
40
80
120
θ, DEGREES
ℓ=0
ℓ=1
ℓ=2
ℓ=3
ℓ=4
ℓ=5, j=9/2
ℓ=5, j=11/2

Figure 3.6.2

Predicted angular distributions for the $^{172}Yb(\alpha,t)^{173}Lu$ reaction at 30 MeV and Q = -14 MeV. The ground state Q-value is -14.8 MeV for this reaction. These angular distributions are seen to be quite featureless at this bombarding energy so it was not felt that measuring angular distributions would be fruitful. Similar shapes of the angular distributions are predicted at E_α = 28.5 MeV.

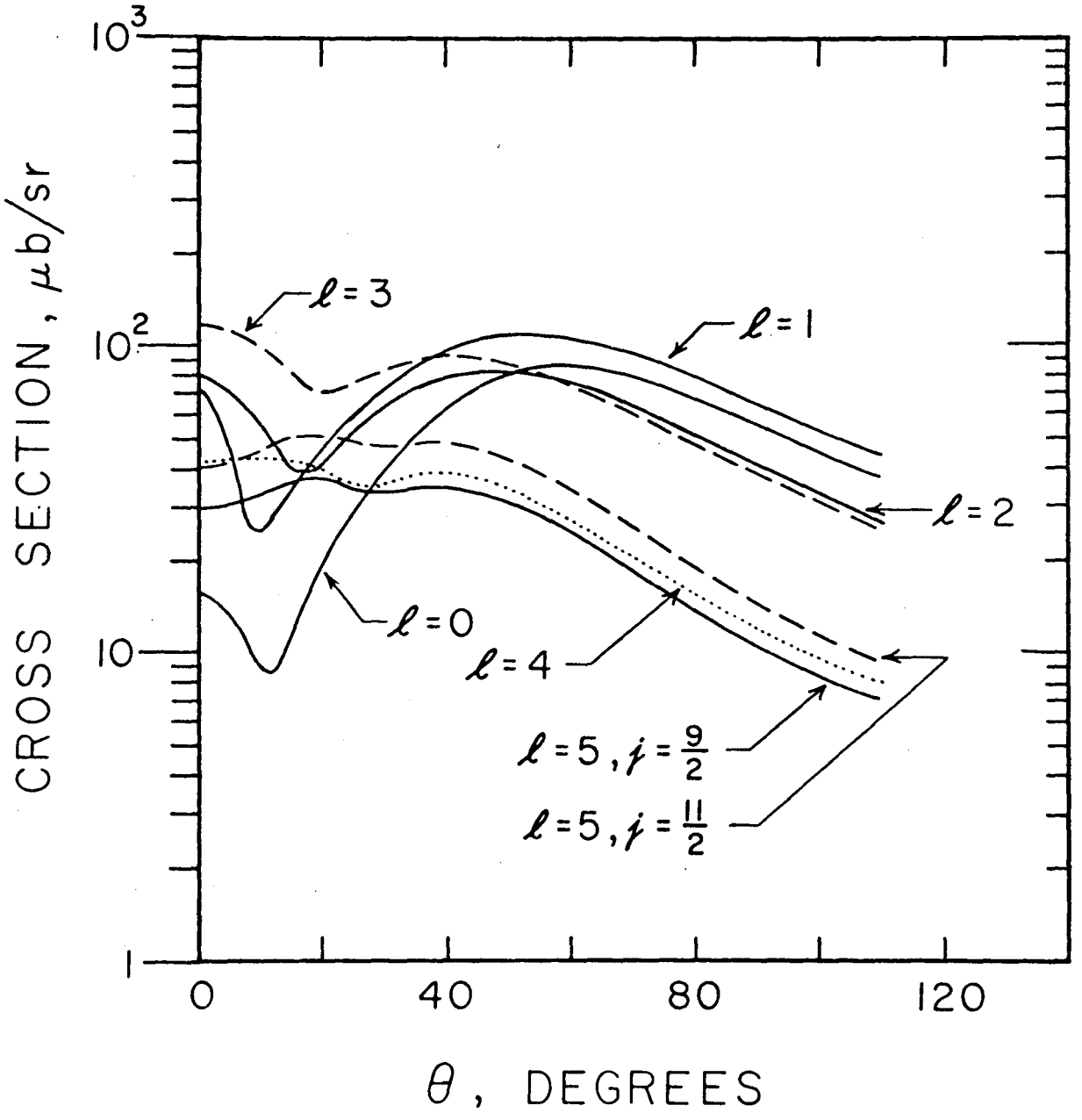
CROSS SECTION, μb/sr
10^3
10^2
10
1
0
40
80
120
θ, DEGREES
ℓ = 3
ℓ = 1
ℓ = 2
ℓ = 0
ℓ = 4
ℓ = 5, j = 9/2
ℓ = 5, j = 11/2

Figure 3.6.3

Predicted angular distributions for the $^{175}Lu(d,t)^{174}Lu$ reaction at 12 MeV and Q = -2 MeV. It may be seen that the cross section falls off quite steeply forward of $\theta_t = 50°$. For high-ℓ transitions in particular the optimum cross sections occur at $\theta_t > 80°$.

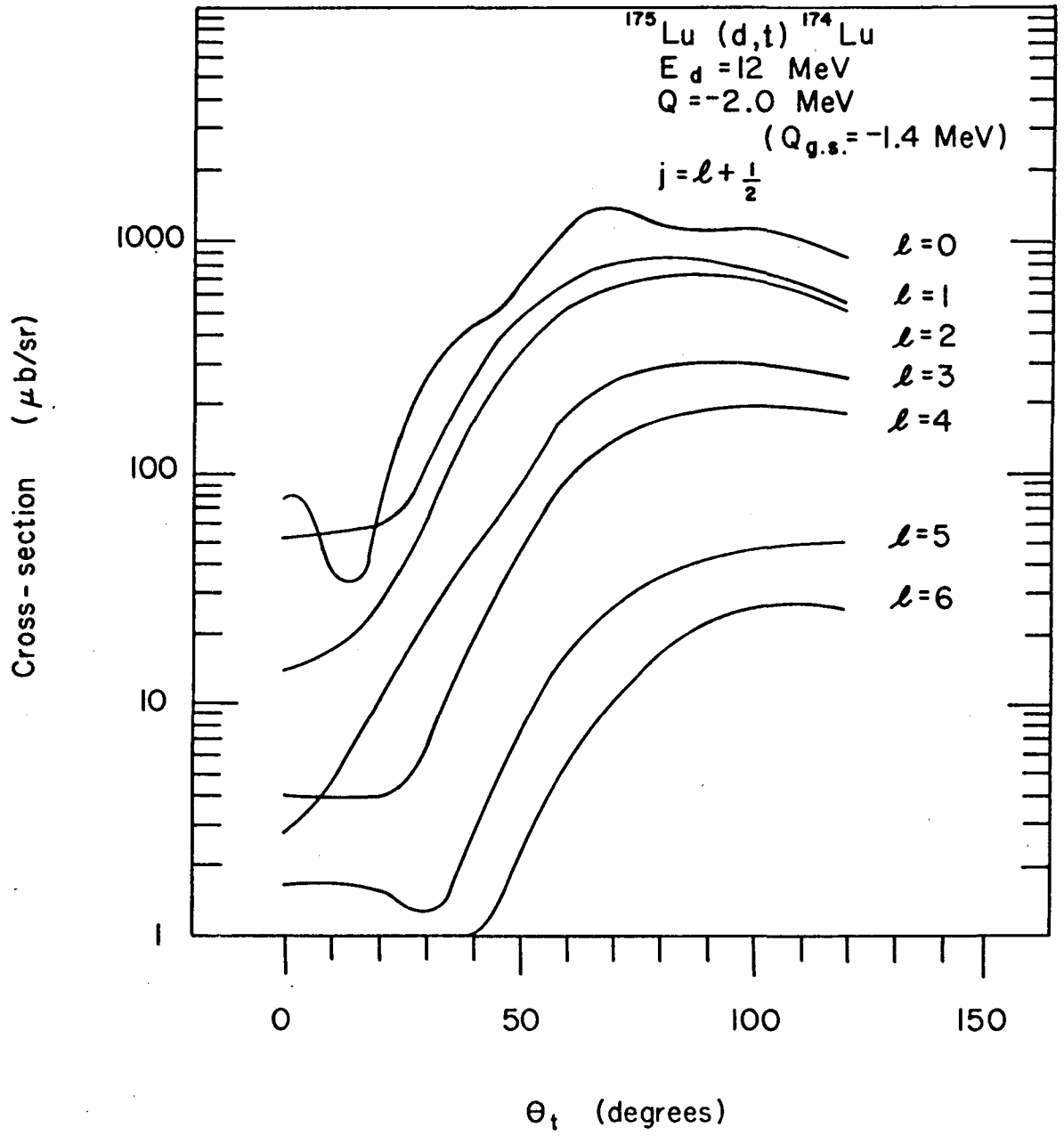
^{175}Lu (d,t) ^{174}Lu
E$_d$ = 12 MeV
Q = -2.0 MeV
(Q$_{g.s.}$ = -1.4 MeV)
j = ℓ + 1/2
ℓ = 0
ℓ = 1
ℓ = 2
ℓ = 3
ℓ = 4
ℓ = 5
ℓ = 6
1000
100
10
1
0
50
100
150
Cross-section (μb/sr)
θ$_t$ (degrees)

Figure 3.6.4

Predicted angular distributions for $^{175}Lu(^{3}He,\alpha)^{174}Lu$ at 24 MeV and Q = 13 MeV. It may be seen here how strongly the high-ℓ states are populated when compared to the low-ℓ states.

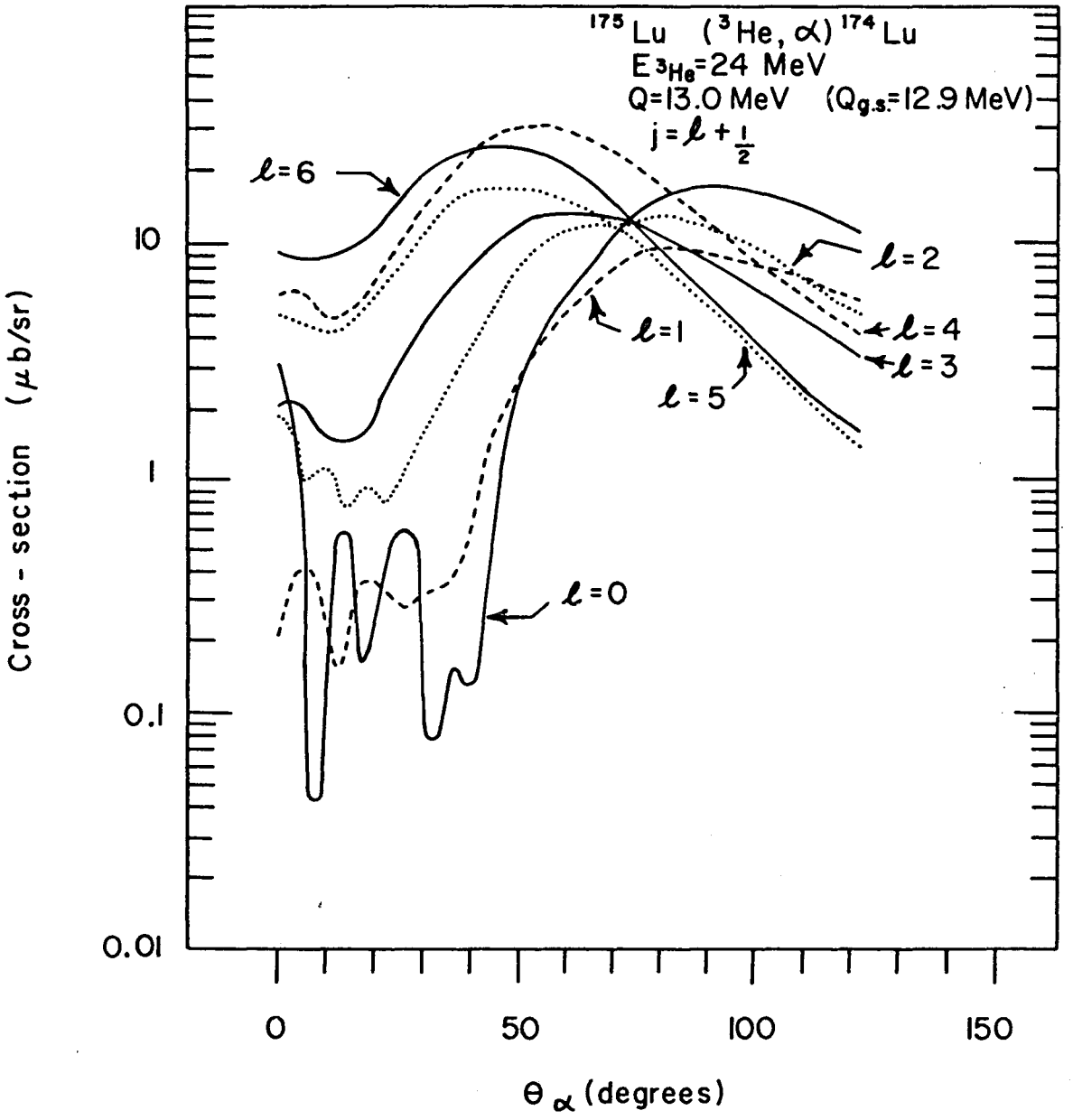
^{175}Lu (^{3}He, α) ^{174}Lu
$E_{^3He}$=24 MeV
Q=13.0 MeV (Q$_{g.s.}$=12.9 MeV)
j = ℓ + 1/2
ℓ=6
ℓ=2
ℓ=1
ℓ=4
ℓ=3
ℓ=5
ℓ=0
10
1
0.1
0.01
0
50
100
150
Cross - section (μb/sr)
θ α (degrees)

Figure 3.6.5

The predicted beam energy dependence of the (^{3}He,d) cross section at θ_d = 50° and Q = -0.2 MeV. Though the cross section does not increase above 26 MeV, more fine structure begins to appear at forward angles in the angular distributions. This diagram assumes the normalization factor is unchanging as the beam energy is increased. The calculations were performed using the same parameters as in Tables 3.6.1 and 3.6.2 for the (^{3}He,d) reaction at 24 MeV.

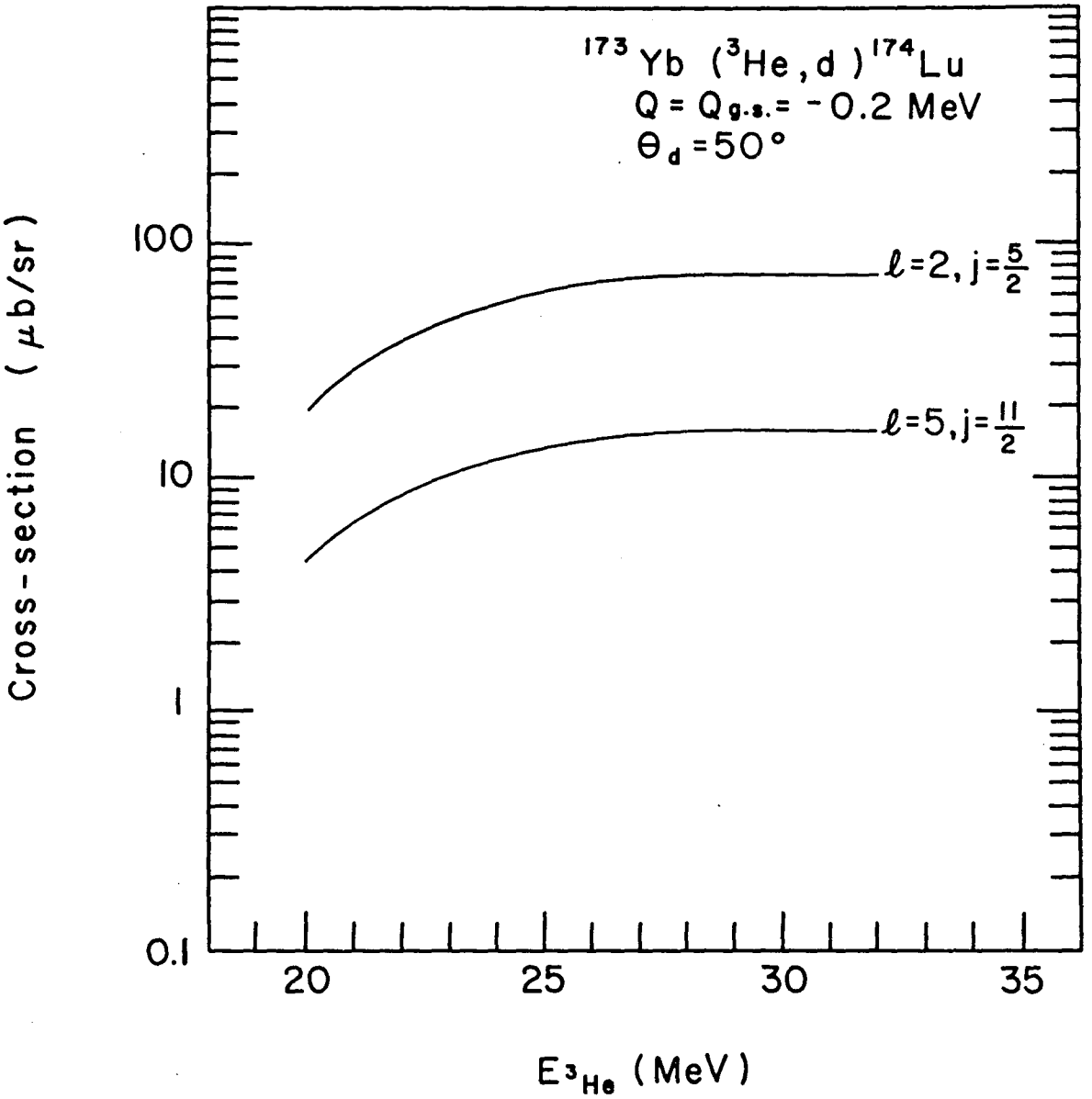
^{173}Yb (^{3}He, d) ^{174}Lu
Q = Q$_{g.s.}$ = -0.2 MeV
θ_d = 50°
ℓ=2, j=5/2
ℓ=5, j=11/2
Cross-section (μb/sr)
100
10
1
0.1
20
25
30
35
$E_{^3He}$ (MeV)

energy.

The (α,t) angular distributions in fig. 3.6.1 may be seen to have very little fine structure. For this reason, no attempt was made to measure the (α,t) angular distributions. Fig. 3.6.6 shows the differential cross sections of the (α,t) reaction as a function of the beam energy. Experiments performed at E_α > 28 MeV have superior cross sections. Above E_α = 30 MeV there does not seem to be much increase in the cross section predicted at lab angle θ_t = 60°; however, the angular distributions are expected to show more structure at forward angles. The (α,t) reaction tends to populate all ℓ-transfers with nearly the same cross section whereas the (^{3}He,d) reaction tends to populate the low-ℓ states more strongly. This observation is a useful tool in the interpretation of the spectra.

The predicted (d,t) angular distributions shown in Figure 3.6.3 shows two things of particular interest. The first is that the cross section for an ℓ=0 transfer is two orders of magnitude greater than for an ℓ=6. The other is the lack of fine structure in the angular distributions themselves. For this reason (d,t) angular distributions were not measured. At higher beam energies the fine structure in the angular distributions becomes apparent because the Coulomb barrier is significantly less than the particle energies. In particular the upward trend at small angles in the ℓ=0 angular distributions becomes quite prominent. For population of high angular momentum transitions the largest cross sections are expected at backward angles. This last point was used as a check on

Figure 3.6.5

The predicted beam energy dependence of the (α,t) cross section at θ_α = 60° and Q = -14.5 MeV. The advantage of high beam energies is in the improved cross section. Though the cross section does not increase much above 28 MeV the angular distributions show more structure as the energy is increased. This diagram assumes the normalization factor remains unchanged as the energy is increased. The calculations were performed using the same parameter set as tabulated in Tables 3.6.1 and 3.6.2 for the (α,t) reaction at 28.5 MeV.

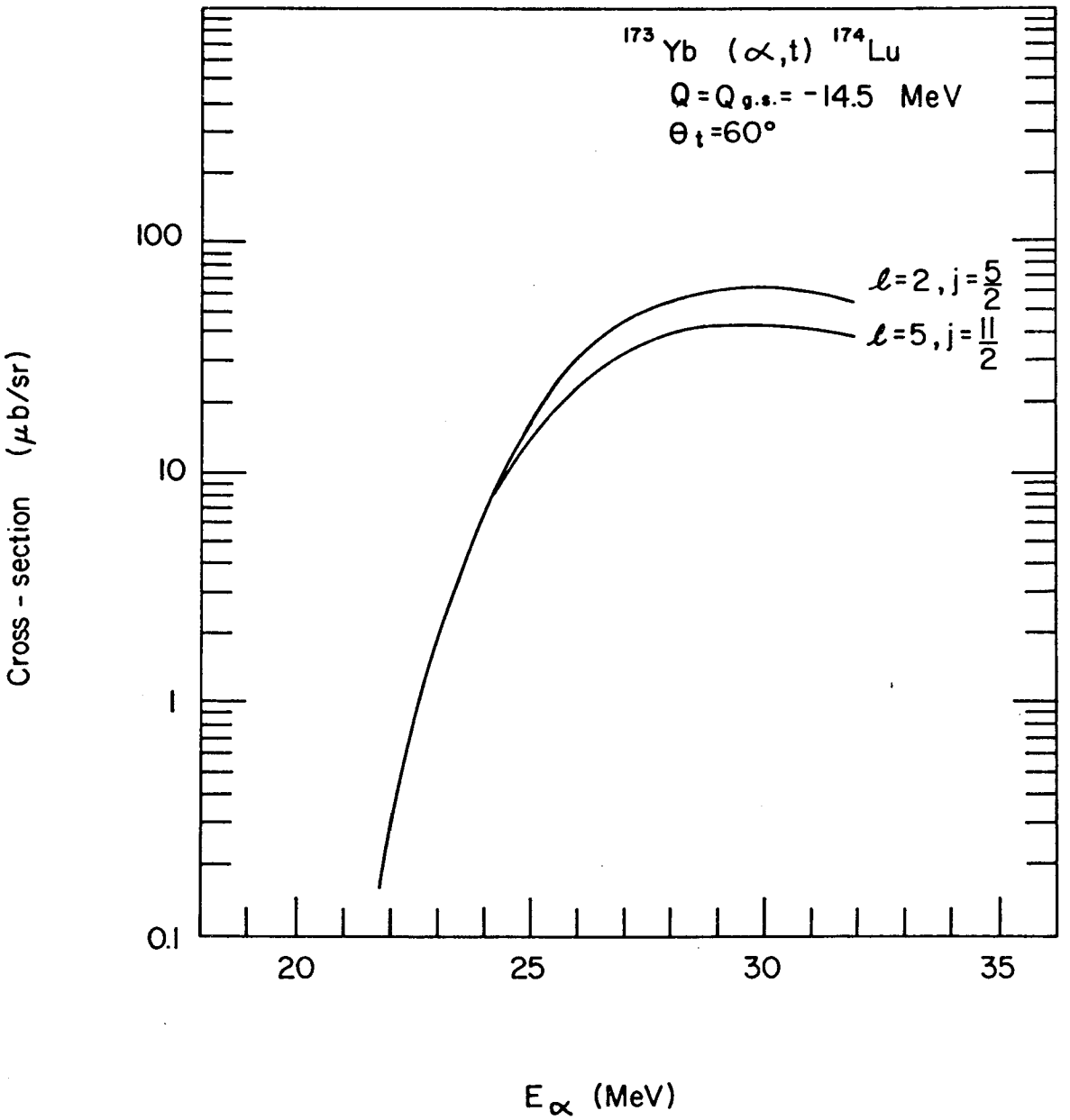
^{173}Yb (α,t) ^{174}Lu
Q = Q g.s. = -14.5 MeV
θ_t = 60°
ℓ = 2, j = 5/2
ℓ = 5, j = 11/2
100
10
1
0.1
20
25
30
35
Cross - section (μb/sr)
E_α (MeV)

the assignment of some ℓ=6 transfers into ^{174}Lu.

Figure 3.6.4 shows the predicted angular distributions for the (^{3}He,α) reaction. The cross sections for this reaction are quite small; the largest is predicted to be $\tilde{>}$20 μb/sr. The high-ℓ transitions are populated most strongly. At lab angle θ_α = 35° the largest single particle cross sections are expected for ℓ=6 transfers. The angular distributions are devoid of strong characteristic features so no attempt was made to measure them.

As has been mentioned, the (^{3}He,d) reaction populates states by low-ℓ transitions more readily than by high-ℓ transitions. The (α,t) reaction is less selective inasmuch as it populates all ℓ-values with roughly the same probability. The expression for the cross section into an odd-A nucleus is:

$$\frac{d\sigma}{d\Omega} = 2C_{j\Omega}{}^2 U^2 \sigma_{j(\ell)} \quad . \qquad (3.5.8)$$

Thus if the ratio of the experimental (^{3}He,d) and (α,t) cross sections is taken, all the nuclear structure information divides out. What is left depends only on the reactions involved and may be calculated using the DWBA programs discussed. Thus a comparison of the predicted ratio and the observed (^{3}He,d) to (α,t) cross section ratio for a specific peak should be a good indication of the ℓ-value of the transition. Taking a certain angle and beam energy for each reaction, it is convenient to make a plot of the predicted ratio for the various

ℓ-values as a function of the Q-value or the excitation energy. Such plots, with some experimental points, are shown in fig. 4.2.1 and 5.2.1. The solid lines represent the predicted (^{3}He,d) to (α,t) cross section ratios for the various ℓ-values. Ratios predicted for the $j = \ell + \frac{1}{2}$ and $j = \ell - \frac{1}{2}$ transfers are identical so only one line has been drawn for each ℓ-value.

When the ratio of the (^{3}He,d) to the (α,t) cross section is taken in the case of an odd-odd final nucleus, the nuclear structure parts in the ratio do not divide out, rendering it less useful. This is quite clear in equations (3.5.7) and (B.9) where the cross section is a sum of different j-values. If the state is populated by a transition of a single ℓ-value, the ratio is expected to lie on one of the predicted ratio curves. Such would be the case if the wavefunction of the transferred orbital has only one large Nilsson coefficient. Some of the orbitals in ^{174}Lu have this property. In these special cases in odd-odd nuclei and in all odd-A nuclei, the (^{3}He,d) to (α,t) cross section ratios should be similar for all members of rotational bands, except for differences in Q-values. If the wave function of the transferred orbital contains several large $C_{j\Omega}$ coefficients then the cross section ratio is expected to show low-ℓ characteristics in the lower spin, I, states of the rotational band. The ratio will indicate higher ℓ-values for the transitions as the spin, I, increases up the band. In the odd-odd nuclei, where the level density is high and states may be unresolved, the (^{3}He,d) to (α,t) cross section ratio

is useful for discriminating between states populated by high or low-ℓ transitions . The error in ascertaining the ℓ-value from the cross-section ratios in such nuclei is likely about one unit in ℓ.

The (d,t) to (^{3}He,α) cross section ratio has been shown (Burke et al. 1971) to be a good indicator of the ℓ-value of the neutron transfer transitions to states in odd-A nuclei. The predicted cross section ratio curve for the neutron transfer reactions into ^{174}Lu is shown in fig. 5.2.2. This curve was not too useful because of the high level density visible in the (d,t) reaction, the very low energy resolution characteristic of the (^{3}He,α) reaction, and the very low (^{3}He,α) cross sections for almost all the states except those populated by ℓ=6 transitions. The (d,t) to (^{3}He,α) cross section ratio has only been used in ^{174}Lu to strengthen the ℓ=6 assignment of some large cross sections in the (^{3}He,α) reaction.

CHAPTER 4

THE ODD MASS LUTETIUM ISOTOPES

A considerable amount of work has been carried out on the study of low-lying intrinsic proton states in the higher-mass region of the deformed rare-earth nuclei. A point of special interest is the fact that several orbitals arising from the N = 5 oscillator shell are strongly depressed in energy with increasing deformation, and are expected to appear among states arising from the N = 4 shell. The states of interest in the present study are indicated in the partial Nilsson diagram shown in fig. 3.1.2 .

Many studies have been made on the lutetium isotopes (Z = 71) in particular, with a view to studying the relative locations of the N = 4 and N = 5 states. In ^{173}Lu, such studies (Valentin et al. 1962; Brenner 1970; Bjørnholm et al. 1965) have led to the identification of the $7/2^+[404]$ ground state band, plus the $1/2^-[541]$, $5/2^+[402]$ and $1/2^+[411]$ bands as excited states. A number of other states have been located at excitation energies near 1 MeV, but have not been identified further. In ^{175}Lu the $7/2^+[404]$ ground state, $5/2^+[402]$, $1/2^-[541]$ and $9/2^-[514]$ bands have been located (Bjørnholm et al. 1965; Johanson et al. 1969; Hatch et al. 1956; Funke et al. 1965). Some of the known levels have been investigated via Coulomb excitation studies (Bernstein and Graetzer 1960), and nuclear resonance fluorescence (Deutch 1962). A study of the ^{176}Lu(d,t)^{175}Lu

reaction has been reported briefly also (Minor et al. 1969). Levels in ^{177}Lu have been studied in the decay (Mize et al. 1956; Brown et al. 1970) of ^{177}Yb, in the decay of an isomeric state (Kristensen et al. 1964; Alexander et al. 1964) in ^{177}Lu, and in the ^{176}Lu(n,γ)^{177}Lu reaction (Maier 1965, Balodis et al. 1966). Once again, the $7/2^+[404]$ ground state, $5/2^+[402]$, $9/2^-[514]$ and $1/2^+[411]$ states are identified. The interesting $1/2^-[541]$ state has not been previously observed in this isotope.

The present study provides another approach to the investigation of the intrinsic states in deformed nuclei by using single proton transfer reactions. By measuring the cross sections for the population of the various rotational band members it is possible to deduce the configuration on which the band is built. Transfer reactions may also provide rather direct information on band mixing.

It turns out that many of the proton states which occur at low excitation energies in this mass region have fingerprints which are not as distinct as those for the neutron states. In some cases, the value of $C^2_{j\Omega}$ is nearly unity for one rotational band member, and therefore only one strong peak is present to represent the band. In such cases the analysis is often limited to testing whether the observed populations agree with the expectations for particular Nilsson states.

In the present study, the assignments noted above for the low-lying intrinsic states have all been confirmed. New assignments have been made for the I = 9/2 members of the

$1/2^-[541]$ band in ^{173}Lu and ^{175}Lu, for the I = 11/2 members of the $9/2^-[514]$ bands in ^{173}Lu and ^{175}Lu, and for the 3/2, 5/2 and 9/2 members of the $1/2^-[541]$ band in ^{177}Lu. In addition, the present results extend the study of these nuclei to a region of excitation not accessible to decay studies. The $1/2^-[530]$ band is identified in all three isotopes near an energy of 1500 keV. The $3/2^-[532]$ band, which shows strong Coriolis mixing with the $1/2^-[541]$ orbital, can be tentatively assigned in ^{173}Lu and ^{175}Lu, and some evidence has been found for its location in ^{177}Lu.

4.1 Experimental results

Figs. 4.1.1, 4.1.2 and 4.1.3 show measured spectra obtained with targets of ^{172}Yb, ^{174}Yb and ^{176}Yb, respectively. Each figure shows the (^3He,d) spectrum at lab angle θ = 40° and the (α,t) spectrum at lab angle θ = 45° plotted to a common scale of excitation energy. This has been done to facilitate visual comparisons of the cross sections for the different reactions to the various final states. The DWBA calculations indicated that the (α,t) angular distributions would have no fine structure and thus no attempt was made to measure angular distributions. The average excitation energies from each reaction, the (^3He,d) cross sections at lab angle θ = 40° and the (α,t) cross sections at lab angle θ = 45°) are presented in tables 4.1.1, 4.1.2 and 4.1.3 for levels in ^{173}Lu, ^{175}Lu and ^{177}Lu, respectively. For strongly populated states the estimated uncertainties are about 2 keV in the excitation energies. The

Figure 4.1.1

The experimental spectra obtained for the $^{172}Yb(^{3}He,d)^{173}Lu$ reaction at $\theta = 40°$ and the $^{172}Yb(\alpha,t)^{173}Lu$ reaction at $\theta = 45°$. A comparison between the intensity of a low spin state ($I = 3/2$) and a high spin state ($I = 9/2$) in the two reactions may be made in the $1/2^{-}[541]$ band.

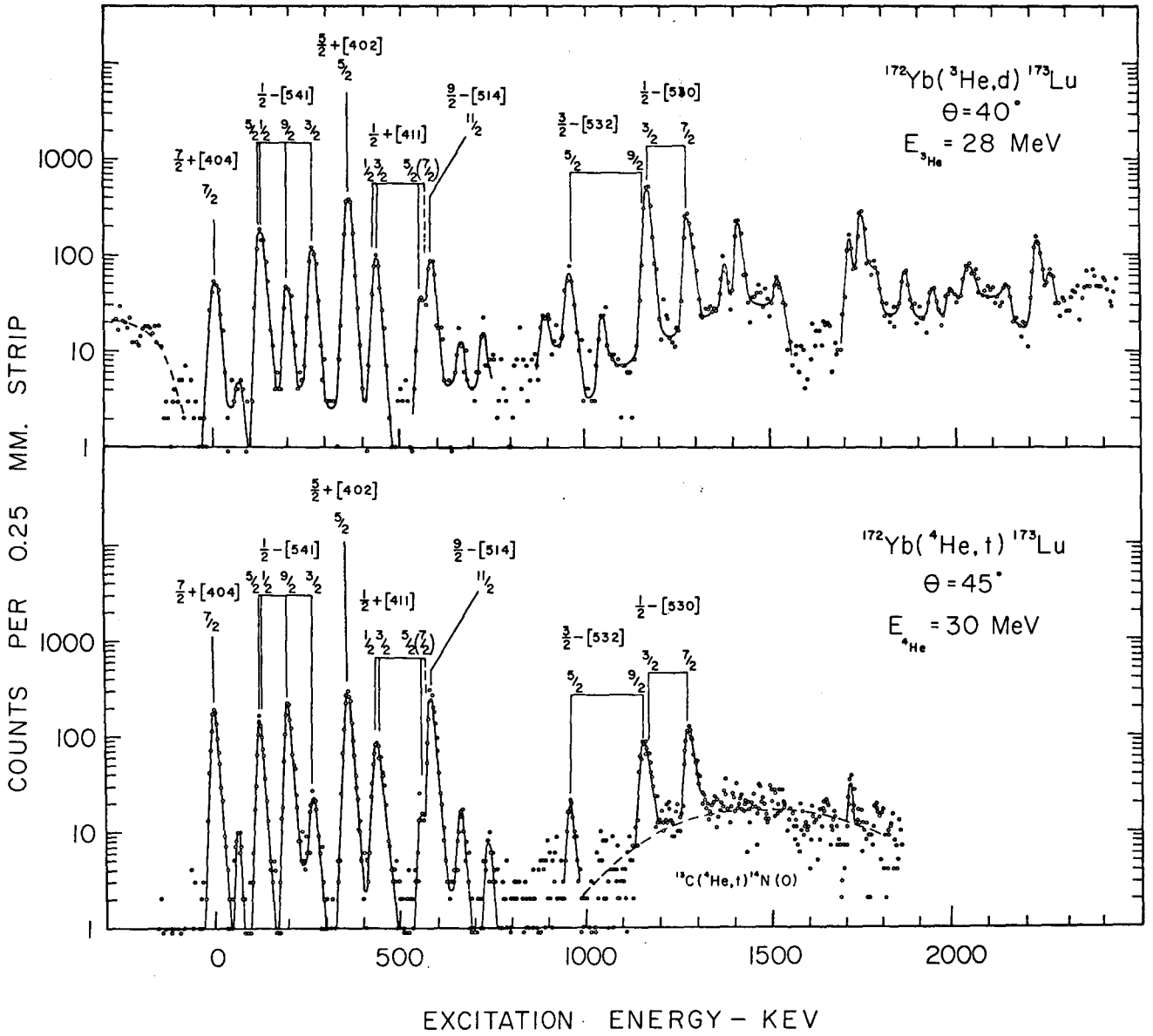
^{172}Yb(^{3}He,d)^{173}Lu
Θ=40°
$E_{^{3}He}$ = 28 MeV
^{172}Yb(^{4}He,t)^{173}Lu
Θ=45°
$E_{^{4}He}$ = 30 MeV
$\frac{5}{2}$+[402]
$\frac{1}{2}$-[541]
$\frac{9}{2}$-[514]
$\frac{1}{2}$+[411]
$\frac{3}{2}$-[532]
$\frac{1}{2}$-[530]
$\frac{7}{2}$+[404]
^{13}C(^{4}He,t)^{14}N (0)
COUNTS PER 0.25 MM. STRIP
EXCITATION ENERGY – KEV
0
500
1000
1500
2000
1
10
100
1000

Figure 4.1.2

The spectra obtained from the $^{174}Yb(^{3}He,d)^{175}Lu$ reaction at $\theta = 40°$ and the $^{174}Yb(\alpha,t)^{175}Lu$ the reaction at $\theta = 45°$.

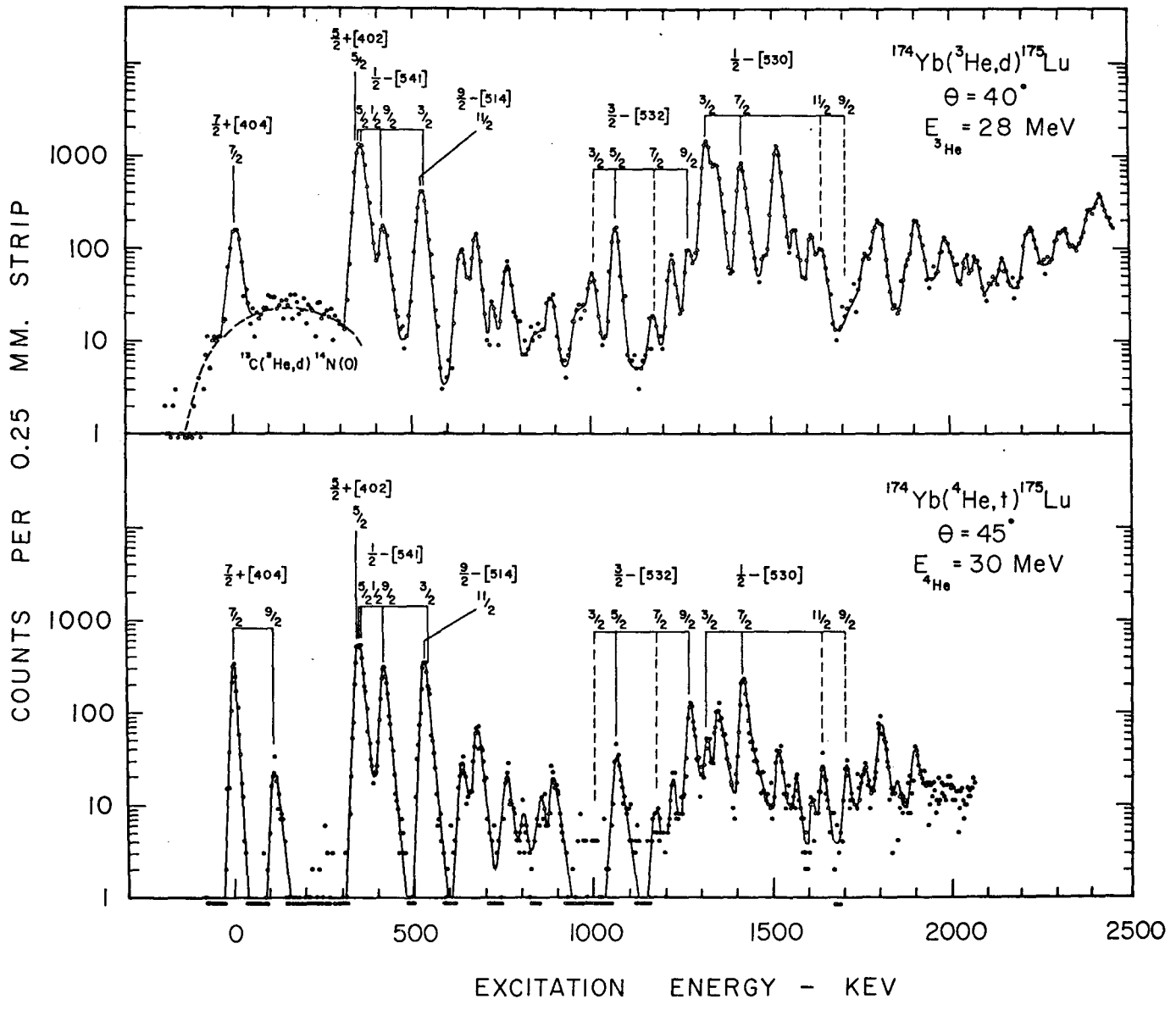
^{174}Yb(^{3}He,d)^{175}Lu
θ = 40°
$E_{^3He}$ = 28 MeV
^{174}Yb(^{4}He,t)^{175}Lu
θ = 45°
$E_{^4He}$ = 30 MeV
5/2+[402]
1/2−[541]
9/2−[514]
7/2+[404]
3/2−[532]
1/2−[530]
^{13}C(^{3}He,d)^{14}N(0)
COUNTS PER 0.25 MM. STRIP
EXCITATION ENERGY − KEV

Figure 4.1.3

The spectra obtained from the $^{176}Yb(^{3}He,d)^{177}Lu$ reaction at $\theta = 40°$ and the $^{176}Yb(\alpha,t)^{177}Lu$ reaction at $\theta = 45°$.

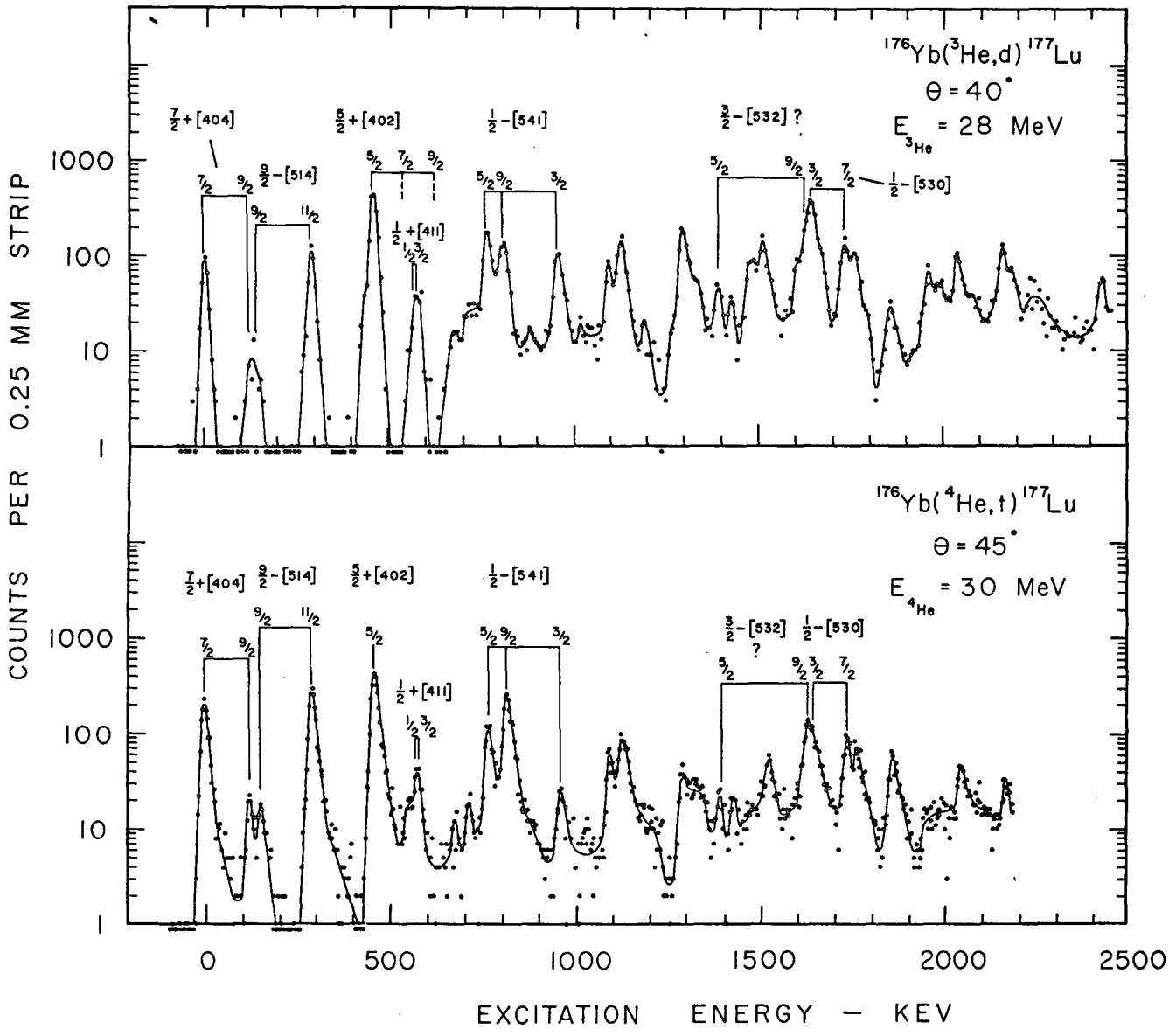
^{176}Yb(^{3}He,d)^{177}Lu
Θ = 40°
$E_{^{3}He}$ = 28 MeV
7/2+[404]
5/2+[402]
1/2-[541]
3/2-[532] ?
9/2-[514]
1/2+[411]
1/2-[530]
^{176}Yb(^{4}He,t)^{177}Lu
Θ = 45°
$E_{^{4}He}$ = 30 MeV
3/2-[532] ?
1/2-[530]
COUNTS PER 0.25 MM STRIP
1000
100
10
1
0
500
1000
1500
2000
2500
EXCITATION ENERGY — KEV

Table 4.1.1

Levels Populated in ^{173}Lu

Energy (keV) Previous	(^{3}He,d)	(α,t)	Assignment $IK^{\pi}[Nn_z\Lambda]$	$\frac{d\sigma}{d\Omega}$ (μb/sr) (^{3}He,d) θ=40°	(α,t) θ=45°
0	0	0	7/2 7/2$^+$[404]	14.5 ±15%	55.1 ± 6%
123, 128	124	123	5/2 1/2$^-$[541]; 1/2 1/2$^-$[541]	49 ±18%	38 ± 6%
	198	198	9/2 1/2$^-$[541]	11 ± 9%	57 ± 7%
263	261	263	3/2 1/2$^-$[541]	29 ± 6%	7.3 ± 9%
357	354	357	5/2 5/2$^+$[402]	100 ± 5%	90 ± 4%
425, 435	428	427	1/2 1/2$^+$[411]; 3/2 1/2$^+$[411]	24 ±18%	25 ± 6%
546	547	545	5/2 1/2$^+$[411]&; 7/2 1/2$^+$[411]?	8 ±16%	3.4 ±21%
	575	579	11/2 9/2$^-$[514]	22 ± 6%	88 ± 7%
	651	656		∿2.4 (±31%)	4.3 ± 12%
	714			∿2.7 (±37%)	
		730			1.8 ± 20%
889	886		3/2 3/2$^-$[532]?	∿6 (±13%)	
	947	953	5/2 3/2$^-$[532]	16 ± 7%	5.9 ± 10%
	1037			6 ±12%	
		1143	9/2 3/2$^-$[532]		21 ± 18%
	1156	1158	1/2 1/2$^-$[530]&; 3/2 1/2$^-$[530]	144 ± 3%	16 ± 46%
	1264	1267	7/2 1/2$^-$[530]	65 ± 4%	40 ± 10%
	1283	1288		20 ±12%	13 ± 9%
	1363			19 ± 8%	≤7 ± 15%

Table 4.1.1 continued

Energy (keV)			Assignment	$\frac{d\sigma}{d\Omega}$ (μb/sr)	
Previous	(^{3}He,d)	(α,t)	$IK^{\pi}[Nn_z\Lambda]$	(^{3}He,d) θ=40°	(α,t) θ=45°
	1399			62 ± 8%	≤4 ±30%
	1504			12 ±12%	
	1700	1705		36 ± 5%	≤7 ±12%
	1731			70 ± 4%	
	1754			14 ±22%	
	1846			21 ±15%	
	1926			∿ 9(±11%)	
	1968			∿10(±25%)	
	2009			∿20(±35%)	
	2038			∿16(±32%)	
	2077			∿10(±22%)	
	2125			∿ 9(±35%)	
	2202			43 ±20%	
	2233			13 ±10%	

Table 4.1.2

Levels Populated in ^{175}Lu

Energy (keV) Previous	Energy (keV) (^{3}He,d)	Energy (keV) (α,t)	Assignment $IK^{\pi}[Nn_z\Lambda]$	$\frac{d\sigma}{d\Omega}$ (^{3}He,d) θ=40° (μb/sr)	$\frac{d\sigma}{d\Omega}$ (α,t) θ=45° (μb/sr)
0	0	0	7/2 $7/2^+[404]$	13 ± 7%	61 ± 8%
114		115	9/2 $7/2^+[404]$		4.8 ±16%
343.4	344	344	5/2 $5/2^+[402]$	137 ± 2%	157 ± 5%
353.6			5/2 $1/2^-[541]$		
358.2			1/2 $1/2^-[541]$		
	413	414	9/2 $1/2^-[541]$	12.5± 7%	79 ± 3%
514.9	513	524	3/2 $1/2^-[541]$ + 11/2 $9/2^-[514]$	39 ± 4%	80 ±19%
	628	629		6.7± 8%	6.9 ± 3%
	668	673		9.7±10%	17 ± 9%
	755	755		5.5± 9%	4.3 ±17%
		∿859			1.6 ±50%
	∿873	872		2.4±11%	5.2 ±52%
	∿951			∿1.7 (±15%)	
	992		3/2 $3/2^-[532]$?	4 ± 8%	
	1056	1060	5/2 $3/2^-[532]$	12 ±11%	7.1 ±17%
	1158	∿1172	7/2 $3/2^-[532]$?	0.6±31%	1.5 ±22%
	1212	1214		4 ±21%	4 ±14%
	1263	1262	9/2 $3/2^-[532]$	5.4±23%	27 ± 8%
	1309	1308	3/2 $1/2^-[530]$ &	123 ± 8%	12 ± 9%
	1338	1338	1/2 $1/2^-[530]$	42 ±17%	28 ± 5%

Table 4.1.2 continued

Energy (keV)			Assignment	$\frac{d\sigma}{d\Omega}$ (μb/sr)	
Previous	(^{3}He,d)	(α,t)	$IK^{\pi}[Nn_z\Lambda]$	(^{3}He,d) θ=40°	(α,t) θ=45°
	1406	1406	7/2 1/2$^-$[530]	63 ± 9%	58 ± 4%
		∿1426			∼10 ± 8%
	1504	1504		96 ± 6%	10 ± 7%
	1550	1557		10 ±37%	∼3.9(±12%)
	1598	1600		12 ±12%	∼2 (±19%)
	1629	1629	11/2 1/2$^-$[530]?	6 ±25%	6 ±11%
		1695	9/2 1/2$^-$[530]?		5 ±14%
	∼1756	∿1743		∿8 (±10%)	6 ±11%
	∼1789	1788		20 ± 5%	18 ± 7%
	∼1888	1890		20 ± 9%	8 ±15%
	1977	1963		8 ±15%	

Table 4.1.3

Levels Populated in ^{177}Lu

Energy (keV) Previous	(^{3}He,d)	(α,t)	Assignment $IK^{\pi}[Nn_z\Lambda]$	$\frac{d\sigma}{d\Omega}$ (^{3}He,d) θ=40°	$\frac{d\sigma}{d\Omega}$ (α,t) θ=45°
0	0	0	7/2 $7/2^+[404]$	12 ± 9%	77 ± 4%
122	≈134	122	9/2 $7/2^+[404]$	∿1 (±84%)	7.3±11%
150		152	9/2 $9/2^-[514]$		5.5±13%
289	288	289	11/2 $9/2^-[514]$	16 ±10%	107 ± 3%
458	455	456	5/2 $5/2^+[402]$	73 ± 6%	161 ± 5%
		∿549			∿6 (±15%)
570	571	571	1/2 $1/2^+[411]$ & 3/2 $1/2^+[411]$	6.7±22%	15 ±10%
574	675	676		4.4±22%	∿3 (±25%)
709	712	708	5/2 $1/2^+[411]$? 7/2 $1/2^+[411]$?	13 ±28%	7.6±10%
720					
762	757	759	5/2 $1/2^-[541]$	32 ±70%	48 ±30%
	790	790?		15 ±48%	≤9 (±20%)
811	810	806	9/2 $1/2^-[541]$	∿15 (±56%)	92 ± 4%
		824			21 ±16%
	946	952	3/2 $1/2^-[541]$	17 ± 7%	8 ±15%
	1086	1092		15 ± 7%	26 ±15%
	1116	1117		25 ±33%	31 ± 9%
	1183	∿1178		5 ±20%	≲5 (±20%)
	1287	1285		28 ± 5%	20 ±10%
	∿1317	∿1320		∿16 (±14%)	∿10 (±14%)
	1383	1381	5/2 $3/2^-[532]$?	8 ±15%	7.5±12%
	1414	1412		5 ±10%	9 ±28%

Table 4.1.3 continued

Energy (keV)			Assignment	$\frac{d\sigma}{d\Omega}$ (μb/sr)			
Previous	(^{3}He,d)	(α,t)	$IK^{\pi}[Nn_z\Lambda]$	(^{3}He,d) θ=40°		(α,t) θ=45°	
	∿1469			21	±20%		
	1501	1517		22	±11%	19	± 8%
	1528			∿8	(±19%)		
	1587	1593		∿13	(±22%)	∿7	(±20%)
	1605	1620	9/2 $3/2^-[532]$?	∿26	(± 8%)	54	±30%
	1633	1638	1/2 $1/2^-[530]$& 3/2 $1/2^-[530]$?	63	± 5%	∿21	(±25%)
	1655	∿1676		∿19	± 9%	∿7	(±20%)
	1718	1724	7/2 $1/2^-[530]$?	26	±12%	41	±12%
	1745	1752		16	±11%	22	±13%
	1841	1850		4.5	±15%	20	±10%
		1883				7	±17%
	1950			10	±11%		
	1981			∿11	(±50%)		
	2028	2037		17	± 6%	18	± 7%
	2148	2061		20	± 6%	7.5	±15%
	∿2168			∿10	±12%		
	2412			9	±11%		

Nilsson model assignments shown in these tables are discussed in section 4.4.

Angular distributions for some of the deuteron groups in the (^{3}He,d) studies are shown in figs. 4.1.4 and 4.1.5. The assignments of ℓ-values to these levels are discussed in section 4.4. The solid curves seen in these figures are the results of DWBA calculations described in the following section.

4.2 The DWBA calculations

As described in section 3.6 a series of appropriate DWBA calculations was carried out for the lutetium isotopes. The calculated angular distributions for ℓ-values of 0 to 5 are shown in fig. 3.6.1 for the (^{3}He,d) reaction and in fig. 3.6.2 for the (α,t) reaction. In the present work, the DWBA results have been used only to obtain the Q-dependence and ℓ-dependence of the reactions. Therefore, only relative values for the nuclear structure factors have been extracted. These were then normalized so that the structure factors for the 5/2 5/2$^+$[402] states had the values expected on the basis of the Nilsson model.

There were several reasons for choosing the 5/2 5/2$^+$[402] level for this purpose. Firstly, the ℓ = 2 transitions leading to it result in some of the largest peaks in the experimental spectra. Also, this state had been previously assigned in

Figure 4.1.4

(^{3}He,d) angular distributions obtained for some known high spin states. The solid lines are the predicted angular distributions from DWBA calculations. Points without error bars may be assumed to have errors approximately equal to the radius of the circles.

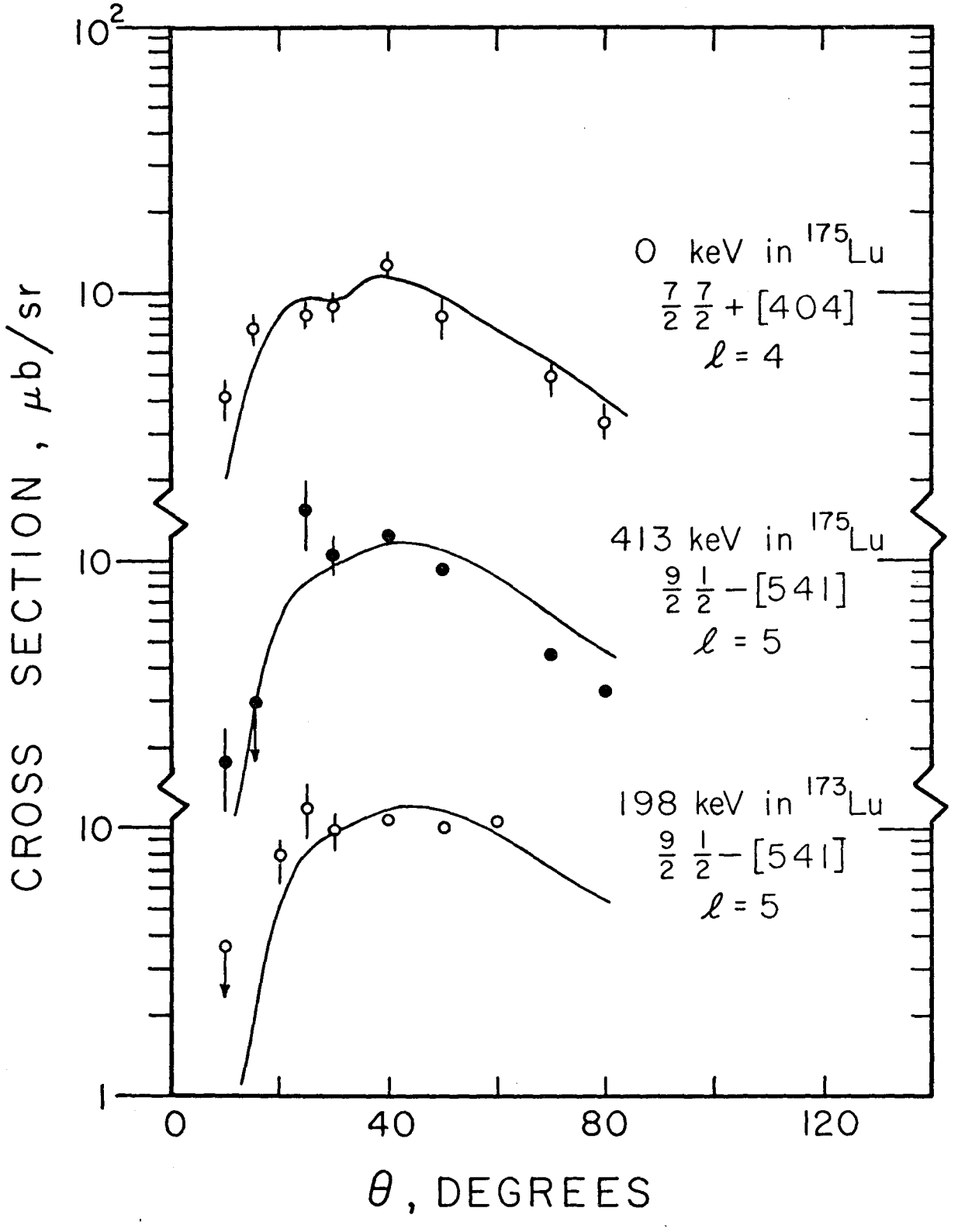
10^2
10
10
10
1
CROSS SECTION, μb/sr
0 keV in ^{175}Lu
$\frac{7}{2}\frac{7}{2}$ + [404]
ℓ = 4
413 keV in ^{175}Lu
$\frac{9}{2}\frac{1}{2}$ − [541]
ℓ = 5
198 keV in ^{173}Lu
$\frac{9}{2}\frac{1}{2}$ − [541]
ℓ = 5
0
40
80
120
θ, DEGREES

Figure 4.1.5

(^{3}He,d) angular distributions obtained for some low spin states. The solid lines result from predictions by DWBA calculations.

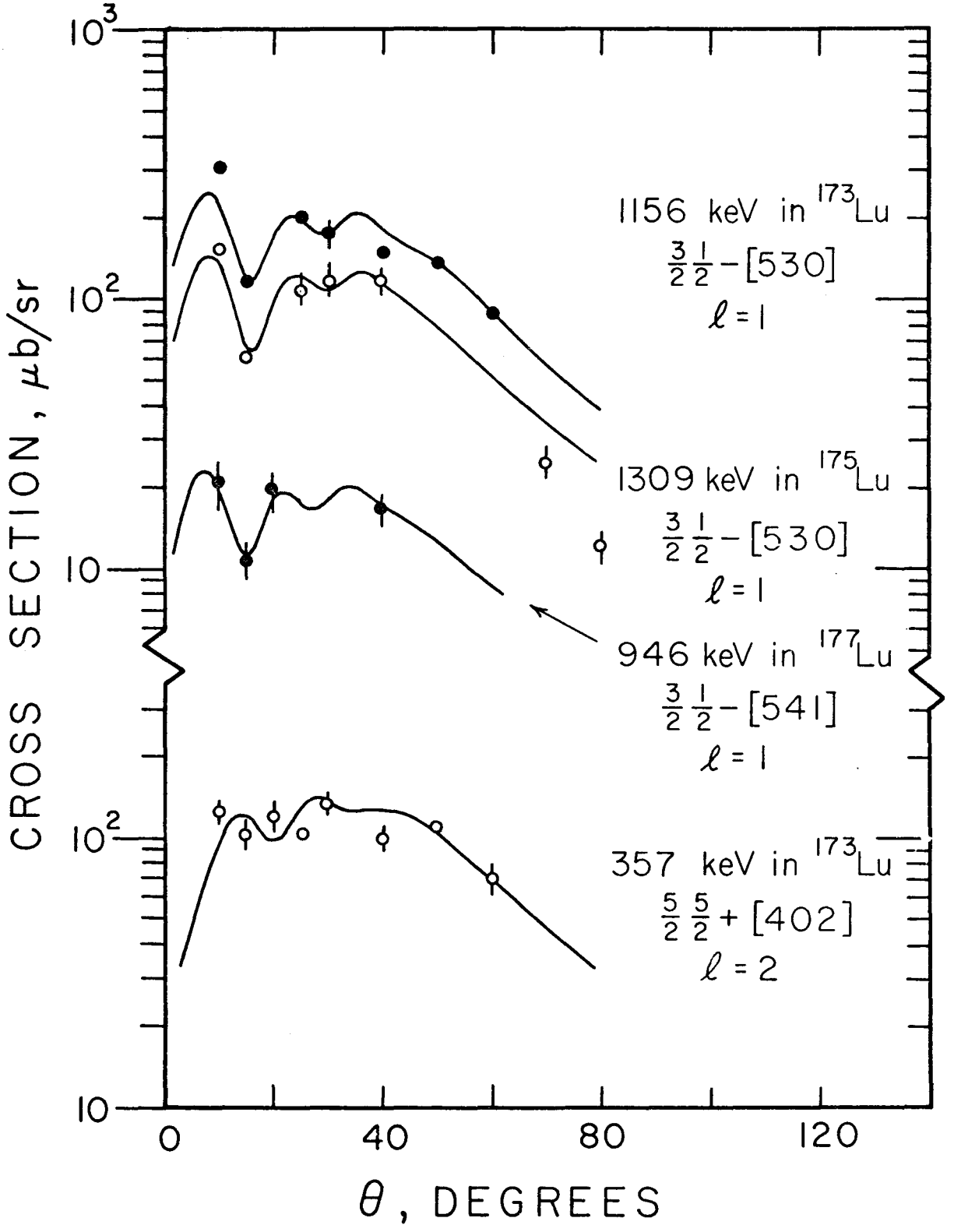
CROSS SECTION, μb/sr
θ, DEGREES
1156 keV in 173Lu
3/2 1/2 − [530]
ℓ = 1
1309 keV in 175Lu
3/2 1/2 − [530]
ℓ = 1
946 keV in 177Lu
3/2 1/2 − [541]
ℓ = 1
357 keV in 173Lu
5/2 5/2 + [402]
ℓ = 2

each of the three final nuclei. Finally, the Nilsson model and pairing theory indicate that the values of $C^2_{j\Omega}$ and U^2 for this state should both be nearly unity and perturbations by the Coriolis interaction are predicted to be negligible. Therefore the uncertainties in the theoretical spectroscopic factors are expected to be smallest for this particular state.

According the Nilsson model calculations, the 5/2 $5/2^+[402]$ state has a value for $C^2_{j\Omega}$ of 0.93. As this level appears at an excitation energy of $\approx$400 keV in each of the three final nuclei, the value of U^2 would be expected to be $\approx$0.9. The normalization factor was therefore chosen so that the average of the values of $C^2_{j\Omega}\,U^2$ for the 5/2 $5/2^+[402]$ states in ^{173}Lu and ^{177}Lu was 0.85. The corresponding group in ^{175}Lu was not included as it was not clearly resolved from other groups. In order to achieve this normalization, the DWBA cross sections for the (^{3}He,d) reaction were all multiplied by a factor of 0.78. In a similar manner, all the DWBA cross sections for the (α,t) reaction were multiplied by a factor of 1.13 in order that the values of $C^2_{j\Omega}\,U^2$ for the 5/2 $5/2^+[402]$ states in ^{173}Lu and ^{177}Lu would have an average of 0.85. The cross sections shown in figs. 3.6.1 and 3.6.2 have already been adjusted by the normalization factors discussed above. It should be pointed out that the uncertainties in the experimental values of the absolute cross sections are of the order of 20%. Thus the absolute values of these

normalization factors cannot be regarded as good tests for the DWBA calculations. However, the ratio of the normalization factors for the two reactions is significant since it involves relative experimental cross sections, for which the uncertainties are only $\lesssim$ 10%.

An examination of the angular distributions in fig. 3.6.1 and 3.6.2 shows that at $\theta = 45°$ the (α,t) cross sections for the various ℓ-values differ by a factor of only 2 or 3. On the other hand, the $(^3He,d)$ cross sections at $\theta = 40°$ exhibit a much stronger ℓ-dependence, varying by a factor of $\approx$ 15 between $\ell = 1$ and $\ell = 5$. Thus it would be expected that the experimental ratio of the $(^3He,d)$ and (α,t) cross sections might be useful as an indicator of the ℓ-value. In studies of levels in rhenium isotopes (Lu and Alford 1971) this ratio was often found to be more useful than a complete angular distribution for the determination of ℓ-values. The ratios of the $(^3He,d)$ and (α,t) cross sections are shown in fig. 4.2.1 plotted as a function of the $(^3He,d)$ Q-value. The solid lines are values obtained from the DWBA calculations and the data points are results from the present experiments for transitions to states of known ℓ. The fact that the $\ell = 2$ points fall quite close to the calculated line is, of course, a consequence of the normalization procedure described above, as the $\ell = 2$ points shown are due to the $5/2\ 5/2^+[402]$ levels. The $\ell = 4$ and $\ell = 5$ data points appear to be in good agreement with the predicted ratios.

Figure 4.2.1

Ratio of the (^{3}He,d) cross section to the (α,t) cross section as a function of the excitation energy for the three nuclei: ^{173}Lu, ^{175}Lu and ^{177}Lu. The incident energy of ^{3}He was 28 MeV and the deuterons were observed at 40°. The incident energy of α's was 30 MeV and the tritons were observed at 45°. The solid lines result from DWBA calculations for the various ℓ transfers. The points represent experimental ratios for states of known ℓ. The two points above the ℓ = 0 line are from experimental ℓ = 1 states. As discussed in section 4.2, the set of predicted curves has effectively been normalized to the two experimental ℓ = 2 points.

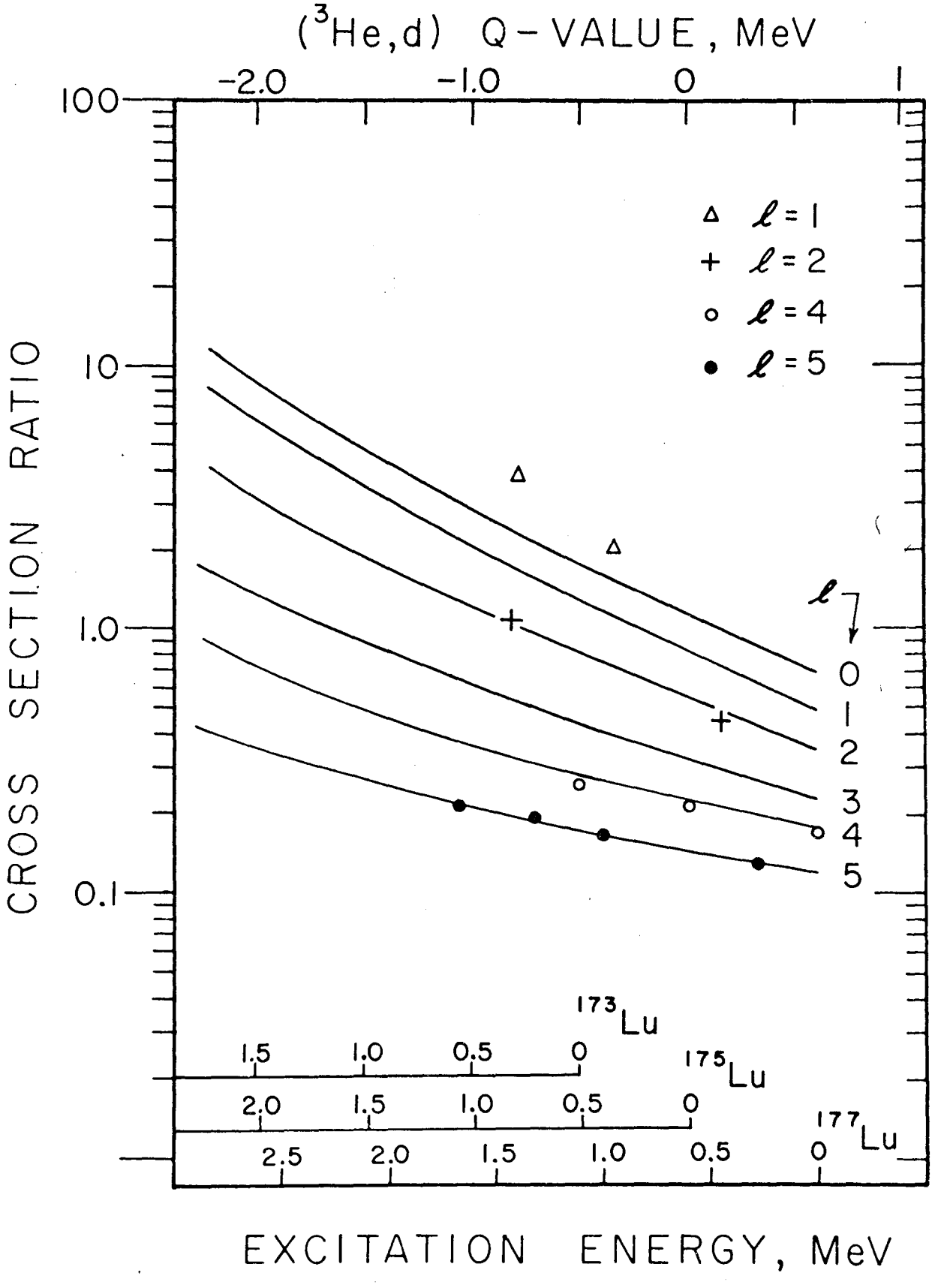
(3He,d) Q-VALUE, MeV
-2.0
-1.0
0
1
100
10
1.0
0.1
CROSS SECTION RATIO
Δ ℓ = 1
+ ℓ = 2
○ ℓ = 4
● ℓ = 5
ℓ
0
1
2
3
4
5
173Lu
1.5
1.0
0.5
0
175Lu
2.0
1.5
1.0
0.5
0
177Lu
2.5
2.0
1.5
1.0
0.5
0
EXCITATION ENERGY, MeV

Table 4.2.1

Spectroscopic Information for ^{173}Lu

State	Energy (keV)	Ratio of (^{3}He,d) and (α,t) cross Sections	Assigned ℓ	Calculated Cross Section Ratio for Assigned ℓ	U^2C^2 From (^{3}He,d) Reaction	U^2C^2 From (α,t) Reaction	U^2C^2 Predicted
7/2 $7/2^+[404]$	0	0.26	4	0.26	0.765	0.76	0.68
5/2 $1/2^-[541]$	123	1.29	3	0.47	0.67[a]	0.23[a]	0.23
1/2 $1/2^-[541]$	218		1	1.45	0.23[a]	0.27[a]	0.03
9/2 $1/2^-[541]$	198	0.19	5	0.19	1.09	0.88	0.94
3/2 $1/2^-[541]$	262	3.9	1	1.6	0.13	0.03	0.06
5/2 $5/2^+[402]$	357	1.11	2	1.1	0.83	0.78	0.83
1/2 $1/2^+[411]$	425	0.95	0	2.7	0.11[a]	0.27[a]	0.04
3/2 $1/2^+[411]$	435		2	1.1	0.23[a]	0.25[a]	0.23
5/2 $1/2^+[411]$	546	2.3	2	1.24	0.06[a]	0.04[a]	0.09
7/2 $1/2^+[411]$			4	0.36	0.36[a]	0.07[a]	0.06
11/2 $9/2^-[514]$	577	0.25	5	0.22	1.35	1.08	1.00
3/2 $3/2^-[532]$	889(?)		1	3.1	0.017		0.003
5/2 $3/2^-[532]$	950	2.7	3	0.84	0.18	0.10	0.08
9/2 $3/2^-[532]$	1143		5	0.27		0.45	0.47
1/2 $1/2^-[530]$	1157		1	3.9	0.46	0.22	0.03
3/2 $1/2^-[530]$			1	3.9			0.21

Table 4.2.1 continued

State	Energy (keV)	Ratio of (^{3}He,d) and (α,t) cross Sections	Assigned ℓ	Calculated Cross Section Ratio for Assigned ℓ	U^2C^2 From (^{3}He,d) Reaction	U^2C^2 From (α,t) Reaction	U^2C^2 Predicted
7/2 1/2$^-$[530]	1266	1.6	3	1.04	0.54	0.37	0.45
	654	0.55					
	1286	1.6					
	1363	2.7					
(I = 1/2)	1399	$\gtrsim$16	(0)	(7.6)	0.21	0.07	
	1700	5.1					
(I = 1/2)	1731	>23	(0)	(11)	0.21	<0.11	
	1733	1.8					

a) Spectroscopic factor if the entire cross section of this doublet is assumed to be of the assigned ℓ

Table 4.2.2

Spectroscopic Information for ^{175}Lu

State	Energy keV	Ratio of (^{3}He,d) and (α,t) cross Sections	Assigned ℓ	Calculated Cross Section Ratio for Assigned ℓ	U^2C^2 From (^{3}He,d) Reaction	U^2C^2 From (α,t) Reaction	U^2C^2 Predicted
7/2 $7/2^+$[404]	0	0.214	4	0.21	0.78	0.77	0.68
9/2 $7/2^+$[404]	115		4	0.22		0.048	0.006
5/2 $5/2^+$[402]	344	1.0	2	0.66	1.2[a]	1.05[a]	0.83
5/2 $1/2^-$[541]			3	0.39	1.51[a]	0.86[a]	0.23
1/2 $1/2^-$[541]			1	1.0	0.71[a]	0.90[a]	0.03
9/2 $1/2^-$[541]	414	0.16	5	0.17	1.14	1.06	0.90
3/2 $1/2^-$[541]	524	0.49	1	1.29	0.17[a]	0.48[a]	0.06
11/2 $9/2^-$[514]			5	0.17	(2.6)	0.86[a]	1.06
3/2 $3/2^-$[532]?	992		(1)	(2.0)	0.02		0.003
5/2 $3/2^-$[532]	1058	1.63	3	0.62	0.14	0.05	0.08
7/2 $3/2^-$[532]	1168	0.4	3	0.69	0.006	0.01	0.01
9/2 $3/2^-$[532]	1262	0.19	5	0.25	0.42	0.35	0.47
3/2 $1/2^-$[530]	1309	10.6	1	2.76	0.45	0.11	0.21
7/2 $1/2^-$[530]	1406	1.09	3	0.84	0.57	0.42	0.45
9/2 $1/2^-$[530]?	1695	0.47	(5)	(0.28)	0.17	0.11	0.08

Table 4.2.2 continued

State	Energy (keV)	Ratio of (^{3}He,d) and (α,t) cross Sections	Assigned ℓ	Calculated Cross Section Ratio for Assigned ℓ	U^2C^2 From (^{3}He,d) Reaction	U^2C^2 From (α,t) Reaction	U^2C^2 Predicted
11/2 1/2$^-$[530]?	1629	1.08	(5)	(0.27)	0.32	0.08	0.07
	628	0.97					
	668	0.57					
	755	1.27					
	872	0.46					
	1213	0.95					
(I = 3/2)	1338	1.45	(2)	(1.5)	0.32	0.19	
(I = 1/2)	1504	9.6	(0)	(4.8)	0.28	0.18	
	1550	0.52					
	1599	6.05					
	1788	11.1					
	1899	2.4					

a) Spectroscopic factor if the entire cross section of this multiplet is assumed to be of the assigned ℓ.

Table 4.2.3

Spectroscopic Information for ^{177}Lu

State	Energy (keV)	Ratio of (^{3}He,d) and (α,t) cross Sections	Assigned ℓ	Calculated Cross Section Ratio for Assigned ℓ	U^2C^2 From (^{3}He,d) Reaction	U^2C^2 From (α,t) Reaction	U^2C^2 Predicted
7/2 7/2$^+$[404]	0	0.16	4	0.17	0.86	0.91	0.68
9/2 7/2$^+$[404]	122	0.15	4	0.18	0.06	0.070	0.006
9/2 9/2$^-$[514]	150	0.2	5	0.12	0.12	0.08	0.01
11/2 9/2$^-$[514]	289	0.14	5	0.13	1.2	1.03	1.06
5/2 5/2$^+$[402]	458	0.45	2	0.48	0.88	0.91	0.83
3/2 1/2$^-$[541]	950	2.12	1	1.1	0.09	0.04	0.00
5/2 1/2$^-$[541]	759	0.66	3	0.35	0.49	0.25	0.23
9/2 1/2$^-$[541]	807	0.16	5	0.16	$\sim$1.4	1.33	0.94
1/2 1/2$^+$[411]	571	0.45	0	1.04	0.04[a]	0.10[a]	0.04
3/2 1/2$^+$[411]			2	0.52	0.09[a]	0.10[a]	0.23
5/2 1/2$^+$[411]	710	1.9	2	0.6	0.11[a]	0.05[a]	0.09
7/2 1/2$^+$[411]			4	0.25	0.59[a]	0.11[a]	0.06
5/2 3/2$^-$[532]	1382	1.05	3	0.51	0.10	0.05	0.08
9/2 3/2$^-$[532]	1612	(1.1)	5	0.21	0.42	0.42	0.47

Table 4.2.3 continued

State	Energy (keV)	Ratio of (^{3}He,d) and (α,t) cross Sections	Assigned ℓ	Calculated Cross Section Ratio for Assigned ℓ	U^2C^2 From (^{3}He,d) Reaction	U^2C^2 From (α,t) Reaction	U^2C^2 Predicted
3/2 1/2$^-$[530]	1635	2.98	1	0.21	0.21	0.17	0.21
7/2 1/2$^-$[530]	1724	0.64	3	0.65	0.26	0.26	0.45
(I = 3/2)	1089	0.47	(2)	(0.76)	0.12	0.22	
(I = 3/2)	1117	0.97	(2)	(0.76)	0.28	0.26	
	1286	1.46					
(I = 3/2)	1517	1.14	(2)	(1.04)	0.21	0.19	
	1748	0.70					
(I = 9/2)	1845	0.22	(5)	(0.22)	0.36	0.36	
	2035	0.95					

a) Spectroscopic factor if the entire cross section of this doublet is assumed to be of the assigned ℓ.

It is seen that the calculated ratios for $\ell = 0$ and $\ell = 1$ transitions both lie below the empirical $\ell = 1$ data points. This is probably due to inadequacies in the DWBA calculations for the (α,t) reaction for the very low ℓ-transfers as there is a serious momentum mismatch for such cases. The predicted (α,t) cross sections for $\ell = 0$ and $\ell = 1$ transitions are thus considered to be not too reliable, and in later sections the spectroscopic factors extracted from the $(^3He,d)$ data will be given more weight than those from the (α,t) results for ℓ-values of 0 and 1. On the other hand, the $\ell = 4$ and $\ell = 5$ transitions have rather small peaks in the $(^3He,d)$ spectra and for these cases the spectroscopic factors from the (α,t) data are considered to be more reliable.

Spectroscopic information for most of the states observed in this study is presented in tables 4.2.1 to 4.2.3. Experimental ratios of the $(^3He,d)$ and (α,t) cross sections are found in column 3 of these tables. For cases where the states were identified, the expected values of ratio are found in column 5.

4.3 The Nilsson and Coriolis mixing calculations

As may be seen in fig. 3.1.2, the general trends of the Nilsson diagram in the region of $\delta = 0.27$ lead one to expect the 71st proton to fall in the $7/2^+[404]$ orbital. This has been previously observed (Nuclear Data Sheets 1966)

as the ground state of the three nuclei ^{173}Lu, ^{175}Lu and ^{177}Lu. With the $7/2^+[404]$ orbital as the ground state it is expected that the $5/2^+[402]$ and the $9/2^-[514]$ orbitals should be seen at approximately the same relatively low excitation energy in all three nuclei. This conclusion is independent of moderate changes in deformation as all three levels exhibit a similar dependence on the deformation. At considerably higher energies, probably well above 1 MeV in the lutetium isotopes, the $1/2^+[400]$, $3/2^+[402]$ and $11/2^-[505]$ orbitals would be expected with an excitation energy again almost independent of the deformation.

In addition to these particle states, the orbitals $1/2^+[411]$, $3/2^+[411]$ and $7/2^-[523]$ would be expected as low lying hole states but these should not be populated strongly in the present experiments.

The other expected low lying states are the $1/2^-[541]$, $3/2^-[532]$ and the $1/2^-[530]$ orbitals which are all low spin states arising from the N = 5 oscillator shell. The energies of all these states as a function of deformation have opposite slope to that of the $7/2^+[404]$ orbital. As a result their energies, compared to the ground state, will depend quite sensitively on the deformation. All three orbitals are expected at about the same excitation relative to each other.

Another group of low lying states might be expected from the N = 6, $i_{13/2}$ spherical state. These are the $1/2^+[660]$, $3/2^+[651]$ and the $5/2^+[642]$ orbitals, which should be near

or below the $1/2^+[400]$ and $3/2^+[402]$ states. Evidence for the identification of all these states except the $5/2^+[642]$ has been obtained by Lu and Alford (1971) in the rhenium isotopes (Z = 73). However, none of the N = 6 states were clearly identified in the present measurements.

The emptiness factor, U^2, and the single quasi-particle energy were found using the results of pairing theory (Elbek and Tjøm 1969). The pairing parameters used were such that the Fermi surface was placed approximately 0.3 MeV below the unperturbed $7/2^+[404]$ band head. A diffuseness parameter, Δ, of 0.8 MeV was used. These parameters lead to a reasonable compression of the energies of the lower lying states as well as fairly good agreement with the observed spectroscopic factors.

In the three nuclei studied, conditions such as energy spacings and the nature of the orbitals allow significant mixing of certain orbitals by the Coriolis interaction. The effects are large enough that they must be considered in accounting for the observed spectroscopic factors but they are not so large that the unperturbed structure is entirely lost, as has been observed in some cases (Borgreen et al. 1969)

A calculation was performed to show typical effects of the Coriolis interaction using unattenuated matrix elements such as given in Appendix A . The Nilsson calculation as described in the previous section was used to obtain unperturbed

band head energies; the effect of pairing was calculated and the rotational bands were formed using a rotational parameter $(\frac{\hbar^2}{2\mathcal{I}})$ of 13 keV. This is the average rotational parameter observed (Burke et al. 1967) in the ground state rotational bands of the even-A ytterbium nuclei. Earlier studies (Valentin et al. 1962, Johansen et al. 1969, Maier 1965) on lutetium nuclei, where Coriolis mixing was not considered, have shown rotational parameters between 12.5 and 14 keV.

A comparison of the structure factors obtained as a result of the basic Nilsson calculation and those obtained after perturbation by the Coriolis interaction is shown in table 4.3.1. These calculations were carried out at a deformation, δ, of 0.27 with the Nilsson well parameters and pairing parameters as previously described. The predicted structure factors quoted in tables 4.2.1, 4.2.2 and 4.2.3, which include the effects of pairing and the Coriolis interaction, result from the same calculation.

In this calculation the following positive parity orbitals were considered: $1/2^+[400]$, $1/2^+[660]$, $1/2^+[411]$, $3/2^+[402]$, $3/2^+[651]$, $5/2^+[402]$, $5/2^+[642]$ and $7/2^+[404]$. None of the N = 6 states were observed, nor were the $1/2^+[400]$, $3/2^+[411]$ or $3/2^+[402]$ orbitals. The effect of the Coriolis interaction on the observed $7/2^+[404]$, $5/2^+[402]$ and $1/2^+[411]$ states was slight as they all arise from different spherical states. Had it been possible to identify the orbitals arising from the $i_{13/2}$ spherical state, very strong Coriolis

Table 4.3.1

Comparison of Predicted Structure Factors Before and After Coriolis Coupling

State	Unperturbed U^2C^2	Perturbed U^2C^2	State	Unperturbed U^2C^2	Perturbed U^2C^2
7/2 $7/2^+[404]$	0.67	0.68	5/2 $5/2^+[402]$	0.81	0.83
9/2	0.01	0.01	7/2	0.04	0.03
			9/2	0.02	0.01
1/2 $1/2^+[411]$	0.04	0.04			
3/2	0.22	0.23	3/2 $3/2^-[532]$	0.01	0.0
5/2	0.08	0.09	5/2	0.12	0.08
7/2	0.06	0.06	7/2	0.05	0.01
9/2	0.01	0.01	9/2	0.76	0.47
			11/2	0.03	0.01
9/2 $9/2^-[514]$	0.01	0.01			
11/2	0.85	1.06			

Table 4.3.1 continued

State	Unperturbed U^2C^2	Perturbed U^2C^2	State	Unperturbed U^2C^2	Perturbed U^2C^2
1/2 $1/2^-$[541]	0.03	0.03	1/2 $1/2^-$[530]	0.02	0.02
3/2	0.04	0.06	3.2	0.22	0.21
5/2	0.19	0.23	5/2	0.0	0.0
7/2	0.04	0.12	7/2	0.48	0.45
9/2	0.58	0.94	9/2	0.16	0.08
11/2	0.02	0.06	11/2	0.09	0.07

perturbations would have been expected. Mixing of the $1/2^+[400]$ and $3/2^+[402]$ states with the $1/2^+[660]$ and $3/2^+[651]$ states might also be significant though $\Delta N = 2$ mixing was not included in these calculations.

The following negative parity states were considered in the Coriolis coupling calculation: $1/2^-[530]$, $1/2^-[541]$, $3/2^-[532]$, $7/2^-[523]$, $9/2^-[514]$ and $11/2^-[505]$. The $h_{9/2}$ spherical state is the origin of both the $5/2^-[523]$ and the $3/2^-[532]$ orbitals. These two states were found to mix strongly even though the $5/2^-[523]$ state lies more than 1 MeV above the $3/2^-[523]$ orbital at a deformation of $\delta = 0.27$. It was noticed that better agreement with the experimental cross sections was obtained for the $1/2^-[541]$, $3/2^-[532]$ and $1/2^-[530]$ orbitals if the $5/2^-[523]$ orbital was not included in the calculation. The $5/2^-[523]$ band is unidentified in the current work. This result may indicate that this orbital, because of its very high excitation energy and many other possible forms of coupling, has ceased to exist as an entity capable of being handled by a simple single particle calculation.

The only negative parity hole state considered was the $7/2^-[523]$ orbital. Pairing considerations indicate this band should be weakly populated and it has not been observed in this work. The mixing of the unidentified 11/2 $11/2^-[505]$ state and the 11/2 $9/2^-[514]$ statetends to increase the structure factor of the latter to slightly more than unity.

The 11/2 $9/2^-$[514] state was strongly populated in all three nuclei.

The remaining strongly mixed states originate from the $1/2^-$[530], the $1/2^-$[541] and the $3/2^-$[532] orbitals. As may be seen from table 4.3.4 the only states with significant perturbations are the I = 5/2, 7/2 and 9/2 members where generally the lower lying $1/2^-$[541] states tend to have increased structure factors mainly at the expense of the $3/2^-$[532] band.

4.4 Interpretation of the results

4.4(i) The $7/2^+$[404] Orbital

This Nilsson orbital has previously been assigned as the ground state of each of the three lutetium isotopes studied. The present results are in good agreement with these assignments. The only rotational member which has a large structure factor is the I=7/2 band head, for which $C^2_{j\Omega} = 0.98$. The three $\ell = 4$ data points in fig. 4.2.1 correspond to these three I = 7/2 ground states. The values $C^2_{j\Omega} U^2$ deduced from the measured (^{3}He,d) and (α,t) cross sections are shown in tables 4.2.1, 4.2.2 and 4.2.3 to range from 0.75 to 0.9. These values are reasonable as U^2 should be appreciably less than unity for the ground states. As these values are all larger than one-half, the Fermi surface must lie below the $7/2^+$[404] orbital for all three nuclei. The variations in these values may be due partly to shifts

in the Fermi surface from one target nucleus to another. However, the combined uncertainties in the relative experimental cross sections and the relative DWBA sections are comparable to the observed variations.

The only other rotational member of the $7/2^+[404]$ band which might be expected to be observed in these reactions is that with j = 9/2 for which $C^2_{j\Omega}$ has the rather small value of 0.01. Small peaks corresponding to the previously known excitation energies for this level can be seen in the (α,t) spectra for ^{175}Lu and ^{177}Lu. These states would be expected to have very small cross sections in the (^{3}He,d) reaction and, although there is evidence for weak peaks in a number of the (^{3}He,d) spectra, a quantitative treatment is not practical. The values of $C^2_{j\Omega}\ U^2$ extracted from the (α,t) cross sections are 0.05 and 0.07, in ^{175}Lu and ^{177}Lu, respectively. These are larger than the expected values but it must be remembered that the cross sections involved are very small, and higher order processes in the reaction mechanism could be contributing to the strength (Burke and Waddington 1972). In fact, the present results are considered to be a good confirmation of the $7/2^+[404]$ assignment to these bands. The 9/2 $7/2^+[404]$ level has not previously been found in ^{173}Lu and has not been observed in the present study. The weak peak expected for this state has most likely been obscured by the strong peaks due to the 5/2 $1/2^-[541]$ and 1/2 $1/2^-[541]$ levels.

4.4(ii) The $5/2^+[402]$ Orbital

This Nilsson state has previously been assigned in ^{173}Lu, (Valentin et al. 1962) ^{175}Lu (Johansen et al. 1969) and ^{177}Lu (Maier 1965) at excitation energies of 358 keV, 353 keV and 458 keV, respectively. As it forms the ground states of the odd-mass rhenium nuclei (Z = 75) it is expected to appear as a particle state in the lutetium isotopes. Thus the emptiness factor, U^2, should be $\approx$0.9. The value of $C^2_{j\Omega}$ is calculated to be 0.93 for I = 5/2 at a deformation δ = 0.27. Therefore the cross sections for the I = 5/2 band heads are expected to be quite large. It was pointed out in section 4.2 that the strong transitions populating these levels have been used for the normalization of the DWBA intensities. The average of the values of $U^2C^2_{j\Omega}$ for this state in ^{173}Lu and ^{177}Lu has been set equal to 0.85. Johansen et al. (1969) have found that the 5/2 $5/2^+[402]$, 5/2 $1/2^-[541]$ and 1/2 $1/2^-[541]$ levels all lie fairly close together at energies of 343.4 keV, 353.6 keV and 358.2 keV, respectively in ^{175}Lu. Although these three levels are not resolved in the present work, the cross section in the large peak observed is consistent with the total expected for all three of these states.

The higher spin members of the $5/2^+[402]$ band are all predicted to have very small cross sections. Although the excitation energies for some of these states are known from previous works, the levels were not identified in the present study because the weak peaks were obscured by large peaks at nearby energies.

4.4(iii) The $9/2^-[514]$ Orbital

According to the Nilsson diagram shown in fig. 3.1.2 this orbital is also expected to appear as a low-lying particle state in the odd-A lutetium nuclei. It originates from the $h_{11/2}$ shell model configuration and thus even at large deformations it has a value of $C^2_{j\Omega} \approx 0.99$ for I = 11/2. The calculations described in section 4.3 predict that the value of $U^2C^2_{j\Omega}$ for this state should be slightly greater than unity, due to admixtures of the 11/2 $7/2^-[523]$ and 11/2 $11/2^-[505]$ states mixed in by Coriolis coupling. Therefore one would expect the I = 11/2 member of the rotational band to be populated by a strong ℓ = 5 transition and the I = 9/2 band head to be populated by a very weak ℓ = 5 transition. The rotational band based on this state has been well studied (Nuclear Data Sheets 1966) up to I = 17/2 in ^{177}Lu, with the I = 9/2 and I = 11/2 levels found at 150 and 289 keV, respectively. The strong transition to the j = 11/2 state is observed in both the (^{3}He,d) and (α,t) reactions and the value of $U^2C^2_{j\Omega}$ extracted from the (α,t) cross section is 1.03. Thus the agreement between experiment and prediction is very good.

The value of $U^2C^2_{j\Omega}$ for the 9/2 $9/2^-[514]$ level in ^{177}Lu is shown in table 4.2.3 to be 0.08. Although this much larger than the predicted value of 0.01, the difference is not considered to be a serious discrepancy. As explained earlier, the extraction of structure factors for weakly populated states may not

be too reliable due to higher order effects in the reaction mechanism.

The $9/2^-[514]$ band head has been previously assigned at 396 keV in ^{175}Lu. The weak peak expected for this state is not seen in the present studies due to the presence of a strongly populated level at 413 keV. However, the I = 11/2 member of the rotational band has been found in the (α,t) reaction at an excitation energy of 524 keV. This state is not completely resolved from the $3/2\ 1/2^-[541]$ level at 515 keV but since the latter is populated by an $\ell = 1$ transition with a small structure factor ($C^2_{j\Omega} \approx 0.04$), it should have a negligible (α,t) cross section. When the (α,t) intensity observed for the doublet is assumed to be due entirely to the $11/2\ 9/2^-[514]$ level, the value of $U^2C^2_{j\Omega}$ obtained is 0.86. In the $(^3He,d)$ reaction, the intensity expected for the $\ell = 1$ transition to the $3/2\ 1/2^-[541]$ state with $U^2C^2_{j\Omega} \approx 0.04$ is comparable to that for the $\ell = 5$ transition with $U^2C^2_{j\Omega} \approx 1$. This is consistent with the observations that the $(^3He,d)$ cross section observed for the composite peak is 2.6 times larger than that for an $\ell = 5$ transition with $U^2C^2_{j\Omega} = 1$. Thus the complex peak in the $(^3He,d)$ spectrum is interpreted as the $\ell = 5$ transition with $U^2C^2_{j\Omega} \approx 0.86$ to the $11/2\ 9/2^-[514]$ level at 524 keV plus the $\ell = 1$ transition with $U^2C^2_{j\Omega} \approx 12\%$ to the $3/2\ 1/2^-[541]$ level previously assigned at 515 keV. The observed centroid position for this doublet is 513 keV in the $(^3He,d)$ reaction.

The $9/2^-[514]$ orbital has not been previously assigned in ^{173}Lu. In the present studies a strong transition with a cross section ratio indicating $\ell = 5$ is observed at 577 keV. The (α,t) cross section corresponds to a value of $U^2C^2 = 1.08$. As the 11/2 $9/2^-[514]$ state is the only one expected to have such a strong $\ell = 5$ population in this energy region, the 577 keV level is assigned to it. The rotational spacing between the I = 9/2 and I = 11/2 members of this band is 139 keV in ^{177}Lu and 133 keV in ^{175}Lu. If the average of these is assumed for the I = 9/2 to I = 11/2 energy difference in ^{173}Lu, the band head would be expected to be at $\sim$446 keV. In the present studies, a weak peak at this energy would be obscured by peaks due to nearby states.

4.4(iv) The $1/2^-[541]$ Orbital

This is perhaps the most interesting of the single particle states studied in the present work. The theoretical value for the decoupling parameter is 3.1, which indicates that the I = 5/2 member of the rotational band should be lowered to an energy just above that of the I = 1/2 band head. Valentin *et al.* (1962) assigned the 123 keV, 128 keV and 263 keV levels in ^{173}Lu to be the I = 5/2, 1/2 and 3/2 band members, respectively. In the original Nilsson calculations, the $1/2^-[541]$ orbital was not predicted to occur at such a low excitation energy in the lutetium isotopes. The parameters used in later calculations were adjusted to lower the energies

of this state and of other states originating from the $h_{9/2}$ shell model configuration.

One of the initial aims of the present study was to make an independent check on this assignment of the $1/2^-[541]$ band. As the orbital in question originates from the $h_{9/2}$ shell model state, the value of $C^2_{j\Omega}$ for I = 9/2 is quite large (0.58). Thus the I = 9/2 rotational member should be populated readily by the single particle transfer reactions. If one makes use of the rotational parameter and decoupling parameter found by Valentin et al. (1962), the I = 9/2 level would be expected at $\approx$190 keV in ^{173}Lu. As there were no other known levels near this energy, the proton transfer studies were undertaken, in order to locate the I = 9/2 state. The peaks seen in fig. 4.1.1 corresponding to an excitation energy of 198 keV have been attributed to this level. The (^{3}He,d) angular distribution for this transition is shown in fig. 4.1.4 and is consistent with the DWBA prediction for an ℓ = 5 transfer. The (^{3}He,d) and (α,t) cross section ratio also indicates that ℓ = 5.

The value of $U^2C^2_{j\Omega}$ extracted from the cross sections is found in table 4.2.1 to be 0.88. This is larger than the expected value for the pure state, for which $C^2_{j\Omega}$ = 0.58, as the emptiness factor U^2 should be $\approx$0.8 at the observed excitation energy. Much better agreement is obtained when one takes into account the Coriolis mixing discussed in section 4.3. The calculation described indicates that the

mixing increases the structure factor for the 9/2 $1/2^-$[541] state mainly at the expense of that for the 9/2 $3/2^-$[532] level. The predicted value of $U^2C^2_{j\Omega}$ for the 9/2 $1/2^-$[541] state, according to the present mixing calculation is 0.90. This is in excellent agreement with the value of $U^2C^2_{j\Omega}$ of 0.88 extracted from the (α,t) cross section.

It can be seen from table 4.2.1 that the populations of the I = 5/2, I = 1/2 and I = 3/2 levels are also in good agreement with expectations, although the first two of these states are unresolved. The combination of the observations described above constitute a very strong confirmation for the previous assignment (Valentin et al. 1962) of the $1/2^-$[541] band in ^{173}Lu.

This orbital has also been observed in ^{175}Lu by Bjørnholm et al. (1965) and by Johansen et al. (1969). The I = 5/2, 1/2 and 3/2 levels were assigned at energies of 353.6 keV, 358.2 keV and 514.9 keV, respectively. The present results are consistent with these assignments, although the I = 1/2 and I = 5/2 levels are not completely resolved from the 5/2 $5/2^+$[402] level. Also the I = 3/2 state is unresolved from the 11/2 $9/2^-$[514] level as described in section 4.4(iii). It is noted, however, that the total (α,t) and (^{3}He,d) cross sections to each of these composite groups are in good agreement with the sums of the expected cross sections for the levels assumed in the groups. Furthermore, a previously unobserved level at 414 keV has been found, which has all the expected properties of the 9/2 $1/2^-$[541] state. The ratio of the

(^{3}He,d) and (α,t) cross sections indicates that this is an ℓ = 5 transition and the (^{3}He,d) angular distribution is consistent with this ℓ-value. The value of $U^2C^2_{j\Omega}$ is shown in table 4.2.2 to be 1.06. As in ^{173}Lu, this is higher than the expected value for the pure 1/2$^-$[541] orbital, and again, the Coriolis mixing offers a reasonable explanation for the increased strength. The increase in the value of $U^2C^2_{j\Omega}$ from 0.88 to 1.06 as one goes from ^{173}Lu to ^{175}Lu is probably due mainly to the increase in U^2, as the band head energy has increased from 128 to 358 keV.

The 1/2$^-$[541] orbital has not been observed previously in ^{177}Lu. On the basis of the present results, the I = 5/2, I = 9/2 and I = 3/2 members of its rotational band have been assigned at 759 keV, 807 keV and 946 keV respectively. The level at 807 keV has a cross section ratio and a (^{3}He,d) angular dependence which indicates ℓ = 5. The value of $U^2C^2_{j\Omega}$ for this state is $\approx$1.3 although there is a fairly large uncertainty on this result due to nearby levels. The 946 keV level has a cross section ratio which indicates $\ell \leq 1$. Also, the (^{3}He,d) angular dependence shows a dip at θ = 15°, a feature expected only for ℓ = 1 transitions. Hence it has been interpreted as the 3/2 1/2$^-$[541] level. The assignment of the I = 5/2 member to the group at 759 keV has been made because the cross section ratio for this group is consistent with an ℓ-value of 2 or 3. Also, it is the only state in this energy region with a cross section as large as that expected for the 5/2 1/2$^-$[541] level. This assignment results

in an energy difference between the I = 5/2 and I = 9/2 levels of 50 keV, which must be compared with 77 keV in ^{173}Lu and 65 keV in ^{175}Lu. The level at 759 keV is probably the same one observed by Michaud et al. (1970) at 761.65 keV by means of (n,γ) studies. They concluded that the spin had a value of either 3/2 or 5/2. It is not clear from the present studies whether the 1/2 1/2$^-$[541] band head is included in the 759 keV group or in another group at 790 keV. The latter is just barely resolved from the I = 9/2 level at 807 keV. Recently, Manfrass et al. (1971) have redone the (n,γ) studies and, using the present data as a starting point, have been able to confirm that spins I = 5/2 and 9/2 of the 1/2$^-$[541] orbital lie at 761.6 and 811.4 keV respectively. Also the spin I = 5/2 member was found to be an isomer with $t_{1/2}$ =35 nsec which seems quite reasonable when compared to the work on the 1/2$^-$[541] isomers in the odd mass lutetium isotopes performed by Bjørnholm et al. (1965).

It is noted that this orbital moves up to higher excitation energies as the neutron number increases. This may be due to differences in deformation for the lutetium isotopes. The 5/2$^+$[402] and 9/2$^-$[514] Nilsson orbitals, which are more or less parallel to the 7/2$^+$[404] state in fig. 3.1.2 have been found to appear at approximately the same excitation energy in each of the three isotopes. The 1/2$^-$[541] orbital has the opposite slope in fig.3.1.2, and thus

the increase in its excitation energy with increasing neutron number could be explained by a decrease in deformation from $\delta \gtrsim 0.27$ for ^{173}Lu to $\delta \gtrsim 0.25$ for ^{177}Lu.

4.4(v) The $1/2^+[411]$ orbital

This orbital appears as a proton hole state in the lutetium nuclei. Therefore it does not have a large value for U^2 and is populated rather weakly in the stripping reactions. The decoupling parameter for this band is typically found to be about - 0.8 and, as a result, the I = 1/2 and I = 3/2 rotational members are at nearly the same energy. In ^{173}Lu, the I = 1/2, I = 3/2 and I = 5/2 band members were previously assigned at 425.0 keV, 434.6 keV and 545.8 keV, respectively. In the present work the first two of these were not resolved. Therefore, the analysis of the data will be restricted to comparing the cross sections in the groups observed at 428 keV with the expected values. For the pure $1/2^+[411]$ state the values of $C^2_{j\Omega}$ predicted for I = 1/2 and I = 3/2 are 0.09 and 0.53, respectively. If the value of U^2 were unity, the predicted total cross sections for the doublet would be 58 μb/sr for the (^{3}He,d) reaction and 65 μb/sr for the (α,t) reaction. The corresponding observed cross sections are 24 μb/sr and 25 μb/sr, respectively, which are ∿40% of the values expected for $U^2 = 1$. Thus, the experimental results are consistent with a value of U^2 of $\gtrsim 0.4$.

The pairing calculations mentioned in section 4.3 indicate that a hole state at an excitation energy of ≳0.5 MeV

would be expected to have an emptiness factor of only ≈0.10. The fact that the observed strength is several times larger than expected is unexplained, but may be due to the presence of another unresolved state near 428 keV in ^{173}Lu.

In ^{177}Lu, the $1/2^+[411]$ band head has been previously assigned at 569.62 keV. If the observed particle groups at 571 keV are assumed to be due to the I = 1/2 and I = 3/2 doublet, the experimental cross sections are consistent with those expected for a pure state with U^2 =0.15. This is in good agreement with the expected value. Manfrass et al. (1971) have placed the spin I = 5/2 and 7/2 states at 694 and 714 keV respectively. The peak at 710 keV in the proton transfer data is more intense than expected for this assignment. However, it is not possible to rule out the assignment of this peak to the $1/2^+[411]$ band.

The $1/2^+[411]$ orbital has not previously been assigned in ^{175}Lu. It is seen from the spectra in fig. 4.1.2 that there are unassigned particle groups at excitation energies of 628, 668, 755 and ≈872 keV. The only one of these groups which has a cross section ratio and structure factor similar to those for the states discussed above in ^{177}Lu is the one at 668 keV. Although the 668 keV level could be due to the I = 1/2 and I = 3/2 members of the $1/2^+[411]$ band, it is felt that there is not sufficient evidence to make an assignment.

4.4(vi) Assignment of the $1/2^-[530]$ and $3/2^-[532]$ orbitals

The observed spectra show a remarkable similarity

at higher excitation energies if one compares regions centered near 1157 keV in ^{173}Lu, 1309 keV in ^{175}Lu and perhaps less clearly above 1635 keV in ^{177}Lu. The larger peaks in these regions have approximately the same intensities and spacings. Corresponding peaks display similar ratios for the (^{3}He,d) and (α,t) cross sections. In the two lighter nuclei where more complete angular distributions were taken, the respective major peaks have similar angular distributions. In ^{177}Lu the partial angular distributions are consistent with the angular distribution for the larger peaks in the ^{173}Lu and ^{175}Lu spectra. It is thus reasonable to assume that the observed structure arises from the same orbitals in each of the three nuclei. An indication of the states involved is provided in that the observed structure lies at an excitation energy of approximately 850 keV above the $1/2^{-}[541]$ state in each nucleus. It is expected that the $3/2^{-}[532]$ and $1/2^{-}[530]$ orbitals, the next low lying states of the N = 5 oscillator shell, would lie at about this excitation above the $1/2^{-}[541]$ rotational band. The detailed evidence for these assignments is discussed in the following subsections.

(a) <u>The $1/2^{-}[530]$ orbital</u> In ^{173}Lu a large peak lies at 1156 keV in the (^{3}He,d) spectrum. As in seen in fig. 4.1.5 this peak possesses a characteristic dip in the angular distribution at θ = 15° indicative of an ℓ = 1 transition. The peak is broader than the single peaks observed at lower

energies however, and the cross section ratio is not in good agreement with those for other $\ell = 1$ transitions. In the (α,t) spectrum the peak has shifted to an energy of 1143 keV. The energy shift and the cross sections in the $(^3He,d)$ and (α,t) reaction are consistent with an $\ell = 5$ transition with a strength, U^2C^2, of 0.45 to a state at 1143 keV and an $\ell = 1$ transition with a strength, U^2C^2, of 0.46 to a state at 1157 keV. The $\ell = 5$ component at 1143 keV is discussed in the next subsection as the $I = 9/2$ member of the $3/2^-[532]$ rotational band. The only Nilsson state with significant $\ell = 1$ strength expected in this region is the $1/2^-[530]$ orbital, for which the calculation in section 4.3 predicts values for the perturbed structure factors (U^2C^2) of 0.02 and 0.23 for the $I = 1/2$ and $I = 3/2$ rotational band members, respectively. The model predicts the two states ought to be less than 50 keV apart. In the light of this information the level seen in this work at 1166 keV has been assigned as the $3/2\ 1/2^-[530]$ state. Valentin et al. (1962) have seen a level at 1160.8 keV in ^{173}Lu which was thought to be an $I = 3/2^-$ or $I = 1/2^-$ state. This level, which was observed by Brenner (1970), decays to the lower angular momentum members of the $1/2^-[541]$ band. Due to the uncertainty in stripping off the $\ell = 5$ strength it is felt that the 1157 keV state possibly corresponds to the level seen by Valentin et al. (1962) at 1160.8 keV.

Fig. 4.1.5 shows the (^{3}He,d) angular distribution for the 1309 keV peak in ^{175}Lu. The characteristic dip at $\theta = 15°$ combined with a structure factor similar to that of the 1166 keV state in ^{173}Lu leads one to assign the 1309 keV level in ^{175}Lu as the 3/2 1/2$^-$[530] state. Its cross section ratio lies between those expected for $\ell = 0$ and $\ell = 1$ transitions. The nuclear structure factor (U^2C^2) for the 3/2 1/2$^-$[530] state is observed to be 0.45 in the (^{3}He,d) reaction. As in ^{173}Lu this is twice that predicted for this state. Again the cross section for the I = 1/2 member of the 1/2$^-$[530] band is predicted to be small compared to that for the I = 3/2 member.

The 7/2 1/2$^-$[530] level is expected to have structure factors (U^2C^2) of approximately 0.5 and to lie about 105 keV above the 3/2 member of the band. In each case such a state exists. This state has been assigned in ^{173}Lu at 1260 keV to a peak for which the value of U^2C^2, averaged between the (^{3}He,d) and (α,t) results, is 0.45. In ^{175}Lu it has been assigned to a peak at 1406 keV which has an average value for U^2C^2 of 0.5. The agreement with the model prediction is very good in these two cases.

The ^{177}Lu spectra do not exhibit clean singlet peaks in the region of the 1/2$^-$[530] rotational band. As in ^{173}Lu, a high spin state appears on the low excitation energy side of the strong peak at 1635 keV in the (^{3}He,d) spectrum. Although complete angular distributions were not taken, the

group at 1635 keV has a dip in the (^{3}He,d) cross section at $\theta = 15°$ as is expected for an $\ell = 1$ transition. This level has a value of U^2C^2=0.21 and has been assigned to the 3/2 1/2$^-$[530] state. The high spin state, seen clearly in the (α,t) spectrum at 1620 keV, has been assigned as the 9/2 3/2$^-$[532] state. The peak assigned to the 7/2 1/2$^-$[530] state at 1732 keV has an average structure factor, U^2C^2, of 0.26. It is interesting to note that the two peaks attributed to the 1/2$^-$[530] orbital in ^{177}Lu have about one half the expected nuclear structure factor, U^2C^2, whereas in the two lighter nuclei the agreement with the model is very good. This may be an indication of the model starting to break down at high excitation energies possibly due to coupling with other higher lying states.

A conjecture has been made for the positions of the I = 9/2 and I = 11/2 members of the 1/2$^-$[530] band in ^{175}Lu. The Coriolis coupling calculation suggests those two states ought to have nuclear structure factors (U^2C^2) of 0.1. The states at 1695 and 1628 keV have approximately the energies expected for the I = 9/2 and the I = 11/2 members, respectively, and the (α,t) strengths agree very well. The (^{3}He,d) structure factors are in poor agreement possibly because these peaks are weak and the level density is high in this region.

(b) <u>The 3/2$^-$[532] orbital</u> At a slightly lower energy than the 1/2$^-$[530] orbital the Nilsson model predicts the existence of the 3/2$^-$[532] state. This orbital is strongly

mixed by the Coriolis interaction with the $1/2^-[541]$ and $1/2^-[530]$ orbitals. As mentioned in the previous subsection the (^{3}He,d) and (α,t) spectra indicated the presence of a state at 1143 keV in ^{173}Lu which was populated by an $\ell = 5$ transition with a strength, U^2C^2, of 0.45. This has been assigned to be the 9/2 $3/2^-[532]$ level. For this state the model predicts a structure factor (U^2C^2) of 0.5, which is in good agreement with the value from the (α,t) cross section. The nearby $\ell = 1$ transition to the 3/2 $1/2^-[530]$ level is so strong in the (^{3}He,d) spectrum that the $\ell = 5$ contribution could not be successfully extracted from the (^{3}He,d) data.

One should expect to see the I = 5/2 rotational band member with a strength (U^2C^2) of 0.07 approximately 210 keV lower than the I = 9/2 level. The only state of sufficient strength in this region is the one at 950 keV. It is probably the 5/2 $3/2^-[532]$ state even though the cross section ratio is not in good agreement with that predicted for an $\ell = 3$ transition. The observed structure factor (U^2C^2) is 0.14 when the results from the reactions are averaged.

Another argument for the assignment of $3/2^-[532]$ orbital in this manner is the existence of a level seen by Valentin et al. (1962) at 888 keV. This level was suspected of having a spin and parity of $3/2^-$ or $1/2^-$ on the basis of measurements of the β-decay of ^{173}Hf. Recent measurements by Brenner (1970) indicate that the level at 889 keV most likely has a spin of 3/2. This level is observed to decay

by E2 transitions to lower spin members of the $1/2^-[541]$ rotational band. In the light of the stripping data, this could very well by the $3/2^-[532]$ band head. On the basis of the Coriolis coupling calculations the I = 3/2 band head is expected to lie 77 keV below the I = 5/2 rotational member. The predicted structure factor (U^2C^2) for this state is less than 0.003 and there is no observed population in the present work. Similarly the 7/2 $3/2^-[532]$ state is unobserved. Although the I = 11/2 member is expected to have a strength, U^2C^2, of about 0.1 it happens to be obscured in a region of very high level density around 1325 keV excitation.

In the ^{175}Lu spectra the peak at 1262 displays an ℓ = 5 cross section ratio and has been assigned as the I = 9/2 member of the $3/2^-[532]$ band. The structure factor (U^2C^2) is 0.42 as compared to a predicted value of 0.5. There is a peak at 1058 keV which has been assigned to the 5/2 $3/2^-[532]$ level. Although this state has a cross section ratio twice as large as expected for an ℓ = 3 transition, the absolute cross sections are not large and thus the ratio is sensitive to any weakly populated unresolved states. The average spectroscopic strength (U^2C^2) is 0.10; the expected value is 0.07.

Almost entirely on the basis of energy considerations, conjectures have been made about the location of the I = 3/2 and I = 7/2 members of this rotational band in ^{175}Lu. A state of low-ℓ transfer is seen at 992 keV with a (^{3}He,d)

structure factor (U^2C^2) of 0.02. Another state lies at 1168 keV with a strength, U^2C^2, of 0.01. These peaks could possibly be the 3/2 $3/2^-[532]$ and the 7/2 $3/2^-[532]$ states respectively.

The (α,t) spectrum of ^{177}Lu reveals a doublet at 1638 keV and 1620 keV. The higher energy component has been already discussed as being the 3/2 $1/2^-[530]$ state. The (α,t) cross section for the lower energy component leads to a structure factor (U^2C^2) of 0.42 for an ℓ = 5 transition. The level at 1620 (with an error of 7 keV) has been assigned as the 9/2 $3/2^-[532]$ state. The observed (α,t) structure factor agrees very well with the model predictions.

The I = 5/2 component of this orbital has been tentatively identified at 1382 keV. As in the other nuclei the weak peak does not possess a cross section ratio in good agreement with an ℓ = 3 transition. The average of the structure factors from the (^{3}He,d) and (α,t) reactions is 0.07.

In each of the three nuclei the assignment of the $3/2^-[532]$ band was based largely on a single ℓ = 5 transition. It is noted that the $11/2^-[505]$ orbital is expected as a particle state in these nuclei and could also result in strong ℓ = 5 transitions. However, it is felt that the ℓ = 5 transitions observed in the present work are more likely due to the $3/2^-[532]$ orbital than the $11/2^-[505]$ state, because their excitation energies all appear to be approximately the same amount above the $1/2^-[541]$ band. This would be expected for the $3/2^-[532]$ orbital as it is parallel to the

$1/2^-[541]$ orbital in fig. 3.1.2. However, the $11/2^-[505]$ orbital has the opposite slope in the Nilsson diagram and should thus appear at a different energy relative to the $1/2^-[541]$ state as the deformation changes between ^{173}Lu and ^{177}Lu. The spacing between the I = 9/2 band members of the $3/2^-[532]$ and the $1/2^-[541]$ orbitals is 945 keV in ^{173}Lu, 848 keV in ^{175}Lu and 805 keV in ^{177}Lu.

4.4(vii) Other Bands

In addition to the states which have been identified in these and in previous measurements, a number of other intrinsic states might be expected to appear in the energy region studied here. The expected bands are difficult to identify unambiguously solely on the basis of stripping measurements since only a single state in each band should be strongly excited. Although it may be difficult to decide whether an observed transition represents a given band, the absence of an appropriate transition makes it possible to conclude that the band in question in not located in the region under study.

Two positive parity bands, $1/2^+[660]$ and $3/2^+[651]$, both arising from the $i_{13/2}$ spherical state, might be expected in the neighbourhood of the observed $3/2^-[532]$ and $1/2^-[530]$ bands. In the absence of Coriolis mixing, each of these positive parity bands would give rise to a strong $\ell = 6$ transition to the spin I = 13/2 member of the band. The Coriolis

mixing is expected to be very strong, however, with the result that most of the $\ell = 6$ strength from both bands should be concentrated in the spin I = 13/2 member of the lower band. Thus these bands would be characterized by a single $\ell = 6$ transition with $U^2C^2>1$ at an excitation of 1.5 to 2 MeV. None of the measured spectra exhibit such a transition; and it must be concluded that these bands do not appear below 2 MeV.

The $9/2^-[514]$ band is well known as a low-lying state in all three isotopes. The next band arising from the $h_{11/2}$ spherical state, $11/2^-[505]$, might then be expected at an excitation of about 2 MeV. Its characteristic signature would be an $\ell = 5$ transition with $U^2C^2 \approx 0.8$ after Coriolis mixing has been considered. No such transition is observed below 2 MeV in ^{173}Lu and ^{175}Lu. In ^{177}Lu, a transition with $\ell = 5$ and $U^2C^2 \approx 0.36$ is observed at 1845 keV. This may represent some of the expected strength, since the companion $9/2^-[514]$ band occurs at lowest excitation in ^{177}Lu.

Two other bands which may be expected to fall rather close together in energy are those based on the $1/2^+[400]$ and $3/2^+[402]$ orbitals. The former should be characterized by an $\ell = 0$ transition with $U^2C^2 \approx 0.8$. Each should give rise to a prominent peak in the deuteron spectrum. These states have been clearly seen in the odd rhenium isotopes (Lu and Alford 1971). There, the strength of the expected strong transition is split into two or more components, but the total expected strength is observed. The centroid of the observed strength lies close to the $11/2^-[505]$ band head, as predicted by the

Nilsson model (fig. 3.1.2). Because of the greater deformation in the lutetium isotopes, we might expect these bands to be located somewhat below the $11/2^-[505]$ orbital in the present measurement.

In ^{173}Lu states are observed at 1399 and 1731 keV, with a cross section ratio consistent with $\ell = 0$ or 1. It is probable that they are in fact $\ell = 0$ transitions, since if $\ell = 1$ they would contain considerably more strength than is expected for $\ell = 1$ transitions in this region. Assuming that they are $\ell = 0$, the total observed strength in both states is about one third of that expected for the $1/2^+[400]$ band. No strong $\ell = 2$ transitions are observed, and there is no evidence for the $3/2^+[402]$ band in ^{173}Lu.

In ^{175}Lu a state is observed at 1338 keV which appears to be populated via an $\ell = 2$ transition, with a strength about one third of that expected for $3/2^+[402]$ band. States at 1504 and 1550 keV show transitions consistent with an $\ell = 0$ assignment and total strengths about half that expected for $1/2^+[400]$ orbital.

In ^{177}Lu, strong transitions are observed to states which are members of poorly resolved groups. States at 1089, 1117 and 1517 keV show cross section ratios consistent with $\ell = 2$ transitions and a total strength of about 75% of that expected for $3/2^+[402]$ orbital. The only possible candidate for an $\ell = 0$ assignment is the state at 1296 keV. The cross section ratio in this case is actually closer to

that for an $\ell = 1$ transition. It should be noted however, that the state is not clearly resolved, and furthermore, that no additional $\ell = 1$ strength is expected in this region. If an $\ell = 0$ assignment is assumed, the state would contain about 25% of the strength expected for $1/2^+[400]$ orbital.

It is thus seen that a substantial fraction of the strength expected in the $1/2^+[400]$ and $3/2^+[402]$ bands may be present in the odd lutetium isotopes studied here. The strength is fragmented, however, and the part observed appears at somewhat lower energy than expected. This is quite analogous to the situation in the odd mass rhenium isotopes where these two bands occur at lower energy, yet still show strong splitting of the total strength. Calculations by Soloviev et al. (1966) have predicted such fragmentation of the strength of these bands in ^{171}Lu.

CHAPTER 5

THE ODD-ODD NUCLEUS ^{174}Lu

The nucleus ^{174}Lu has been carefully studied by Jones and Sheline (1970) using the ^{175}Lu(d,t)^{174}Lu reaction. The odd target proton is in the $7/2^+[404]$ orbital and thus the only states identified in the (d,t) reaction are those formed by coupling the $7/2^+[404]$ proton to the unpaired neutron remaining after the reaction. The present chapter describes the results of a study of ^{174}Lu using the ^{175}Lu(^{3}He,α)^{174}Lu, ^{173}Yb(α,t)^{174}Lu, ^{173}Yb(^{3}He,d)^{174}Lu and the ^{175}Lu(d,t)^{174}Lu reactions. It has been shown in Chapter 4 and also by Lu and Alford (1971) that the ratio of the (^{3}He,d) and (α,t) cross sections can be a good indicator of the orbital angular momentum, ℓ, transferred in a reaction on a doubly even target. Similarly, the same has been found to be true (Burke et al. 1971) for the ratio of the cross section in a (d,t) reaction to that in the corresponding (^{3}He,α) reaction. Though the states populated in the doubly odd nucleus ^{174}Lu by single nucleon transfer reactions are formed by mixed-ℓ transitions, the technique of using cross section ratios still provides useful clues about the ℓ-values transferred. This information and the characteristic intensity patterns formed by rotational bands built on intrinsic states enabled many new

levels to be interpreted in terms of the Nilsson model with pairing and Coriolis mixing effects included.

The major part of this chapter deals with the very restricted set of states which may be observed using the $^{173}Yb(^{3}He,d)^{174}Lu$ and $^{173}Yb(\alpha,t)^{174}Lu$ reactions. Energy levels populated in these reactions are those in which the odd target neutron, in the $5/2^{-}[512]$ orbital, couples to the transferred proton. The only states which the proton transfer reactions show in common with the neutron transfer data are members of the $K^{\pi}=1^{-}$ ground state band and the $K^{\pi}=6^{-}$ band formed by the $5/2^{-}[512]$ neutron and the $7/2^{+}[404]$ proton, which form the ground states of the respective targets. As was expected from the study of states in the odd mass lutetium nuclei (Chapter 4), strong Coriolis coupling occurs between proton states arising from the $h_{9/2}$ shell model states.

5.1 Experimental results

Figure 5.1.1 shows representative $^{173}Yb(^{3}He,d)^{174}Lu$ and $^{173}Yb(\alpha,t)^{174}Lu$ spectra. The $(^{3}He,d)$ exposures were made at laboratory angles θ = 30°, 38° and 50° with resolutions between 16 and 20 keV (FWHM). The (α,t) exposures were made at θ = 20°, 60° and 75° with a typical resolution of 12 keV. The (α,t) process tends to populate higher spin states more strongly than the $(^{3}He,d)$ reaction. For example in fig. 5.1.1 it may be seen that the ground state band, which is populated entirely by

Figure 5.1.1

The spectra obtained from the $^{173}Yb(^{3}He,d)^{174}Lu$ reaction at $\theta = 50°$ and the $^{173}Yb(\alpha,t)^{174}Lu$ reaction at $\theta = 60°$. In these spectra all the larger peaks up to 800 keV have been assigned to Nilsson configurations. Those remaining unassigned below 800 keV are due to impurities, for example, the weak peak below the ground state.

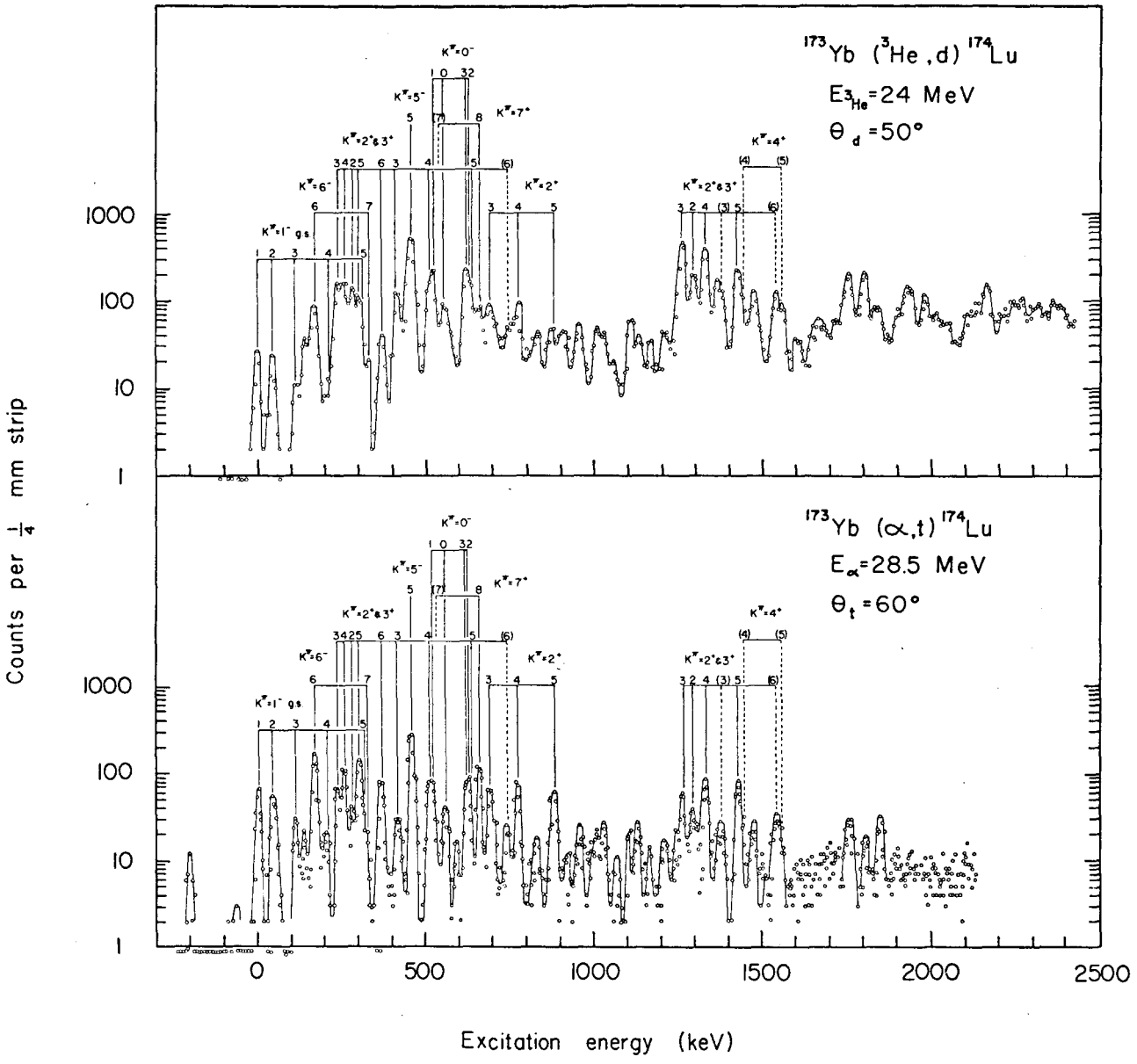
^{173}Yb (^{3}He ,d) ^{174}Lu
$E_{^3He}$=24 MeV
θ_d=50°
^{173}Yb (α,t) ^{174}Lu
E_α=28.5 MeV
θ_t=60°
Counts per 1/4 mm strip
Excitation energy (keV)
1000
100
10
1
0
500
1000
1500
2000
2500

ℓ=4 transitions, gives rise to large peaks in the (α,t) spectrum when compared to the (^{3}He,d) results. It is interesting to compare fig. 5.1.1 with the spectra for the same reactions into ^{173}Lu (fig. 4.1.1).

Figure 5.1.2 shows typical ^{175}Lu(d,t)^{174}Lu and ^{175}Lu(^{3}He,α)^{174}Lu spectra. The (d,t) exposures were made at laboratory angles of θ = 40°, 60° and 120° with resolutions between 7 and 12 keV. There is no change in the interpretation proposed by Jones and Sheline (1970) for the largest peaks but the (d,t) spectrum is shown in order to contrast with the (^{3}He,α) exposures where the resolution is approximately 30 keV. The (^{3}He,α) exposures were done at θ = 25°, 35° and 45°. The (d,t) reaction tends to populate the low angular momentum components of the transitions whereas the (^{3}He,α) reaction tends to populate the higher angular momentum transfers. For comparison with fig. 5.1.2, the ^{172}Yb(d,t)^{173}Yb and ^{172}Yb(^{3}He,α)^{173}Yb spectra are shown in fig. C.2. The simplicity of the spectra of the odd mass nucleus is rather striking.

The cross sections were normalized in each reaction using the number of incident particles elastically scattered into a semiconductor monitor counter located in the target chamber. The error in the absolute cross section is estimated to be approximately 20%. Tables 5.1.1 and 5.1.2 list the energies and cross sections of the states observed in the proton transfer and neutron transfer reactions respectively. Only the statistical

Figure 5.1.2

The spectra obtained from the $^{175}Lu(d,t)^{174}Lu$ reaction at $\theta=60°$ and the $^{175}Lu(^{3}He,\alpha)^{174}Lu$ reaction at $\theta=35°$. The intense peaks attributed to the transfer of the $7/2^{+}[633]$ neutron may be seen in the $(^{3}He,\alpha)$ reaction.

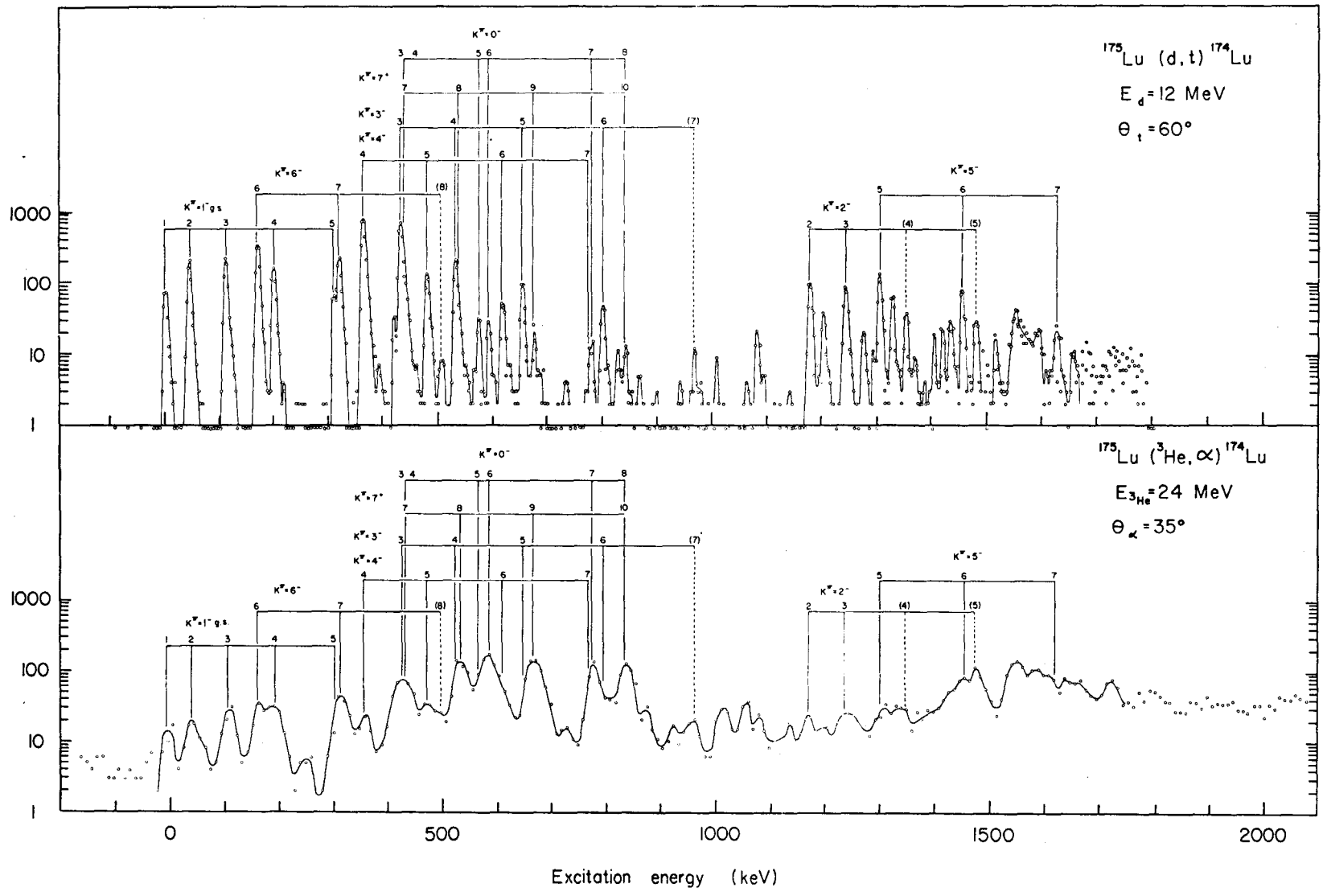
^{175}Lu (d,t) ^{174}Lu
E_d = 12 MeV
θ_t = 60°
^{175}Lu (^{3}He,α) ^{174}Lu
$E_{^3He}$ = 24 MeV
θ_α = 35°
Counts per ¼ mm. strip
Excitation energy (keV)
0
500
1000
1500
2000
1
10
100
1000

Table 5.1.1

Observed Energies and Cross sections of Proton Transfer Reactions Into ^{174}Lu

I,K^{π}	Assignment	$^{173}Yb(^{3}He,d)^{174}Lu$ Average Energy (keV)	$^{173}Yb(^{3}He,d)^{174}Lu$ $\frac{d\sigma}{d\Omega}$ @ θ= 50° (μb/sr)	$^{173}Yb(\alpha,t)^{174}Lu$ Average Energy (keV)	$^{173}Yb(\alpha,t)^{174}Lu$ $\frac{d\sigma}{d\Omega}$ @ θ= 60° (μb/sr)	$\frac{\sigma(^{3}He,d)}{\sigma(\alpha,t)}$ Experimental
$1,1^{-}$	$7/2+[404]_p$-$5/2-[512]_n$	0	2.7±62%	0	7.6± 8%	0.35
$2,1^{-}$	$7/2+[404]_p$-$5/2-[512]_n$	43	2.5±21%	45.3	6.8± 7%	0.37
$3,1^{-}$	$7/2+[404]_p$-$5/2-[512]_n$	111	1.3±20%	112.6	4.1± 8%	0.31
	^{175}Lu	141	4.8±10%	139.6	2.4±11%	
$6,6^{-}$	$7/2+[404]_p$+$5/2-[512]_n$	169	10.0± 6%	170.6	19.9±15%	0.5
$4,1^{-}$	$7/2+[404]_p$-$5/2-[512]_n$	202	1.6±17%	202	3.0±28%	0.53
	^{175}Lu			212	0.7?	
$3,2^{+}$	$1/2-[541]_p$-$5/2-[512]_n$	237	17.3± 8%	240	9.7± 6%	1.8
$4,2^{+}$	$1/2-[541]_p$-$5/2[512]_n$	255	16.7± 8%	259	14.5± 5%	1.15
$2,2^{+}$	$1/2-[541]_p$-$5/2-[512]_n$	278	15.4± 7%	284	4.8±10%	3.2
$5,2^{+}$	$1/2-[541]_p$-$5/2-[512]_n$	298	11.9±10%	302	16.7± 5%	0.71
$7,6^{-}$	$7/2+[404]_p$+$5/2-[512]_n$	$\approx$317	$\approx$2	323	2.1±17%	0.95
$5,1^{-}$	$7/2+[404]_p$-$5/2^{-}[512]_n$					

(continued next page)

Table 5.1.1 (continued)

I,K^{π}	Assignment	$^{173}Yb(^{3}He,d)^{174}Lu$ Average Energy (keV)	$^{173}Yb(^{3}He,d)^{174}Lu$ $\frac{d\sigma}{d\Omega}$ @ θ= 50° (μb/sr)	$^{173}Yb(\alpha,t)$ Average Energy (keV)	$^{173}Yb(\alpha,t)$ $\frac{d\sigma}{d\Omega}$ @ θ= 60° (μb/sr)	$\frac{\sigma(^{3}He,d)}{\sigma(\alpha,t)}$ Experimental
$6,2^{+}$	$1/2-[541]_p-5/2-[512]_n$	366	4.8± 9%	367	10.5±15%	0.46
$3,3^{+}$	$1/2-[541]_p+5/2-[512]_n$	414	16.1±10%	412	4.0±11%	3.2
				428?	1.3±26%	
$5,5^{-}$	$5/2+[402]_p+5/2-[512]_n$	455	61.2± 3.5%	455.4	38.7± 3%	1.57
$4,3^{+}$	$1/2-[541]_p+5/2-[512]_n$	507	11.6±31%	505	5.0±32%	2.3
$1,0^{-}$ and $7,7^{+}$ (?)	$5/2+[402]_p-5/2-[512]_n$ and $9/2-[541]_p+5/2-[512]_n$	521	20.7±14%	516	7.7±28%	1.5
				527	6.5±32%	
$0,0^{-}$	$5/2+[402]_p-5/2-[512]_n$	555	11.7± 6%	553	4.3±24%	1.8
				561	2.0±60%	
		≈578	4.0±11%			
	^{173}Lu?			591	1.4±20%	
3 and $2,0^{-}$	$5/2+[402]_p-5/2-[512]_n$	621	28.7± 6%	619	8.2±24%	1.82
				627	7.6±23%	
$5,3^{+}$	$1/2-[541]_p+5/2-[512]_n$	640	7.6±26%			

(continued next page)

Table 5.1.1 (continued)

I,K^{π}	Assignment	$^{173}Yb(^{3}He,d)^{174}Lu$ Average Energy (keV)	$^{173}Yb(^{3}He,d)^{174}Lu$ $\frac{d\sigma}{d\Omega}$ @ θ= 50° (μb/sr)	$^{173}Yb(\alpha,t)^{174}Lu$ Average Energy (keV)	$^{173}Yb(\alpha,t)^{174}Lu$ $\frac{d\sigma}{d\Omega}$ @ θ= 60° (μb/sr)	$\frac{\sigma(^{3}He,d)}{\sigma(\alpha,t)}$ Experimental
$8,7^{+}$	$9/2-[514]_p+5/2-[512]_n$	659	10.0±10%	658	14.1± 5%	0.71
$3,2^{+}$	$9/2-[514]_p-5/2-[512]_n$	692	11.6± 6% [a]	691	9.1± 6%	1.3
		714	5.5±11% [a]	723	0.8±26%	7.
$6,3^{+}$ (?)	$1/2-[541]_p-5/2-[512]_n$	746	10.4±24% [a]	745	3.0±11%	3.5
$4,2^{+}$	$9/2-[514]_p-5/2-[512]_n$	771	8.2±27%	771	9.4± 6%	0.87
		809	4.9±27% [a]	808	0.6±31%	8.
		833	5.2± 9%	829	1.9±14%	2.7
$5,2^{+}$	$9/2-[514]_p-5/2-[512]_n$	875	5.5±14%	875	8.6±10%	0.64
		903	5.7±11%	908	1.0±25%	5.7
		923	3.3±17%			
		951	6.2±10%	955	1.2±21%	5.2
		1005	6.6± 9%	1008	2.3±20%	2.9
		1027	5.1±10%	1028	2.7±15%	1.9
				1061	0.8±25%	
		1107	8.3± 7%	1108	1.6±50%	5.2

(continued next page)

Table 5.1.1 (continued)

I^{π}	Assignment	$^{173}Yb(^{3}He,d)^{174}Lu$ Average Energy (keV)	$^{173}Yb(^{3}He,d)^{174}Lu$ $\frac{d\sigma}{d\Omega}$ @ θ= 50° (μb/sr)	$^{173}Yb(\alpha,t)^{174}Lu$ Average Energy (keV)	$^{173}Yb(\alpha,t)^{174}Lu$ $\frac{d\sigma}{d\Omega}$ @ θ= 60° (μb/sr)	$\frac{\sigma(^{3}He,d)}{\sigma(\alpha,t)}$ Experimental
		1133	4.5±10%	1130	3.0±11%	1.5
		1164	4.0±10%	1168	1.4±17%	2.8
		1206	5.8±10%	1211	2.2±12%	2.6
				1240	2.1±13%	
$3,3^{+}$	$1/2-[530]_{p}+5/2-[512]_{n}$	1262	55	1260	7.7± 6%	7.1
				1286	4.6±11%	
$2,2^{+}$	$1/2-[530]_{p}-5/2-[512]_{n}$	1293	26.9± 8%			3.9
				1301	2.3±19%	
$4,3^{+}$	$1/2-[530]_{p}+5/2-[512]_{n}$	1326	46.4± 4%	1329	11.2± 5%	4.14
		1362	19.2± 7%	1363	2.3±17%	8.3
		1378	9.4±12%	1379	2.5±16%	3.8
		1391	3.8±15%			
$5,3^{+}$	$1/2-[530]_{p}+5/2-[512]_{n}$	1421	29.5± 5%	1423	10.7±30%	2.77
$4,4^{+}$ (?)	$3/2-[532]_{p}+5/2-[512]_{n}$	1439	8.3±15%	1437	2.5±40%	3.3
				1460	1.6±27%	
		1474	14.9± 6%	1477	2.5±19%	6.0

Table 5.1.1. (continued)

Assignment		$^{173}Yb(^{3}He,d)^{174}Lu$		$^{173}Yb(\alpha,t)^{174}Lu$		$\frac{\sigma(^{3}He,d)}{\sigma(\alpha,t)}$
I,K^{π}		Average Energy (keV)	$\frac{d\sigma}{d\Omega}$ @ θ=50° (μb/sr)	Average Energy (keV)	$\frac{d\sigma}{d\Omega}$ @ θ= 60° (μb/sr)	Experimental
	^{173}Lu?	1500	4.4±13%	1498	1.1±20%	4.0
$6,3^{+}$ (?)	$1/2-[530]_p+5/2-[512]_n$	1533	18.6±15%[a]	1537	2.1±28%	8.9
$5,4^{+}$ (?)	$3/2^{-}[532]_p+5/2-[512]_n$	1558	9.5±15%	1558	$\lesssim$4.1±30%	2.3
		1592	3.4±25%			
		1609	3.9±22%			
		1640	5.7±10%			
		1664	6.8±10%			
		1689	5.7±10%			
		1716	8.7±23%[a]			
		1738	9.4±13%			
		1753	23.0± 5%	1753	3.7± 9%	6.2
		1771	7.2± 9%			
		1800	26.6± 4%	1801	2.5± 9%	11.6
		1829	8.5± 9%			
		1847	9.1±10%	1847	3.0 30%	3.0
		1868	5.3±14%			

Table 5.1.1 (continued)

Assignment I,K^{π}	$^{173}Yb(^{3}He,d)^{174}Lu$ Average Energy (keV)	$^{173}Yb(^{3}He,d)^{174}Lu$ $\frac{d\sigma}{d\Omega}$ @ $\theta = 50°$ (μb/sr)	$^{173}Yb(\alpha,t)^{174}Lu$ Average Energy (keV)	$^{173}Yb(\alpha,t)^{174}Lu$ $\frac{d\sigma}{d\Omega}$ @ $\theta = 60°$ (μb/sr)	$\frac{\sigma(^{3}He,d)}{\sigma(\alpha,t)}$ Experimental
	1903	13.1±25%			
	1927	16.9± 9%			
	1940	14.3±11%			
	1979	13.7± 7%			
	≈2012	8.6± 8%			
	2096	8 ± 8%			
	2120	8.8±13%			
	2155	8.1±12%			

a) possible unresolved multiplet.

Table 5.1.2

Observed Energies and Cross sections of Neutron Transfer Reactions Into ^{174}Lu

I,K^{π}	Assignment	$^{175}Lu(d,t)^{174}Lu$ Average Energy (keV)	$^{175}Lu(d,t)^{174}Lu$ $\frac{d\sigma}{d\Omega}$ @ θ=60° (μb/sr)	$^{175}Lu(^3He,\alpha)^{174}Lu$ Average Energy (keV)	$^{175}Lu(^3He,\alpha)^{174}Lu$ $\frac{d\sigma}{d\Omega}$ @ θ=35° (μb/sr)	$\frac{\sigma(d,t)}{\sigma(^3He,\alpha)}$ Experimental
$1,1^-$	$5/2-[512]_n-7/2+[404]_p$	0	20 ± 7%	≈10	0.5±56%	40
$2,1^-$	$5/2-[512]_n-7/2+[404]_p$	44.4	50.7± 4%	47	1.3±28%	39
$3,1^-$	$5/2-[512]_n-7/2+[404]_p$	111.2	57.8± 4%	119	1.8±23%	32
$6,6^-$	$5/2-[512]_n+7/2+[404]_p$	169.9	89.1± 4%	178	2.8±50%	32
$4,1^-$	$5/2-[512]_n-7/2+[404]_p$	199.9	42.0± 4%	197	1.9±50%	22
$5,1^-$	$5/2-[512]_n-7/2+[404]_p$	310.4	16.9±12%	324	3.6±15%	21
$7,6^-$	$5/2-[512]_n+7/2+[404]_p$	319.3	57.8± 8%			
$4,4^-$	$1/2-[512]_n+7/2+[404]_p$	364	217.9± 7%	369	1.5±25%	140
		395?	1.9±25%			
		419	5.5±21%			
$7,7^+$	$7/2+[633]_n+7/2+[404]_p$					
$3,3^-$	$1/2-[521]_n-7/2+[404]_p$	432	176.7± 4%[a]	433	10.0±6%	17
3 and $4,0^+$	$7/2+[633]_n-7/2+[404]_p$					

(continued next page)

Table 5.1.2 (continued)

I,K^{π}	Assignment	$^{175}Lu(d,t)^{174}Lu$ Average Energy (keV)	$^{175}Lu(d,t)^{174}Lu$ $\frac{d\sigma}{d\Omega}$ @ θ=60° (μb/sr)	$^{175}Lu(^{3}He,\alpha)^{174}Lu$ Average Energy (keV)	$^{175}Lu(^{3}He,\alpha)^{174}Lu$ $\frac{d\sigma}{d\Omega}$ @ θ=35° (μb/sr)	$\frac{\sigma(d,t)}{\sigma(^{3}He,\alpha)}$ Experimental
		442	11.9±25% [a]			
		458	1.7±30%			
$5,4^{-}$	$1/2-[521]_n+7/2+[404]_p$	480	38.5± 5%	490	3.6±15%	11
$8,6^{-}$ (?)	$5/2-[512]_n+7/2+[404]_p$	506	2.6±20%			
$4,3^{-}$	$1/2-[521]_n-7/2+[404]_p$	532	58.4± 5% [a]			
$8,7^{+}$	$7/2+[633]_n+7/2+[404]_p$			538	13.9±28%	4.2
$5,0^{+}$	$7/2+[633]_n-7/2+[404]_p$	573	6.9±17%	582	20.8± 6%	0.67
$6,0^{+}$	$7/2+[633]_n-7/2+[404]_p$	593	7.1±11%	592		
$6,4^{-}$	$1/2-[521]_n+7/2+[404]_p$	618	14.7± 8%			
$5,3^{-}$	$1/2-[521]_n-7/2+[404]_p$	655	25.4± 6%			
$9,7^{+}$	$7/2+[633]_n+7/2+[404]_p$	676	5.5±16%	676 [a]	18.1± 6%	0.3
		694	0.8±47%			
		735	1.1±34%	741?	0.9±46%	1.2

(continued next page)

Table 5.1.2 (continued)

I,K^{π}	Assignment	$^{175}Lu(d,t)^{174}Lu$ Average Energy (keV)	$^{175}Lu(d,t)^{174}Lu$ $\frac{d\sigma}{d\Omega}$ @ θ=60° (μb/sr)	$^{175}Lu(^{3}He,\alpha)^{174}Lu$ Average Energy (keV)	$^{175}Lu(^{3}He,\alpha)^{174}Lu$ $\frac{d\sigma}{d\Omega}$ @ θ=35° (μb/sr)	$\frac{\sigma(d,t)}{\sigma(^{3}He,\alpha)}$ Experimental
$7,4^{-}$	$1/2-[512]_n+7/2+[404]_p$	779	3.9±19%			
$7,0^{+}$	$7/2+[633]_n-7/2+[404]_p$			788	10.7±40%	1.5
$6,3^{-}$	$1/2-[521]_n-7/2+[404]_p$	801	12.3± 8%			
$8,0^{+}$	$7/2+[633]_n-7/2+[404]_p$	842	3.4±17%	847	13.6± 9%	0.25
$10,7^{+}$	$7/2+[633]_n+7/2+[404]_p$					
		866?	1.3±30%			
$7,3^{-}$ (?)	$1/2-[521]_n-7/2+[404]_p$	968	2.5±21%	966	1.6±27%	1.6
		1010	1.1	1027	2.5±18%	0.44
			<0.7	1071	2.9±24%	
		1081	5.1±13%			
				1156	1.1±39%	
$2,2^{-}$	$3/2-[521]_n-7/2+[404]_p$	1178	28.2±10%			
		1203	9.3±10%	1194	2.0±22%	4.6

(continued next page)

Table 5.1.2 (continued)

Assignment		$^{175}Lu(d,t)^{174}Lu$		$^{175}Lu(^{3}He,\alpha)^{174}Lu$		$\frac{\sigma(d,t)}{\sigma(^{3}He,\alpha)}$
I,K^{π}		Average Energy (keV)	$\frac{d\sigma}{d\Omega}$ @ θ=60° (μb/sr)	Average Energy (keV)	$\frac{d\sigma}{d\Omega}$ @ θ=35° (μb/sr)	Experimental
$3,2^-$	$3/2-[521]_n-7/2+[404]_p$	1243	23.6± 6%	1250	3.3±11%	7.2
		1275	5.6±13%			
		1294	2.6±21%			
$5,5^-$	$3/2-[521]_n+7/2+[404]_p$	1304	32.7± 5%	1310	2.6±18%	13
		1329	17.0± 6%			
$4,2^-$ (?)	$3/2-[521]_n-7/2+[404]_p$	1353	11.0± 9%			
		1370?	2.5±20%			
		1406	3.4±25%			
		1421	6.2±12%	1429	3.6± 5%	4.4
		1436	9.7±20%			
$6,5^-$	$3/2-[521]_n+7/2+[404]_p$	1456	19.3±27%	1456	7.3±19%	2.6
$5,2^-$ (?)	$3/2-[521]_n+7/2+[404]_p$	1481	9.5±12%	1484	10.2±17%	0.93
		1516	4.0±15%			
		1551	17.1±25%	1555	16.6± 5%	1.0

(continued next page)

Table 5.1.2 (continued)

Assignment		$^{175}Lu(d,t)^{174}Lu$		$^{175}Lu(^{3}He,\alpha)^{174}Lu$		$\frac{\sigma(d,t)}{\sigma(^{3}He,\alpha)}$
I,K^{π}		Average Energy (keV)	$\frac{d\sigma}{d\Omega}$ @ θ=60° (μb/sr)	Average Energy (keV)	$\frac{d\sigma}{d\Omega}$ @ θ=35° (μb/sr)	Experimental
		1564	10.1±30%			
		1576	5.2±23%			
		1589	3.7±32%	1587	7.9±10%	
		1596	5.7±21%			
$7,5^{-}$	$3/2-[521]_{n}+7/2+[404]_{p}$	1628	7.2±30%[a]	1617	9.2± 9%	
		1660	4.5±23%[a]	1651	9.1±11%	
		1681	5.3±30%[a]	1682?	6.5±15%	
				1732	8.4± 7%	
				1840	3.2±12%	
				2041	5.0±11%	
				2082	5.4±11%	

a) possible unresolved multiplet.

errors in the cross sections for a particular reaction are shown. The energies have an error of less than 2 keV except in the cases of unresolved doublets or very weak peaks.

5.2 Calculations

The cross sections for the states expected to be populated in the single nucleon transfer reactions were calculated using Nilsson model wave functions. The effects of pairing, which alter the occupation probabilities for target orbitals were included. In several cases it was found necessary to include Coriolis coupling between the two-quasiparticle states of ^{174}Lu. A discussion of the Nilsson calculation performed may be found in section 3.1. In ^{174}Lu, as in the odd mass isotopes a deformation of δ=0.27 was used. The cross sections for a single particle transfer reaction starting with an odd-mass target were calculated using equations (3.5.7) and (B.9).

The fullness factors, V^2, for the states observed in the neutron pick-up reactions were obtained using the standard expressions from pairing theory for one quasiparticle states (eq. (3.2.1)). the calculations were performed using a gap, Δ_n of 700 keV. The Fermi surface was set to be slightly above the $5/2^-$[512] neutron orbital. These results are consistent with the V^2 found in the ^{174}Yb(d,t)^{173}Yb study (Burke et al. 1966). The emptiness probabilities, U^2, for the proton stripping reactions were calculated in a similar manner. The proton energy gap parameter, Δ_p,

used in this case was 850 keV. The Fermi energy was set approximately 300 keV below the $7/2^+[404]$ orbital, which is consistent with the cross sections observed in the $^{172}Yb(^3He,d)^{173}Lu$ and $^{172}Yb(\alpha,t)^{173}Lu$ experiments (Chapter 4).

The normalization of the proton transfer intrinsic cross sections predicted by DWBA calculations was found by summing the cross sections of the observed members of the $K^\pi = 1^-$ ground state band and the $K^\pi = 6^-$ band at 170 keV. These states are populated by pure $\ell=4$ transitions in the proton transfer reactions and by a mixture of $\ell=3$ and 5 in the neutron transfer reactions. Initially, the normalization factor of the DWBA calculation for each reaction was adjusted so the total cross section predicted for these states was in agreement with the total observed cross sections. Though these states have low intensities in the $(^3He,\alpha)$ and $(^3He,d)$ reactions, this procedure gave acceptable results when the normalization factors obtained were applied to more strongly populated states. Except in the case of the (α,t) reaction the normalization factors so found were close enough to the standard values (Elbek and Tjøm 1969), that the standard values were used. The normalization factors are included in table 3.6.2.

It appears that the DWBA calculations did not yield a satisfactory Q-dependence for the (α,t) cross section. At higher excitation energies the (α,t) cross section is predicted to decrease much more rapidly than it appears to do in the

observed spectrum. The (^{3}He,d) cross sections may also show a similar effect but not nearly to the same degree. Thus in making assignments, the cross sections predicted for the (^{3}He,d) reaction were given much more weight than those from the (α,t) reaction. It was found that over ranges of approximately 300 keV excitation energy, such as found within a rotational band, the relative (α,t) cross sections were still quite useful.

The ratio of the (^{3}He,d) and (α,t) cross sections as a function of the Q-value were calculated from the DWBA results and are plotted in fig. 5.2.1 for various ℓ-values. The points marked are the observed ratios, taken from table 5.1.1,for states which have been identified in this work. The points are identified by the total spin, I, that has been assigned to the state. If a state is populated by transition of a single ℓ-value the experimental points should fall on the predicted curves. It is seen in fig. 5.2.1 that the agreement between the predicted ratio and the observed ratio for peaks populated by a single ℓ-value is not too satisfactory. As it is, the (^{3}He,d) to (α,t) cross section ratios are useful for discriminating between states populated by high or low-ℓ transitions; the error in ascertaining the ℓ-value from the cross section ratios for the proton transfer reaction is likely about one unit in ℓ.

The ratio of the (d,t) cross section to the (^{3}He,α) cross section has been shown to be remarkably good for predicting ℓ-values (Burke et al. 1971). However, because the low cross sections observed in the ^{175}Lu(^{3}He,α)^{174}Lu reaction, this ratio has not

Figure 5.2.1

The ratio of the (^{3}He,d) cross section to the (α,t) cross section as a function of the excitation energy in ^{174}Lu. The solid lines represent the predicted ratio for the transfer of a proton with a single ℓ-value. The points are the observed ratios for states identified in ^{174}Lu and are labelled by the spin I of the state. The predicted curves have been effectively normalized to the observed cross section ratios of the states formed by the transfer of the $7/2^{+}[404]$ proton which takes place by essentially pure ℓ=4 transitions. Configurations resulting from the transfer of the $1/2^{-}[541]$, $3/2^{-}[532]$ and $1/2^{-}[530]$ protons are populated by mixed ℓ transitions.

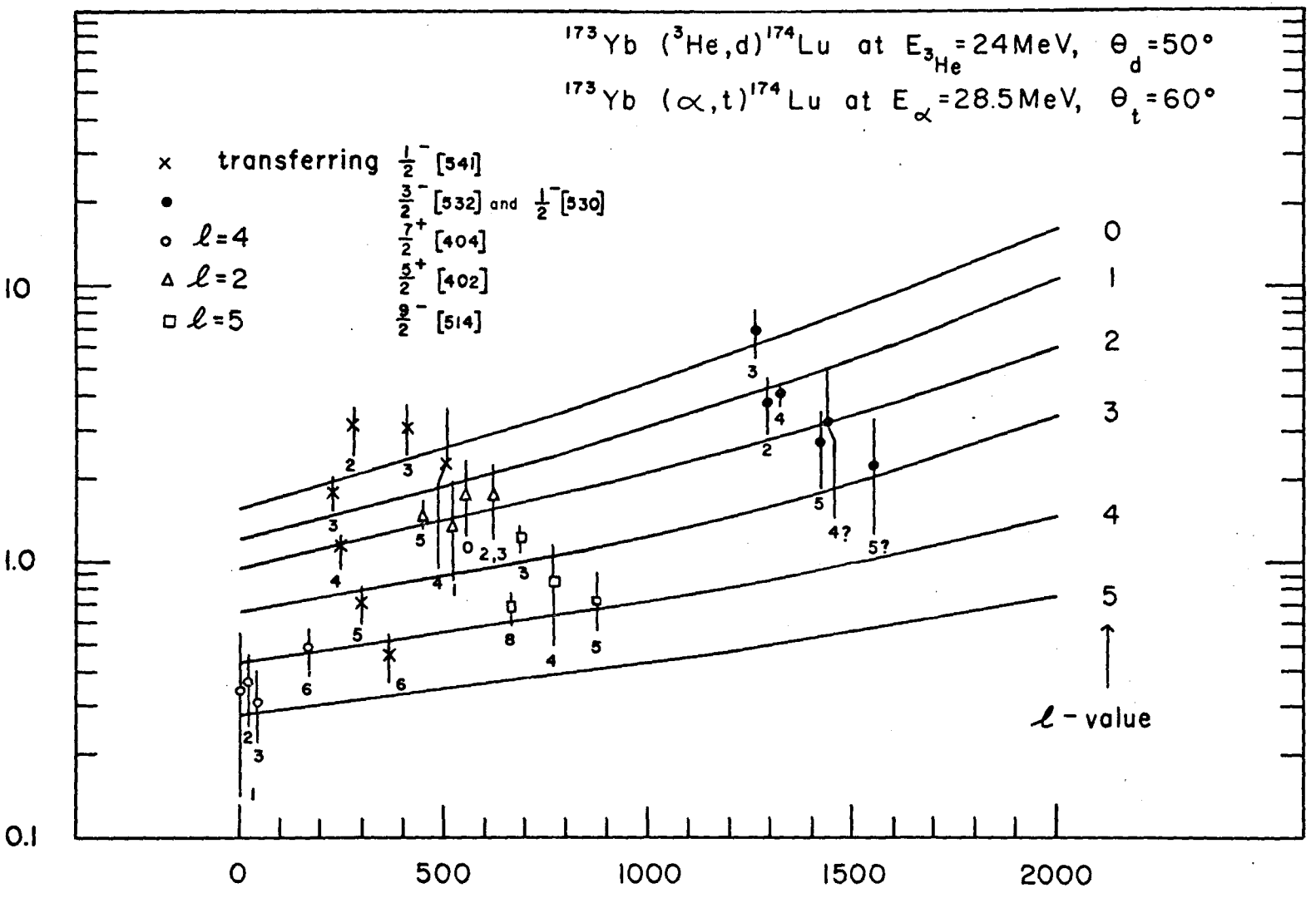

$\frac{d\sigma}{d\Omega}$ (^{3}He,d) / $\frac{d\sigma}{d\Omega}$ (α,t)

been considered too useful. Fig. 5.2.2 shows the predicted (d,t) to (^{3}He,α) cross section ratio curve. The only states included on this diagram arise from the transfer of the $5/2^-$[512] and $7/2^+$[633] neutrons. The latter states are the only ones with sufficient cross section in the (^{3}He,α) reaction to really be identified in the (^{3}He,α) spectra below 1 MeV. With the low resolution associated with the (^{3}He,α) reaction, and the high level density, even these strong states were not completely resolved from those populated by lower ℓ-value transitions. It was considered significant that certain states were populated strongly in the (^{3}He,α) reaction; such a strength could be attributed only to transitions with orbital angular momentum ℓ = 5 or 6, the most likely states being formed by removing a neutron from the $7/2^+$[633] orbital. As may be seen from fig. 5.1.2, there are some strongly populated states in the (^{3}He,α) spectrum near 1 MeV of excitation. It was not felt that the (d,t) spectrum was well enough understood in this region to be able to draw any conclusions from the (^{3}He,α) data.

The only states considered in the neutron pick-up reactions were those formed by coupling the $7/2^+$[404] target proton to an unpaired neutron. Similarly, in the proton stripping reaction, the states considered were restricted to those for which the transferred proton was coupled to the $5/2^-$[512] target neutron. Coriolis coupling calculations described in section 3.3 were performed using these two sets independently.

It is possible for some members of one set to couple with members of the other set. For example, in such a situation, one might expect to see a peak in the (d,t) spectrum having the same energy as that of a state populated in the (α,t) experiment. This could be due to the state having a mixed wavefunction of which one of the components is from the proton transfer set and one is from the neutron transfer set. This phenomenon has been observed (Khoo et al. 1972) in ^{176}Hf. No such peaks have been observed in the low energy spectra of ^{174}Lu. There are many combinations of neutron and proton orbitals which could form low lying configurations in ^{174}Lu and which are not members of the two sets of states considered. These states would not be populated by single particle transfer reactions unless their wavefunctions contained admixtures of the simple configurations which may be seen in such a reaction. Some of the weakly populated uninterpreted levels may be of this type.

Because of the very restricted set of states considered, standard expressions for the Coriolis matrix elements, such as found in Bunker and Reich (1971) could be employed. However, because of differences in the phase factors, a more general expression (eq. (A.8)) for the Coriolis coupling of two-quasiparticle states in a doubly-odd nucleus was used. The mixing amplitudes resulting from the diagonalization of the rotational Hamiltonian were used to calculate the perturbed cross sections of the bands.

Figure 5.2.2

The ratio of the (d,t) cross section to the (^{3}He,α) cross section as a function of the excitation energy in ^{174}Lu. The solid lines represent the predicted ratio for the transfer of a neutron with a single ℓ-value. The points represent the predicted and observed cross section ratios for the transfer of two different neutrons. The transfer of the $5/2^{-}[512]$ neutron proceeds largely by ℓ=3 transitions. The states which have been attributed to the $\{7/2^{+}[633]_{n} \pm 7/2^{+}[404]_{p}\}$ configuration have ratios in good agreement with the predicted values. Such states should be populated by almost pure ℓ=6 transitions.

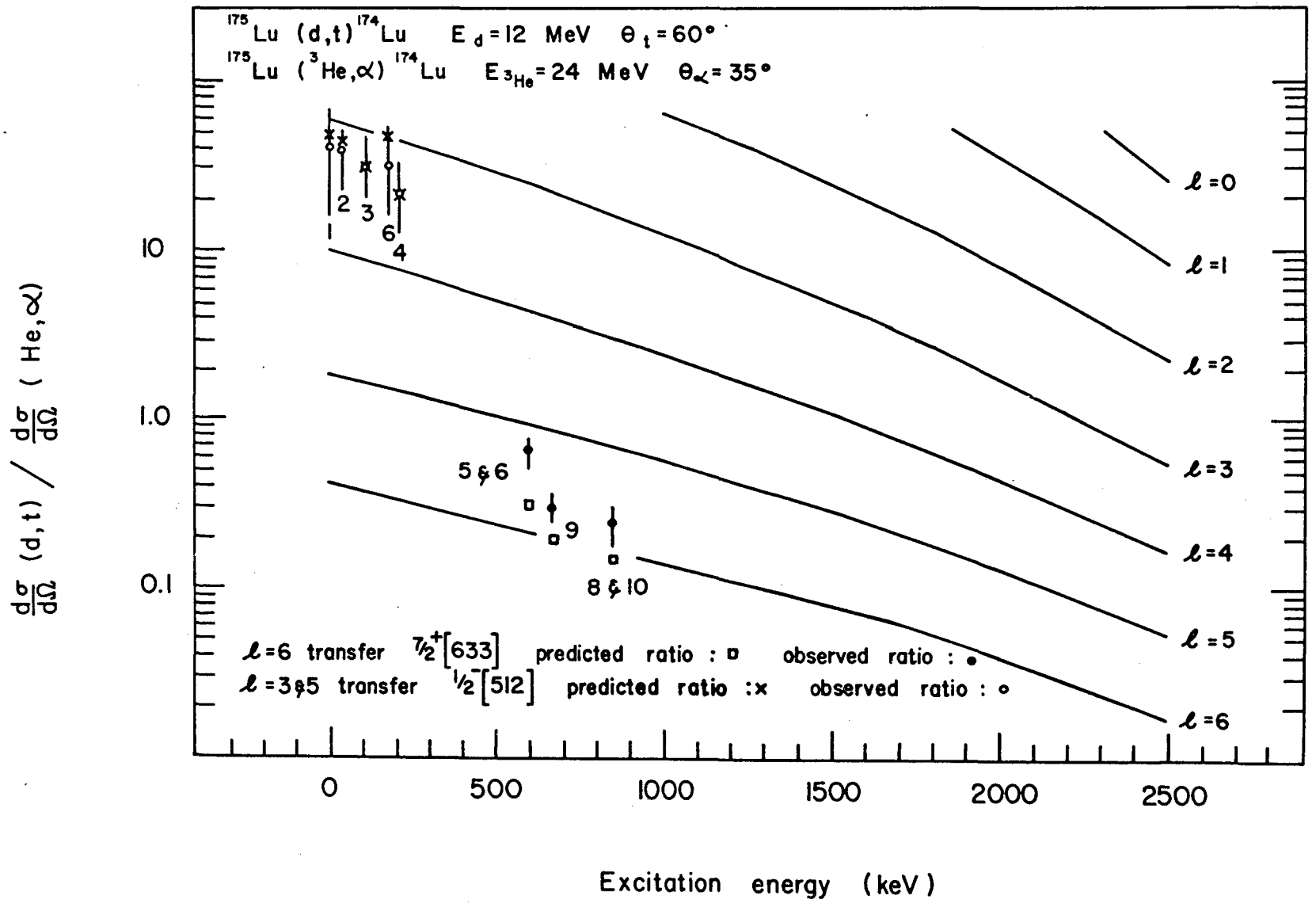
^{175}Lu (d,t) ^{174}Lu E_d = 12 MeV θ_t = 60°
^{175}Lu (^{3}He,α) ^{174}Lu $E_{^3He}$ = 24 MeV θ_α = 35°
ℓ = 0
ℓ = 1
ℓ = 2
ℓ = 3
ℓ = 4
ℓ = 5
ℓ = 6
1
2
3
6
4
5 & 6
9
8 & 10
ℓ = 6 transfer 7/2+[633] predicted ratio : □ observed ratio : ●
ℓ = 3 & 5 transfer 1/2−[512] predicted ratio : × observed ratio : ○
10
1.0
0.1
0
500
1000
1500
2000
2500
dσ/dΩ (d,t) / dσ/dΩ (He,α)
Excitation energy (keV)

The unperturbed bandhead energies were adjusted so there was good agreement between the energy spectrum predicted when Coriolis coupling was included and the observed spectrum. In general, this procedure also produced acceptable agreement between the predicted and observed fingerprints. It was not found necessary to vary the rotational parameters from band to band.

Table 5.2.1 lists the unperturbed energies and cross sections of the states expected to be seen in ^{174}Lu by means of single proton transfer reactions. The rotational parameter $(\frac{\hbar^2}{2\mathcal{J}})$ of 11.1 keV,which is the value obtained from the ground state band,was used for all the bands. The matrix elements used in this calculation were unattenuated but were corrected for pairing effects. With the exception of the $5/2^-[512]$ target neutron orbital coupled to the $1/2^+[411]$ and possibly the $3/2^-[532]$ proton orbitals all these states have been identified in ^{174}Lu. The odd-even shift in the $K^\pi = 0^-$ band has not been included because the cross sections of the states do not change much over the $\sim$50 keV that the odd spin states are displaced from their simple I(I+1) energy rule positions. Table 5.2.1 also shows the effect of Coriolis coupling on the states populated in the (^{3}He,d) and (α,t) reactions. In addition to the states listed, the calculation included the configurations with lower energy proton states arising from the N=6 oscillator shell as well as the $11/2^-[505]$, $1/2^+[400]$ and $3/2^+[402]$ proton orbitals

Predicted Energies and Cross Sections of Proton transfer reactions into ^{174}Lu

			Unperturbed			Coriolis Perturbed				
				Cross Section			Cross Section			
I,K^{π}	Configuration	U^2 of transferred proton	Energy (keV)	(^{3}He,d) $\theta = 50^{o}$ (μb /sr)	(α,t) $\theta = 60^{o}$ (μb/sr)	Energy (keV)	(^{3}He,d) $\theta = 50^{o}$ (μb/sr)	(α,t) $\theta = 60^{o}$ (μb/sr)	$\frac{\sigma(^3He,d)}{\sigma(\alpha,t)}$ predicted	Exp. Energy (keV)
1, 1^-	$7/2+[404]_p-5/2-[512]_n$	0.75	0	3.6	7.7	0	3.6	7.8	0.46	0
2,			44	3.4	7.2	44	3.4	7.1	0.48	44.7
3,			111	2.0	4.0	110	2.0	4.1	0.49	111.7
4,			200	0.7	1.4	199	0.7	1.4	0.5	200
5,			311	0.2	0.3	309	0.2	0.3	0.66	(311)
$6,6^-$	$7/2+[404]_p+5/2-[512]_n$	0.75	171	10.1	20.0	169	10.2	20.3	0.5	170.8
7,			326	0.1	0.2	324	0.1	0.2	0.5	(320)
$5,5^-$	$5/2+[402]_p+5/2-[512]_n$	0.91	458	60.3	44.2	455	61.5	45.3	1.36	455
6,			591	0.5	0.8	582	0.4	0.8	0.5	(591)?
7,			747	0.1	0.2	734	0.2	0.3	0.66	
$0,0^-$	$5/2+[402]_p-5/2^-[512]_n$	0.91	555	10.3	7.0	555	10.3	7.0	1.47	555
1,			577	22.4	14.9	576[a]	22.6	15.0	1.51	521
2,			622	19.1	12.4	619	19.7	12.8	1.54	621
3,			688	9.3	5.9	683[a]	9.8	6.2	1.6	
4,			777	2.6	1.7	770	2.9	2.0	1.45	833 ?
5,			888	0.4	0.3	877[a]	0.4	0.4	1	

Table 5.2.1

Table 5.2.1 (continued)

I,K^{π}	Configuration	U^2 of transferred proton	Unperturbed			Coriolis Perturbed				
				Cross Section			Cross Section			
			Energy (keV)	(^{3}He,d) $\theta = 50^o$ (μb /sr)	(α,t) $\theta = 60^o$ (μb/sr)	Energy (keV)	(^{3}He,d) $\theta = 50^o$ (μb/sr)	(α,t) $\theta = 60^o$ (μb/sr)	$\frac{\sigma(^3He,d)}{\sigma(\alpha,t)}$ predicted	Exp. Energy (keV)
$7,7^+$	$9/2-[514]_p+5/2-[512]_n$	0.9	507	3.7	10.5	500	3.8	10.9	0.35	530
8,			685	8.3	21.9	659	10.1	27	0.37	659
$2,2^+$	$9/2-[514]_p-5/2-[512]_n$	0.9	635	0	0.1	632	0.	0.1		
3,			702	3.9	10.2	692	4.4	11.6	0.38	692
4,			790	4.5	11.4	772	5.2	13.3	0.39	771
5,			901	2.7	6.6	871	3.2	7.8	0.41	875
6,			1035	1.0	2.3	991	1.2	2.7	0.44	
7,			1190	0.2	0.4	1131	0.2	0.5	0.4	
$2,2^+$	$1/2-[541]_p-5/2-[512]_n$	0.84	287	7.3	5.6	279	7.7	6.2	1.2	278
3,			354	7.7	7.8	234	10.7	12.1	0.88	237
4,			442	6.1	8.5	254	11.6	18.5	0.63	255
5,			553	3.7	7.1	300	9.1	20.2	0.45	298
6,			687	1.7	3.9	367	5.1	14.3	0.36	366
7,			842	0.4	1.0	455	1.7	4.6	0.37	
$3,3^+$	$1/2-[541]_p+5/2-[512]_n$	0.84	327	9.9	7.7	417	10.6	7.1	1.5	414
4,			416	8.5	9.5	528	10.2	8.5	1.2	507

Table 5.2.1 (continued)

I,K^{π}	Configuration	U^2 of transferred proton	Unperturbed Energy (keV)	Unperturbed Cross Section (^{3}He,d) $\theta = 50^{o}$ (μb /sr)	Unperturbed Cross Section (α,t) $\theta = 60^{o}$ (μb/sr)	Coriolis Perturbed Energy (keV)	Coriolis Perturbed Cross Section (^{3}He,d) $\theta = 50^{o}$ (μb/sr)	Coriolis Perturbed Cross Section (α,t) $\theta = 60^{0}$ (μb/sr)	$\sigma(^3He,d)/\sigma(\alpha,t)$ predicted	Exp. Energy (keV)
5,			527	5.4	8.7	649	7.0	7.3	0.96	640
6,			660	2.6	5.7	784	3.3	4.0	0.83	(746)
7,			815	0.8	1.9	934	0.6	1.4	0.43	
$2,2^{-}$	$1/2+[411]_p-5/2-[512]_n$	0.2	200	5.1	3.8	200	5.3	4.0	1.3	
3,			267	4.1	3.4	252	6.3	5.4	1.2	
4,			355	1.7	1.5	328	3.1	2.7	1.2	
5,			466	0.4	0.4	427	0.5	0.6	0.8	
$3,3^{-}$	$1/2+[411]_p-5/2-[512]_n$	0.2	300	6.8	4.8	313	5.3	3.3	1.6	
4,			389	3.9	3.1	412	3.4	2.6	1.3	
5,			500	0.8	0.8	523	0.7	0.6	1.2	
6,			633	0.1	0.1	547	0.1	0.1	1	
$1,1^{+}$	$3/2-[532]_p-5/2-[512]_n$	0.96	1370	2.4	0.9	1370	2.4	0.9	2.67	
2,			1414	4.7	2.5	1424	5.4	2.5	2.16	
3,			1481	6.0	4.5	1506	6.7	4.1	1.63	
4,			1570	5.7	6.1	1614	6.2	4.7	1.32	
5,			1681	4.0	5.0	1749	3.8	2.9	1.31	

Table 5.2.1 (continued)

I,K^{π}	Configuration	U^2 of transferred proton	Unperturbed Energy (keV)	Unperturbed Cross Section (^{3}He,d) $\theta = 50^{\circ}$ (μb /sr)	Unperturbed Cross Section (α,t) $\theta = 60^{\circ}$ (μb/sr)	Coriolis Perturbed Energy (keV)	Coriolis Perturbed Cross Section (^{3}He,d) $\theta = 50^{\circ}$ (μb/sr)	Coriolis Perturbed Cross Section (α,t) $\theta = 60^{\circ}$ (μb/sr)	$\frac{\sigma(^3He,d)}{\sigma(\alpha,t)}$ predicted	Exp. Energ (keV)
6,			1814	1.7	2.2	1911	1.3	0.9	1.44	
7,			1969	0.3	0.4	2102	0.2	0.2	1	
$4,4^+$	$3/2-[532]_p+5/2-[512]_n$	0.96	1440	7.8	3.8	1463	11.0	4.8	2.3	1439 ?
5,			1551	9.1	7.1	1599	10.3	7.3	1.4	1558 ?
6,			1684	5.8	7.1	1760	5.7	5.8	0.98	
7,			1840	2.3	3.2	1944	1.6	2.1	0.76	
8,			2017	0.1	0.1	2150	0.1	0.1	1	
$3,3^+$	$1/2-[530]_p+5/2-[512]_n$	0.96	1297	32.4	8.7	1267	47.4	14.4	3.29	1262
4,			1386	30.3	11.7	1326	35.6	16.0	2.23	1326
5,			1497	18.5	10.6	1411	19.5	11.2	1.74	1421
6,			1630	8.1	5.1	1519	6.3	4.1	1.5	1533 ?
7,			1785	0.7	1.1	1650	0.5	0.6	0.83	
8,			1963	0.2	0.2	1804	0.1	0.1	1	
$2,2^+$	$1/2-[530]_p-5/2-[512]_n$	0.96	1297	23.9	6.1	1295	22.6	5.7	4.0	1293
3,			1364	27.4	9.3	1399	5.7	2.3	2.5	1379 ?
4,			1452	21.5	10.5	1521	2.1	1.8	1.2	
5,			1563	13.0	7.5	1664	1.4	1.8	0.78	

I,K^{π}	Configuration	U^2 of transferred proton	Unperturbed Energy (keV)	Unperturbed Cross Section (^{3}He,d) $\theta = 50^{o}$ (μb /sr)	Unperturbed Cross Section (α,t) $\theta = 60^{o}$ (μb/sr)	Coriolis Perturbed Energy (keV)	Coriolis Perturbed Cross Section (^{3}He,d) $\theta = 50^{o}$ (μb/sr)	Coriolis Perturbed Cross Section (α,t) $\theta = 60^{o}$ (μb/sr)	$\frac{\sigma(^3He,d)}{\sigma(\alpha,t)}$ predicted	Exp. Energy (keV)
6,			1697	4.1	2.9	1830	0.9	1.0	0.9	
7,			1852	0.5	0.7	2019	0.1	0.2	0.5	
8,			2030	0.1	0.1	2230	0.	0.		

a) subtract 55 keV to account for odd-even shift

Table 5.2.1 - continued

coupled individually to the $5/2^-[512]$ neutron. The $1/2^+[411]$, $7/2^-[523]$ and $3/2^+[411]$ orbitals from below the Fermi surface were also included in the calculation. These additional states were found to have little effect on the levels identified in the low energy spectrum of ^{174}Lu.

Though it will be discussed in more detail in sect. 5.3, it is interesting to point out the strong Coriolis coupling which exists between the $K^\pi=2^+$ and 3^+ configuration formed by coupling the $5/2^-[512]$ neutron and the $1/2^-[541]$ proton orbital. The resultant states are almost 50% admixtures of each configuration. It is not so easily interpreted in the case where the $3/2^-[532]$ and $1/2^-[530]$ proton orbitals couple individually to the $5/2^-[512]$ neutron orbital, forming states of $K^\pi= 1^+$, 2^+, 3^+ and 4^+ which are greatly perturbed by the Coriolis interaction.

A similar calculation was performed for the states expected to be populated in ^{174}Lu by the (d,t) and (^{3}He,α) reactions. In the neutron transfer work, it was found necessary to reduce the Coriolis matrix element by approximately a factor of 0.7 as was done by Løvhøiden et al. (1970) in the neutron states of ^{155}Gd. In addition, due in part to the coupling between $\{5/2^-[512]_n \pm 7/2^+[404]_p\}$ and the $\{3/2^-[521]_n \pm 7/2^+[404]_p\}$ configurations, the unperturbed rotational parameter used for all the bands populated in the neutron transfer reactions was $\frac{\hbar^2}{2\mathcal{J}}$ = 12.1 keV. It would have been more elegant to be able to use the same rotational parameter in the proton transfer cal-

Table 5.2.2

Predicted energies and cross sections of neutron transfer reactions into ^{174}Lu

I,K^{π}	Configuration	V^2 of transferred neutron	Unperturbed			Coriolis Perturbed				Experimental energy (keV)
			Energy (keV)	Cross-section (d,t) θ=60° (μb/sr)	Cross-section (^{3}He,α) θ=35° (μb/sr)	Energy (keV)	Cross-section (d,t) θ=60° (μb/sr)	Cross-section (^{3}He,α) θ=35° (μb/sr)	σ(d,t) / σ(^{3}He,α) predicted	
$1,1^-$	$5/2+[512]_n-7/2+[404]_p$	0.7	0	14.4	0.3	0	14.3	0.3	48.	0
2,			44	41.2	0.9	44.5	43.4	1.0	43.	44.4
3,			121	49.4	1.5	112	56.8	1.7	33.	111.2
4,			218	32.8	1.4	201	42.0	1.9	22.	200
5,			339	12.8	0.9	313	18.6	1.4	13.	310
6,			484	2.8	0.4	448	4.8	0.7	6.8	
7,			653	0.3	0.1	604	0.6	0.2	3.0	
$6,6^-$	$5/2-[512]_n+7/2+[404]_p$	0.7	180	73.5	1.5	171	85.7	1.8	47.6	169.9
7,			349	63.2	2.1	326	70.0	2.7	25.9	319
8			543	0.8	0.6	504	1.4	1.1	1.3	506?
$0,0^+$	$7/2+[633]_n-7/2+[404]_p$	0.92	349	0	0	349[a)]	0.	0.		
1,			373	0.4	0.1	363	0.4	0.1	4	
2,			422	1.1	0.2	391[a)]	1.6	0.3	5.3	
3,			494	1.7	1.1	435	2.8	1.3	2.2	433

(continued next page)

Table 5.2.2 (continued)

I,K^{π}	Configuration	V^2 of transferred neutron	Unperturbed Energy (keV)	Unperturbed Cross-section (d,t) θ=60° (μb/sr)	Unperturbed Cross-section (^{3}He,α) θ=35° (μb/sr)	Coriolis Perturbed Energy (keV)	Coriolis Perturbed Cross-section (d,t) θ=60° (μb/sr)	Coriolis Perturbed Cross-section (^{3}He,α) θ=35° (μb/sr)	$\frac{\sigma(d,t)}{\sigma(^3He,\alpha)}$ predicted	Experimental energy (keV)
4,			591	1.8	3.5	496[a)]	3.9	5.2	0.75	433
5,			712	1.6	6.1	574	3.7	9.1	0.4	573
6,			857	1.2	6.3	672[a)]	3.3	12.4	0.26	593
7,			1027	0.6	4.1	789	1.7	8.8	0.19	788
8,			1220	0.2	1.7	926[a)]	0.7	4.8	0.14	847
9,			1438	0.	0.4	1085	0.2	1.3	0.15	1071?
7,7	$7/2+[633]_n+7/2+[404]_p$	0.92	461	2.5	1.4	414	4.9	2.7	1.8	433
8,			655	3.5	6.2	541	7.1	11.4	0.6	538
9,			872	1.6	10.2	691	3.5	17.9	0.19	676
10,			1114	0.7	5.8	865	1.5	9.7	0.15	847
$4,4^-$	$1/2-[521]_n+7/2+[404]_p$	0.89	368	238.3	0.9	364	248.0	1.0	248.	364
5,			489	45.9	1.8	480	42.0	2.0	21	480
6,			634	16.6	1.9	619	14.0	2.2	6.46	618
7,			804	3.3	1.1	782	2.6	1.3	2.	779
8,			997	0.2	0.3	968	0.2	0.3	0.66	

(continued next page)

I,K^{π}	Configuration	V^2 of transferred neutron	Unperturbed			Coriolis Perturbed				Experimental energy (keV)
			Energy (keV)	Cross-section (d,t) θ=60° (μb/sr)	Cross-section (^{3}He,α) θ=35° (μb/sr)	Energy (keV)	Cross-section (d,t) θ=60° (μb/sr)	Cross-section (^{3}He,α) θ=35° (μb/sr)	$\frac{\sigma(d,t)}{\sigma(^3He,\alpha)}$ predicted	
$3,3^-$	$1/2-[521]_n-7/2+[404]_p$	0.89	433	190.7	0.7	433	190.7	0.7	272	432
4,			530	60.6	1.5	532	55.4	1.3	43	532
5,			651	21.7	1.8	654	26.8	1.7	16	655
6,			796	6.9	1.4	802	9.8	1.2	8.2	801
7,			965	1.2	0.6	973	2.0	0.5	4.	968 ?
$3,3^-$	$1/2-[510]_n-7/2+[404]_p$	0.05	1400	3.2	0.1	1402	4.2	0.1	42	(1081)
4,			1497	2.0	0.1	1500	4.2	0.2	21	
5,			1618	0.5	0.1	1617	1.8	0.3	6	
6,			1763	0.1	0.	1761	0.2	0.5	0.6	
7,			1932	0.	0.	1949	0.	0.1		
$4,4^-$	$1/2-[510]_n+7/2+[404]_p$	0.05	1500	3.3	0.1	1506	1.6	0.5	3.2	(1203)
5,			1621	1.5	0.2	1637	1.3	0.8	1.6	
6,			1766	0.2	0.1	1775	0.2	0.2	1.0	
7,			1936	0.	0.	1949	0.1	0.1		

(continued next page)

Table 5.2.2

Table 5.2.2 (continued)

I,K^{π}	Configuration	V^2 of transferred neutron	Unperturbed			Coriolis Perturbed				
			Energy (keV)	Cross-section (d,t) θ=60° (μb/sr)	Cross-section (^{3}He,α) θ=35° (μb/sr)	Energy (keV)	Cross-section (d,t) θ=60° (μb/sr)	Cross-section (^{3}He,α) θ=35° (μb/sr)	σ(d,t)/σ(^{3}He,α) predicted	Experimental energy (keV)
$2,2^-$	$3/2-[521]_n-7/2+[404]_p$	0.95	1178	15.8	0.6	1178	13.9	0.5	28	1178
3,			1251	16.3	2.1	1249	10.3	1.9	5.4	1243
4,			1347	14.0	3.5	1344	8.0	3.6	2.2	1353?
5,			1468	7.6	3.5	1468	4.4	3.7	1.2	1481?
6,			1614	2.3	2.1	1609	1.4	2.1	0.66	
7,			1783	0.3	0.8	1778	0.2	0.7	0.3	
$5,5^-$	$3/2-[521]_n+7/2+[404]_p$	0.95	1303	26.4	2.1	1303	25.8	2.2	12	1304
6,			1448	16.3	5.1	1458	15.7	4.3	3.6	1456
7,			1618	6.3	4.3	1639	5.6	2.6	2.2	1628
8,			1811	0.2	1.3	1856	0.1	0.6	0.2	
$1,1^+$	$5/2+[642]_n-7/2+[404]_p$	0.96	1100	0.3	0.	1002	0.	0.		
2,			1148	0.6	0.2	1162	0.5	0.2	2.5	
3,			1221	1.1	0.8	1242	1.0	0.5	2	
4,			1318	1.4	2.6	1349	1.3	1.6	0.8	
5,			1439	1.2	5.5	1483	1.0	2.0	0.5	
6,			1584	0.8	7.5	1642	0.8	4.7	0.2	

(continued next page)

Table 5.2.2 (continued)

I,K^{π}	Configuration	V^2 of transferred neutron	Unperturbed			Coriolis Perturbed				Experimental energy (keV)
				Cross-section			Cross-section		$\frac{\sigma(d,t)}{\sigma(^3He,\alpha)}$	
			Energy (keV)	(d,t) θ=60° (μb/sr)	(^{3}He,α) θ=35° (μb/sr)	Energy (keV)	(d,t) θ=60° (μb/sr)	(^{3}He,α) θ=35° (μb/sr)	predicted	
7,			1753	0.4	6.3	1826	0.3	3.3	0.1	
8,			1947	0.1	3.2	2032	0.1	3.3	0	
9,			2165	0.	0.9	2260	0.	1.1		
6,6	$5/2+[642]_n+7/2+[404]_p$	0.96	1200	1.5	0.9	1167	2.6	1.6	1.6	
7,			1369	2.2	4.3	1345	2.8	5.9	0.5	
8,			1563	1.4	9.1	1547	1.4	9.2	0.15	
9,			1781	0.5	9.3	1771	0.3	6.6	0.45	
10,			2023	0.1	3.7	2019	0.1	1.6	0.1	
$6,6^-$	$5/2-[523]_n+7/2+[404]_p$	0.95	1200	13.0	3.6	1195	10.7	3.8	2.8	
7,			1369	7.6	6.7	1364	5.6	7.0	0.8	
8,			1563	1.0	3.9	1556	1.0	3.8	0.26	
$1,1^-$	$5/2-[523]_n-7/2+[404]_p$	0.95	1250	2.9	0.5	1251	2.9	0.5	5.8	
2,			1298	5.0	1.5	1305	5.7	1.5	3.8	
3,			1371	5.2	3.2	1384	7.1	2.8	2.5	
4,			1468	3.6	4.1	1487	5.0	2.6	1.9	

(continued next page)

Table 5.2.2 (continued)

I,K^{π}	Configuration	V^2 of transferred neutron	Unperturbed			Coriolis Perturbed			$\frac{\sigma(d,t)}{\sigma(^3He,\alpha)}$ predicted	Experimental energy (keV)
			Energy (keV)	Cross-section (d,t) θ=60° (μb/sr)	Cross-section (^{3}He,α) θ=35° (μb/sr)	Energy (keV)	Cross-section (d,t) θ=60° (μb/sr)	Cross-section (^{3}He,α) θ=35° (μb/sr)		
5,			1589	0.5	3.3	1613	1.7	1.2	1.4	
6,			1734	0.1	1.6	1795	0.5	0.4	1.2	
$1,1^+$	$9/2+[624]_n-7/2+[404]_p$	0.05	1000	0.	0.	1001	0.	0.		
2,			1048	0.	0.	1053	0.	0.		
3,			1121	0.	0.1	1127	0.2	0.4	0.5	
4,			1218	0.	0.3	1224	0.2	0.1	2.	
5,			1339	0.	0.4	1341	0.6	3.0	0.2	
6,			1484	0.	0.3	1479	0.3	1.4	0.2	
7,			1653	0.	0.1	1638	0.4	4.4	0.1	
8,			1847	0.	0.	1818	0.1	1.9	0.1	
9,			2065	0.	0.	2019	0.	1.1	-	
$8,8^+$	$9/2+[624]_n+7/2+[404]_p$	0.05	1100	0.1	0.2	926	0.7	0.1	7	
9,			1318	0.1	0.6	1340	0.2	0.2	1	
10,			1560	0	0.6	1586	0.	0.		

a) subtract $\approx$ 79 keV to account for odd-even shift

culation as in the neutron transfer work. This difference may in fact indicate that these two sets of states are not completely independent has has been assumed in these calculations. The only other free parameters in the calculation were the location of the band heads and the odd-even shift in the $K^{\pi} = 0^{+}$ band. This calculation is discussed in detail in section 5.4(i). Table 5.2.2 lists the unperturbed energies and cross sections as well as the energies and cross sections when Coriolis coupling is included.

Tables 5.2.1 and 5.2.2 may be compared to Tables 5.1.1 and 5.1.2 directly to see the agreement between the predicted and observed cross sections for states populated by these reactions into ^{174}Lu.

No attempt was made to calculate the two quasi-particle energies of the states from the Nilsson model, nor was any attempt made to calculate effects due to the residual neutron-proton interaction. The splitting between the spin singlet and spin triplet configurations as well as the odd-even shift are due to the residual interaction. The particle vibrational couplings which could be important above about 1 MeV of excitation have also been ignored.

5.3 Interpretation of the proton transfer spectra

5.3(i) The $\{7/2^{+}[404]_{p} \pm 5/2^{-}[512]_{n}\}$ states

The ground state band of ^{174}Lu is formed in the proton transfer reactions by transferring a proton to the $7/2^{+}[404]$

orbital. This nucleon couples to the $5/2^-[512]$ neutron of the target to form states with $K^\pi = 1^-$ or $K^\pi = 6^-$. The $K^\pi = 1^-$ spin triplet configuration forms the ground state band as expected by the Gallagher-Moszkowski rule (Gallagher and Moszkowski 1958). The $K^\pi = 6^-$ spin singlet coupling is experimentally found to lie 171 keV higher.

Figure 5.3.1 shows a comparison of the predicted and observed fingerprints for the states arising from the $K^\pi = 1^-$ and $K^\pi = 6^-$ configurations. The DWBA calculation for the (α,t) reaction was effectively normalized using these states hence the remarkable agreement. Because the $7/2^+[404]$ proton is the odd particle in ^{175}Lu and the $5/2^-[512]$ neutron is the odd particle in ^{173}Yb, the $\{7/2^+[404]_p \pm 5/2^-[512]_n\}$ configurations may be populated by all four reactions. These two configurations are the only ones which may be populated in both neutron and proton transfer reactions. The population of these states by the neutron transfer reactions is referred to briefly in section 5.4.

The ground state band is quite strongly populated in the (α,t) reaction and the energies of these states agree very well with those measured by Jones and Sheline (1970) and with earlier decay work (Harmatz et al. 1960 and Lederer et al. 1967). The spin I = 1, 2, 3, 4 and perhaps 5 members of the ground state band have been identified in the proton transfer work. The states formed by stripping a $7/2^+[404]$ proton are not very intensely populated in the $(^3$He,d) spectra because this reaction favours low

Figure 5.3.1

A comparison of the predicted and observed fingerprints of the $\{7/2^+[404]_p \pm 5/2^-[512]_n\}$ configurations. The bars are identified by the spin I of the state. The $I,K^\pi = 6,1^-$ state is possibly obscured by other strongly populated states in the (d,t) reaction. As may be seen, the cross sections for these states are very low in the (^{3}He,α) reaction because these configurations are populated mainly by ℓ=3 transitions in the neutron transfer case. The proton transfer reactions to these states is by pure ℓ=4 transitions hence the rather small (^{3}He,d) cross sections.

Fingerprint of $\{\frac{7}{2}^+[404]_p \pm \frac{5}{2}^-[512]_n\}$

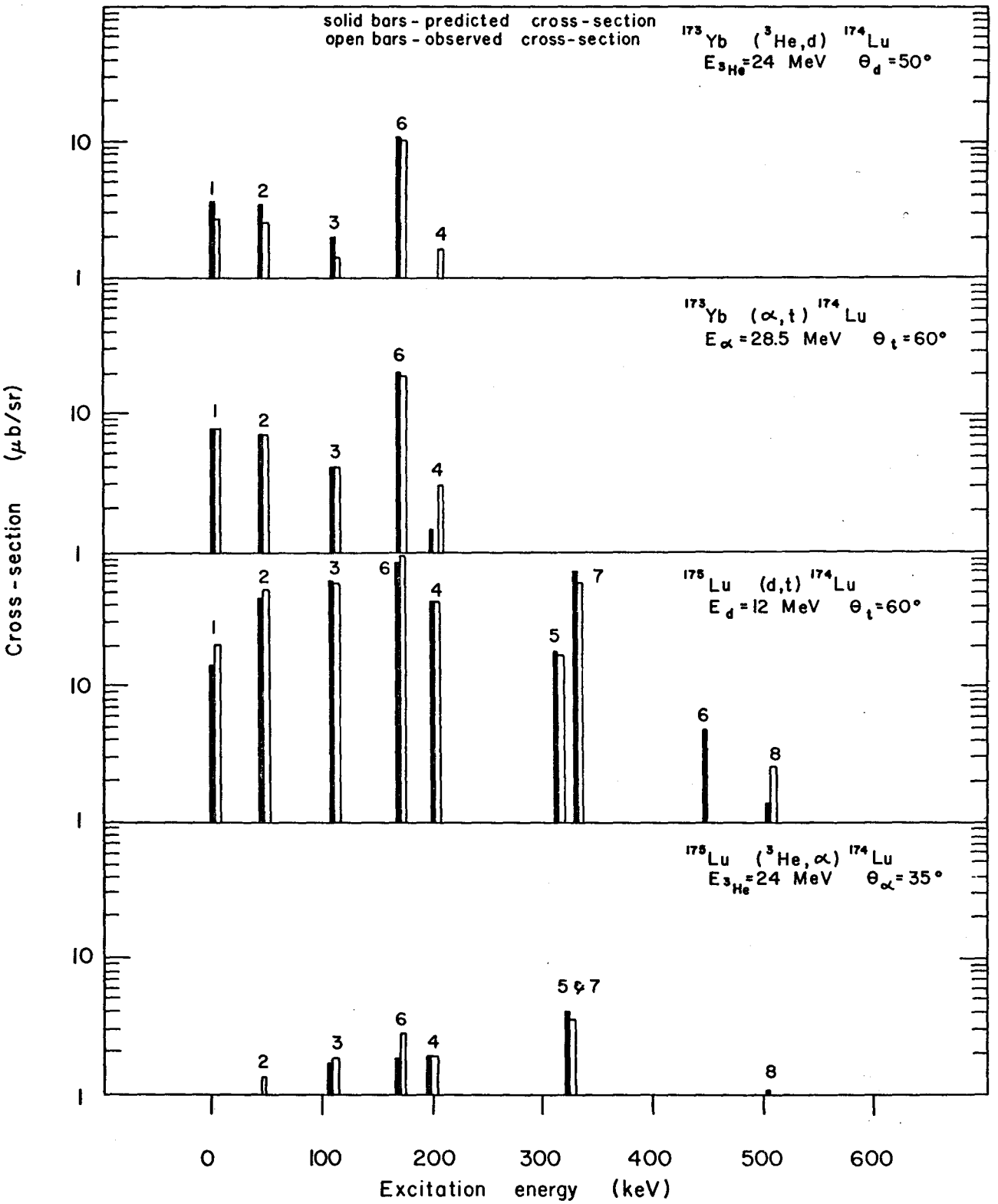

orbital angular momentum transfers. Since $C_{7/2,7/2}$ is almost unity for the $7/2^+[404]$ orbital, the above states are populated almost entirely by $\ell=4$ transitions.

The $K^\pi = 6^-$ configuration $\{7/2^+[404]_p + 5/2^-[512]_n\}$ has its band head at 171 keV. The spin I=7 member of this band is weakly populated and is not resolved from the I=5 member of the ground state band and another strongly populated state at 298 keV.

The cross sections for the first three members of the ground state band and the $I,K^\pi = 6,6^-$ coupling of the $7/2^+[404]$ proton to the target neutron were used to normalize the DWBA calculations. The experimental $\ell=4$ cross section ratios in fig. 5.2.1 were obtained from these two bands. Due to large uncertainties in the (^{3}He,d) cross sections for these levels, the lower spin states do not fall exactly on the predicted $\ell=4$ line.

The Coriolis coupling calculations showed that none of the configurations which could be populated in the present proton transfer reactions would be expected to mix strongly with the ground state band or the $K^\pi = 6^-$ band. However, it may be possible for other configurations to mix into the ground state band altering its rotational parameter. When calculating the Coriolis interaction for the other states in the nucleus which could be observed by proton transfer reactions, a rotational parameter of 11.1 keV was used. This is the value observed in the ground state band.

5.3(ii) The $\{5/2^+[402]_p \pm 5/2^-[512]_n\}$ states

The $5/2^+[402]$ proton orbital may couple with the $5/2^-[512]$ neutron orbital to either $K^\pi = 0^-$ or $K^\pi = 5^-$. The Gallagher-Moszkowski rule (Gallagher and Moszkowski 1958) predicts the $K^\pi = 5^-$ spin triplet state to lie at a lower energy than the spin singlet $K^\pi = 0^-$ configuration. The splitting energy between the two band heads is observed to be 100 keV. As may be seen from table 5.2.1, neither of the bands is expected to be significantly perturbed by the Coriolis interaction. The $5/2^+[402]$ proton orbital originates from the $d_{5/2}$ shell model state and has essentially all of its wavefunction in the $j = 5/2$ component; thus the two configurations containing the orbital are expected to be populated by strong $\ell=2$ transitions.

The $K^\pi = 5^-$ band head is predicted to be the most intense peak observed in both the low energy (^{3}He,d) spectra and the (α,t) spectra. The largest cross sections observed in these spectra below one MeV are at 455 keV. The (^{3}He,d) to (α,t) cross section ratio of this peak is consistent with that for an $\ell=2$ transition. The 455 keV level has been assigned as the band head of the $K^\pi = 5^-$, $\{7/2^+[404]_p + 5/2^-[512]_n\}$ configuration. The other members of this band have not been identified as they are expected to have cross sections less than 1 μb/sr.

The $K^\pi = 0^-$ band, because of the residual interaction, has an odd-even shift. In this band, the even spin members form a rotational band and the odd spin members form a second band

displaced about 50 keV from the position predicted by a simple I(I+1) energy spacing rule. The $K^{\pi} = 0^{-}$ band has been assigned at 555 keV, 521 keV, 619 keV and 627 keV for the spin I=0 to I=3 members respectively. The spin I=2 and 3 members are in an unresolved multiplet; however, the total cross-section of the peak in the (^{3}He,d) exposure is consistent with the assignment of the peak to these two band members and an I=5 member from the $1/2^{-}[541]$ proton orbital coupling to the target neutron. Similarly the spin I=1 band member is unresolved from an I=4 state formed by transferring a proton into the $1/2^{-}[541]$ orbital. Higher spin members of the $K^{\pi} = 0^{-}$ band have not been assigned. The (α,t) cross section of the state at 853 keV agrees very well with what is expected for the spin I=4 member of this band; however, this energy is considerably higher than the expected energy of the state. It is possible that the $I,K^{\pi} = 4,0^{-}$ state is unresolved from the $I,K^{\pi} = 4,2^{-}$ state at 771 keV. The (^{3}He,d) to (α,t) cross section ratios for the peaks assigned to the $K^{\pi} = 0^{-}$ band are in good agreement with the predicted ℓ=2 cross section ratios.

Figure 5.3.2 shows the predicted cross sections for the $\{5/2^{+}[402]_{p} \pm 5/2^{-}[512]_{n}\}$ configurations and compares them to the cross sections attributed to these states. The agreement is excellent.

Figure 5.3.2

A comparison of the predicted and observed fingerprints of the $\{5/2^{+}[402]_{p} \pm 5/2^{-}[512]_{n}\}$ configurations. The bars are identified by the spin I of the state. The odd-even shift and the relative band head energies were treated as free parameters in this fit. There are essentially no free parameters in the calculation of the predicted cross sections.

Fingerprint of $\left\{\frac{5}{2}^{+}\,[402]_p \pm \frac{5}{2}^{-}\,[512]_n\right\}$

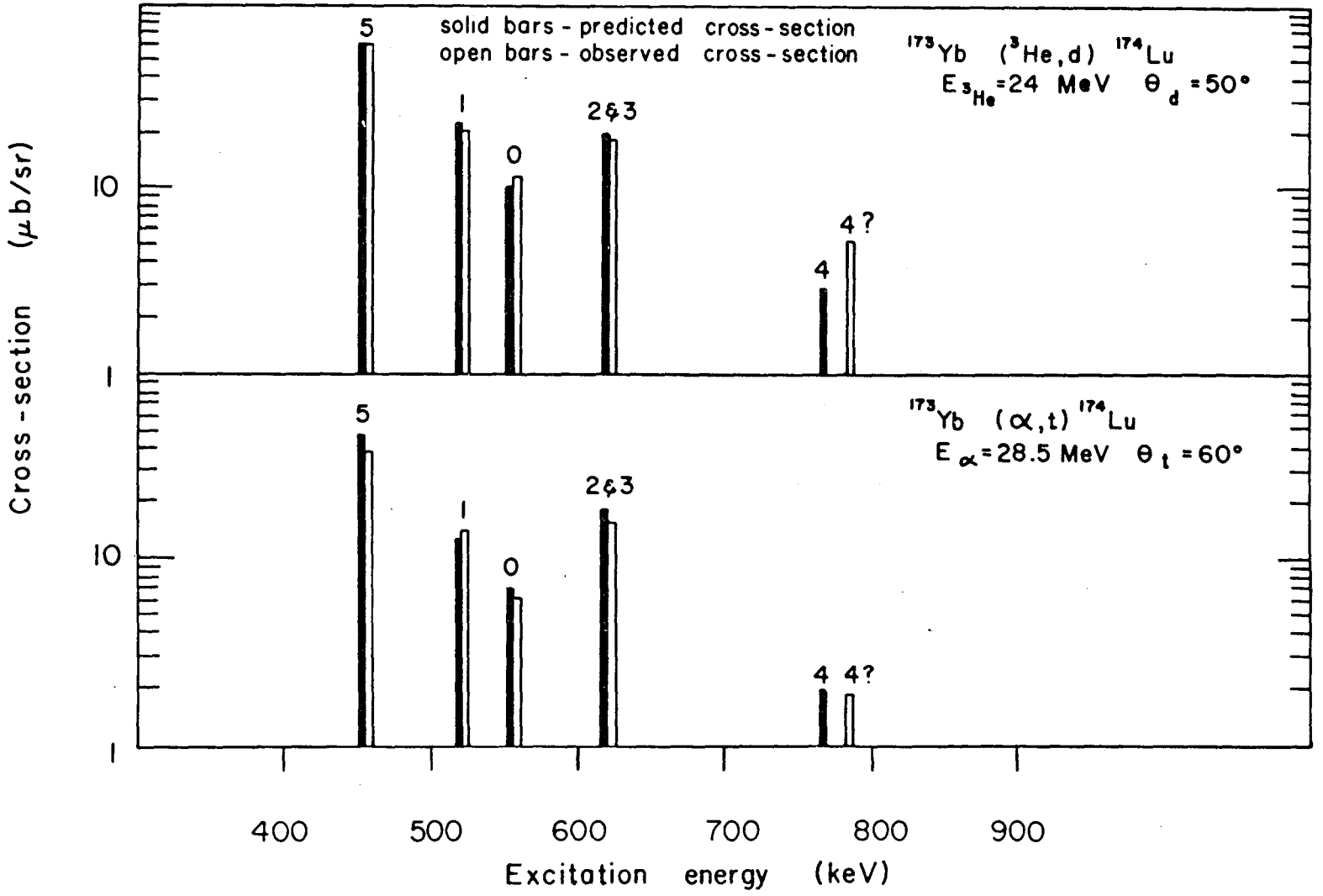

5.3(iii) The $\{9/2^-[514]_p \pm 5/2^-[512]_n\}$ states

The only orbitals in the 71 proton, deformation δ=0.27 region of the Nilsson diagram which may be populated by high-ℓ transfers are the $7/2^+[404]$, the $1/2^-[541]$ and the $9/2^-[514]$ states. The $7/2^+[404]$ orbital, which is transferred to form the ground state band, has been discussed in subsection 5.3(i). The $1/2^-[541]$ proton orbital coupled to the $5/2^-[512]$ target neutron has a strongly perturbed fingerprint due to the Coriolis interaction and is discussed in subsection 5.3(iv). Thus the remaining states to be populated by high angular momentum transitions in the low energy spectrum of ^{174}Lu should arise from the $\{9/2^-[514]_p \pm 5/2^-[512]_n\}$ configurations. In that the $9/2^-[514]$ orbital originates from the $h_{11/2}$ shell model state the rotational bands build on these configurations should be populated exclusively by ℓ=5 transitions.

The $9/2^-[514]$ proton couples with the $K^\pi = 5/2^-$ target neutron to form $K^\pi = 7^+$ and $K^\pi = 2^+$ rotational bands. The Gallagher-Moszkowski rule predicts the $K^\pi = 7^+$ state should lie at the lower energy. The predicted fingerprints of these two rotational bands are shown in Fig. 5.3.3.

The spin I=8 member of the $K^\pi = 7^+$ triplet coupling of the $\{9/2^-[514]_p + 5/2^-[512]_n\}$ configuration has been assigned at 659 keV. This state has a (^{3}He,d) to (α,t) cross section ratio (fig. 5.2.1) which is consistent with an ℓ=4 transition rather than ℓ=5 which is expected for such a state. The experi-

Figure 5.3.3

A comparison of the predicted and observed fingerprints of the $\{9/2^{-}[514]_{p} \pm 5/2^{-}[512]_{n}\}$ configurations. The spin I=7 state is masked by some other strongly populated states. The spin $I,K^{\pi} = 8,7^{+}$ and $I,K^{\pi} = 3,2^{+}$ states lie in a region which apparently has a very high level density.

Fingerprint of $\{\frac{9}{2}^-[514]_p \pm \frac{5}{2}^-[512]_n\}$

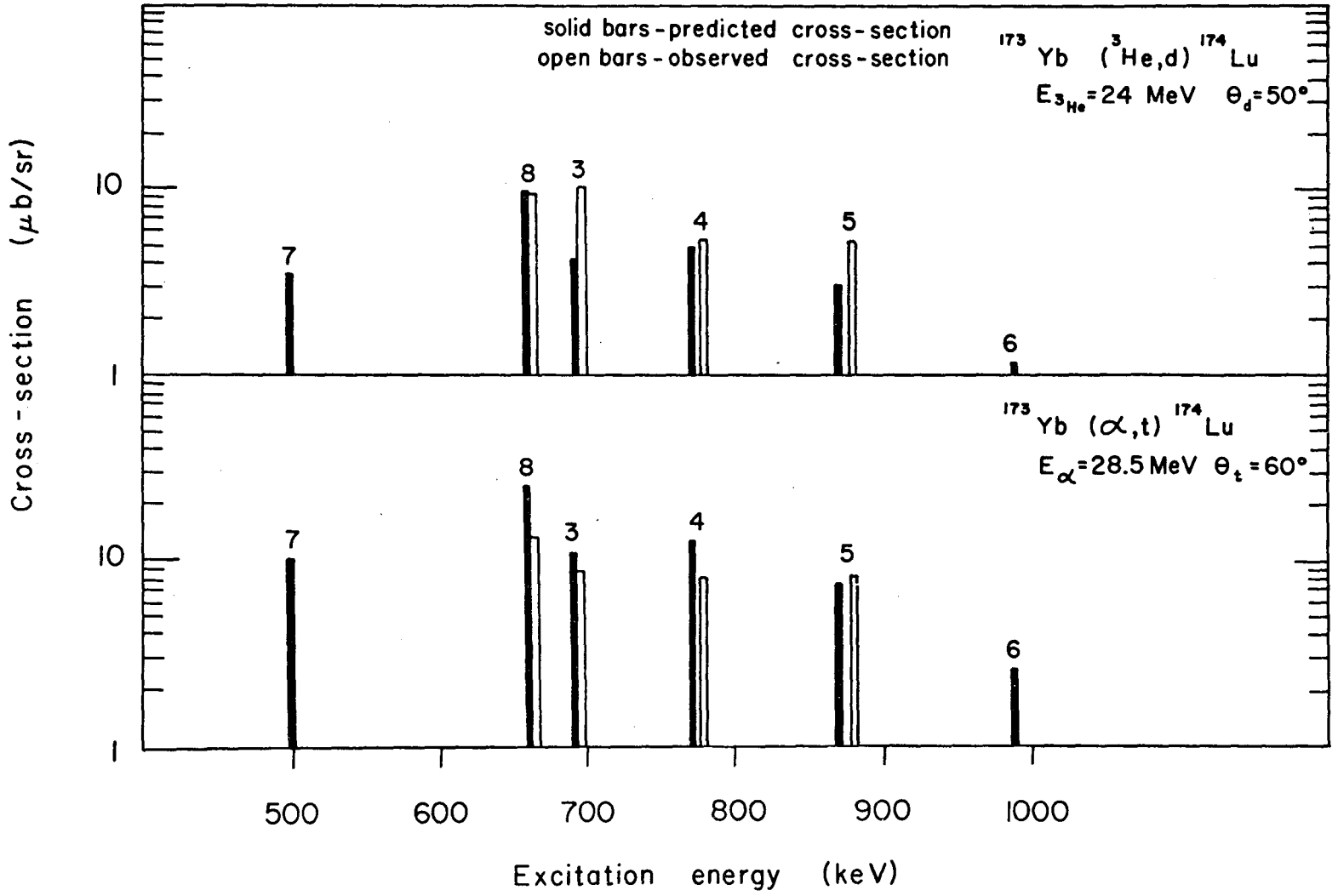

mental (^{3}He,d) cross section for this level is in good agreement with the predicted value; however, the observed (α,t) cross section is smaller than the predicted value by almost a factor of two. It is felt that this is due to the DWBA calculations not predicting the Q-dependence of the (α,t) reactions accurately. Similar problems in using the ratios of (^{3}He,d) and (α,t) cross sections to distinguish between ℓ=4 and ℓ=5 transitions have been encountered in the study of ^{151}Pm levels using proton transfer reactions (Burke and Waddington 1972). Based on the above assignment for the spin I=8 member and assuming a reasonable rotational parameter, the spin I=7 band head would be expected to fall near 500 keV. This lies in the neighbourhood of a broad peak in the (α,t) spectrum which has a (^{3}He,d) to (α,t) cross section ratio indicative of a low-ℓ transition. The intensity of the corresponding peak in the (^{3}He,d) spectra can be attributed to other states. The predicted contribution of the I=7 state to the (^{3}He,d) peak is only about 10% of the observed (^{3}He,d) intensity. The observed (α,t) cross section may also be attributed to other states. Thus the relatively small peaks expected for the spin I=7 member would be obscured by larger ones so a definite assignment is difficult to make.

The spin I=3, 4 and 5 members of the $K^\pi = 2^+$, $\{9/2^-[514]_n - 5/2^-[512]_n\}$ configuration have been assigned at 692 keV, 771 keV and 875 keV respectively. The band head is expected to be very weakly populated and has not been identified. The spin I=3 member of the band is likely in an unresolved multi-

plet with a low-ℓ state because the (^{3}He,d) to (α,t) cross section ratio indicates a lower value than expected for this assignment. The spins I=4 and 5 members of this band have experimental (^{3}He,d) to (α,t) cross section ratios which are in good agreement with that observed for the $I,K^\pi = 8,7^+$ state formed from the $\{9/2^-[514]_p + 5/2^-[512]_n\}$ configuration. The I=6 member of the band is predicted to be about 991 keV. In this region of the proton spectra there are several small peaks which could be attributed to this level though it remains unassigned.

A comparison of the predicted cross sections and the cross sections for the peaks attributed to these configurations is shown in fig. 5.3.3. Though the agreement is not particularly good for individual states, other evidence such as the cross section ratios indicating a high angular momentum (ℓ) transfer and energy considerations tend to strengthen these assignments.

The $K^\pi = 7^+$ and $K^\pi = 2^+$ bandheads are not observed in the present work but their splitting is estimated, from the positions of higher spin band members, to be 132 keV. Coriolis coupling exists between the rotational bands formed by transferring the $9/2^-[514]$ proton orbital and those originating from the transfer of the $7/2^-[523]$ hole state and the $11/2^-[505]$ particle state. The $\{7/2^-[523]_p \pm 5/2^-[512]_n\}$ and $\{11/2^-[505]_n \pm 5/2^-[512]_n\}$ configurations were placed at energies greater than 1800 keV in the coupling calculation. This energy was estimated as being the minimum energy at which they were likely to appear. The $11/2^-[505]$

orbital was not identified in the odd-A lutetium isotopes (Chapter 4) nor are there are any states in the ^{174}Lu spectra which are obviously due to this orbital below 2 MeV excitation. The $7/2^-[523]$ orbital lies below the Fermi surface so the $\{7/2^-[523]_p \pm 5/2^-[512]_n\}$ configurations are not expected to be populated. The main effect of this Coriolis coupling, as may be seen from table 5.2.1, is to reduce the rotational parameter of the $\{9/2^-[514]_p \pm 5/2^-[512]_n\}$ configurations and to slightly increase the cross sections to most of the band members.

5.3(iv) The $\{1/2^-[541]_p \pm 5/2^-[512]_n\}$ states

Two rotational bands, with $K^\pi = 2^+$ and $K^\pi = 3^+$, are expected to be formed by transferring a proton into the $1/2^-[541]$ orbital and coupling it with the $5/2^-[512]$ neutron in the target. These two bands should be strongly mixed by the Coriolis interaction as the calculated j_+ matrix element has a value of -3.4. The transfer of the $1/2^-[541]$ proton involves mainly ℓ=5 transitions as this orbital originates from the $h_{9/2}$ shell. However, there are also appreciable ℓ=1 and ℓ=3 components in its wavefunction. In studies of the odd lutetium isotopes with (^{3}He,d) and (α,t) reactions several strong peaks were assigned to the $1/2^-[541]$ band, which started at an excitation energy of approximately 125 keV in ^{173}Lu and approximately 350 keV in ^{175}Lu.

The experimental (^{3}He,d) and (α,t) spectra in the present work do not exhibit structures which resemble the predicted unperturbed fingerprints for the $K^\pi = 2^+$ and $K^\pi = 3^+$ bands. However,

there is a series of states starting at an excitation energy of approximately 235 keV which has not been assigned and which has approximately the same total cross section as would be expected for the transfer of a $1/2^-[541]$ proton. A set of mixing calculations was done to test whether the observed structure in the spectra could be explained by Coriolis coupling of the two bands. These calculations assumed an unperturbed rotational parameter of 11.1 keV for both bands, as in previous subsections. The Coriolis matrix elements were not attenuated but were corrected for pairing effects. The only free parameter was the separation of the two bandheads. The actual calculations also included the higher-lying $\{3/2^-[532]_p \pm 5/2^-[512]_n\}$ and $\{1/2^-[530]_p \pm 5/2^-[512]_n\}$ configurations but these did not have strong effects on the predicted results.

It was found that for an unperturbed separation of 40 keV for the $I,K^\pi = 2,2^+$ and $I,K^\pi = 3,3^+$ states, with the $K^\pi = 2^+$ states lowest as predicted by the Gallagher-Moszkowski rule, the predicted fingerprints were similar in appearance to the observed spectra. This is shown in fig. 5.3.4 where the solid bars represent the predicted cross sections and the open bars show the observed values. The mixing is so strong that the I(I+1) spacing has been lost and all band members have comparable amplitudes of the $K^\pi = 2^+$ and $K^\pi = 3^+$ configurations.

It is seen in fig. 5.3.4. that the level spacings have been fitted very well and the predicted relative (α,t)

Figure 5.3.4

A comparison of the predicted and observed fingerprints of the $\{1/2^-[541]_p \pm 5/2^-[512]_n\}$ configurations. The bars are identified by the spin I of the state. The only free parameter in this calculation is the energy separation between $K^\pi = 2^+$ and $K^\pi = 3^+$ bandheads.

Fingerprint of $\{\frac{1}{2}^-[541]_p \pm \frac{5}{2}^-[512]_n\}$

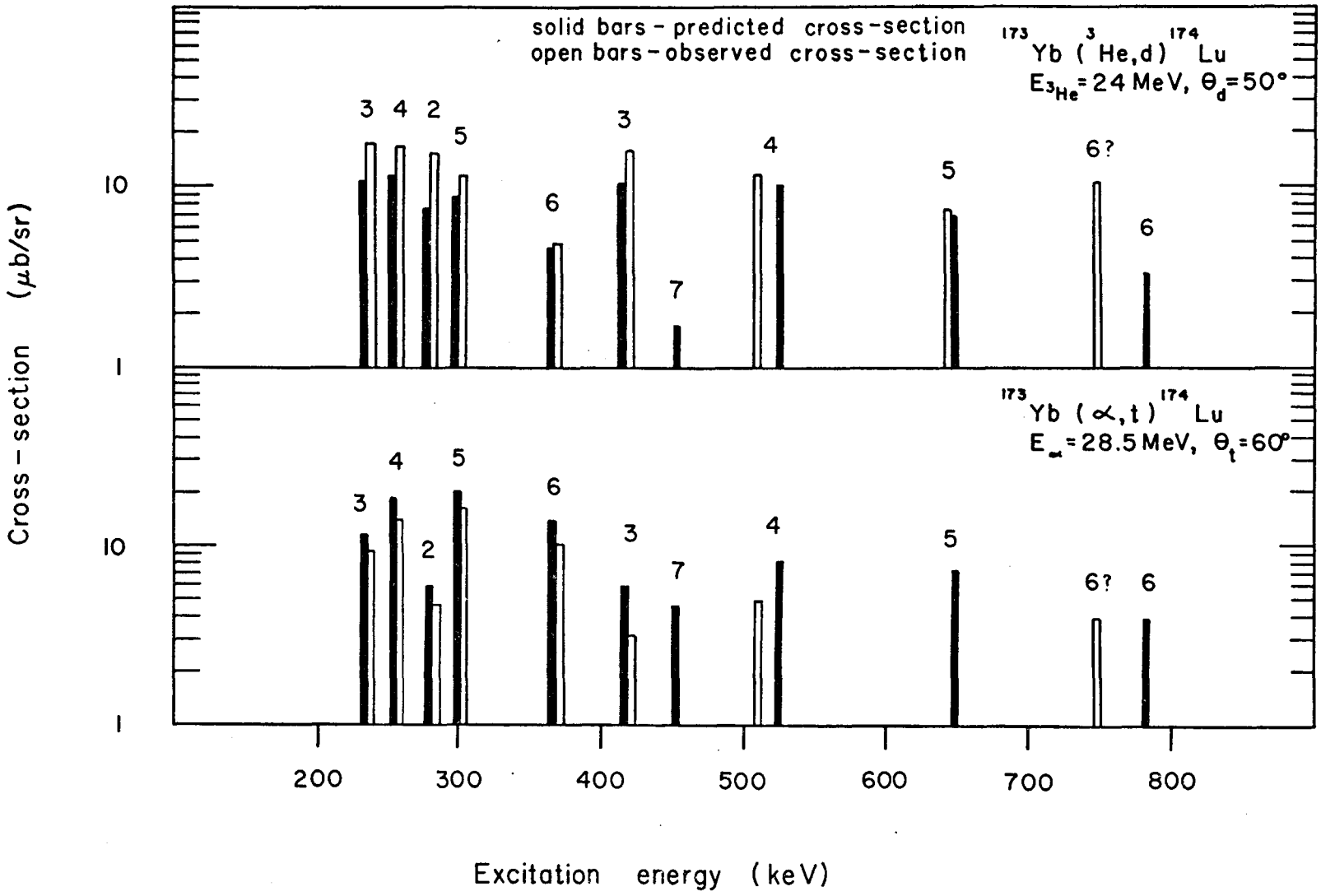

cross sections are also in very good agreement with experiment. The (^{3}He,d) relative cross sections for the lower band are also in good agreement with the calculated fingerprint except for the I=2 member at approximately 270 keV which may be an unresolved doublet in the spectrum. The I=7 member of this band is expected to be weak and has likely been obscured by the strong peak due to the $I,K^{\pi} = 5,5^-$ state at 455 keV.

The observed members of the higher energy band are in fair agreement with the energies and cross sections predicted in the Coriolis coupling calculation. The spin I=4 state is part of an unresolved multiplet between 507 and 521 keV so its energy is not accurately known. Similarly the spin I=5 member at 640 keV is part of an unresolved multiplet. In this case the total (^{3}He,d) cross section is in good agreement with the sum of the individual cross sections for states assigned to the multiplet though the (α,t) cross section is too small by a factor of almost two. The spin I=6 member has not been definitely assigned though there is a state at 746 keV which has the expected (α,t) cross section. The (^{3}He,d) cross section for this peak is too large for such an assignment and the energy is 40 keV lower than predicted by the coupling calculation, though it might be possible to account for the displacement by mixing to some additional states.

The (^{3}He,d) to (α,t) cross section ratios for the two bands are observed to decrease as the spin I of the state increases.

This indicates that as the spin increases, larger contributions to the cross sections are being made from the high-ℓ components. From fig. 5.3.4 it may be seen that the predicted (^{3}He,d) cross section is larger than expected by almost a constant amount, and the (α,t) cross section is smaller than predicted. This causes the ratios observed for the $\{1/2^-[541]_p \pm 5/2^-[512]_n\}$ configurations to be larger than the predicted values.

It is concluded that the observed states represented in fig. 5.3.4 are most likely due to the $\{1/2^-[541]_p \pm 5/2^-[512]_n\}$ configurations, which are strongly perturbed by the Coriolis mixing. The band head separation of 40 keV which resulted in the best fit to the experimental data is somewhat smaller than the typical spin triplet-singlet splittings of 100-200 keV reported (Jones et al. 1971) for other two quasi-particle states in this region.

5.3(v) The $\{1/2^-[530]_p \pm 5/2^-[512]_n\}$ and $\{3/2^-[532]_p \pm 5/2^-[521]_n\}$ states

It may be seen in the proton transfer spectra of fig. 5.1.1 that the region from 1250 keV to 1600 keV contains some large peaks in the (^{3}He,d) experiment. It is likely that these peaks arise from the $\{1/2^-[530]_p \pm 5/2^-[512]_n\}$ and the $\{3/2^-[532]_p \pm 5/2^-[512]_n\}$ configurations since the $1/2^-[530]$ and $3/2^-[532]$ proton orbitals in ^{173}Lu lie between 1150 keV and 1300 keV excitation.

The $\{3/2^-[532]_p \pm 5/2^-[512]_n\}$ configurations, forming rotational bands with $K^\pi = 1^+$ and 4^+ are not expected to be strongly

populated in these experiments. Only tentative assignments have been made for states formed from this orbital. However, the presence of these states influences the rotational spacings for members of the $\{1/2^-[541]_p \pm 5/2^-[512]_n\}$ bands and the fingerprints of the $\{1/2^-[530]_p \pm 5/2^-[512]_n\}$ configurations through the Coriolis interaction.

The $1/2^-[530]$ proton orbital combines with the target neutron to form states of $K^\pi = 2^+$ and 3^+. These states are expected to be fairly strongly coupled by the Coriolis interaction as the j_+ matrix element between them has a value of 2.16. A coupling calculation was performed simultaneously to the one described in subsect 5.3(iv).Again,the only free parameters were the unperturbed band head energies. It was found that the observed cross sections of the peaks at 1262, 1293, 1326 and 1421 keV could be explained by the coupling of the $K^\pi = 2^+$ and $K^\pi = 3^+$ configurations. Though the Gallagher-Moszkowski rule predicts the $K^\pi = 3^+$ band to lie at the lower energy, optimum agreement of the observed fingerprint with the predicted one was obtained with the $K^\pi = 2^+$ and 3^+ bandheads degenerate before mixing. The states at 1262, 1293, 1326 and 1421 keV have been assigned as the spin I=3, 2, 4 and 5 states respectively arising mostly from the $\{1/2^-[530]_p \pm 5/2^-[512]_n\}$ configurations. Figure 5.3.5 displays the predicted fingerprint and compares it to the assigned peaks. As may be seen, the agreement is very good in the (^{3}He,d) case. The spin I=6 member of the band may be located at 1533 keV though this energy is higher than predicted by the

Figure 5.3.5

A comparison of the predicted and observed fingerprints of the $\{1/2^{-}[530]_{p} \pm 5/2^{-}[512]_{n}\}$ configurations. The bars are identified by the spin I of the state.

Fingerprint of $\{\frac{1}{2}^{-}[530]_p \pm \frac{5}{2}^{-}[512]_n\}$

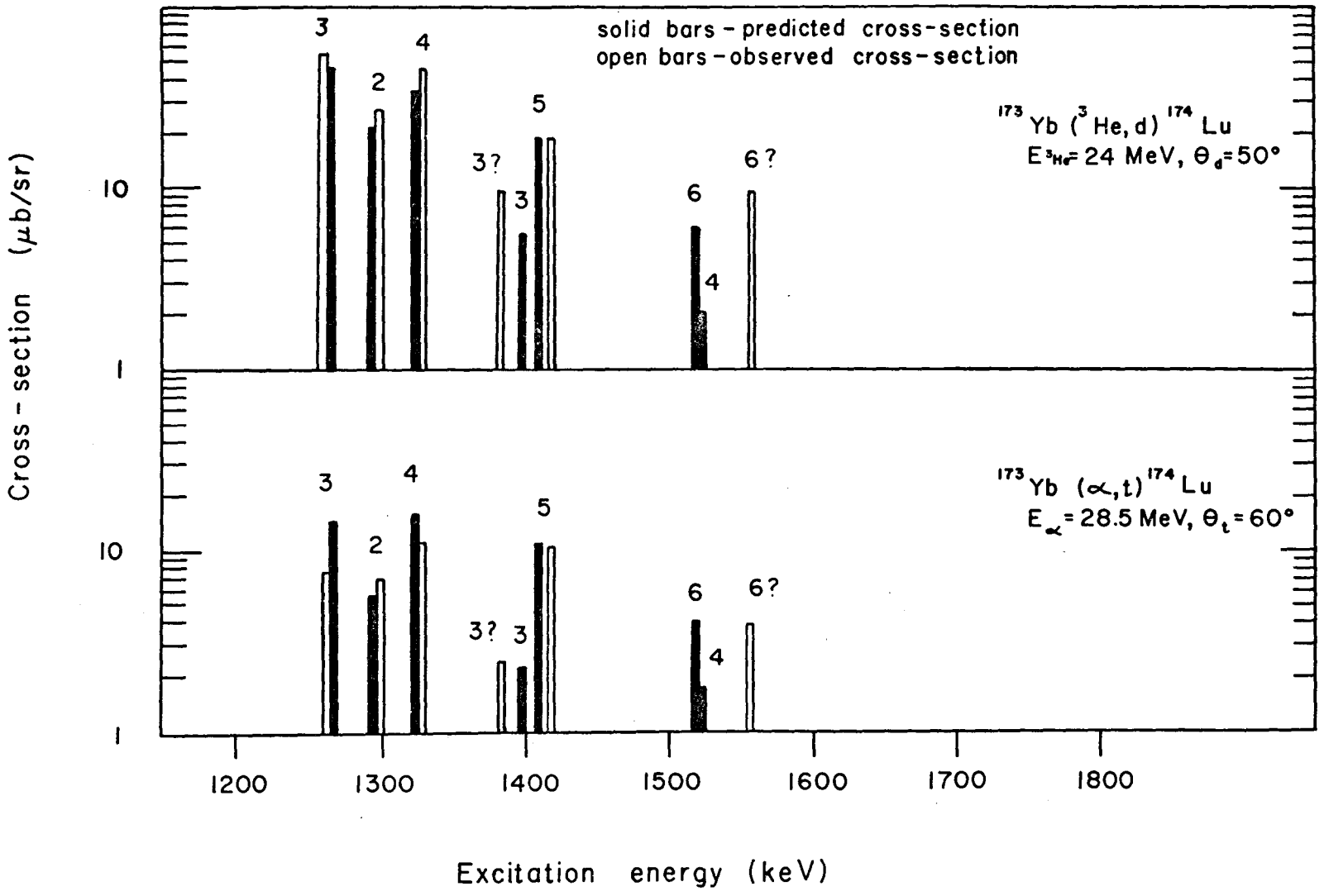

calculation. Only one band is strongly populated as almost all the intensity is shifted from the higher energy state into the lower state of the same spin by the Coriolis interaction.

The positions of the $\{3/2^-[532]_p \pm 5/2^-[512]_n\}$ configurations were varied in an attempt to improve the fit of the large peaks due to the transfer of the $1/2^-[530]$ proton. In the odd mass lutetium isotopes the bandhead of the $3/2^-[532]$ orbital has been assigned at a lower excitation than that of the $1/2^-[530]$ band. It was found that unless the $K^\pi=1^+$ and 4^+ states arising from the transfer of the $3/2^-[532]$ proton were above the unperturbed $K^\pi = 2^+$ and 3^+ bandheads, the spacing of the band members of the strongly mixed $\{1/2^-[530]_p \pm 5/2^-[512]_n\}$ configuration could not be reproduced. Adding the $5/2^-[523]$ and the $3/2^-[521]$ proton orbitals to the calculation at reasonable excitation energies failed to account for the observed compression of the $K^\pi = 2^+$ and 3^+ bands if the $\{3/2^-[532]_p \pm 5/2^-[512]_n\}$ configurations were placed below the $K^\pi = 2^+$ and 3^+ bandheads. Furthermore, placement of the $\{3/2^-[532]_p \pm 5/2^-[512]_n\}$ states in the region from 950 to 1200 keV resulted in poorer fits of the fingerprint for the transfer of the $1/2^-[541]$ proton orbital.

The $I,K^\pi = 4,4^+$ and $5,4^+$ states are the only ones from the $\{3/2^-[532]_p \pm 5/2^-[512]_n\}$ configuration which are expected, on the basis of the Coriolis coupling calculation, to have cross sections greater than 10 μb/sr in the (^{3}He,d) experiment. The spacing between these two strong peaks is predicted to be 135 keV. A tentative assignment is proposed that the spin I=4

and 5 members of the $K^{\pi} = 4^{+}$, $\{3/2^{-}[532]_{p}+5/2^{-}[532]_{n}\}$ configuration lie at 1439 keV and 1558 keV respectively. This is shown in fig. 5.3.6. One difficulty with this assignment is that there is no peak in the (α,t) spectrum which might correspond to the I=6 band member. The Coriolis coupling calculation was not able to predict the $I,K^{\pi} = 4,4^{+}$ state to lie in the vicinity of the 1378 keV peak as this was too close to the spin I=4 state of the mixed $K^{\pi} = 2^{+}$ and 3^{+} bands. The $K^{\pi} = 1^{+}$ coupling of this configuration is expected to lie at lower energies but it is not strongly populated and hence remains unidentified. The assignment of the $K^{\pi} = 4^{+}$ band should be considered very tentative as one cannot exclude the possibility that other strongly populated states such as those at 1362, 1378, 1474, 1533 and perhaps 1609 keV could be band members.

5.3(vi) Other states in the proton transfer spectrum

The $1/2^{+}[411]$ proton hole state has been identified (subsection 4.4(v)) in ^{173}Lu and ^{177}Lu at low excitation energies. Table 5.2.1 includes the predicted cross sections for the $\{1/2^{+}[411]_{p}\pm5/2^{-}[512]_{n}\}$ configurations in ^{174}Lu. Though some unresolved states may exist in the proton transfer spectra below 700 keV, it may be seen that virtually all the intensity in this region has been accounted for. The possible exceptions are weak states at 428 keV and 561 keV in the (α,t) exposure which appear to be doublets of which only one member has been assigned. These states have cross sections roughly comparable to what may

Figure 5.3.6

A comparison of the predicted and observed fingerprints of the $\{3/2^-[532]_p \pm 5/2^-[512]_n\}$ configurations and two states which may belong to the $K^\pi = 4^+$ rotational band. These configurations are strongly coupled to the states arising from the transfer of the $1/2^-[530]$ proton and also of the $1/2^-[541]$ proton .

Fingerprint of $\left\{\frac{3}{2}^{-}[532]_p \pm \frac{5}{2}^{-}[512]_n\right\}$

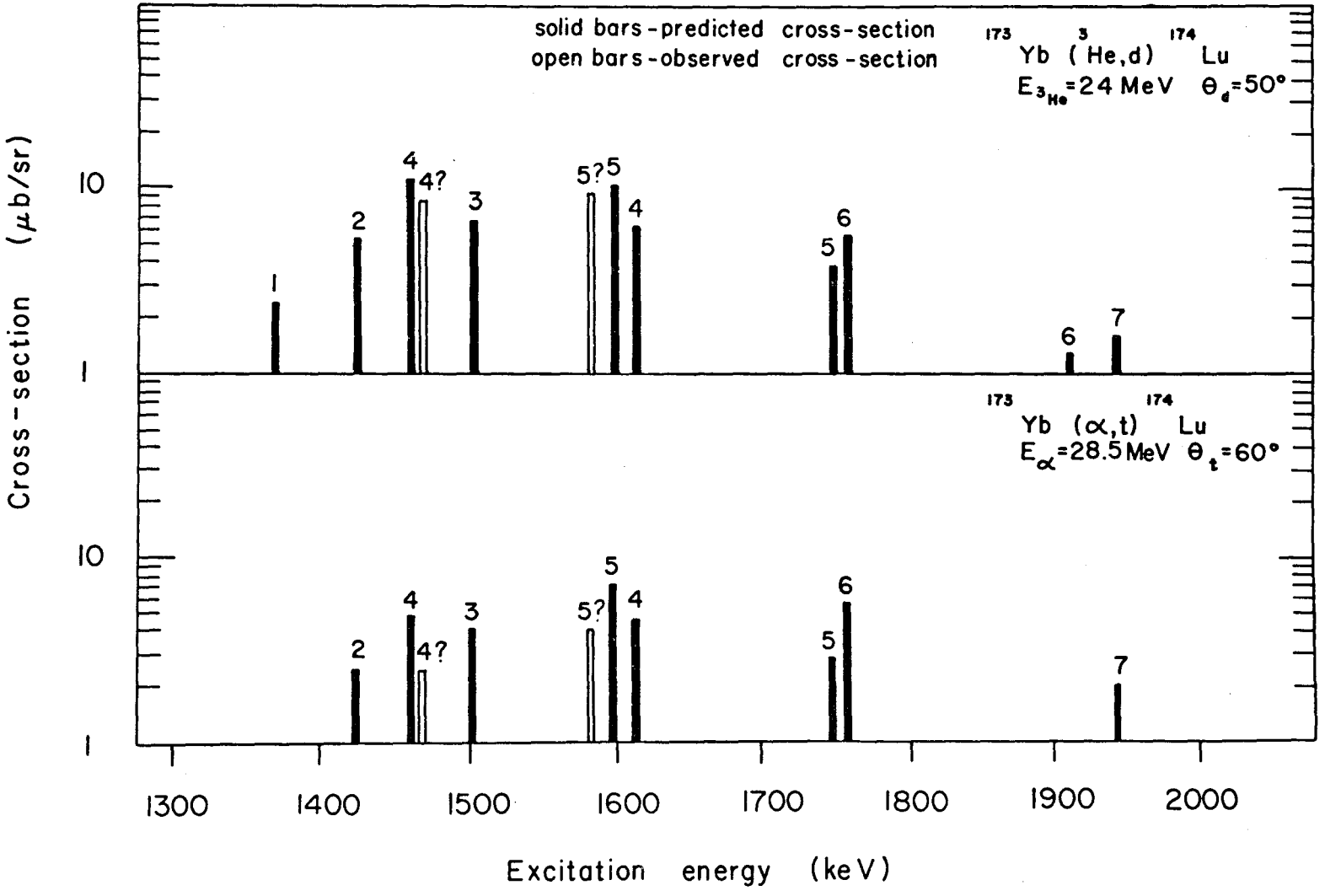

be expected from the transfer of the $1/2^+[411]$ orbital. However, no other band members are seen to support the assignment of these peaks to the $\{1/2^+[411]_p \pm 5/2^-[521]_n\}$ configurations.

Numerous unassigned states lie between 700 keV and 1250 keV excitation. These states are not strongly populated. Though some of these states have cross sections similar to what might be expected from the $\{3/2^-[532]_p\ 5/2^-[512]_n\}$ configurations, the Coriolis coupling calculations lead one to believe this to be unlikely. These peaks could also be due to the coupling of other sets of states into the simple proton transfer set considered. It is noted that several unassigned peaks of comparable intensity were found (Chapter 4) in the proton transfer spectra leading to ^{173}Lu, ^{175}Lu and ^{177}Lu within the same region of excitation energies. It is known in neighbouring even nuclei that vibrations occur in the region from 900 to 1200 keV. The suggestion was made that the unidentified peaks may result from the $1/2^+[400]$ and $3/2^+[402]$ orbitals coupled into gamma vibrations, for example, built on the $5/2^+[402]$ and $7/2^+[404]$ orbitals respectively. This effect spreads the intensity of these strong low-ℓ transitions into several peaks in the spectrum. It is possible that states formed in an analogous manner may also exist in ^{174}Lu.

The transfer of the $3/2^+[402]$ and $1/2^+[400]$ proton orbitals is characterised by extremely strong $\ell=0$ and $\ell=2$ transitions. The largest remaining unassigned states in the (^{3}He,d) spectrum,

such as those at 1753 keV and 1800 keV, have cross sections of about one fifth what is expected for these states. Though these configurations could lie at energies above those considered in the present work a strong possibility exists that these states are highly fragmented in the doubly-odd nucleus ^{174}Lu. Such fragmentation is predicted in the odd-mass nucleus ^{171}Lu. (Soloviev et al. 1966) and it seems reasonable to qualitatively generalize this prediction to the doubly-odd nucleus ^{174}Lu.

The Nilsson diagram predicts the $11/2^-[505]$ proton orbital to be at higher excitation energies than the $1/2^-[530]$ proton orbital. The rotational bands built on the $\{11/2^-[505]_p \pm 5/2^-[512]_n\}$ configurations would be populated by pure $\ell=5$ transitions. Such states are expected to have comparable (^{3}He,d) and (α,t) cross sections. No such states are seen below 2 MeV in the spectrum.

States formed by the transfer of the $1/2^+[660]$ and $3/2^+[651]$ proton orbitals are also expected in the region of the $\{1/2^-[530]_p \pm 5/2^-[502]_n\}$ configurations. These states should be populated by $\ell=6$ transitions as the $1/2^+[660]$ and $3/2^+[651]$ proton orbitals originate from the $i_{13/2}$ shell. The $\ell=6$ character of these states should not be altered by the strong Coriolis coupling known to exist between $i_{13/2}$ states. Such levels would be fairly strongly populated in the (α,t) reaction but using the (^{3}He,d) to (α,t) cross section ratio there appears to be no high-ℓ strength between 900 and 2000 keV excitation.

5.4 Interpretation of the neutron transfer data

Jones and Sheline (1970), using the $^{175}Lu(d,t)^{174}Lu$ reaction, have assigned the majority of the states below 1400 keV and have offered tentative assignments for several others. The rotational bands built on the following configurations have been assigned by these workers: $K^{\pi} = 1^-$ and 6^-, $\{5/2^-[512]_n \pm 7/2^+[404]_p\}$; $K^{\pi} = 3^-$ and 4^-, $\{1/2^-[521]_n \pm 7/2^+[404]_p\}$; $K^{\pi} = 2^-$ and 5^-, $\{3/2^-[521]_n \pm 7/2^+[404]_p\}$; and $K^{\pi} = 7^+$, $\{7/2^+[633]_n + 7/2^+[404]_p\}$. It was proposed that the $K^{\pi} = 7^+$, $\{7/2^+[633]_n + 7/2^+[404]_p\}$ configuration had its band head at 677 keV. The first four assignments have not been altered in the present work.

The Coriolis coupling calculation performed by Jones and Sheline gave very good agreement between the experimental data and the predicted energies and cross sections. Their calculation used the moments of inerita as well as the band head energies as free parameters.

The splittings between the spin singlet and spin triplet energies in ^{174}Lu were compared with those predicted by a spin-spin type of residual interaction. The calculations, which were further refined in a later paper by Jones et al. (1971) predicted the sign and the magnitude of the splitting quite well.

5.4(i) The $\{7/2^+[633]_n \pm 7/2^+[404]_p\}$ states

Jones and Sheline tentatively assigned the states at 677, 843 and 1016 keV to the spin I=7, 8 and 9 members of the

$K^{\pi} = 7^{+}$, $\{7/2^{+}[633]_{n}+7/2^{+}[404]_{p}\}$ rotational band. The agreement of the (d,t) cross sections with the predicted values was not too satisfactory. It may be seen from table 5.2.2 that the (d,t) fingerprint of this band is very weak in comparison to the other peaks in the spectrum. The $7/2^{+}[633]$ neutron wave-function, arising from the $i_{13/2}$ shell model state, is largely $\ell=6$ in character so the $^{175}Lu(^{3}He,\alpha)^{174}Lu$ reaction should be ideal for locating the states formed by transfer of this neutron. Figure 5.1.2 shows one of the spectra obtained in these experiments. It is significant that no strongly populated states exist in the $(^{3}He,\alpha)$ spectrum between 900 keV and 1400 keV excitation. The spin I=9 and 10 members of the $K^{\pi} = 7^{+}$ band are expected, from table 5.4.2 to be quite intensely populated in the $(^{3}He,\alpha)$ reaction so it is unlikely they lie above 900 keV as Jones and Sheline suggested.

The $\{7/2^{+}[633]_{n}\pm7/2^{+}[404]_{p}\}$ couplings should form rotational bands of $K^{\pi} = 0^{+}$ and 7^{+}. The states arising from $i_{13/2}$ neutron orbitals are known (Kleinheinz et al. 1972) to be very strongly Coriolis coupled in odd mass nuclei, and thus the bands built on configurations containing these states are also expected to be strongly coupled in the present case. A Coriolis coupling calculation was performed using matrix elements attenuated by a factor of 0.75 and corrected for pairing. Configurations arising from the $7/2^{+}[633]$, $5/2^{+}[642]$, $3/2^{+}[651]$ and $1/2^{+}[660]$ neutron hole states and the $9/2^{+}[624]$ particle state, coupled to the $7/2^{+}[404]$ proton were included.

As a first approximation the band head energies were taken from a Nilsson calculation and the Fermi surface was placed about one third of the way between the $7/2^+[633]$ and $9/2^+[624]$ states. The actual energies of the intrinsic two particle states formed were then varied somewhat in order to obtain a calculated fingerprint which resembled the experimental results. The spin singlet-triplet splittings of the observed configurations and the odd-even shift in the $K^\pi = 0^+$ band were also varied in later iterations to optomize the fit. It was typical of these calculations that the lowest bands should receive most of the strength expected from the transfer of $7/2^+[633]$ neutrons plus some of that due to the deeper hole states, in particular the $5/2^+[642]$ state. Some of the strength from the $1/2^+[660]$ and $3/2^+[651]$ orbitals is predicted to be drained into the bands which contain the remainder of the $5/2^+[642]$ strength and these are expected to occur several hundred keV higher than the bands mentioned above.

In the (^{3}He,α) spectrum of fig. 5.1.2 the group of states between 400 keV and 900 keV excitation can reasonably be associated with the $\{7/2^+[633]_n \pm 7/2^+[404]_p\}$ bands and their admixtures. The strongly populated group of peaks in the vicinity of 1500 keV excitation in the (^{3}He,α) spectrum is then most likely the second group of bands predicted.

The unperturbed energies of the $\{5/2^+[642]_n \pm 7/2^+[404]_p\}$ states were adjusted, relative to those of the $\{7/2^+[633]_n \pm 7/2^+[404]_p\}$ states so that the main (^{3}He,α) strength in this

second group would be predicted to occur at about 1500 keV. The calculation showed that the position of these states could be varied by ± 100 keV without seriously affecting the fingerprints of the lower $K^{\pi} = 0^{+}$ and $K^{\pi} = 7^{+}$ bands.

The $\{9/2^{+}[624]_{n} \pm 7/2^{+}[404]_{p}\}$ configurations should not be strongly populated in the present work as the $9/2^{+}[624]$ state is above the Fermi surface. However, they have an effect on the rotational spacing of the $\{7/2^{+}[633]_{n} \pm 7/2^{+}[404]_{p}\}$ bands because of Coriolis mixing. In the present calculation, the unperturbed rotational parameter, $\frac{\hbar^2}{2\mathcal{J}}$, was set at 12.1 keV for all bands. In order to obtain the value of 8.1 keV for the perturbed rotational parameter of the lower bands, as implied by the present interpretation of the data, the $\{9/2^{+}[624]_{n} \pm 7/2^{+}[404]_{p}\}$ band heads had to be placed 650±50 keV above the $\{7/2^{+}[633]_{n} \pm 7/2^{+}[404]_{p}\}$ bandheads.

In addition to adjusting the relative energies of the various intrinsic configurations, the unperturbed splitting between the $K^{\pi} = 0^{+}$ triplet and the $K^{\pi} = 7^{+}$ singlet couplings was varied. The optimum unperturbed energy difference between the band heads was found to be 112 keV. Finally, the last parameter to be varied was the odd-even shift of the $K^{\pi} = 0^{+}$, $\{7/2^{+}[633]_{n} - 7/2^{+}[404]_{p}\}$ band. It is expected that the odd spin states should be shifted to higher energies (Jones et al. 1972 and Valentin et al. 1962) as has been found for this band in ^{172}Lu. With a shift in this direction and a magnitude

of 79 keV, the predicted fingerprints as shown in fig. 5.4.1 are produced. This figure also shows, for comparison, the experimental results. The predicted energies and cross sections also appear in Table 5.2.2.

As may be seen from fig. 5.4.1 the $^{175}Lu(d,t)^{174}Lu$ fingerprint is not reproduced too satisfactorily for these very weak states. However, there are several band members unresolved from peaks with much greater cross sections in the (d,t) spectra and these weak peaks are also subject to errors because of the difficulties in predicting the cross sections of states with large angular momentum transfers.

The spin I=5 and I=6 members of the $K^{\pi}=0^{+}$ bands are predicted to have similar cross sections in the (d,t) spectrum and these have been assigned to the states observed at 573 keV and 593 keV. The strength observed in the ($^{3}He,\alpha$) spectrum is also in excellent agreement with this interpretation. However, from the present results it is not certain which is the I=5 state and which is the I=6. The best overall fit to the remaining band members was obtained when the odd-even shift was set to put the I=5 state lower in energy than the I=6 state. In order to do this the even spin states had to be displaced 79 keV downwards with respect to the odd spin states as mentioned above; thus the spin I=5 and I=6 members have been assigned at 573 keV and 593 keV respectively.

Figure 5.4.1

A comparison of the predicted and observed fingerprints of the $\{7/2^+[633]_n \pm 7/2^+[404]_p\}$ configurations. In this case the contributions to the $(^3He,\alpha)$ cross sections from other unresolved states identified in the (d,t) reaction have been removed. If the states in these bands are unresolved, the cross sections of the band members have been summed; for example, the spins I=5 and 6 states are unresolved in the $(^3He,\alpha)$ reaction.

Fingerprint of $\left\{\frac{7}{2}^+\,[633]_n \pm \frac{7}{2}^+\,[404]_p\right\}$

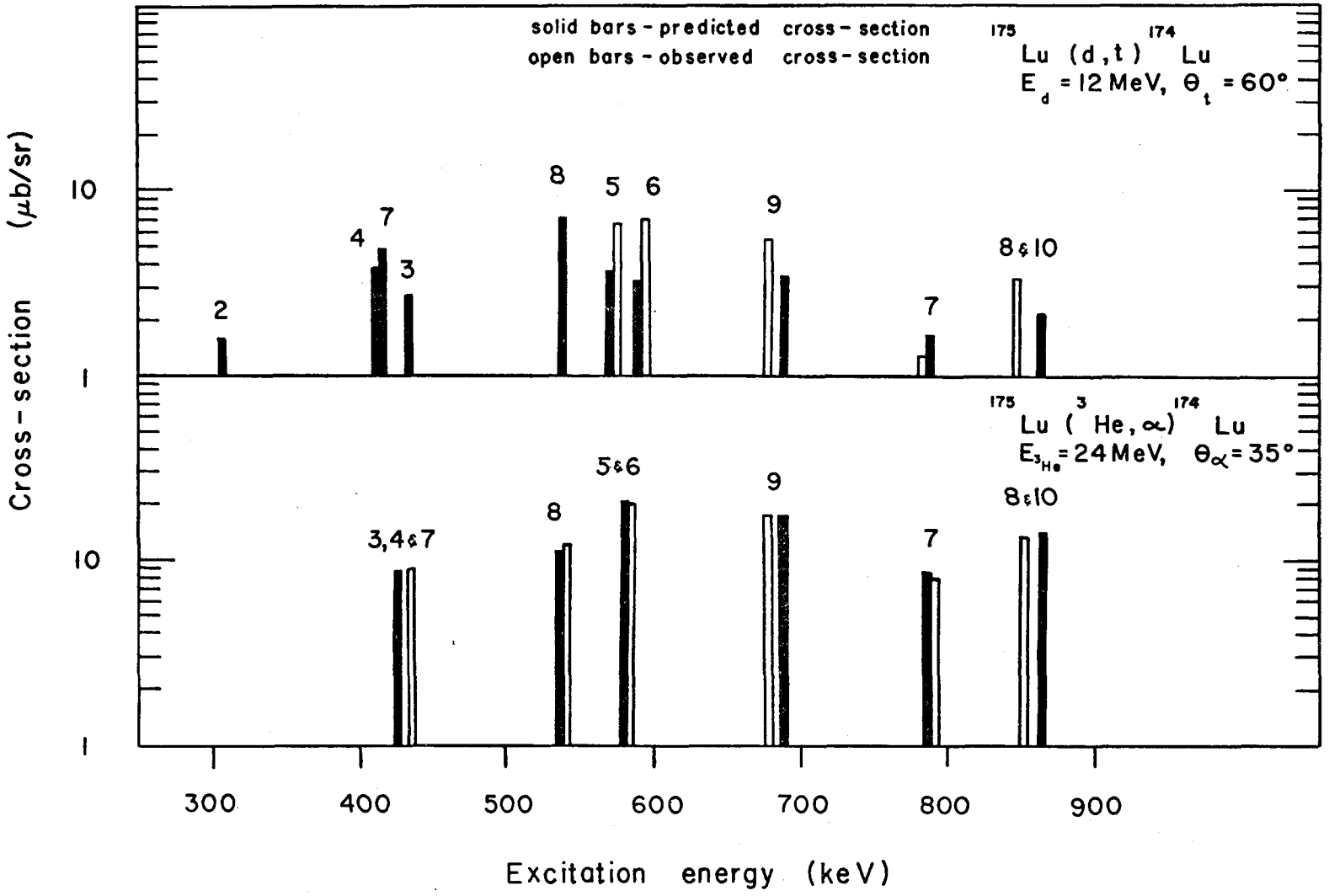

The proposed interpretation places many of the $\{7/2^+[633]_n \pm 7/2^+[404]_p\}$ states close in energy to other strongly populated states in the (d,t) spectrum. Hence, the weak peaks expected for the bands under discussion are masked. In such cases the large intensities observed in the (^{3}He,α) reaction were used to advantage although in some cases the contributions due to known peaks in the vicinity had to be taken into account. In the case of the (^{3}He,α) reaction the resolution is not adequate to resolve all the closely spaced levels. In particular, the particle group at $\approx$ 433 keV excitation energy in the spectrum has been attributed to the unresolved spin I=3 and I=4 members of the $K^\pi = 0^+$ band the I=7 member of the $K^\pi = 7^+$ band. According to the present interpretation, the predicted spread of the energies for these three states is 31 keV. Although it is difficult to prove all these states exist at $\approx$ 433 ± 15 keV, the summed (^{3}He,α) cross section is consistent with this assignment.

In general, the predicted (^{3}He,α) fingerprint is in excellent agreement with the experimental results, as can be seen from Fig. 5.4.1. It is to be noted that the interpretation given for these two bands has used reasonable values for all the parameters which were varied in the calculation. It is also consistent with all the data currently available on ^{174}Lu. However, it is difficult to demonstrate that the proposed assignments of spins and K-values represent a unique explanation of the experimental

data and further experiments to test the spins would be desirable.

5.4(ii) Other states in the neutron transfer spectra

Jones and Sheline (1970) have assigned the $K^{\pi} = 1^{-}$ ground state band up to spin I=5 as well as the $K^{\pi} = 6^{-}$ band which forms the spin singlet coupling of the $\{5/2^{-}[512]_n + 7/2^{+}[404]_p\}$ configuration. The present work confirms these assignments and has added the tentative assignment of the weakly populated $I, K^{\pi} = 8, 6^{-}$ state at 506 keV. Table 5.2.2 shows essentially the same predicted cross sections as obtained by Jones and Sheline for these bands. The fingerprints for these states obtained in the present work are included in fig. 5.3.1.

Similarly the interpretation of the $K^{\pi} = 2^{+}$ and 3^{+} bands formed from the $\{1/2^{-}[521]_n \pm 7/2^{+}[404]_p\}$ configuration is also in agreement with what Jones and Sheline have obtained. Though the present Coriolis coupling calculation contains more bands, the results are virtually the same. Figure 5.4.2 shows the excellent agreement between the predicted and observed cross-sections for these states.

Above 1 MeV excitation the $K^{\pi} = 5^{-}$ and 2^{-} couplings of the $3/2^{-}[521]$ neutron coupled to the target proton have been assigned. It may be seen in fig. 5.4.3 that the $K^{\pi} = 5^{-}$ states have cross sections in good agreement with the predictions: however, the $K^{\pi} = 2^{-}$ states are anomalously strong. The $K^{\pi} = 2^{-}$

Figure 5.4.2

A comparison of the predicted and observed fingerprints of the $\{1/2^{-}[521]_n \pm 7/2^{+}[404]_p\}$ configurations. The bars are labelled by the spin I of the state. These states are expected to be weakly populated in the $(^3He,\alpha)$ reaction and have not been observed, with the exception of the $I,K^{\pi} = 4,4^{-}$ state.

Fingerprint of $\{\frac{1}{2}^{-}[521]_n \pm \frac{7}{2}^{+}[404]_p\}$

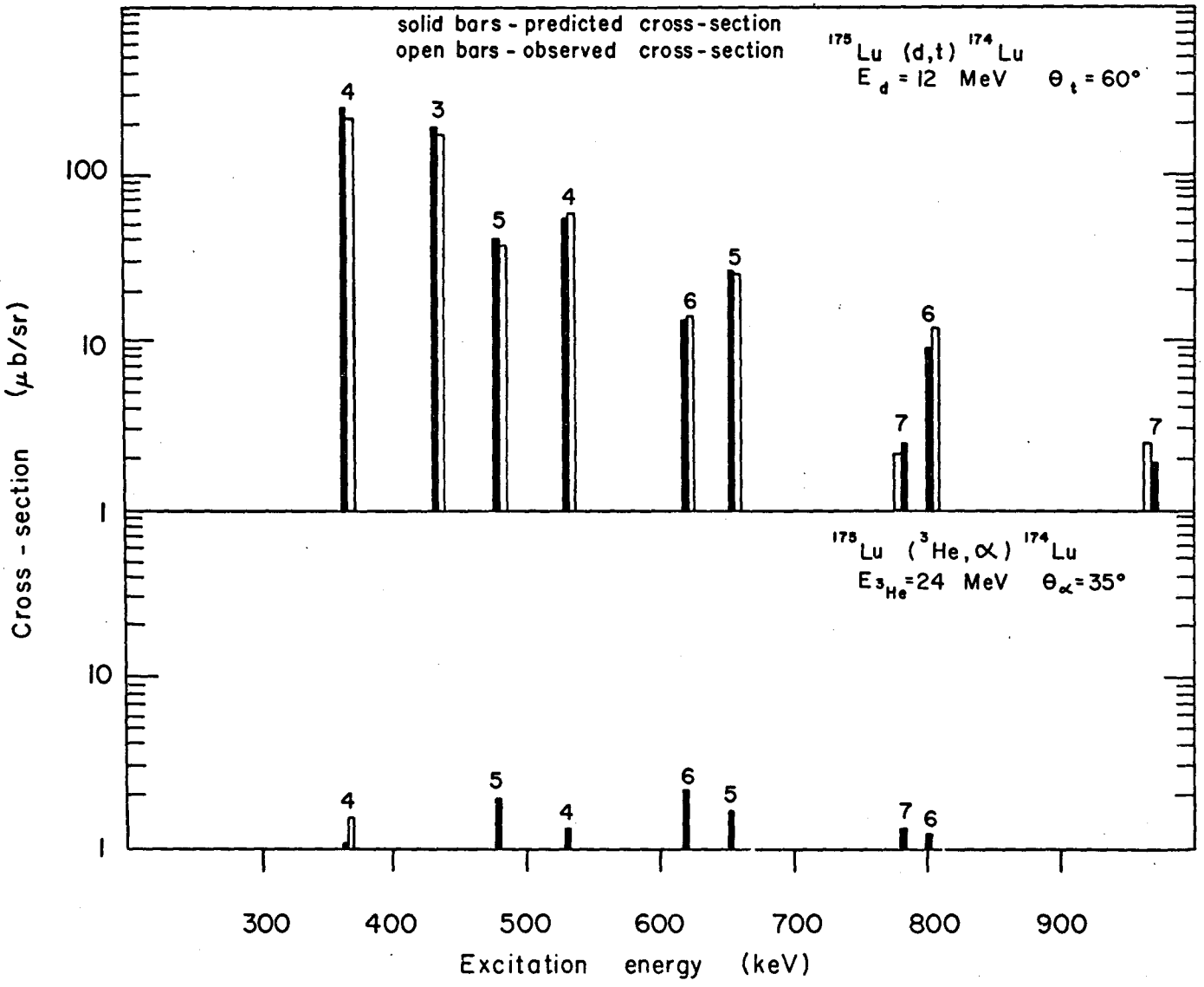

Figure 5.4.3

A comparison of the predicted and observed fingerprints of the $\{3/2^{-}[521]_n \pm 7/2^{+}[404]_p\}$ configuration. The bars are labelled by the spin I of the state. The observed (^{3}He,α) cross sections in this region are much larger than what could be reasonably assigned to these states. This is likely due to the high level density and the low energy resolution of the (^{3}He,α) reaction.

Fingerprint of $\{\frac{3}{2}^{-}[521]_n \pm \frac{7}{2}^{+}[404]_p\}$

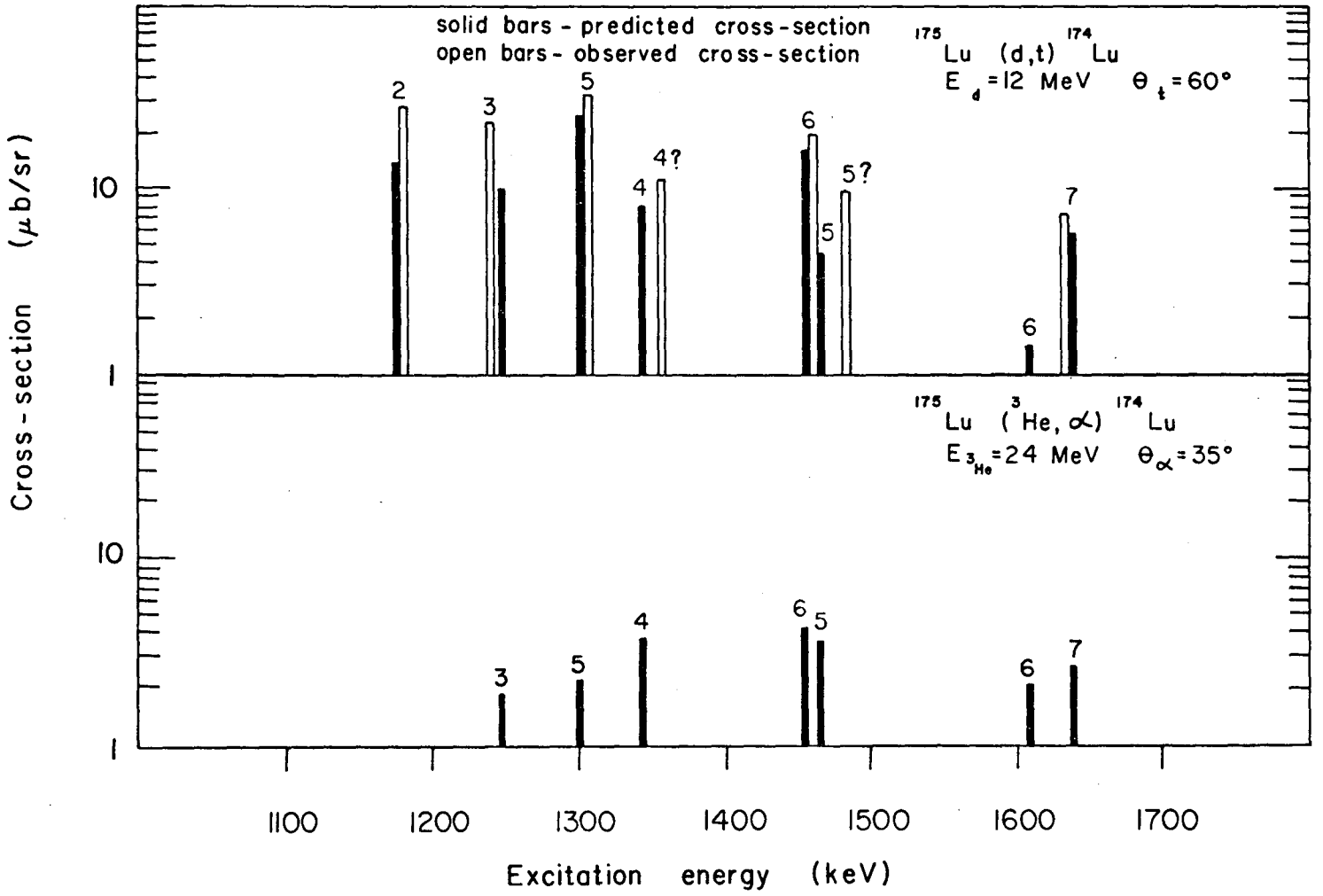

band was assigned by Jones and Sheline at 1185, 1252, 1337 and 1442 keV for the spins I=2 to 5 respectively, though the spin I=4 and 5 states were tentative assignments. The Coriolis coupling calculations performed with a 12.1 keV rotational parameter favour the assignment of the 1353 keV level to the $I,K^{\pi} = 4,2^{-}$ member of the $\{3/2^{-}[521]_n - 7/2^{+}[404]_p\}$ configuration. The same calculations also predict the I=5 member of the same band to be close to the peak at 1481 keV. It is possible this peak is an unresolved multiplet of the I=5 state and some high-ℓ state because it has a large $(^3He,\alpha)$ cross-section. Coriolis coupling of states at higher energies to the $K^{\pi} = 2^{-}$ band would reduce the rotational parameter so that the assignments by Jones and Sheline (1970) of the spin I=4 and 5 members would be more satisfactory than those proposed here. The assignments of the I=4 and 5 states of the $K^{\pi} = 2^{-}$ band remain tentative.

The region just above 1 MeV is also expected to contain the rotational states built on the $\{5/2^{-}[523]_n \pm 7/2^{+}[404]_p\}$ configuration. These are quite strongly coupled to the $\{3/2^{-}[521]_n \pm 7/2^{+}[404]_p\}$ states so the relative energies of these four bands can have a large effect on the fingerprints. In Table 5 the energies of the $\{5/2^{-}[523]_n \pm 7/2^{+}[404]_p\}$ configurations are quite arbitrary and though a variation of these energies was attempted it did not appear to account for the anomalously large cross sections of the $K^{\pi} = 2^{-}$, $\{3/2^{-}[521]_n \pm 7/2^{+}[404]_p\}$ states. The calculation was extended to include

several additional neutron orbitals from this region such as the $3/2^-[532]$ and $1/2^-[530]$ states coupled to the target, but no better results were obtained. The same table shows fairly large (d,t) cross sections to the four bands originating from the transfer of the $3/2^-[521]$ and $5/2^-[523]$ neutrons. However only the latter exhibits appreciable (^{3}He,α) strength. It is possible that some of the (^{3}He,α) intensity in the region of 1500 keV excitation is due to the transfer of this neutron state though it has not been assigned.

Speculation was made by Jones and Sheline (1970) that the two peaks at 1081 keV and 1203 keV were due to the band heads of the $\{1/2^-[510]_n \pm 7/2^+[404]_p\}$ configurations. This would involve the pick-up of a particle from an almost unoccupied orbital; hence, very low cross sections are expected. This orbital has been identified as a particle state in ^{173}Yb where it was populated at approximately 1031 keV by a (d,p) reaction and very weakly by the (d,t) reaction. The $\{1/2^-[510]_n \pm 7/2^+[404]_p\}$ configurations couple quite strongly to the $K^\pi = 2^-$ and 3^-, $\{1/2^+[521]_n \pm 7/2^+[404]_p\}$ states. From the observed rotational parameter of the latter bands, the $\{1/2^-[510]_n \pm 7/2^+[404]_p\}$ states must have a minimum energy of about 1 MeV.

The $\{5/2^+[642]_n \pm 7/2^+[404]_p\}$ configurations have not been identified in ^{174}Lu. As discussed in subsect. 5.4.(i) it is

suspected that these states have most of their intensity above 1400 keV excitation in order to account for several strong peaks in this region of the (^{3}He,α) spectra. Table 5.2.2 shows that the $K^{\pi} = 1^+$ band has some of its spectroscopic strength transferred to lower lying states by the Coriolis interaction. In particular the configurations formed from the transfer of the $7/2^+[633]$ neutron orbital are enhanced by Coriolis coupling. The number of possibilities for the fragmentation of the higher lying configurations based on the transfer of the $i_{13/2}$ neutron orbitals and the low resolution associated with the (^{3}He,α) exposures hindered the identification of the characteristic fingerprints of these bands.

CHAPTER VI

CONCLUSIONS

The low lying structure of three odd mass lutetium isotopes has been studied using the (^{3}He,d) and (α,t) reactions. Many of the largest peaks in the spectra have been interpreted in terms of the Nilsson model. The level schemes of the single proton states observed in ^{173}Lu, ^{175}Lu and ^{177}Lu are shown in figs. 6.0.1, 6.0.2 and 6.0.3 respectively. In addition to these states, there also exist unassigned peaks in the spectra of all three nuclei whose energies and cross sections have been measured. The location of these latter states with respect to the more strongly populated, assigned peaks may be seen in the experimental spectra (figs. 4.1.1, 4.1.2 and 4.1.3).

It may be seen from the level diagrams that the structures of all three nuclei are similar. The levels of ^{171}Lu (Gregory, 1972) are shown in fig. C.2 and ^{169}Lu has been recently studied by Foin et al. (1972). The structures for each of the lighter two isotopes of lutetium is very similar to those of the heavier isotopes reported in the present work. Such similarities in the single particle structure of the lutetium isotopes are expected from the Nilsson model provided the deformation does not change greatly.

The single particle states which are identified in the lutetium isotopes are in good agreement with the predictions of the Nilsson model. The populations of the ro-

Figure 6.0.1

A level scheme of ^{173}Lu for assigned levels populated in the proton transfer reactions.

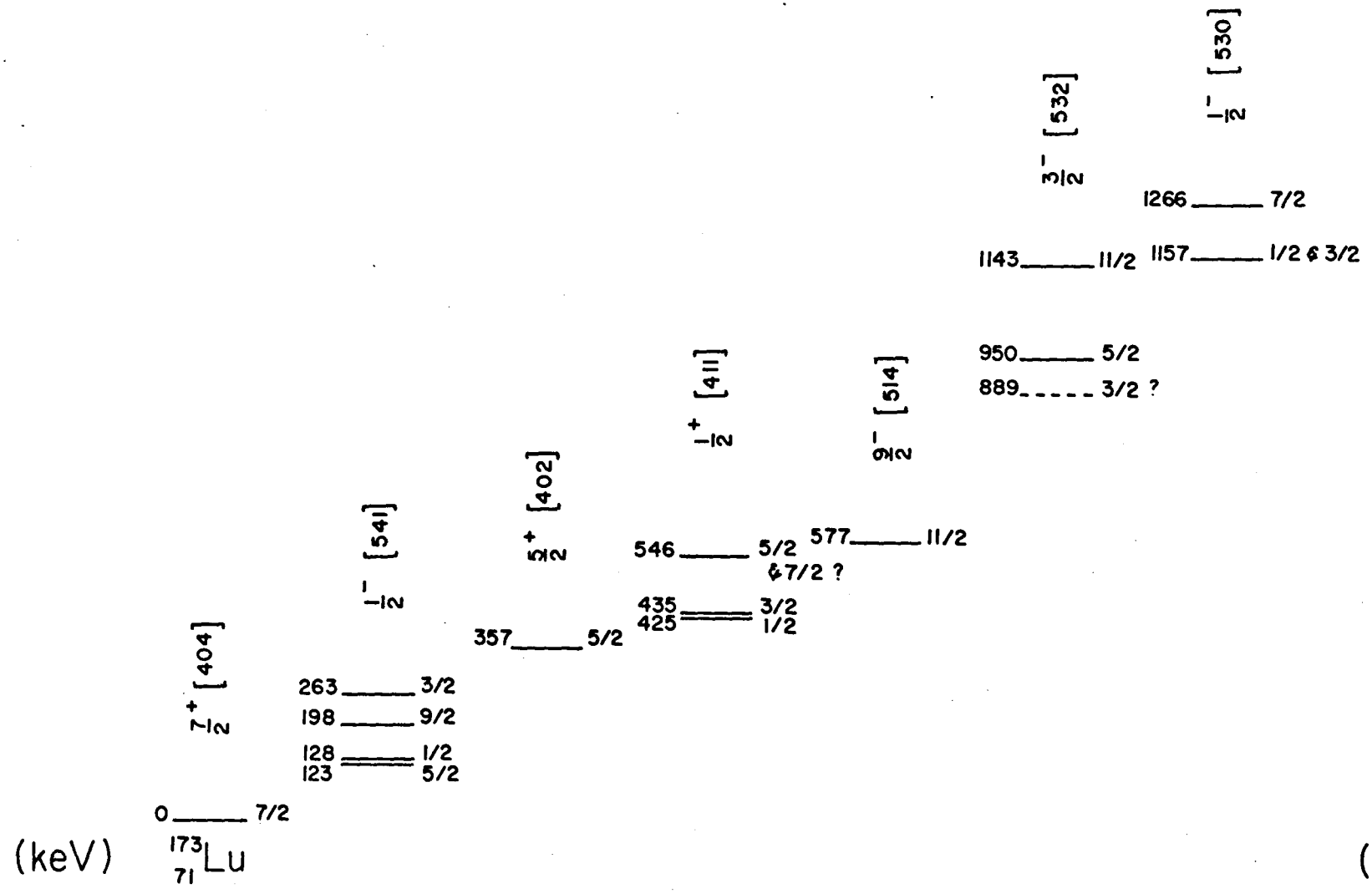
(keV)
$^{173}_{71}Lu$
0 7/2
263 3/2
198 9/2
128 1/2
123 5/2
357 5/2
546 5/2
&7/2 ?
435 3/2
425 1/2
577 11/2
1143 11/2
950 5/2
889 3/2 ?
1266 7/2
1157 1/2 & 3/2
$7^+_{\frac{1}{2}}[404]$
$1^-_{\frac{1}{2}}[541]$
$5^+_{\frac{2}{2}}[402]$
$1^+_{\frac{1}{2}}[411]$
$9^-_{\frac{2}{2}}[514]$
$3^-_{\frac{1}{2}}[532]$
$1^-_{\frac{1}{2}}[530]$

(I)

Figure 6.0.2

A level scheme of ^{175}Lu for assigned levels populated in the proton transfer reactions.

(keV)
175 71 Lu
0 7/2
114 9/2
7+/2 [404]
515 3/2
414 9/2
358 1/2
354 5/2
1+/2 [541]
343 5/2
5+/2 [402]
524 11/2
413 9/2
9-/2 [514]
1695 9/2 ?
1629 11/2 ?
1406 7/2
1309 3/2
1262 9/2
1168 7/2 ?
1058 5/2
992 3/2 ?
3-/2 [532]
1-/2 [530]
(I)

Figure 6.0.3

A level scheme of ^{177}Lu for assigned levels populated in the proton transfer reactions.

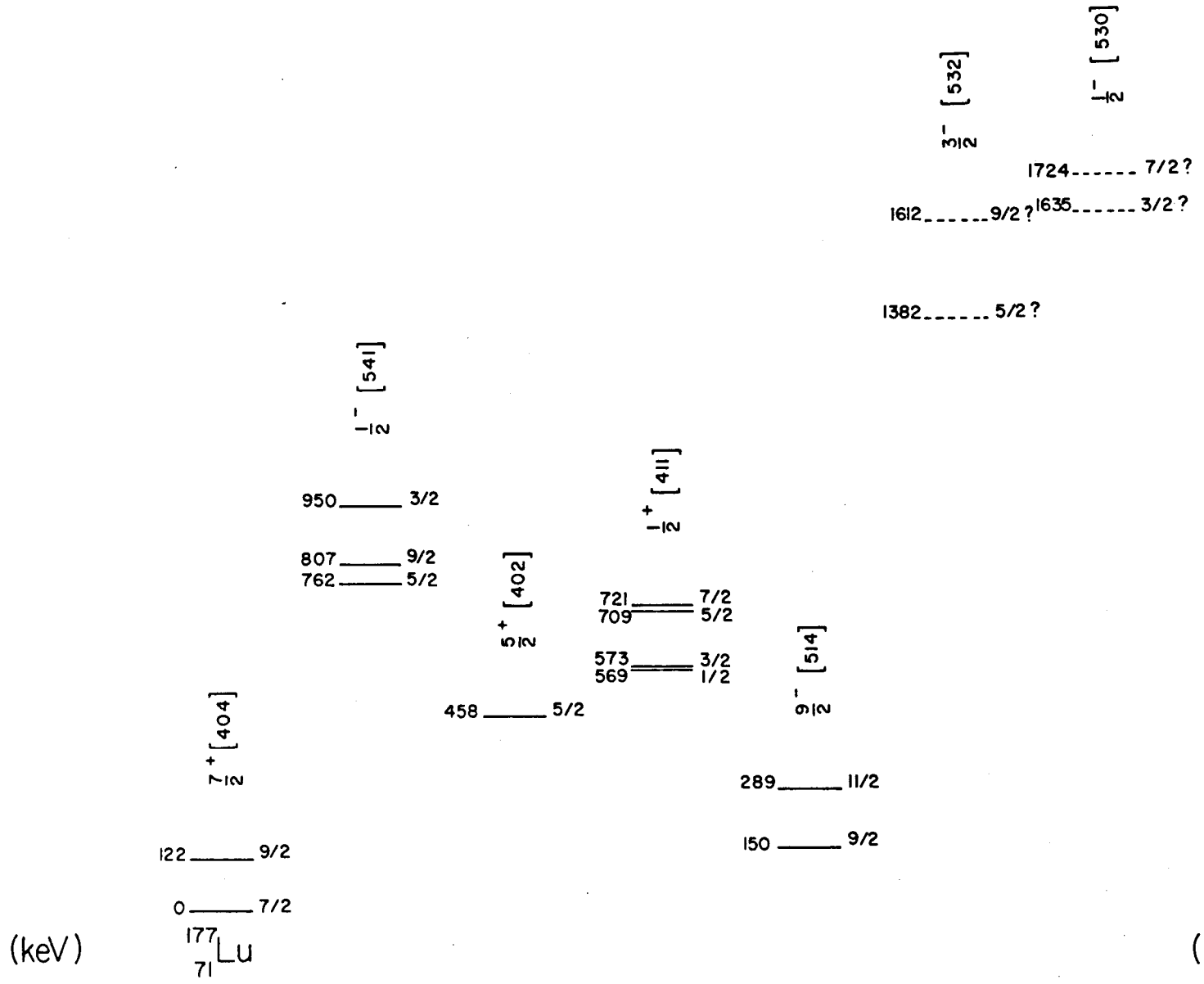
(keV)
$^{177}_{71}Lu$
0 7/2
122 9/2
7^+_{12} [404]
458 5/2
289 11/2
150 9/2
9^-_{12} [514]
721 7/2
709 5/2
573 3/2
569 1/2
1^+_{12} [411]
5^+_{12} [402]
950 3/2
807 9/2
762 5/2
1^-_{12} [541]
1382 5/2?
1612 9/2?
1724 7/2?
1635 3/2?
3^-_{12} [532]
1^-_{2} [530]
(I)

tational bands based on the $7/2^+[404]$, $5/2^+[402]$, $9/2^-[514]$, $1/2^+[411]$, $1/2^-[541]$, $3/2^-[532]$ and $1/2^-[530]$ orbitals by the single proton transfer reactions are consistent with the predictions when pairing effects and Coriolis coupling are taken into account. Recent calculations by Soloviev and Fedatov (1971) using the data presented in Chapter 4 have shown that for the states identified, vibrational effects are not expected to seriously alter the single particle spectra of these nuclei. It is unfortunate these same calculations do not include couplings to the $1/2^+[400]$, $3/2^+[402]$, $1/2^+[660]$ and $3/2^+[651]$ proton orbitals which are expected to lie at higher energies than the orbitals listed above. Experimentally at higher excitation energies, the observed cross sections are often smaller than those predicted for the Nilsson orbitals arising from the $i_{13/2}$ and $s_{1/2}$ states in this region. Thus there must be appreciable fragmentation of the single particle states at the higher energies as has been observed in the odd neutron nuclei.

The doubly-odd nucleus ^{174}Lu has been investigated using four single particle transfer reactions. This was one of the first times that four single particle transfer reactions have been brought to bear on a single final deformed nucleus. Most of the large peaks below 1.5 MeV have been interpreted in the light of the Nilsson model. Figs. 6.0.4 and 6.0.5 show the states which have been interpreted in the present work and by

Figure 6.0.4

A level scheme of ^{174}Lu for assigned levels populated in the neutron transfer reactions.

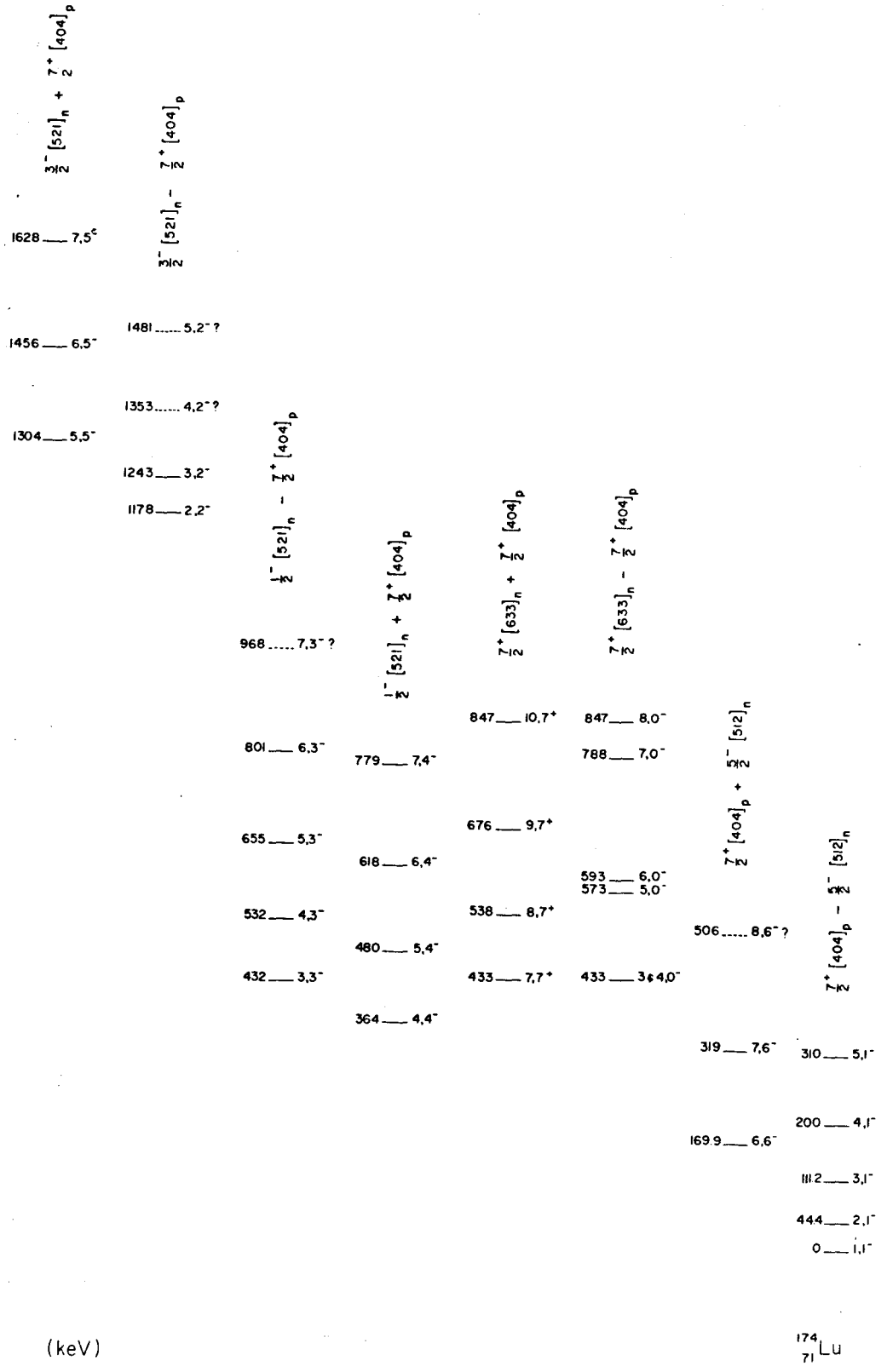
3/2⁻ [521]n + 7/2⁺ [404]p
3/2⁻ [521]n − 7/2⁺ [404]p
1/2⁻ [521]n − 7/2⁺ [404]p
1/2⁻ [521]n + 7/2⁺ [404]p
7/2⁺ [633]n + 7/2⁺ [404]p
7/2⁺ [633]n − 7/2⁺ [404]p
7/2⁺ [404]p + 5/2⁻ [512]n
7/2⁺ [404]p − 5/2⁻ [512]n
1628 — 7,5⁺
1481 ..... 5,2⁻ ?
1456 — 6,5⁻
1353 ..... 4,2⁻ ?
1304 — 5,5⁻
1243 — 3,2⁻
1178 — 2,2⁻
968 ..... 7,3⁻ ?
801 — 6,3⁻
779 — 7,4⁻
655 — 5,3⁻
618 — 6,4⁻
532 — 4,3⁻
480 — 5,4⁻
432 — 3,3⁻
364 — 4,4⁻
847 — 10,7⁺
676 — 9,7⁺
538 — 8,7⁺
433 — 7,7⁺
847 — 8,0⁻
788 — 7,0⁻
593 — 6,0⁻
573 — 5,0⁻
433 — 3 ó 4,0⁻
506 ..... 8,6⁻ ?
319 — 7,6⁻
169.9 — 6,6⁻
310 — 5,1⁻
200 — 4,1⁻
111.2 — 3,1⁻
44.4 — 2,1⁻
0 — 1,1⁻
(keV)
174 71 Lu
(I, K^π)

Figure 6.0.5

A level scheme of ^{174}Lu for assigned levels populated in the proton transfer reactions.

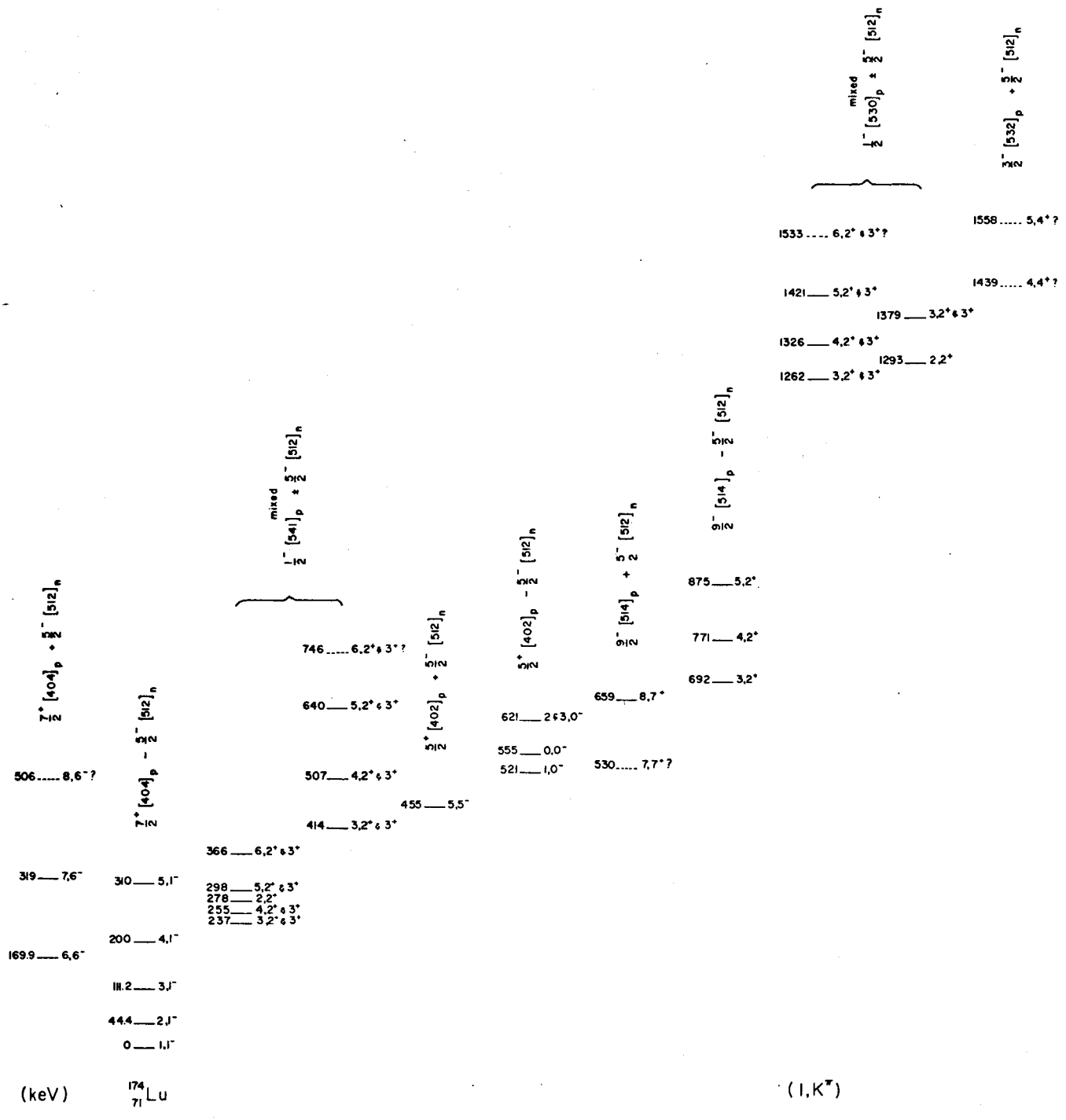
mixed
$\frac{1}{2}^-[530]_p \pm \frac{5}{2}^-[512]_n$
$\frac{3}{2}^-[532]_p + \frac{5}{2}^-[512]_n$
1558 ..... 5,4⁺?
1533 ..... 6,2⁺ ⊕ 3⁺?
1439 ..... 4,4⁺?
1421 ___ 5,2⁺ ⊕ 3⁺
1379 ___ 3,2⁺ ⊕ 3⁺
1326 ___ 4,2⁺ ⊕ 3⁺
1293 ___ 2,2⁺
1262 ___ 3,2⁺ ⊕ 3⁺
$\frac{9}{2}^-[514]_p - \frac{5}{2}^-[512]_n$
875 ___ 5,2⁺
771 ___ 4,2⁺
692 ___ 3,2⁺
$\frac{9}{2}^-[514]_p + \frac{5}{2}^-[512]_n$
659 ___ 8,7⁺
530 ..... 7,7⁺?
$\frac{5}{2}^+[402]_p - \frac{5}{2}^-[512]_n$
621 ___ 2 ⊕ 3,0⁻
555 ___ 0,0⁻
521 ___ 1,0⁻
mixed
$\frac{1}{2}^-[541]_p \pm \frac{5}{2}^-[512]_n$
$\frac{5}{2}^+[402]_p + \frac{5}{2}^-[512]_n$
746 ..... 6,2⁺ ⊕ 3⁺?
640 ___ 5,2⁺ ⊕ 3⁺
507 ___ 4,2⁺ ⊕ 3⁺
455 ___ 5,5⁻
414 ___ 3,2⁺ ⊕ 3⁺
366 ___ 6,2⁺ ⊕ 3⁺
298 ___ 5,2⁺ ⊕ 3⁺
278 ___ 2,2⁺
255 ___ 4,2⁺ ⊕ 3⁺
237 ___ 3,2⁺ ⊕ 3⁺
$\frac{7}{2}^+[404]_p + \frac{5}{2}^-[512]_n$
506 ..... 8,6⁻?
319 ___ 7,6⁻
169,9 ___ 6,6⁻
$\frac{7}{2}^+[404]_p - \frac{5}{2}^-[512]_n$
310 ___ 5,1⁻
200 ___ 4,1⁻
111,2 ___ 3,1⁻
44,4 ___ 2,1⁻
0 ___ 1,1⁻
(keV)
$^{174}_{71}Lu$
(I,K$^\pi$)

Jones and Sheline. The states in fig. 6.0.4 were populated in the neutron transfer whereas those in fig. 6.0.5 were observed using proton transfer reactions. In the latter case, the only states considered were those where the transferred proton was coupled to the $5/2^-[512]$ neutron orbital. Similarly the analysis of the neutron transfer data considered states where the neutron was coupled to the $7/2^+[404]$ target proton. In all, seventeen intrinsic configurations of the odd-proton and odd-neutron have been identified or tentatively identified in ^{174}Lu.

It has been shown that several rotational bands in ^{174}Lu are very strongly perturbed by the Coriolis interaction. In particular, the two configurations arising from the transfer of the $1/2^-[541]$ proton are very strongly coupled, resulting in one set of states to be grouped into a rotational band with an extremely small rotational parameter ($\frac{\hbar^2}{2\mathcal{I}}$) and another set with $\frac{\hbar^2}{2\mathcal{I}}$ larger than the unperturbed value. In general, the effect of Coriolis coupling has been found to alter the rotational parameters and cross sections in much the same manner as has been observed in odd-A deformed rare earth nuclei.

In all the configurations observed, the band head of the spin singlet coupling of the proton and neutron lies at a higher energy than the band head of the triplet coupling, as predicted by the Gallagher-Moszkowski rule. The present work has not included any attempt to calculate the effects of the residual interaction. This has been done by Jones et al. (1971)

for the states expected to be populated in the neutron transfer reaction. It is hoped that the data from the proton transfer reactions will be used in future studies of the residual interaction. Because of the great deal of attention odd-odd nuclei are presently receiving experimentally in the rare earth region, such a calculation should be able to make use of a significantly larger number of measured splitting energies and odd-even shifts.

The understanding of the low energy spectrum of ^{174}Lu has now progressed to the point where it is feasible to do on line γ-ray and conversion electron studies using experiments such as the ^{174}Yb (d,2nγ) ^{174}Lu or ^{170}Er (^{7}Li,3nγ) ^{174}Lu reactions. Using high resolution detection systems it should be possible to measure spins and transition rates to confirm the assignments made by Jones and Sheline and in the present work. It is expected that these reactions will not be so selective as the direct reactions are to the sets of states populated. Thus several additional configurations below one MeV will likely be found which have not been identified using the single particle transfer reactions.

APPENDIX A

Matrix Elements of the Rotational Hamiltonian

The various matrix elements of the total rotational Hamiltonian (eg. 3.0.2) are evaluated in various standard references, for example Davidson (1968). The matrix elements for the rotational particle coupling and particle-particle coupling in the odd-odd nucleus are identical to those evaluated by Jones (1969). The approach here must be regarded as the conventional method. The results for the odd-A nuclei quoted here seem to differ from those obtained by Scholz and Malik (1968) using a slightly different formalism.

The matrix element of H_{rot} is a diagonal element in the representation we have chosen:

$$E_{rot} = \langle IMK\Omega_p\Omega_n | H_{rot} | IMK\Omega_p\Omega_n \rangle$$

$$= \frac{\hbar^2}{2\mathcal{J}} [I(I+1)-K^2-\Omega_p^2-\Omega_n^2] \qquad (A.1)$$

For an odd-Z nucleus this may be written:

$$E_{rot} = \langle IMK | H_{rot} | IMK \rangle = \frac{\hbar^2}{2\mathcal{J}} [I(I+1)-2K^2] \qquad (A.2)$$

The matrix element of H_{prot}, which may be interpreted as the rotational energy of the odd proton is also a diagonal element.

$$E_{prot} = \langle IMK\Omega_p\Omega_n | H_{prot} | IMK\Omega_p\Omega_n \rangle$$

$$= \frac{\hbar^2}{2\mathcal{J}} \sum_{j_p} |C_{j_p\Omega_p}|^2 j_p(j_p+1) \qquad (A.3)$$

The matrix element of H_{nrot} is identical except the reference is to the odd neutron rather than the odd proton.

$$E_{nrot} = \frac{\hbar^2}{2\mathcal{J}} \sum_{j_n} |C_{j_n\Omega_n}|^2 j_n(j_n+1) \qquad (A.3)$$

This matrix element is often included in the Nilsson energy of the state. Its effect is to move the states with larger angular momentum components to higher energies. Though it may not be justified, the contribution of this term was ignored in the calculation of the excitation energies.

In the calculation of the particle-particle and rotational particle coupling, the matrix elements of the I_+ and j_- operators are needed. These are (Kerman 1956):

$$\langle IMK|I_\pm|I'M'K'\rangle = \delta_{I,I'}\delta_{MM'} \quad \delta_{K\pm1,K'}\sqrt{(I\mp K)(I\pm K+1)}$$

$$\langle j_p\Omega_p|j_{p\mp}|j_p'\ \Omega_p'\rangle = \delta_{j_pj_p'} \quad \delta_{\Omega_p+1,\Omega_p'}\sqrt{(j_p\mp\Omega_p)(j_p\pm\Omega_p+1)}$$

and similarly for the $j_{n\mp}$ matrix element. (A.4)

Using these expressions the matrix element of H_{rpc} the so called Coriolis matrix element, for an odd-Z nucleus is:

$$\langle IMK|H_{rpc}|I'M'K'\rangle$$

$$= \frac{-\hbar^2}{2\mathcal{J}} \delta_{II'}\delta_{MM'} \sum_j C_{jK'}C_{jK} \left[\delta_{K',K+1}\sqrt{(I-K)(I+K+1)(j-K)(j+K+1)}\right.$$

$$\left. + (-1)^{I-j}\delta_{K=1/2,K'=1/2}(I+1/2)(j+1/2)\right] \qquad (A.5)$$

Both K and K′ are taken to be positive and K is the minimum of the two K-values. It is seen from equation (A.5) that only rotational

bands of the same parity but differing by K'-K=1 are coupled by the Coriolis interaction. This off-diagonal element is the same as the expression of Bunker and Reich (1971). It should be noticed that a K=1/2 band may couple to itself by the Coriolis interaction because the +Ω term of the wave function may mix with the -Ω term. In such a case there is a diagonal contribution to the energy of the rotational band.

$$E_d = \langle IM\ \tfrac{1}{2}\ |H_{rpc}|\ IM\ \tfrac{1}{2}\rangle$$

$$= \frac{\hbar^2}{2\mathfrak{J}}\, a(-1)^{I+1/2}(I+1/2)\,\delta_{K,\frac{1}{2}} \qquad (A.6)$$

The decoupling parameter, a, is defined as

$$a = -\sum_j (-1)^{j+1/2}(j+1/2)\ C^2_{j\frac{1}{2}} \qquad (A.7)$$

The expression for the Coriolis matrix element in an odd-odd nucleus is quite complicated (Jones, 1969).

$$\langle I'M'K'\Omega'_p\Omega'_n|H_{rpc}|IMK\Omega_p\Omega_n\rangle = \frac{-\hbar^2}{2\mathfrak{J}}\ \delta_{I'I}\ \delta_{M'M}$$

$$\sum_{j_p}\ \sum_{j_n} C_{j_p\Omega'_p}\, C_{j_p\Omega_p}\, C_{j_n\Omega'_n}\, C_{j_n\Omega_n}\ \{\delta_{K',K-1}\sqrt{(I+K)(I-K+1)}$$

$$\cdot[\delta_{\Omega'_p,\Omega_p-1}\delta_{\Omega'_n,\Omega_n}\sqrt{(j_p+\Omega_p)(j_p-\Omega_p+1)} + \delta_{\Omega'_p,\Omega_p}\delta_{\Omega'_n,\Omega_n-1}$$

$$\cdot\sqrt{(j_n+\Omega_n)(j_n-\Omega_n+1)}]$$

$$+\ \delta_{K',K+1}\sqrt{(I-K)(I+K+1)}$$

$$\cdot[\delta_{\Omega_p',\Omega_p+1}\delta_{\Omega_n',\Omega_n}\sqrt{(j_p-\Omega_p)(j_p+\Omega_p+1)} + \delta_{\Omega_p',\Omega_p}\delta_{\Omega_n',\Omega_n+1}\sqrt{(j_n-\Omega_n)(j_n+\Omega_n+1)}]$$

$$+ \delta_{K',-K+1}\sqrt{(I+K)(I-K+1)}$$

$$\cdot(-1)^{I-j_p-j_n}[\delta_{\Omega_p',-\Omega_p+1}\delta_{\Omega_n',-\Omega_n}\sqrt{(j_p+\Omega_p)(j_p-\Omega_p+1)} \qquad (A.8)$$

$$+ \delta_{\Omega_p',-\Omega_p}\delta_{\Omega_n',-\Omega_n+1}\sqrt{(j_n+\Omega_n)(j_n-\Omega_n+1)}]\}$$

The Coriolis matrix element in the case of odd-odd nuclei again couples only states of the same parity differing by $|K-K'|=1$. There is, however, an additional selection rule which requires, for example, the proton orbitals in the two configurations to differ in Ω by one unit, and the neutron must be in the same orbital in both configurations though it may have the opposite Ω-projection in the two configurations.

The particle-particle matrix element is:

$$\langle I'M'K'\Omega'_p\Omega'_n|H_{pp}|IMK\Omega_p\Omega_n\rangle = \frac{\hbar^2}{2\mathcal{J}}\delta_{I'I}\,\delta_{M'M}\,\delta_{K'K} \qquad (A.9)$$

$$\sum_{j_p}\sum_{j_n} C_{j_p\Omega_p'}C_{j_p\Omega_p}C_{j_n\Omega_n'}C_{j_n\Omega_n}$$

$$\cdot\{\sqrt{(j_p-\Omega_p)(j_p+\Omega_p+1)(j_n+\Omega_n)(j_n-\Omega_n+1)}$$

$$\cdot[\delta_{\Omega_p',\Omega_p+1}\delta_{\Omega_n',\Omega_n-1}+(-1)^{I-j_p-j_n}\delta_{KO}\delta_{\Omega_p',-\Omega_p-1}\delta_{\Omega_n',-\Omega_n+1}]$$

$$+ \sqrt{(j_p+\Omega_p)(j_p-\Omega_p+1)(j_n-\Omega_n)(j_n+\Omega_n+1)}$$

$$\cdot[\delta_{\Omega_p',\Omega_p-1}\delta_{\Omega_n',\Omega_n+1}+(-1)^{I-j_p-j_n}\delta_{KO}\delta_{\Omega_p',-\Omega_p+1}\delta_{\Omega_n',-\Omega_n-1}]\}$$

In this case both Ω_p and Ω_n must differ by one unit between bands for the matrix element to be non-zero. One of these matrix elements occurs along the diagonal when both $|\Omega_n| = |\Omega_p| = 1/2$ and couple to form a K=0 rotational band.

$$E_{pp} = \langle IMK\Omega_p\Omega_n | H_{pp} | IMK\Omega_p\Omega_n \rangle$$

$$= \frac{\hbar^2}{2\mathcal{J}} (-1)^{I+1} a_p a_n \delta_{KO} \delta_{|\Omega_p|, 1/2} \qquad (A.10)$$

the neutron and proton decoupling parameters a_n and a_p are defined in analogy to equation (A.7)

In the evaluation of the Coriolis and particle-particle coupling it is important to notice the signs of the various Ω's and to use the correct phase on the $C_{j\Omega}$. The phase relationship is:

$$C_{j-\Omega} = (-1)^{j - 1/2} \pi C_{j\Omega} \qquad (3.1.6)$$

when π is the parity of the orbital

It has been suggested (Brockmeier et al. 1965) that the Coriolis matrix elements and the particle-particle matrix elements be corrected for the effects of pairing. The correction can most simply be made to the $j_\pm$ matrix element (eq. A.4). The correction factor is:

$$P_{K,K'} \approx (U_K U_{K'} + V_K V_{K'}) \qquad (A.11)$$

multiplying the j_+ matrix elements. Thus equation (A.5) can be multiplied on the right side by $P_{KK'}$. Similarly the matrix elements of the Coriolis and particle-particle interactions in the odd-odd case (eq. A.8 and eq. A.9) must also be corrected by a factor.

$$(P_{KK'})_{neutron}\ (P_{KK'})_{proton} \approx (U_p U_{p'} + V_p V_{p'})(U_n U_{n'} + V_n V_{n'}) \tag{A.12}$$

This correction due to pairing is usually small.

The total diagonal energy for an odd-Z nucleus is given by:

$$E = E_o + E_{rot} + E_{prot} + E_d \tag{A.13}$$

E_d is the decoupling energy (eq.(A.6)). E_o is the quasiparticle energy defined in equation (3.2.4) The total diagonal energy for an odd-odd nucleus is given by:

$$E = E_{po} + E_{no} + E_{rot} + E_{prot} + E_{nrot} + E_{pp} + E_{int} \tag{A.14}$$

E_{int} is the residual proton-neutron interaction. The effects of the residual interaction are briefly discussed in sect. 3.4.

It is usually more convenient to work in terms of the excitation energies of the nucleus. To obtain the excitation energy E_{ex} of a state it is only necessary to subtract the energy E_{gs} of the ground state configuration as calculated from either eq.(A.13) or (A.14) from the energy, E, calculated in a similar manner for the state of interest.

$$E_{ex} = E - E_{gs}$$

The matrix elements contained in this appendix are expected to be useful for the calculation of the properties of pure two quasi-particle states, and the mixings thereof due to the Coriolis interaction, in even-even nuclei as well. In even-even nuclei, though, the mixing is much more complicated because the first two quasi-particle states occur at comparable energies to the vibrations. It has been shown experimentally in ^{172}Yb (O'Neil and Burke 1972) that even relatively pure two quasi-particle configurations may be strongly coupled to vibrational states.

APPENDIX B

The Transition Amplitude

The transition amplitude between the initial and final states in a single particle transfer reaction is:

$$S_{fi} = \langle \phi_f | V_{pb} | \phi_i \rangle \qquad (3.5.5)$$

where the definitions of the wavefunctions and the potential V_{pb} may be found in section 3.5

$$S_{fi} = \int \psi_f \chi_B^* \chi_b^* V_{pb} \chi_a \chi_A \psi_i d\tau_b d\tau_A d\tau_B d\tau_a d\tau_i d\tau_f \qquad (B.1)$$

This integral extends over all the coordinates (center of mass) of the outgoing and incoming particles ($d\tau_i$, $d\tau_f$). The remaining integrations are over all the internal coordinates of the target, residual nucleus, projectile and the scattered particle.

Examining the integral:

$$\int \psi_B^* \psi_b^* V_{pb} \psi_a \psi_A d\tau_A d\tau_B d\tau_a d\tau_b \ ,$$

it is possible to perform the integration over the internal coordinates of the target and residual nucleus first.

$$\int \langle f | i \rangle \ \chi_b^* V_{pb} \chi_a \ d\tau_a d\tau_b$$

The problem is now to evaluate the overlap of the nuclear wavefunctions beforeand after the reaction.

$$\langle f | i \rangle = \int \chi_B^* \chi_A d\tau_A d\tau_B$$

$$= \langle I_f M_f K_f \Omega_{pf} \Omega_{nf} | I_i M_i K_i \Omega_i \rangle \qquad (B.2)$$

The subscripts i and f refer to the initial and final nucleus. The problem will be examined for the transition from an odd target nucleus (with an odd neutron, n) to an odd-odd nucleus, that is with an odd proton p and the same neutron n as was in the target. This last statement is very important as it is the reason the single particle transfer reactions populate only a certain type of configuration in the odd-odd nucleus. It is also assumed that the adiabatic wavefunction (3.3.10) and (3.3.11) may be used to represent the nucleus.

$$
\begin{aligned}
\langle f|i\rangle = & \sqrt{\frac{2I_i+1}{16\pi^2}}\sqrt{\frac{2I_f+1}{16\pi^2}} \sum_{j_{ni}} \sum_{j_{nf}} \sum_{j_p} C^{(f)}_{j_n\Omega_n} C_{n_p\Omega_p} C^{(i)}_{j_n\Omega_n} \\
& \delta_{j_{nf}\, j_{ni}} \int \{\delta_{\Omega_{nf},\Omega_i} D^{I_f*}_{M_fK_f} D^{I_i}_{M_iK_i} \chi^{\Omega_p*}_{j_p} \\
& + (-1)^{I_f-j_{nf}-j_p} \delta_{-\Omega_{nf},\Omega_i} D^{I_f*}_{M_f-K_f} D^{I_i}_{M_i-K_i} \chi^{-\Omega_p*}_{j_p} \\
& + (-1)^{I_i-j_{ni}} \delta_{\Omega_{nf},-\Omega_i} D^{I_f*}_{M_fK_f} D^{I_i}_{M_i-K_i} \chi^{\Omega_p*}_{j_p} \\
& + (-1)^{I_f-j_{nf}-j_p+I_i-j_{ni}} \delta_{-\Omega_{nf},-\Omega_i} D^{I_f*}_{M_f-K_f} D^{I_i}_{M_i-K_i} \chi^{-\Omega_p*}_{j_p} \}d\theta
\end{aligned}
\tag{B.3}
$$

Jones (1969) emphasizes the necessity now of using the consistent phases of the $C_{j\Omega}$ coefficients.

$$
\sum_j C_{j\Omega} C_{j\Omega} = 1 \tag{B.4}
$$

$$
\text{and} \qquad \sum_j C_{j\Omega} C_{j-\Omega} (-1)^{I-j} = (-1)^{I-1/2}\pi
$$

As Jones points out, the last expression here results in the only difference between Jones (1969) and Macfarlane and French (1960).

Because the reaction is performed in the lab frame, it is most convenient to rotate the wavefunction of the transferred particle into the space fixed orientation

$$\chi^{\Omega_p}_{j_p} = \sum_{m_p} D^{j_p}_{m_p \Omega_p} \psi_{j_p m_p}(\nu'). \qquad \text{(B.5)}$$

This may be seen to lead to integrals of the following form in the equation for $\langle f|i\rangle$

$$\int D^{I_1}_{M_1 K_1} D^{I_2}_{M_2 K_2} D^{I_3 *}_{M_3 K_3} \, d\theta$$

$$= \frac{8\pi^2}{(2I_3+1)} \langle I_1 I_2 M_1 M_2 | I_3 M_3 \rangle \langle I_1 I_2 K_1 K_2 | I_3 K_3 \rangle . \qquad \text{(B.6)}$$

Now using the symmetry properties of the Clebsch Gordan coefficients the overlap integral reduces to

$$\langle f|i\rangle = \sum_{j_p} \sqrt{\frac{2I_i+1}{2I_f+1}} \, C_{j_p \Omega_p} \langle I_i, j_p m_i, m_f - m_i | I_f m_f \rangle$$

$$\psi^{*}_{j_p, m_f - m_i}(\omega') [\langle I_i j_p K_i \Omega_p | I_f K_f \rangle$$

$$+ (-1)^{I_i - \frac{1}{2}} \pi_n \langle I_i, j_p, K_i, -\Omega_p | I_f - K_f \rangle]$$

$$= \sum_{j_p} \langle I_i, j_p, m_i, m_f - m_i | I_f m_f \rangle \psi^{*}_{j_p, m_f - m_i}(\omega') \beta_{j_p}(\ell_p) \qquad \text{(B.7)}$$

The last line defines the reduced particle width β. The quantity β has a value for each j_p; because of parity conservation there is a corresponding ℓ_p. In β it is customary to include the positive root of the occupation probability $\sqrt{U^2}$ and the core overlap factor:

$$\langle\phi_f|\phi_i\rangle \tilde{\simeq} 1 . \qquad (B.8)$$

The core overlap factor is the degree to which the initial and final vibrational states are the same. It does not seem unreasonable that the overlap should be near unity because both the initial and final nuclei are assumed to be in their vibrational ground states and they only differ by one nucleon. Thus:

$$\beta_{j_p} = \sqrt{\frac{2I_i+1}{2I_f+1}}\,\langle\phi_f|\phi_i\rangle U C_{j_p\Omega_p}$$

$$[\langle I_i j_p K_i \Omega_p | I_f K_f\rangle + (-1)^{I_i-\frac{1}{2}}\,\pi_n \langle I_i, j_p, K_i, -\Omega_p | I_f, -K_f\rangle] \qquad (B.9)$$

If the target spin $I_i=0$ it is a straightforward calculation to evaluate β_{j_p} using the properly symmetrised wavefunction for the ground state of an even-even target:

$$|IMK\rangle = D^I_{MK} + (-1)^I D^I_{M-K} . \qquad (B.10)$$

In the case of a stripping reaction on an even-even target leading to an odd-Z nucleus β_{j_p} becomes:

$$\beta_{j_p} = \sqrt{2}\,\sqrt{\frac{2I_i+1}{2I_f+1}}\,U\langle\phi_f|\phi_i\rangle C_{j_p\Omega_p}\,\delta_{\Omega_p K_p}\,\delta_{j_p I_f} . \qquad (B.11)$$

Now returning to the discussion of the scattering amplitude, we have shown that (from eq. (B.1)):

$$S_{fi} = \int \psi_f^* \sum_{j_p} \beta_{j_p} \langle I_i, j_p, m_i m_f - m_i | I_f m_f \rangle \int \psi^*_{j_p, m_f - m_i}(\omega) \cdot$$

$$V_{pb} \chi_b \; \psi_i d\tau_a d\tau_b d\tau_i d\tau_f \qquad \text{(B.12)}$$

The integral

$$F_{j,m} = F_{j, m_f - m_i} = \int \psi^*_{j_p, m_f - m_i}(\omega) \chi_b^* \; V_{pb} \; \chi_a \; d\tau_a \; d\tau_b \qquad \text{(B.13)}$$

is called the form factor and the integration of this is much simplified by using the "zero-range" approximation.

$$V_{pb} \chi_a (\vec{r}_b - \vec{r}_p) = D_o \, \delta (\vec{r}_b - \vec{r}_p) \; . \qquad \text{(B.14)}$$

This approximation means that the proton and the outgoing particle must be at the same place before an interaction of strength D_o can take place. This implies the incoming particle must also be at the same place as the reaction taking place. The form factor essentially gives the degree to which the incoming particle looks like the outgoing particle plus a proton in a specific shell model orbit with the given interaction. Some type of wavefunction for these particles must be assumed. This integration with a specific wavefunction for the incident and scattered particles also generates the normalizing factor for the predicted cross section. The form factor is referred to again in section 3.6.

Thus the scattering amplitude is:

$$S_{fi} = \int \psi_f^* \sum_{j_p} \beta_{j_p} \langle I_i, j_p, m_i, m_f - m_i | I_f m_f \rangle F_{j, m_f - m_i} \psi_i d_{\tau i} d_{\tau f} \cdot \quad \text{(B.15)}$$

A NOTE ON THE PHASES USED

The correct $C_{j\Omega}$ coefficients must be used in the wave-function for an odd-odd nucleus (eq. (3.3.10)). This is particularly important if an Ω-value is negative for an orbital in the configuration under consideration. The $C_{j\Omega}$ coefficient for an orbital with a negative Ω is related to the coefficient of the same orbital with a positive Ω-value in the following manner:

$$C^{\nu}_{j-\Omega} = (-1)^{j-1/2} \pi C^{\nu}_{j\Omega} \quad .$$

This phase relationship must also be carefully included in the Coriolis matrix element (eq. (A.8)), the particle-particle matrix element (eq. A.9) and in the partial width for the single particle transitions (eq. (B.9)).

The expressions for the matrix elements of the rotational Hamiltonian (Appendix A) and the partial width for the single particle transitions are consistent with the wave-function chosen in equation (3.3.10).

APPENDIX C

Energy Levels of Some Neighbouring Nuclei

The level scheme of ^{171}Lu as determined by Gregory (1972), is shown in fig. C.1. This is to be compared with the level schemes reported in the present work for ^{173}Lu, ^{175}Lu and ^{177}Lu. The structure of ^{171}Lu is very similar to that of the heavier lutetium isotopes shown in figs. 6.0.1, 6.0.2 and 6.0.3.

A comparison of the (^{3}He,α) and (d,t) spectra of ^{173}Yb is shown in fig. C.2. This is to be contrasted with figure 5.1.2 for ^{174}Lu. The odd-odd nucleus ^{174}Lu has one more proton than ^{173}Yb and this proton may couple in two ways to the transferred neutron, hence a more complicated spectrum.

Figure C.1

An energy level diagram for ^{171}Lu (Gregory 1972). These data were obtained using single proton transfer reactions as well as (HI,xn) reactions and observing γ-rays in singles and coincidence. Internal conversion electron studies were done with the (α,2n) reaction.

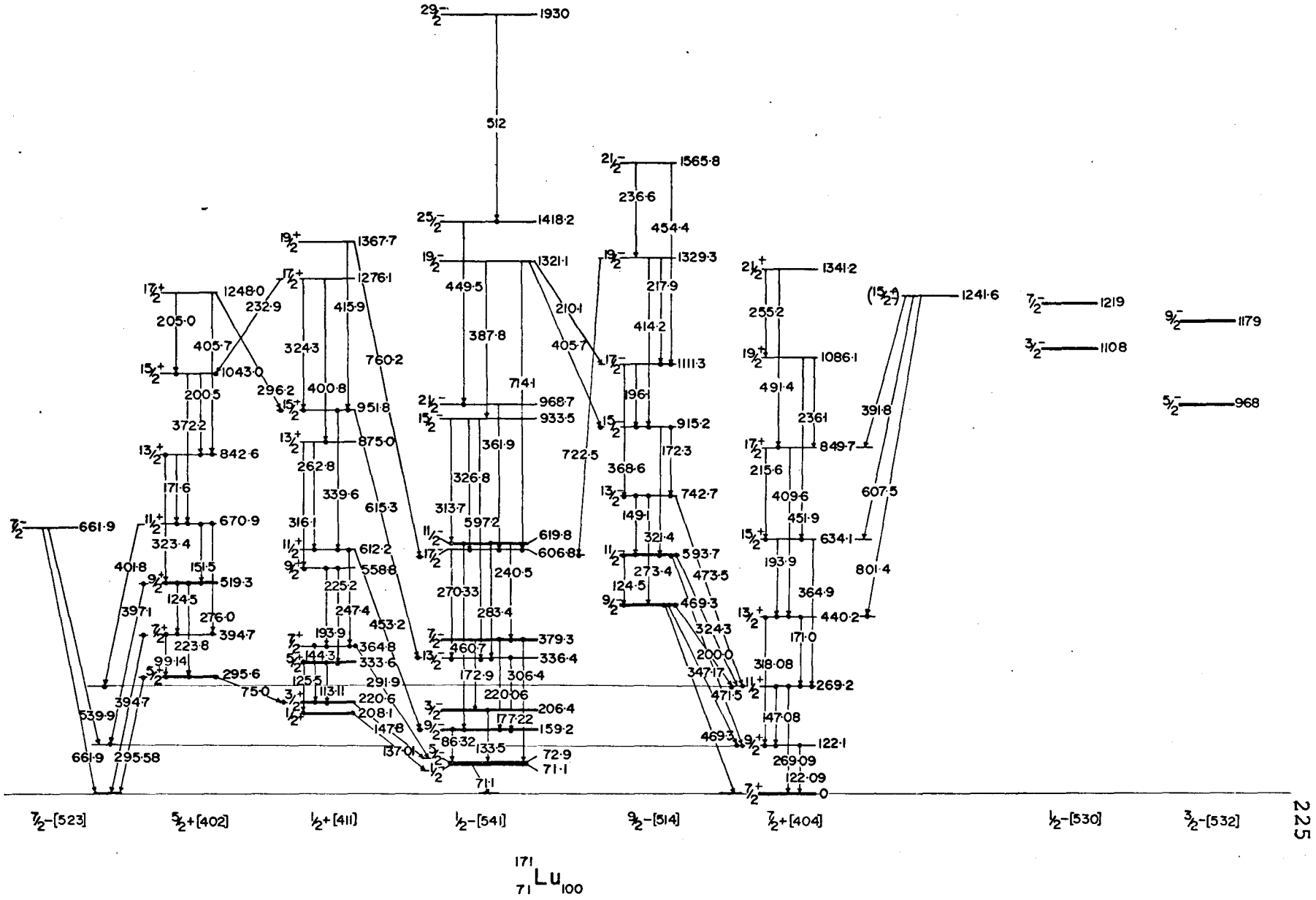
29/2− 1930
512
25/2− 1418.2
19/2− 1321.1
449.5
387.8
714.1
21/2− 968.7
15/2− 933.5
361.9
326.8
313.7
597.2
11/2− 619.8
17/2− 606.8
240.5
270.33
283.4
7/2− 379.3
460.7
13/2− 336.4
172.9
306.4
220.06
3/2− 206.4
177.22
9/2− 159.2
86.32
133.5
5/2− 72.9
1/2− 71.1
21/2− 1565.8
236.6
454.4
19/2− 1329.3
217.9
414.2
17/2− 1111.3
196.1
15/2− 915.2
722.5
172.3
368.6
13/2− 742.7
149.1
321.4
11/2− 593.7
273.4
473.5
124.5
9/2− 469.3
324.3
200.0
347.17
471.5
11/2+ 269.2
147.08
469.3
9/2+ 122.1
269.09
122.09
7/2+ 0
405.7
210.1
19/2+ 1367.7
1276.1
17/2+ 1248.0
232.9
415.9
205.0
324.3
760.2
15/2+ 1043.0
405.7
400.8
296.2
200.5
15/2+ 951.8
372.2
13/2+ 875.0
842.6
262.8
339.6
171.6
316.1
615.3
11/2+ 612.2
11/2+ 670.9
9/2+ 558.8
323.4
225.2
401.8
151.5
247.4
453.2
9/2+ 519.3
397.1
124.5
193.9
276.0
7/2+ 364.8
7/2+ 394.7
223.8
5/2+ 144.3 333.6
99.14
5/2+ 295.6
1255
291.9
75.0
3/2+ 113.11 220.6
1/2+ 208.1
539.9
394.7
1478
137.01
7/2− 661.9
661.9 295.58
1341.2
255.2
19/2+ 1086.1
491.4
236.1
17/2+ 849.7
215.6
409.6
451.9
15/2+ 634.1
193.9
364.9
13/2+ 440.2
171.0
318.08
11/2+ 269.2
(15/2+) 1241.6
391.8
607.5
801.4
7/2− 1219
3/2− 1108
9/2− 1179
5/2− 968
7/2−[523]
5/2+[402]
1/2+[411]
1/2−[541]
9/2−[514]
7/2+[404]
1/2−[530]
3/2−[532]
171 71 Lu 100

Figure C.2

Representative spectra from the $^{174}Yb(d,t)^{173}Yb$ and $^{174}Yb(^{3}He,\alpha)^{173}Yb$ reactions. These spectra have been adapted from Burke et al. (1971) and Burke et al. (1966).

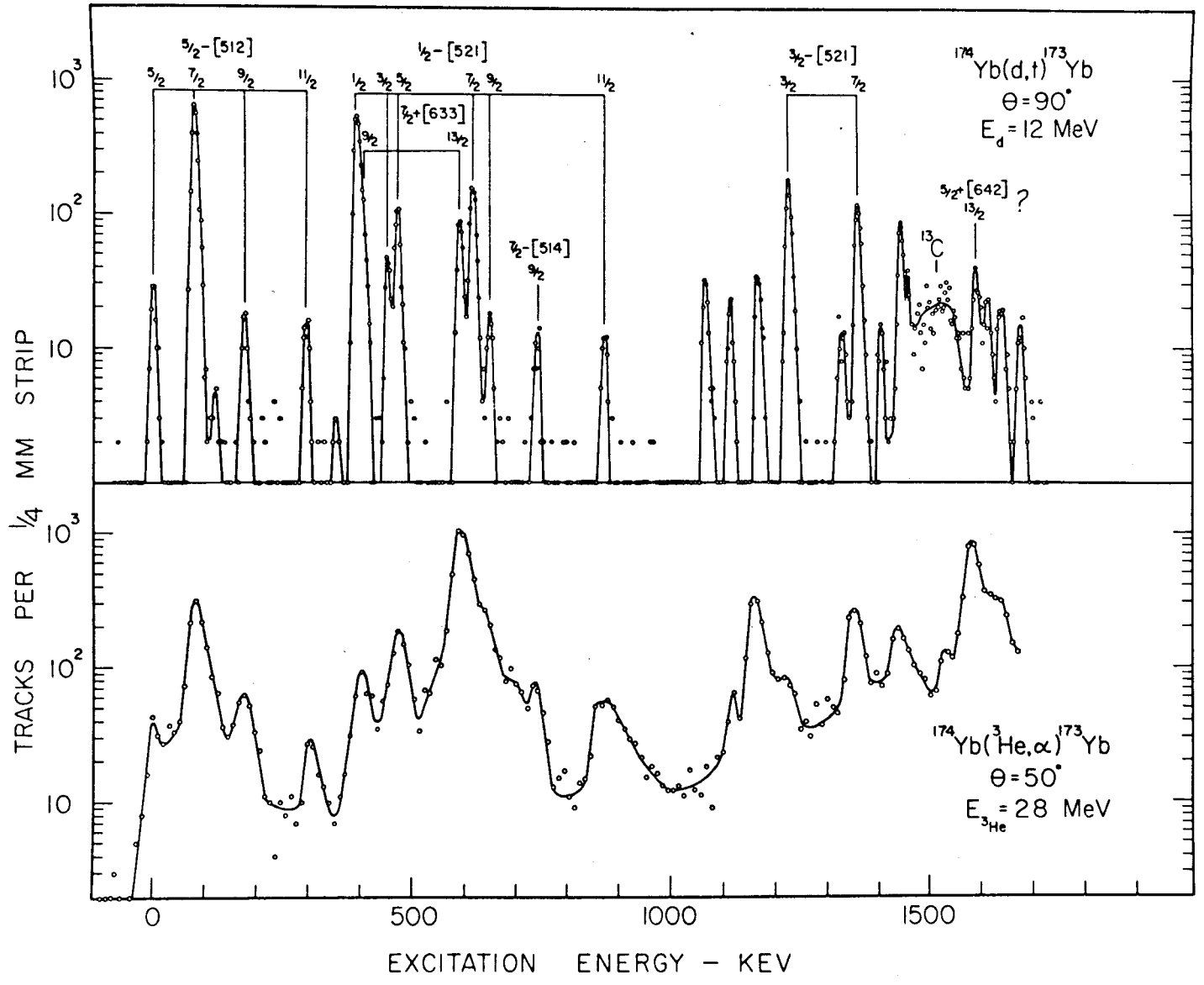
5/2-[512]
1/2-[521]
3/2-[521]
174Yb(d,t)173Yb
Θ=90°
Ed=12 MeV
7/2+[633]
7/2-[514]
5/2+[642]
13C
174Yb(3He,α)173Yb
Θ=50°
E3He=28 MeV
TRACKS PER 1/4 MM STRIP
EXCITATION ENERGY – KEV

REFERENCES

Alexander, P., Boehm, F. and Kankeleit, E. 1964. Phys. Rev. 133, B284.

Balodis, M. K., Kramer, N.D., Prokofiev, P. T. and Fainer, U.M. 1966. Sov. J. Nucl. Phys. (English translation) 3, 141.

Bassel, R. H., Drisko, R. M. and Satchler, G. R. 1962. Oak Ridge National Laboratory Report. #3240. unpublished.

Bernstein, E.M. and Graetzer, R. 1960. Phys. Rev. 119, 1321.

Bjørnholm, S., Borggreen, J., Frahm, H. J. and Sigurd Hansen, N. J. 1965. Nucl. Phys. 73, 593.

Blair, A. G. and Armstrong, D. D. 1966. Phys. Rev. 151, 930.

Bohr, N. 1948. Mat. Fys. Medd. Dan. Vid. Selsk. 18, #8.

Borggreen, G., Løvhøiden, G. and Waddington, J.C. 1969. Nucl. Phys. A.131, 241.

Brenner, D. 1970. Private communication to D. G. Burke.

Brockmeier, R. T., Walborn, S., Seppi, E. J., and Boehm, F. 1965. Nucl. Phys. 63, 102.

Brown, R. A., Roulston, K. I., Ewan, G. T., and Andersson, G.I. 1970. Nucl. Phys. 154, 626.

Bunker, M.E., and Reich, C. W., 1971. Rev. Mod. Phys. 43, 348.

Burke, D. G., Zeidman, B., Elbek, B., Herskind, B. and Olesen, M. 1966. Mat. Phys. Medd. Dan. Vid. Selsk, 35, #2.

Burke, D. G. and Tippett, J. C., 1968. Nucl. Inst. 49, 181.

Burke, D. G., Alford, W. P., and O'Neil, R. A. 1971. Nucl. Phys. A161, 129.

Burke, D. G. and Waddington, J. C. 1972. Can. J. Phys. 50, 700. (Indirect Excitation)

Burke, D. G. and Waddington, J. C. 1972. Accepted for publication by Nucl. Phys. (^{151}Pm)

Cairns, J. E. 1972. McMaster University, proposed M.Sc. thesis.

Chi, B. E. 1967. State University of New York, Department of Physics, preprint. Corrected from Chi, B. E. 1966. Nucl. Phys. 83, 97.

Christensen, P. R., Berinde, A., Neamu, I. and Scentai, N. 1969. Nucl. Phys. A129, 337.

Davidson, J. P. 1968. Collective Models of the Nucleus, Page 83. Academic Press, New York.

Deutch, B. I. 1962. Nucl. Phys. 30, 191.

Edmonds, A. R. 1957. Angular Momentum in Quantum Mechanics, Princeton University Press, Princeton, N. J.

Elbek, B. and Tjøm, P. O. 1969. Advances in Nuclear Physics, 3, 759. Ed. M. Baranger and E. Vogt, Plenum Press, New York.

Elliot, J. P. 1958. Collective Motion in Nuclei, Part B, Page 76. (Notes compiled by H. M. Macfarlane, Department of Physics, University of Rochester, Rochester, New York)

Enge, H. A. 1966. Introduction to Nuclear Physics, Addison-Wesley (Canada) Limited, Don Mills, Ontario.

Foin, C., Barnéoud, D., and Hjorth, S. A., 1971. Annual Report, Research Institute for Physics, Stockholm, Sweden.

Funke, L., Graber, H., Kaun, K. H., Sodan, H. and Werner, L. 1965. Nucl. Phys. 70, 347.

Gallagher, C. J. Jr., and Moszkowski, S. A. 1958. Phys. Rev. 111, 1282.

Glendenning, N.K. 1963. Ann. Rev. Nucl. Sci. 13, 191.

Gregory, P. R. 1972. Ph. D. Thesis, McMaster University, unpublished. (And a portion thereof to be submitted to Can. J. Phys.)

Harmatz, B., Handley, T. H. and Mihelich, J. W. 1960. Phys. Rev. 119, 1345.

Harmatz, B. and Handley, T. H. 1966. Nucl. Phys. 81, 481.

Hatch, E. N., Boehm, F., Marmier, P. Dumond, J. W. M. 1956. Phys. Rev. 104, 745.

Hering, W. R., Becker, H. Wiedner, C. A. and Thompson, W. J. 1970. Nucl. Phys. A151, 33.

Jaskola, M., Nybø, K., Tjøm, P. O. and Elbek, B., 1967. Nucl. Phys. A96, 52.

Johansen, K. H., Bengston, B., Hansen, P. G. and Hornshøj, P. Nucl. Phys. A133, 213.

Jones, H. D., 1969. Ph.D. dissertation, The Florida State University. #70-3320, University Microfilms, Inc., Ann Arbor, Michigan.

Jones, H. D., and Sheline, R. K., 1970. Phys. Rev. C1, 2030.

Jones, H. D., Onishi, N., Hess, T. and Skeline, R. K. 1971. Phys. Rev. C3, 529.

Kerman, A. K., 1956. Mat. Fys. Medd. Dan. Vid. Selsk. 30, #15.

Khoo, T. L., Waddington, J. C., O'Neil, R. A., Prebisz, Z., Burke, D. G. and Johns, M. W., 1972. Phys. Rev. Lett. 28, 1717.

Kleinheinz, P., Løvhøiden, G., and Mogelvang, A., 1972. To be published.

Kristensen, L., Jørgensen, M., Nielsen, O. B. and Sidenius, G. 1964. Phys. Lett. 8, 61.

Kunz, P. D., 1969. University of Colorado, computer program DWUCK and write up thereof, unpublished.

Lamm, I-L., 1969. Nucl. Phys. A125, 504.

Lederer, C. M., Hollander, J. M., and Perlman, I., 1968. Table of Isotopes, 6th ed., John Wiley & Sons, New York.

Lilley, T. S. and Stein, N., 1967. Phys. Rev. Lett. 19, 709.

Liran, S. and Zeldes, N., 1969. Nucl. Phys. A130, 190.

Løvhøiden, G., Waddington, J. C., Hagemann, K. A., Hjorth, S.A., and Ryde, H., 1970. Nucl. Phys. A148, 657.

Lu, M. T. and Alford, W. P., 1971. Phys. Rev. C3, 1243.

Macfarlane, M. H. and French, J. B., 1960. Rev. Mod. Phys. 32, 567.

Maier, B. P. K., 1965. Z. Physik 184, 153.

Manfrass, P., Prade, H., Beitins, M. T., Bondarenko, W. A., Kramer, N. D., and Prokofjew, P. T., 1971. Nucl. Phys. A172, 298, and subsequent private communication to R. A. O'Neil.

Marion, J.B. and Young, F.C. 1968. Nuclear Reaction Analysis-Graphs and Tables, North Holland Publishing Co., Amsterdam.

Michaud, B., Kern, J. and Schaller, L.A. 1970. Helv. Phys. Acta. 43, 424.

Minor, M.M., Skeline, R.K. and Jurney, E.T. 1969. Phys. Rev. 187, 1516

Mize, J.P., Bunker, M.E. and Starner, J.W. 1956. Phys. Rev. 103, 182.

Nathan, O. and Nilsson, S.G. 1965 . Alpha Beta and Gamma Ray Spectroscopy, 601. ed. K. Siegbahn, North Holland Publishing Co., Amsterdam.

Neergård, K. and Vogel, P. 1970. Nucl. Phys. A145, 33.

Newby, N.D. Jr. 1962. Phys. Rev. 125, 2063.

Nilsson, S.G. 1955. Mat. Fys. Medd. Dan. Vid. Selsk. 29, #16.

Nilsson, S.G., Tsang, C.F., Sobiczewski, A., Szymanski, Z., Wycech, S., Gustafson, C., Lamm, I-L., Möller, P. and Nilsson, B, 1969. Nucl. Phys. A131, 1.

Nuclear Data Sheets (1959-1965) 1966. ed. K. Way. Academic Press, New York.

O'Neil, R.A., Burke, D.G. and Alford, W.P. 1971. Nucl. Phys. A167, 481.

O'Neil, R.A. and Burke, D.G. 1972. Nucl. Phys. A182, 342.

O'Neil, R.A. 1972. McMaster University, computer programs GREAT, GREATER and SPECTR, unpublished.

Preston, M.A. 1962. Physics of the Nucleus, Addison-Wesley Publishing Co. Inc., Reading, Mass.

Pyatov, N.I., 1963. Ivz. Akad, Nauk, SSSR Ser. Fiz. 27, 1409 (trans. Bull. Acad. Sci. USSR Phys. Ser. 27, 1409).

Rost, E. 1967. Phys. Rev. 154, 994.

Satchler, G.R. 1958. Ann. Phys. (N.Y.) 3, 275.

Satchler, G.R. 1964. Nucl. Phys. 55, 1.

Scholz, W. and Malik, F.B., 1968. Phys. Rev. 176, 1355.

Spencer, J.E. and Enge, H.E. 1967. Nucl. Inst. 49, 181.

Soloviev, V.G., Vogel, P. and Jungklaussen, G. 1966. Preprint #E4-3051. Joint Institute for Nuclear Research, Dubna.

Soloviev, V. G. and Fedotov, S. I., 1971. Preprint #E4-6055, Joint Institute for Nuclear Research, Dubna.

Valentin, J., Horen, D. J. and Hollander, J. M., 1962. Nucl. Phys. 31, 353. (^{173}Lu).

Valentin, J. Horen, D. J. and Hollander, J. M., 1962. Nucl. Phys. 31, 373. (^{172}Lu).

Westgaard, L. and Bjørnholm, S., 1966. Nucl. Inst. 49, 77.

Wildenthal, B. B., Preedom, B. M., Newman, E., and Cates, M. R. 1967. Phys. Rev. Lett. 19, 960.